

University of Southampton Research Repository

Copyright © and Moral Rights for this thesis and, where applicable, any accompanying data are retained by the author and/or other copyright owners. A copy can be downloaded for personal non-commercial research or study, without prior permission or charge. This thesis and the accompanying data cannot be reproduced or quoted extensively from without first obtaining permission in writing from the copyright holder/s. The content of the thesis and accompanying research data (where applicable) must not be changed in any way or sold commercially in any format or medium without the formal permission of the copyright holder/s.

When referring to this thesis and any accompanying data, full bibliographic details must be given, e.g.

Thesis: Author (Year of Submission) "Full thesis title", University of Southampton, name of the University Faculty or School or Department, PhD Thesis, pagination.

Data: Author (Year) Title. URI [dataset]

University of Southampton

Faculty of Medicine

School of Cancer Sciences

**CD8+ tissue resident memory T lymphocytes and disease control in human
oesophageal adenocarcinoma**

by

Samuel Luke Hill

ORCID ID 0000-0002-9590-2116

Thesis for the degree of Doctor of Philosophy - Cancer Sciences

November 2022

University of Southampton

Abstract

Faculty of Medicine

School of Cancer Sciences

Thesis for the degree of Doctor of Philosophy - Cancer Sciences

CD8+ tissue resident memory T lymphocytes and disease control in human oesophageal adenocarcinoma

by

Samuel Luke Hill

The development of novel treatments for oesophageal adenocarcinoma (OAC) represents an area of significant unmet need. Incidence has increased across western populations in recent decades, and despite improvements in oncological therapies and surgical techniques, 5 year survival remains at approximately 17%. Despite features suggesting potential response to treatment with immune checkpoint blockade, the benefits of such approaches in OAC have been modest.

A flow cytometric approach has been adopted to undertake immune phenotyping of human OAC specimens, obtained during curative resection, to assess factors related to lymphocyte dysfunction and exhaustion. It was observed that OAC are variously, but often highly, infiltrated with a population of antigen experienced CD8+ T lymphocytes (TILs) that express high levels of both PD-1 and CD39 and an abundance of this population was associated with improved progression free and overall survival. While a small sub population within this group express multiple exhaustion markers, these TILs do not appear to conform to the classical picture of lymphocyte exhaustion.

The dominant PD-1+ and CD39+ lymphocyte population was investigated utilising bulk RNA sequencing and flow cytometric based functional analysis. This has demonstrated a population dominated by precursor exhausted-like tissue resident memory CD8+ lymphocytes, identified through their transcriptomic profile as well as by their CD103+ and TIM3- phenotypes, and is consistent with TILs described as being associated with improved survival in various cancers. This population demonstrated a maintained proliferative potential, and an ability to degranulate and produce the key effector molecules IFN- γ , TNF- α and Granzyme B. The minority TIM3+ LAG3+ group among PD-1 and CD39 positive TILs corresponds to a terminally exhausted-like tissue resident memory CD8+ lymphocyte phenotype previously described as correlating with

therapeutic response to immune checkpoint blockade, and the relative lack of this population in OAC points to a potential mechanism for the poor responses seen to immunotherapy.

Table of Contents

1.4	Oesophageal cancer.....	27
1.4.1	Background demographics and aetiology	27
1.4.2	Oesophageal Adenocarcinoma and Barrett’s oesophagus.....	28
1.4.3	Curative Treatment – surgery, chemotherapy and radiotherapy	30
1.4.4	Treatment of inoperable and metastatic oesophageal adenocarcinoma	31
1.4.5	Rationale for immunotherapy - tumour microenvironment, inflammatory phenotype and TMB	32
1.4.6	Early immunotherapy trials	34
Chapter 2	Materials and Methods.....	37
2.1	Experimental protocols.....	37
2.1.1	Access to samples	37
2.1.2	Tumour disaggregation.....	37
2.1.3	Flow cytometry	38
2.1.4	Tumour infiltrating lymphocyte culture	39
2.1.5	Cell Freezing.....	39
2.1.6	RNA extraction	40
2.1.7	RNA quantification.....	41
2.1.8	Smart-seq2 RNA sequencing.....	41
2.1.8.1	Primer preparation	41
2.1.8.2	Reverse transcription.....	42
2.1.8.3	PCR pre-amplification and cDNA clean up.....	42
2.1.8.4	Tagmentation and Indexing	43
2.1.8.5	Library pooling and DNA sequencing.....	43
2.1.9	Post-sequencing data processing	44
2.1.10	Lymphocyte proliferation assay.....	44
2.1.11	Lymphocyte stimulation assay.....	45
2.2	Experimental procedure development and optimisation	46
2.2.1	RNA sequencing experiment optimisation	46
2.2.1.1	Assessment of RNA extraction techniques.....	46
2.2.1.2	Assessment of expected yield of TILs isolated by fluorescence-activated cell sorting (FACS)	49

2.2.1.3	Assessment of feasibility of RNA sequencing using SmartSeq2 protocol	51
2.2.1.4	cDNA production and indexing of sequencing library from RNA extracted from oesophageal adenocarcinoma TILs	52
2.2.1.5	RNA sequencing of sorted TILs from human oesophageal adenocarcinoma	53
2.2.1.6	Processing of transcriptomic data.....	55
2.2.2	CD8+ proliferation assay development and testing.....	56
Chapter 3 Immunophenotyping of exhausted CD8+ T lymphocytes in human oesophageal adenocarcinoma		59
3.1	Introduction.....	59
3.2	Results	60
3.2.1	Patient Characteristics	60
3.2.2	Flow Cytometry assessment	63
3.2.3	Lymphocyte infiltration	66
3.2.3.1	Immunohistochemistry analysis.....	66
3.2.3.2	Flow cytometry analysis	67
3.2.4	Antigen experienced CD8+ lymphocyte infiltration.....	70
3.2.5	PD-1 and CD39.....	73
3.2.5.1	PD-1	73
3.2.5.2	CD39	75
3.2.5.3	PD-1 and CD39 dual positivity	78
3.2.6	Tbet and Eomes.....	81
3.2.7	Cell surface markers of exhaustion	85
3.2.7.1	TIM3 and LAG3	85
3.2.7.2	TIGIT, CD244 and CD38	87
3.2.8	Exhaustion marker expression and degree of PD-1 expression	91
3.3	Discussion	94
Chapter 4 Transcriptomic assessment of exhausted CD8+ T lymphocyte populations in human oesophageal adenocarcinoma		97

Table of Contents

4.1	Introduction	97
4.2	Results.....	98
4.2.1	RNA sequencing pipeline optimisation.....	98
4.2.2	Preliminary data analysis	100
4.2.3	Expansion of data set.....	105
4.2.4	Data analysis of full data set.....	106
4.2.5	Comparison of treatment naïve and chemotherapy treated samples from expanded data set	107
4.2.6	Comparison of DP and DN populations from all treatment naïve and chemotherapy pre-treated samples.....	110
4.2.6.1	Gene ontology term and Reactome pathway analysis with GSEA	110
4.2.6.2	Ingenuity Pathway Analysis	114
4.2.6.3	GSEA phenotypic assessment indicating tissue resident memory lymphocyte phenotype and potential immunotherapy resistance....	115
4.2.7	Comparing the LExh and DP phenotype from all analysed samples.	117
4.2.7.1	Ingenuity Pathway Analysis	117
4.2.7.2	Gene ontology term and Reactome pathway analysis with GSEA	121
4.2.7.3	GSEA phenotypic assessment	124
4.2.8	Comparison of all experimental phenotypes from combined treatment naïve and chemotherapy pre-treated samples.....	125
4.2.8.1	Gene set variation analysis	125
4.2.8.2	Key effector molecule and transcription factor expression	129
4.3	Discussion.....	131
Chapter 5	Functional assessment of exhausted CD8+ T lymphocyte populations in human oesophageal adenocarcinoma.....	133
5.1	Introduction	133
5.2	Results.....	134
5.2.1	Multi-parametric flow cytometric assessment of the DP population.....	134
5.2.1.1	T-bet and Eomes expression.....	135

5.2.1.2	Characterisation of T-bet ^{High} Eomes ^{Low} and T-bet ^{Low} Eomes ^{High} populations.....	138
5.2.1.3	Expression of CD8+ lymphocyte effector molecules.....	140
5.2.2	CD8+ Lymphocyte stimulation assays.....	142
5.2.2.1	Stimulation of degranulation	143
5.2.2.2	Stimulation of effector molecule production	145
5.2.3	CD8+ lymphocyte proliferation assay	147
5.2.3.1	CD8+ proliferation assay development and testing.....	148
5.2.3.2	Proliferation assay of sorted OAC TILs	148
5.2.4	Assessment of the CD4+ compartment of the OAC TILs.....	151
5.2.5	Assessment for expression of markers of tissue resident memory phenotype	155
5.3	Discussion.....	158
Chapter 6 Discussion.....		161
6.1	Oesophageal adenocarcinoma – an area of unmet need.....	161
6.2	Key Findings.....	162
6.3	Interpretation of results.....	165
6.4	Limitations.....	168
6.5	Future research	170
6.6	Concluding summary.....	172
Appendix A Classification and staging of human oesophagogastric cancer		175
A.1	Siewert system of classification for adenocarcinomas of the oesophagogastric junction.....	175
A.2	TNM cancer staging categories for cancer of the oesophagus and oesophagogastric junction.....	176
A.3	Mandard tumour regression score	177
Appendix B List of flow cytometry antibodies		179
Appendix C SmartSeq 2 reaction mixtures and reaction conditions.....		181
C.1	Reverse transcription and template switching reaction.....	181

Table of Contents

C.1.1	Reverse transcription/template switching reaction mixture	181
C.1.2	Reverse transcription PCR conditions.....	181
C.2	PCR pre-amplification reaction	182
C.2.1	PCR pre-amplification reaction mixture	182
C.2.2	Pre-amplification PCR conditions	182
C.3	Tagmentation and adapter-ligated fragment amplification.....	183
C.3.1	Tagmentation reaction mixture.....	183
C.3.2	Amplification of adapter-ligated fragment reaction mixture.....	183
C.3.3	Adapter-ligated fragment amplification PCR conditions.....	183
Appendix D Script for DEG analysis using DESeq2		185
Appendix E Metadata and read count example		189
E.1	RNA sequencing metadata	189
E.2	Example RNA sequencing read counts data for analysis.....	190
Glossary of Terms		193
List of References.....		197

Table of Tables

Table 1	RNA extraction technique analysis.	47
Table 2	Assessment of the Zymo Direct-zol™ RNA Microprep Kit.	48
Table 3	Cells recovered from trial FACS sorts of human oesophageal adenocarcinoma specimens.	50
Table 4	Patient demographics and clinical characteristics of individuals with oesophageal tumours included in the study.	62
Table 5	Siewert classification of oesophagogastric adenocarcinomas.	175
Table 6	Cancer staging for cancer of the oesophagus and oesophagogastric junction.	177
Table 7	Classification of tumour regression using the Mandard scoring system.	177
Table 8	Fluorophore labelled antibodies used for flow cytometry.	180
Table 9	Reverse transcription/template switching reaction mixture.	181
Table 10	Reverse transcription PCR conditions.	182
Table 11	PCR pre-amplification reaction mixture.	182
Table 12	Pre-amplification PCR conditions.	182
Table 13	Tagmentation reaction mixture.	183
Table 14	Amplification of adapter-ligated fragment reaction mixture.	183
Table 15	Adapter-ligated fragment amplification PCR conditions.	184
Table 16	Metadata for RNA sequencing analysis	189
Table 17	Example of read counts generated by RNA sequencing.	190

Table of Figures

Figure 1	Potential developmental relationship between exhausted, effector and memory CD8+ T lymphocytes.....	14
Figure 2	Metabolism of extracellular ATP to Adenosine.....	24
Figure 3	RNA quality assessment using Agilent 2100 Bioanalyzer.....	49
Figure 4	Trial library preparation using SmartSeq2 protocol.....	52
Figure 5	Successful cDNA production from oesophageal adenocarcinoma TILs using SmartSeq2 protocol.....	53
Figure 6	cDNA from 3 populations of TILs extracted from 3 oesophageal adenocarcinomas.....	54
Figure 7	Analysis of tagmented and indexed cDNA from first 3 oesophageal adenocarcinomas.....	55
Figure 8	CFSE proliferation assay development utilising HD PBMC samples.....	57
Figure 9	Exemplar antibody titration experiment showing anti-CD8a FITC antibody.....	63
Figure 10	Comparison of fresh vs freeze-thawed sample analysis.....	65
Figure 11	Immunohistochemistry staining of resected oesophageal adenocarcinoma specimen for lymphocyte markers.....	67
Figure 12	Lymphocyte infiltration in human oesophageal adenocarcinoma.....	69
Figure 13	CD8+CD44+ tumour infiltrating lymphocytes from human oesophageal adenocarcinoma.....	71
Figure 14	PD-1 expression on CD8+CD44+ tumour infiltrating lymphocytes from human oesophageal adenocarcinoma.....	74
Figure 15	CD39 expression on CD8+CD44+ tumour infiltrating lymphocytes from human oesophageal adenocarcinoma.....	77
Figure 16	PD-1 and CD39 dual expression on CD8+CD44+ tumour infiltrating lymphocytes from human oesophageal adenocarcinoma.....	79

Table of Figures

Figure 17	T-bet and Eomes expression by CD8+CD44+ tumour infiltrating lymphocytes from human oesophageal adenocarcinoma.	84
Figure 18	TIM3 and LAG3 expression by CD8+CD44+ tumour infiltrating lymphocytes from human oesophageal adenocarcinoma.	86
Figure 19	TIGIT, CD244 and CD38 expression by CD8+CD44+ tumour infiltrating lymphocytes from human oesophageal adenocarcinoma.	89
Figure 20	Exhaustion marker expression on DN and DP TILs in human oesophageal adenocarcinoma.	91
Figure 21	Cell surface exhaustion marker and T-box transcription factor expression in human oesophageal adenocarcinoma by degree of PD-1 expression.	93
Figure 22	Gating strategy for FACS sorting of lymphocyte populations of interest.	99
Figure 23	Analysis of preliminary dataset showing DEG profiling and GSEA.	104
Figure 24	Differential gene expression analysis and GSEA comparing DP with DN populations in treatment naïve samples.	109
Figure 25	Comparison of DP and DN populations from all post chemotherapy and treatment naïve patient samples.	113
Figure 26	GSEA comparison of DP and DN phenotypes.	116
Figure 27	Comparison of the LExh and DP populations with Qiagen IPA analysis.	120
Figure 28	GSEA comparing the LExh and DP populations using GO terms and Reactome pathways.	123
Figure 29	GSEA comparison of LExh and DP phenotypes.	125
Figure 30	GSVA analysis of GO terms and Reactome pathways of interest.	127
Figure 31	GSVA analysis using gene sets for phenotypes of interest.	129
Figure 32	Normalised gene expression for effector molecules and TRM associated markers.	130
Figure 33	Expression of T-bet and Eomes in PD-1 and CD39 expressing antigen experienced lymphocyte populations.	136

Figure 34	Differential expression of markers of exhaustion and effector molecules between T-bet^{High} Eomes^{Low} and T-bet^{Low} Eomes^{High} populations.....	139
Figure 35	Effector molecule expression by populations of interest from antigen experienced CD8+ lymphocytes.	141
Figure 36	Degranulation of CD8+ lymphocyte populations on stimulation by autologous tumour alone, anti-CD3/CD28 antibodies or PMA/Ionomycin.	144
Figure 37	Production of key cytokines and cytolytic granule products by CD8+ lymphocyte populations on stimulation by autologous tumour, anti-CD3/CD28 antibodies or PMA/Ionomycin.	146
Figure 38	CFSE assay examining proliferative capacity of OAC TIL populations of interest.	149
Figure 39	CD3, CD4 and CD8 positivity of OAC TILs.	152
Figure 40	Positivity for PD-1 and CD39 among CD3+ lymphocytes of either CD8+, CD4+ or CD8- CD4- subgroup.	154
Figure 41	CD103 and CD57 positivity in human OAC TILs.....	156
Figure 42	Similarities between tissue resident memory cell and classically exhausted lymphocyte populations of interest.	167

Research Thesis: Declaration of Authorship

Print name: Samuel Luke Hill

Title of thesis: CD8+ tissue resident memory T lymphocytes and disease control in human oesophageal adenocarcinoma

I declare that this thesis and the work presented in it are my own and has been generated by me as the result of my own original research.

I confirm that:

1. This work was done wholly or mainly while in candidature for a research degree at this University;
2. Where any part of this thesis has previously been submitted for a degree or any other qualification at this University or any other institution, this has been clearly stated;
3. Where I have consulted the published work of others, this is always clearly attributed;
4. Where I have quoted from the work of others, the source is always given. With the exception of such quotations, this thesis is entirely my own work;
5. I have acknowledged all main sources of help;
6. Where the thesis is based on work done by myself jointly with others, I have made clear exactly what was done by others and what I have contributed myself;
7. None of this work has been published before

Signature: Samuel Luke Hill..... Date: 28/06/2022

Acknowledgements

Sincere thanks to the patients who generously consented to donate tissue to this study at such a difficult time in their treatment journey. These tumour samples were essential for the completion of this project. In addition, the experiences of these patients when heard through my clinical practice provided the inspiration and motivation to persevere with this study.

Thank you to Prof Tim Elliott for his encouragement, guidance and kindness throughout my time working with his group, I appreciate the risk taken releasing a clinician into a research laboratory. Thanks too to Dr Gessa Sugiyarto for her excellent post-doctoral supervision, and all members of the Elliott/James Lab group and the wider community at the Centre for Cancer Immunology for their help and their time. Thank you to Prof Tim Underwood for his advice, support and investment in this project and to his extended laboratory group for their help. A particular thank you to Jack Harrington for sharing his time and his knowledge of RNA sequencing and to Ben Grace for his help in accessing patient samples.

I am indebted to Cancer Research UK and the Southampton Cancer Research UK Centre led by Prof Peter Johnson for their funding that made it possible for me to step out of clinical training to pursue a doctoral degree.

Finally, thank you to my family and close friends for their support throughout this project. Particularly, the most heartfelt gratitude goes to Lucy, Olivia and Emily for their patience, unwavering support, understanding and love, without which completing this project would not have been possible.

Definitions and Abbreviations

2B4	Natural Killer Receptor 2B4
APC.....	Antigen presenting cell
ATP	Adenosine triphosphate
BCG.....	Bacillus Calmette-Guérin
BE	Barrett's oesophagus
BFA	Brefeldin A
CAF	Cancer-associated fibroblasts
CCR.....	Chemokine receptor (β group)
CD.....	Cluster of differentiation
CFSE.....	Carboxyfluorescein succinimidyl ester
CT	Computerized tomography
CTL.....	Cytotoxic CD8 positive T lymphocyte
CTLA-4	Cytotoxic T lymphocyte associated antigen 4
CXCR.....	Chemokine receptor (α group)
DC.....	Dendritic Cell
DEG.....	Differentially expressed genes
DMSO	Dimethyl sulfoxide
DN	PD-1 CD39 double negative lymphocyte population
DP	PD-1 CD39 double positive lymphocyte population
eATP	extracellular adenosine triphosphate
EExh.....	Early exhausted group
EGF	Epidermal growth factor
Eomes	Eomesodermin
FACS	Fluorescence-activated cell sorting
FasL	Fas ligand
FDR.....	False discovery rate

Definitions and Abbreviations

FMO	Full minus one
FSC-A.....	Forward scatter-area
FSC-W.....	Forward scatter-width
GO	Gene ontology
GOJ.....	Gastro-oesophageal junction
GORD	Gastro-oesophageal reflux disease
GZM	Granzyme
HBV	Hepatitis B virus
HCC	Hepatocellular carcinoma
HCV	Hepatitis C virus
HD PBMC.....	Healthy donor peripheral blood mononuclear cell
HER-2	Human epidermal growth factor receptor 2
HGD.....	High grade dysplasia
HIV	Human immunodeficiency virus
ICB.....	Immune checkpoint blockade
IDO	Indoleamine 2,3-deoxygenase
IFN.....	Interferon
Ig	Immunoglobulin
IL	Interleukin
ITIM.....	immunoreceptor tyrosine-based inhibition motif
LAG3.....	Lymphocyte-activation gene 3
LCMV.....	Lymphocytic choriomeningitis virus
LExh.....	Late exhausted group
LGD	Low grade dysplasia
LRS	Leukocyte reduction system chamber
MHC.....	Major histocompatibility complex
MMRd	Deficiency of mismatch repair genes
MSigDM	The molecular signatures database

MSI-high	High microsatellite instability
NDBE	Non-dysplastic BE
NES	Normalised Enrichment Score
NHS	National Health Service
NICE	National Institute for Health and Care Excellence
NKT	Natural killer T cells
OAC	Oesophageal adenocarcinoma
PBMC.....	Peripheral Blood Mononuclear cell
PCA	Principle Component Analysis
PD-1.....	programmed death receptor 1
PD-L1	Programmed death-ligand 1
PExh.....	Precursor exhausted
PI3K	Phosphoinositide 3-kinases
pMHC	Peptide MHC complex
PRF1	Perforin
RCC	Renal cell carcinoma
Rlog	Regularized logarithm
SSC-A	Side scatter-area
TAM.....	Tumour associated macrophage
T-bet.....	T-box expressed in T cells
TCF-1	T-Cell factor 1
TCM.....	Central memory T cells
TCR	T cell receptor
TEFF.....	Effector T lymphocyte
TEM	Effector memory T cells
TExh.....	Terminally differentiated exhausted
TGF- β	Transforming growth factor β

Definitions and Abbreviations

TIGIT.....	T cell immunoreceptor with immunoglobulin and immunoreceptor tyrosine-base inhibitory motif [ITIM] domains
TIL	Tumour infiltrating lymphocyte
TIM3.....	T-cell immunoglobulin and mucin-domain containing-3 (Hepatitis A virus cellular receptor 2)
TMB.....	Tumour mutational burden
TNF	Tumour Necrosis Factor
TOX	Thymocyte selection-associated high mobility group box protein
TREG	FoxP3+ regulatory CD4+ T lymphocytes
TRM.....	Tissue resident memory cells (CD8+ T lymphocytes unless otherwise stated)
US FDA	United States Food and Drug Administration
VST	Variance stabilizing transformation

Chapter 1 Introduction

1.1 Cancer Immunotherapy

The appeal of harnessing the immune system in the fight against cancer has long been recognised, though until recently has been considered by many as not widely applicable (1). As early as the 1890s an immune response was implicated in tumour regression noted in some sarcoma patients purposefully injected with *Streptococcus pyogenes* cultures (2). While occasional examples of spontaneous tumour regression or prolonged dormancy were recorded, pointing to a form of host restraint, such responses were hard to replicate (3). With the development of surgical oncology techniques, the advent of radiotherapy and in the mid twentieth century chemotherapy, enthusiasm for an immune therapy faded. It was not until the 1960s that the first widely used immunotherapy was adopted with the use of intravesical Bacillus Calmette-Guérin (BCG) to treat superficial bladder tumours (4).

As the science of immunology developed towards the end of the 20th century, a viral aetiology for cancer was considered. As such, interest developed in the effectors of an antiviral response, such as antibodies and cytokines, and their potential role in targeting malignancy. Interleukin (IL)-2 and interferon (IFN)- α were shown to modulate tumours in vivo and large scale clinical trials were undertaken using these molecules as therapeutics during the 1980s with mixed results (5). IFN- α whose functions appeared to be numerous, including immunoregulatory, anti-proliferative and anti-angiogenic properties, showed a response rate of between 10 and 20% in patients with metastatic melanoma with some proving durable (6). Results such as this prompted the licensing of IFN- α for use as treatment for hairy cell leukaemia in 1986 and adjuvant treatment for resected stage IIB/III melanoma in 1995. IL-2, a cytokine stimulating lymphocytes, followed suit and was licensed for use in treatment of solid tumours including melanoma and renal cell carcinoma (RCC) (6,7).

The invention of hybridoma technology in 1975 allowed large quantities of specific immunoglobulin to be manufactured, overcoming previous difficulties (8). This allowed antibodies to be tested that targeted tumour antigens directly for the first time. Results were initially disappointing owing to short half-life and poor recruitment of human immune effector mechanism by these murine antibodies. The further refinement of this technology to allow incorporation of human constant regions resulted in greater successes. A treatment targeting the human cluster of differentiation (CD) 52 antigens on lymphoma cells by the Campath-1H antibody represented a landmark achievement (9). This was followed by the licencing of Rituximab in 1997.

Chapter 1

This chimeric monoclonal antibody targeting CD20 has several mechanisms of action including activating antibody-dependant cytotoxicity and complement dependent cytotoxicity as well as driving apoptosis (10). Initial concerns about the effects of depleting normal B cells appeared unfounded and it has so significantly improved outcomes in B cell lymphomas that it has been classified by the world health organisation as an essential medicine for all health economies (11).

This approach of directing humanised monoclonal antibodies against cancer antigens or other targets within the tumour microenvironment has proven successful. There are now a host of antibody treatments licensed for use in cancer medicine. They can be used either to directly evoke effector immune mechanisms, in a similar manner to rituximab (10), or they can inhibit specific stimulatory pathways. An example being the use of trastuzumab to block the epidermal growth factor (EGF) pathway in human epidermal growth factor receptor 2 (HER-2)-positive breast cancer (1).

More recently, antibody technology has proven essential in driving forward another form of immunotherapy, targeting inhibitory mechanisms on cytotoxic T lymphocytes to release their effector functions against tumours. These so called immune checkpoint inhibitors have demonstrated such pronounced and durable improvements in survival in patients with the highly immunogenic cancers such as metastatic malignant melanoma (12,13) that it has led the way to combination immunotherapy being considered a viable potential treatment for a wide range of cancers.

1.2 Cytotoxic T lymphocytes

1.2.1 Thymic development

Central to recent developments in cancer immunotherapy has been an increasing understanding of the adaptive immune response, and the role and function of the cytotoxic CD8 positive T lymphocyte (CTL). These cells through possession of highly variable T-cell receptors, recognise 8-9 amino acid peptides presented on major histocompatibility complex (MHC) class I molecules. They possess the ability to initiate killing of dysfunctional cells, identified through presentation of non-self peptides, and play a crucial role in anti-viral immunity, as well as clearing cells showing signs of malignant transformation (14,15).

T-lymphocytes arise from the common lymphoid progenitor stem cells located in the bone marrow, and migrate to mature within the thymus as early thymic progenitor cells (16). These thymocytes initially lack CD4 and CD8 expression and undertake recombination of the variable regions of their T cell receptor (TCR) genes (17). The TCR β gene undertakes rearrangement first,

accompanied by the TCR γ and TCR δ genes utilising a combination of the lymphoid-specific recombinase enzymes (RAG1 and RAG2) with ubiquitously expressed DNA repair proteins. RAG proteins create a double strand break in the recombination signal sequences that flank the TCR variable (V), diversity (D) and joining (J) regions, before being repaired using non-homologous end joining. This combination of one of a number of V, D, and J fragments, trimmed at potentially varied loci, and repaired using a mechanism with inherent scope for error results in the high levels of diversity among TCRs (18). Following recombination of the TCR β , γ and δ genes, the developing thymocytes commit to either an $\alpha\beta$ or $\gamma\delta$ lineage dependent on successful assembly of the $\gamma\delta$ TCR or the $\alpha\beta$ TCR using pre-T α gene. Successful recombination of one of these TCRs promote downregulation of recombinase expression and differentiation to a CD4+CD8+ phenotype. Those committed to the $\alpha\beta$ lineage then undertake recombination of the TCR α genes V and J regions, adding further diversity on dimerization (18). This process allows the formation of a vast repertoire of potential TCRs, allowing binding of a large array of peptide MHC complexes (pMHC) at varying affinities.

The double positive progenitor T cells undertake a period of maturation within the thymus allowing their newly recombined $\alpha\beta$ TCR or $\gamma\delta$ TCR to engage with the diverse pMHC complexes presented within the thymic cortex. These cortical thymic epithelial cells express the autoimmune regulator (AIRE) gene, a transcriptional regulator allowing expression of an array of tissue specific proteins to ensure developing thymocytes are exposed to a broad range of self antigens (19).

The affinity of these interactions between the TCR and the varied pMHC molecules on display govern the survival of these progenitor T cells. Thymocytes lacking any stimulation via the TCR die by neglect, while negative selection deletes those with high affinity binding for pMHC. This leaves a population of T cells completing positive selection, with a low affinity for self pMHC, that can go on to leave the thymus.

By completion of this process the majority of immature thymocytes will have been deleted by apoptosis. Those remaining will be restricted to either detection of MHC class I or class II molecules when bound to peptides and will remain positive for either CD8 or CD4 respectively. The survivors should have displayed too low an affinity for self peptides to result in autoimmunity but retain the potential to recognise MHC molecules presenting non-self peptides, be they from viral origin or due to malignant transformation (19).

1.2.2 Activation and function

Naïve CD8 + T lymphocytes on leaving the thymus circulate through the secondary lymphoid organs, awaiting activation through recognition of antigen. This priming requires recognition of a

Chapter 1

target pMHC complex, stimulating the T cell receptor, this is typically from presentation of pathogenic material to naïve CD8 + lymphocytes by a professional antigen presenting cell (APC) such as a dendritic cell (20). APCs also provide the second signal required for activation, engagement of CD28 molecules on the T cell, with its target ligands CD80 or CD86 (B7-1 or B7-2 respectively). Achieving maximal expansion requires integration of multiple signals, alongside TCR and costimulatory pathways, including the pro-inflammatory cytokines such as IL-2 and type I interferon. Members of the tumour necrosis factor (TNF) receptor family such as 4-1BB, OX-40 and CD27 among others may also provide additional co-stimulatory signals (16,20).

On activation, naïve CD8 + T lymphocytes will undergo a period of clonal expansion with the assistance of IL-2 produced by activated CD4+ T lymphocytes. This is rapid and can continue for a period of up to 1 week following initial viral infection, and results in cell division every 4-6 hours. This can lead to a 500,000 fold expansion in the number of activated effector CTLs, with accompanied changes in migration behaviour, gene expression and function, governed by the unique mix stimulatory signals they receive (15).

Upon activation in the lymphoid organs, activated CD8+ T lymphocytes will upregulate expression of the inflammatory cytokine receptor CXCR3, allowing their entry to peripheral tissues and sites of primary infection (15,20). These terminally differentiated effector cells can infiltrate a site of inflammation and initiate killing of target cells expressing their cognate peptide antigen. The two principle methods of target cell killing undertaken by activated CD8+ lymphocytes are through the granule exocytosis pathway and expression and release of death ligands such as Fas ligand (FasL) or the TNF-related apoptosis inducing ligand (TRAIL) (15,16,21).

Activation of the granule exocytosis pathway leads to rapid directional release of pre-formed cytoplasmic granules towards the contact site with the target cell, the immunological synapse. These granules principally contain the pore forming protein perforin (PRF1) and granule-associated enzymes (granzymes; GZM), a family of serine proteases. GZMA and GZMB have been most studied but there are 5 human granzymes as well as other granule associated proteins. Once inside the target cell GZMB activates the classical caspase dependent apoptotic pathway while GZMA activates a caspase independent apoptotic pathway(16,21). The characteristics of the granules and death ligands released into the immunological synapse appear to differ dependent on the circumstance such as in the context of viral infection or type of malignancy as well as under the influence of mediators of the immune response such as checkpoint inhibitors (21).

Activated CTLs engaging antigen will also release interferon- γ (IFN- γ) and tumour necrosis factor- α (TNF- α) modulating the effects of other inflammatory cells such as macrophages and dendritic cells, influencing the wider immune microenvironment.

1.2.3 Lymphocytes in the tumour microenvironment

For a developing cancer to be controlled and eliminated, the host immune system must recognise the threat, produce an effective response, and overcome inhibitory or regulatory signals coming from the tumour microenvironment. As described by Chen and Mellman's cancer immunity cycle, neoantigens created by oncogenesis and genome mutation, must be released and captured by antigen presenting cells. CTLs must be activated in the lymphatic organs as described above and migrate to the local tumour microenvironment before undertaking killing of target malignant cells, leading to release of more potentially immunogenic neoantigens and a continued cycling towards effective cancer elimination (22). An occult cancer, by its existence, has overcome, interrupted or benefited from a deficiency in this process.

The cancer immunity cycle can be interrupted in a multitude of ways. Tumour antigens can remain undetected, Dendritic Cells (DC) and CTLs can treat tumour antigens as self rather than pathological resulting in immune tolerance and a regulatory T cell response, failure of homing or infiltration of immune cells into tumours, or through the development of a suppressive tumour microenvironment (22).

The immune suppressive tumour microenvironment is complex and possesses different characteristics in individual tumours. Examples of such inhibitory mechanisms include tumour derived soluble molecules, such as transforming growth factor β (TGF- β) and Interleukin 10 (IL-10), which lead to a more tolerogenic immune state. Likewise, IFN- γ production can drive expression of co-inhibitory molecules programmed death receptor 1 (PD-1) on CTLs and its ligand PD-L1 on tumour cells and dendritic cells. Hypoxia and lactic acidosis, common conditions within a tumour, can also influence immune cell characteristics resulting in more T regulatory response and release of immunosuppressive molecules from DCs such as indoleamine 2,3-deoxygenase (IDO) and prostaglandin E2 (23). Another soluble factor known to promote an anti- rather than pro-inflammatory environment within tumours is adenosine. The conversion of extracellular adenosine triphosphate (ATP) to adenosine by cell surface proteins including CD39 and CD73 occurs following stimulation by immune inhibitory transforming growth factor- β (TGF β). CD39 is highly expressed on regulator T lymphocytes (T_{reg}) but also on activated CD8+ T lymphocytes as well as B lymphocytes and macrophages (24).

Tumour control by cytotoxic CD8+ T lymphocytes requires contact between the cancer cells and the immune cells. It has been shown in multiple tumour types, including colorectal cancer, ovarian cancer and oesophageal adenocarcinoma, that long-term survival is correlated with the

Chapter 1

presence and number of tumour infiltrating lymphocytes (TILs) (25–27). CTL exclusion can occur as a result post translational modification of chemokines by the tumour microenvironment, a vasculature that is hostile to lymphocytes by expression of death signals such as Fas-L, and through the direct effects of stromal cells such as cancer-associated fibroblasts (CAFS) among other mechanisms (25).

The influence of a suppressive microenvironment can inhibit tumour specific activated cytotoxic CD8 positive T lymphocytes from expanding, migrating to their site of interest, and undertaking effective killing of cancer cells(28,29). In addition to these extrinsic factors limiting lymphocyte dependent tumour killing, factors intrinsic to lymphocytes can have a bearing on their ability to control tumour growth. This includes the composition of subsets of CTLs of varying phenotypes in the CD8+ lymphocyte compartment, their ability to undertake effector functions, and the impact of phenomena such as lymphocyte exhaustion, anergy and senescence among this highly heterogeneous cell type(29).

1.3 Lymphocyte dysfunction

1.3.1 T cell exhaustion

T cell exhaustion is a state of dysfunction observed in chronic infections and cancer, and is characterised by a loss of effector functions. In the case of the cytotoxic CD8+ T lymphocytes this includes a stepwise loss of proliferative capacity, up-regulation of cell surface inhibitory receptors, loss of interferon and granzyme production, and ultimately complete loss of functional ability and apoptosis as affected cells progress towards a terminally exhausted phenotype. This dysfunction is linked to persistent antigen exposure, occurs in T cells that have acquired effector function, and is distinct from other types of dysfunction, such as anergy where cells fail to acquire effector functions because of insufficient co-stimulatory priming, or T memory cells where reactivation can happen rapidly after re-exposure to antigen (30).

The concept of exhaustion was described simultaneously in two contexts during the late 1990s. Firstly, within a murine viral infection model where the chronic variant of the infection and persistent antigen exposure resulted in loss of functional effector CD8+ T lymphocytes when compared to the response observed from acute infection (31,32). Secondly, in the observation that patients infected with the human immunodeficiency virus (HIV) develop persistent infection and that this was linked to a loss of functional CD8+ T cells specific for viral targets, after an initial response (33). The similarities observed in loss of effective CTL response in the context of an experimental murine model and a clinical scenario, alongside a greater understanding of the

heterogeneity of lymphocyte populations and techniques to investigate them, resulted in the development of this hypothesis and an understanding of its importance in multiple disease states.

While initial hypotheses were based on a single population of exhausted lymphocytes which gradually progress to loose function as a result of consistent antigen exposure, more recent insights through single cell RNA sequencing, special analysis of individual clusters, and differential responses to immune checkpoint blockade (ICB) therapy, have led to a more complex model being accepted. It is now considered that a stem-like CD8⁺ T cell exhausted population, which is responsive to ICB therapy, may reside in a peripheral rather than intratumoural position, and gives rise to a terminally differentially exhausted population. This terminally differentiated exhausted population possess diminishing anti-tumour effects, are found in the tumour microenvironment, and are refractory to immunotherapy (29,34).

1.3.2 LCMV model

A state of T cell exhaustion was first described within antigen specific CD8 lymphocytes following persistent stimulation in a mouse model of chronic viral infection. It was noted that in mice with persistent infection with the lymphocytic choriomeningitis virus (LCMV) a population of CD8 positive T lymphocytes specific for a viral epitope persisted. This population showed the presence of activation markers, CD69 and CD44, but were unable to perform any antiviral effector functions (32,35).

It was observed that different strains of the LCMV can result in either acute infection with clearance of the disease, or chronic infection. The Armstrong strain of LCMV is reproducibly cleared by day 8 of infection, whereas the LCMV Clone-13 (Cl-13) strain results in persistent infection with ongoing viraemia at 3 months and virus persisting in some tissues indefinitely. This difference is noted despite significant homogeneity between the viruses. There are just two base pair differences and one amino acid change between the strains, preserving all known T-cell epitopes (32,35–37), a feature that allowed direct comparison between the CD8 T cell response in acute and chronic infection.

Taking advantage of this model, a predictable stepwise loss of effector functions, as CD8 T cells progressed towards exhaustion in chronic infection, was demonstrated. Lymphocyte effector profiles were comparable at an early stage of infection with the Armstrong and Cl-13 strains, until day 5 post infection. From this point on the lymphocytes of the Cl-13 infected mice progressively lost their in-vitro lytic capacity. This loss was accompanied by an early loss of IL-2 production as well as a reduction in the level of IFN- γ production and developing loss of TNF- α production with 10% of cells unable to secrete the cytokine. With time, complete loss of TNF- α was observed and

Chapter 1

finally loss of IFN- γ as well (37). Ultimately, with persisting infection these lymphocytes appear to be deleted as they reach the terminal phase of exhaustion, demonstrated by the loss of CD8+ lymphocyte clones reactive to known dominant antigens as shown by loss of staining with MHC-peptide tetramers (37).

Similarly, the expression of inhibitory receptors was identified as a hallmark of lymphocyte exhaustion. Principle among them is PD-1. Expressed on T-cells following TCR engagement and activation where its physiological function is in limiting immunopathology and maintaining tolerance to self-antigens. While PD-1 expression quickly declines in resolving infection, with persistent antigen exposure PD-1 is sustained and levels of expression rise (38,39).

On engagement with its ligands PD-L1 or PD-L2, PD-1 suppresses T cell function through multiple mechanisms, including antagonising TCR function through recruitment of phosphatases such as SHP2 repressing expression of T cell effector genes (40).

In addition to PD-1, on progression towards terminal exhaustion, numerous other inhibitory receptors are over-expressed by lymphocytes experiencing persistent antigen exposure. This includes T cell immunoglobulin and mucin domain 3 protein (TIM3), Lymphocyte-activation gene 3 (LAG3), Cytotoxic T lymphocyte antigen-4 (CTLA-4), and T cell immunoglobulin and ITIM domain (TIGIT), among others (41). Co-expression of these receptors, especially in combination with PD-1, indicates a greater degree of exhaustion and effector dysfunction (39,42).

Viral load was shown to correlate with loss of CTL functionality. Higher virus levels in the LCMV model of chronic infection showed a strong association with exhaustion. This was progressive, in the manner described above, with loss of IFN- γ more marked at day 30 compared to day 15 despite stable viraemia over time (37).

Not all T-cell populations were affected equally during chronic LCMV infections. Viral epitopes presented at high frequency or persistently during CI-13 infection such as NP396 and GP34 appeared to drive clonal deletion. In contrast those epitopes with lesser stimulatory capacity, such as GP33 and GP276 resulted in a persistent but functionally exhaustion phenotype among CD8 T-cells (37).

Of note CD4 T-cells show an exhausted and dysfunctional phenotype in chronic infection, though this remains less clearly characterised.

Building on this early work the LCMV model has proven a valuable tool for further dissecting the process of T cell exhaustion and allowing development of an understanding of this process in human disease. Understanding the transcriptional profile of T cell exhaustion in the mouse model

has allowed insight into the variety of intrinsic and extrinsic factors resulting in dysfunction (41) and the complex interplay between them which can lead to a different molecular and clinical picture dependant on context (43,44). Such insights have also led to understanding of the developmental origins and transcription factor controls of exhausted lymphocytes as depicted in figure 1.

1.3.3 Lymphocyte exhaustion in human infection

As outlined above, alongside the characterisation of exhausted CD8 T lymphocytes in the mouse model, similar phenomena were observed in human disease. As research accelerated into HIV infection, an inverse relationship between viral load and functionality of effector CD8 T cell response was identified (33). In fact effector functions in viral antigen specific CD8 T-cells were lost in a stepwise fashion, similar to those seen in the mouse model, with IL-2 production lost early and IFN- γ again the more persistent (45).

Additionally the level of PD-1 expression on HIV-1 specific CD8+ CTLs was shown to be correlated with increased viral load and reduction in CD4+ count as well as being associated with early progression to AIDS (46). And it is not just PD-1 whose expression appears to predict progression to an exhausted CD8 CTL state, but also other cell surface exhaustion markers too. LAG3 appears to have an association, while TIM3 shows less correlation. The ability of expression of these cell surface markers to identify non-progressors compared to early-progressors of HIV infection as well as the functional capacity of CTLs demonstrates commonly shared features of lymphocyte exhaustion, while the variation in the nature of this dysfunction from LCMV infection are an example of the context specific nature of this process (45,47).

Aside from HIV infection, lymphocyte exhaustion has been shown to be relevant in responses to other chronic infections including Hepatitis C virus (HCV) and Hepatitis B virus (HBV) infections. HCV is a highly transmissible blood borne RNA virus which after an initial, often asymptomatic, acute infection is cleared in fewer than half of patients. The remainder will develop a chronic infection, leading to liver fibrosis and cirrhosis in many, with between 1-7% of these going on to develop hepatocellular carcinoma (HCC) every year (48,49). Viral elimination relies upon strong and sustained CD8+ and CD4+ T lymphocyte responses, though this is significantly impaired once chronic infection develops. There is a strong body of evidence that the dysfunction in CD8+ CTLs is due to progressive exhaustion in this compartment, with increased PD-1 expression, marked reduction in cytolytic capacity and IFN- γ production. This was somewhat reversible with PD-1 blockade and culture in cytokine rich environments, though not fully. Other hallmarks of exhaustion have also been observed, such as reduced granzyme A production, impaired TNF- α

Chapter 1

secretion and lower proliferation (49). The transcriptional control of the exhaustion processes in HCV is directly analogous to that seen in LCMV with the transcription factors TOX and TCF1 identified as central mediators (50).

A significant role for lymphocyte exhaustion in HBV infection has also been identified, with recovery of cytolytic capacity by HBV specific exhausted CTLs with anti-PD-1 therapy observed(51). Additionally, in non-viral chronic infections, exhaustion is shown to be relevant in the inability to clear Mycobacterium tuberculosis infection, despite evidence of an effective initial T-cell immune response (52).

Since the emergence of the novel severe acute respiratory syndrome coronavirus 2 (SARS-CoV2) and its associated clinical manifestation of Coronavirus disease 2019 (COVID-19) in December 2019, this has dominated research agendas in particular viral immunology science. Though principally an acute viral infection, from which most will fully recover, CD8+ CTLs specific to SARS-CoV2 bearing transcriptional profiles and multiple cell surface exhaustion markers in keeping with exhaustion have been identified, mostly in patients with severe COVID-19. These findings are not uniformly replicated and the importance of lymphocyte exhaustion to the immune response in this context is disputed (53). This however, does demonstrate the far reaching impact of the translational changes observed in lymphocyte exhaustion in responses to human viral disease.

1.3.4 Exploiting lymphocyte exhaustion and dysfunction in human cancer

Following the identification of exhaustion in murine models and human viral infections, the importance of this phenomenon in the ineffectual immune response to malignancy quickly became apparent. In common with chronic viral infection, malignancy produces a state where by persistent antigen can be presented to CD8+ CTLs as a result of progressive cancer. This similarity and the presence of dysfunctional tumour infiltrating CD8+ lymphocytes expressing high levels of PD-1 was observed early, and an appreciation made that exhausted TILs represented a potential pool of tumour reactive CTLs that could be recruited and reactivated to treat cancer (54,55).

Gene expression profiles of tumour infiltrating CTLs from both human and murine tumours when compared to those from chronic viral infections demonstrated exhausted lymphocytes present in both contexts (56). Upregulation of inhibitory surface receptors is noted as a core feature of lymphocyte exhaustion, and this too has been observed in tumour infiltrated CTLs. Their co-expression is again associated with an increasingly dysfunctional phenotype and they are strongly co-expressed with PD-1 (44,57).

As in a chronic viral infection setting, a progressive loss of effector functions, including IFN- γ , TNF- α and IL-2, is observed in dysfunctional CD8+ TILs, and this has been observed across tumour types including, but not exclusively in melanoma, lung cancer and gastric cancer (56–58). Of interest too, is that the pattern of inhibitory receptors and the order in which loss of effector functions develop appears context specific, not only different between infection and cancer, but also between tumour types (59). The shared features suggests a common mechanism with dysfunction in chronic viral infection, but it is not surprising that the nature of the dysfunctional state diverges from this given the tumour microenvironment will only partially correlate with a chronically infected site.

As is often true, while the molecular underpinning of lymphocyte exhaustion was being uncovered, with PD-1 identified as an important player in this process, quick progress was made to inhibit its function in pre-clinical models and then in humans (38,54). PD-1 inhibition demonstrated promising early responses in a meaningful proportion of patients with metastatic melanoma, a highly aggressive skin cancer, known to possess high levels of DNA mutations due to ultraviolet light exposure and to possess an immune rich microenvironment. Previously largely refractory to treatment with chemotherapy in the metastatic setting, encouraging response rates heralded the start of the checkpoint blockade era. Response rates with single agent anti-PD-1 therapy, Nivolumab, showed a response rate in an expanded phase I trial of patients with advanced disease of 28% in melanoma, 27% in renal cell carcinoma and 18% in non-small cell lung cancer (60). Such response rates, including a number of complete radiological responses defined by an inability to measure the cancer on computerized tomography (CT) scan after treatment, were hugely encouraging. Even more so was the emergence of the so called 'tail' among patients responding. This meant that a large proportion of those responding to treatment continued to long term, even after completion of the therapy, without progressive disease, death or need for further treatment, creating the picture of a tail on Kaplan-Meier survival curves.

Alongside the development of anti-PD-1 therapies, similar monoclonal antibody antagonist targeting the cytotoxic T lymphocyte associated antigen 4 (CTLA-4) were being developed, and in fact won the race for publication of impressive evidence of clinical responses and drug licensing (61). CTLA-4 is upregulated at the cell surface after T lymphocyte activation, and acts to inhibit lymphocyte activity through a number of mechanisms, including out-competing CD28 for its target ligand B7 as well as inducing T cell arrest. Pre-clinical investigations into mouse models showed CTLA-4 inhibition could lead to impressive tumour rejection in mice prompting investigation in human disease (62,63). Two humanised anti-CTLA-4 monoclonal antibodies entered clinical trials, and while survival benefit was disappointing for tremelimumab, potentially for multiple reasons of trial design, ipilimumab showed a significant improvement in response

Chapter 1

rate and overall survival when given to patients with advanced melanoma. Two important outcomes of these trials were firstly that again while response rates were modest at around 20%, a large proportion of these experienced long term disease control, and secondly, immune mediated toxicity of such drugs could be severe and required a new way of considering anti-cancer drug side effects (61,64,65).

The early phase trials in inhibitory antibody drugs targeting PD-1 and CTLA-4 in melanoma were such a success that these therapies have quickly moved on to become standard of care treatments for patients with metastatic melanoma (66,67). Subsequently this quickly resulted in evaluation of combination treatment consisting of both strategies, resulting in even greater response rates and prolonged survival at over 50% at 5 years. This spurred the trial of immune checkpoint blockade in a host of other malignancies (12).

While the model of lymphocyte exhaustion as defined in LCMV and observed in human viral infections and cancer, was taking hold and developing, the therapeutic implications of exploiting the themes uncovered raced past the knowledge base. The development of cohorts of patients, with varying clinical features, cancer types and response rates treated with immune checkpoint inhibitors subsequently produced an array of models for uncovering the details of lymphocyte dysfunction in human cancers.

Early investigations into anti-PD-1 therapies demonstrated a reinvigoration of the PD-1+ exhausted T cell pool rather than recruitment from a PD-1- naïve T cell source, leading to the hypothesis of such treatments reversing progression along a linear pathway to exhaustion(38). This linear progression model made intuitive sense given exhausted lymphocytes shared a developmental relationship with differentiated effector lymphocytes but were driven to their phenotype by persistent TCR activation. However, as exploration of the response to anti-PD-1 immunotherapy progressed, it became apparent that such treatment did not result in recruitment of less exhausted PD-1^{low} CTLs from a PD-1^{high} terminally exhausted population, but rather that responses arose from recruitment and proliferation of a less exhausted precursor population (68).

Recent work has attempted to combine the evolving knowledge of the development of lymphocyte dysfunction in cancer with clinical responses to immune checkpoint blockade and high dimensional analysis techniques such as single cell RNA sequencing and cytometry by time of flight (CyTOF). Such work has allowed characterisation of distinct gene signatures that can potentially predict response to treatment and have helped to develop the non-linear model of lymphocyte exhaustion, based upon distinct populations (69–72).

The use of the anthropomorphised term exhaustion was initially appropriate, but increased appreciation of the complexity of these processes and the identification of distinct sub-populations of exhausted lymphocytes, has rendering this terminology confusing.

The existence of two key populations of exhausted lymphocytes has now been broadly agreed upon, though how to label them remains open for debate. A population of precursor exhausted or stem cell-like lymphocytes which demonstrate a stem-like capacity, likely derived from antigen specific effector cells that have gained the capacity to be long lived has now been confirmed. This stem-like population can give rise to terminally differentiated exhausted lymphocytes, which display the progressive dysfunction outlined as characteristic in early exhaustion studies.

For the sake of clarity, these populations will be labelled precursor exhausted (PExh), and terminally differentiated exhausted (TExh) lymphocytes respectively, in this report. The term exhaustion will be reserved for discussing the phenomenon broadly, rather than referring to a specific lymphocyte population.

1.3.5 Precursor exhausted lymphocytes

As stated above, initial hypotheses suggesting exhausted lymphocytes derived from terminally differentiated T lymphocytes have now been replaced by a consensus that a heterogeneous population of exhausted lymphocytes arise early in an infection or cancer formation from effector cells and in the presence of high levels of antigen survive the contraction phase of the immune response and are long lived (34). During initial development these cells arise from the same pool of KLRG1^{low} effector cells that give rise to T memory cells following acute infection. It was also noted that senescent KLRG1⁺ effector cells could not give rise to exhausted cells suggesting a distinct population from senescence (73).

A key property of memory T cells is their ability to persist in the absence of stimulatory antigen via the effects of IL-7 and IL-15. On re-exposure to antigen this population of memory cells can subsequently be re-energised and undergo cell division and clonal expansion, as well as activate effector functions. The precursor exhausted phenotype however is not maintained by IL-7 and IL-15 and cannot be maintained in the absence of stimulatory antigen (74,75), suggesting an alternative origin through early differentiation from activated T effector cells. Despite this there is a close association observed with memory T cells particularly with sharing of crucial transcription factor, T-Cell factor 1 (TCF1), and common transcriptional profiles with effector memory T cells (T_{EM}) (Figure 1).

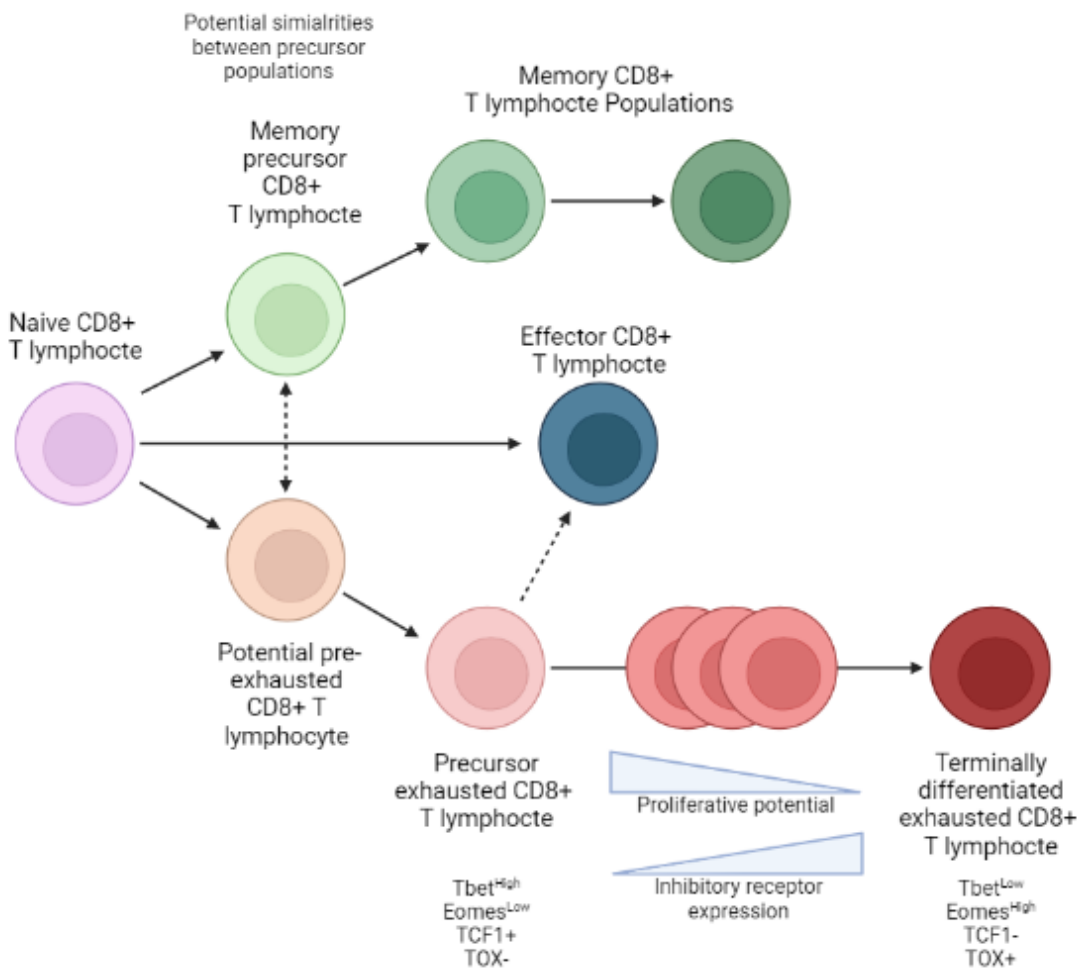


Figure 1 Potential developmental relationship between exhausted, effector and memory CD8+ T lymphocytes.

Dominant hypothesis for developmental pathway of exhausted CD8+ T lymphocytes within the context of chronic LCMV infection. High level of similarities between pre-exhausted and memory precursor lymphocytes. Progressive antigen exposure drives precursor exhausted to terminally differentiated exhausted CD8+ T lymphocytes resulting in reduced proliferative potential and increased inhibitory receptor expression. Classical transcription factor profile displayed for both precursor and terminally differentiated exhausted phenotypes. Adapted from Blank et al 2019 (76). Created with BioRender.com.

An essential component of the exhausted lymphocyte pool is a precursor exhausted lymphocyte population commonly defined as PD-1^{High} TIM3^{Low}TCF1+. This population possess characteristics of both stem cells and memory cells, such as self renewal and an ability for rapid expansion. TCF1, also commonly known as Transcription Factor 7 (TCF7), encoded by the *TCF7* gene, is a transcription factor essential in differentiation and persistence of memory CD8 T cells, and was found to be a main component signature in melanomas responding to anti-PD-1 immune

checkpoint blockade (69). Subsequently this population has been shown to be the source of tumour specific terminally differentiated exhausted lymphocytes, produced from this pool in response to PD-1 blockade and responsible for tumour regression, both in animal transfection models and in human cancers (69,77,78).

While precursor exhausted lymphocytes express PD-1, this is typically at a lower level than among the terminally differentiated exhausted lymphocyte population. In addition, they typically do not express other surface markers associated with exhaustion and are commonly defined as having negative or low expression levels of the TIM3 and low levels of LAG3 and TIGIT, which are all commonly upregulated in terminally differentiated exhausted lymphocytes. For this reason this precursor exhausted population is often described as PD-1^{low} TIM3⁻, PD-1^{low} or PD-1^{low}/TCF1^{high} (29,79)(Figure 1).

With regard to CD8+ T lymphocyte effector molecules, precursor exhausted lymphocytes maintain an ability to secrete IFN- γ , IL-2 and granzyme B, the production of which is inhibited with progression towards a terminally differentiated exhausted phenotype (80). Reinvigoration of the precursor exhausted population by PD-1 blockade will also result in release of terminally differentiated exhausted lymphocyte population that can themselves transiently produce effector molecules.

1.3.6 Terminally differentiated exhausted lymphocytes

The second key population of exhausted lymphocytes is the terminally differentiated exhausted lymphocyte population. This group contains lymphocytes in a range of states of progressive dysfunction, from their development from precursor exhausted lymphocytes, through functional effector-exhausted states to a terminally exhausted hypo-functional state. It has been demonstrated through single cell RNA sequencing studies and mass cytometry studies that this group, often characterised as PD-1^{High} TIM3⁺ TCF1⁻, can maintain a range of effector functions, particularly in the context of cancer (44). This group is important in maintaining an anti-tumour immune response, and are the cell population responsible for tumour killing secondary to immune checkpoint blockade after being released from the precursor exhausted population following treatment with anti-PD-1 immunotherapies (78,80).

In addition to TCF1 negativity, thymocyte selection-associated high mobility group box protein (TOX) expression is maintained in these terminally differentiated exhausted lymphocytes and is responsible for persistent PD-1 expression. TOX also plays a role in the upregulation of other surface markers of exhaustion such as TIM3, LAG3, TIGIT and the Natural Killer Receptor 2B4 (2B4/CD244). TOX expression is also essential to ensure survival of this cell population. T-bet

Chapter 1

expression levels fall with progression towards terminal exhaustion, and an accompanied rise in the transcription factor Eomesodermin (Eomes) observed in chronic viral infections, though this is equivocal in tumour models(81). Eomes expression plays an important role in enhancing the proliferation of memory CD8+ lymphocytes, has been regularly identified through transcriptomic analysis to be upregulated in the terminally exhausted lymphocyte phenotype(82). Eomes expression appears to be under the control of TOX, whereas Eomes co-expression with TCF1 is not observed (82,83)(Figure 1).

As already eluded to, as terminally differentiated exhausted lymphocytes progress along their path towards a hypofunctional, terminally exhausted state, increasing expression levels of surface markers of exhaustion are observed. TIM3, LAG3, TIGIT and 2B4 have already been mentioned, and a range of other surface proteins are observed as associated with this state, including the activation marker CD38, CTLA-4 and CD160. The precise repertoire of surface markers expressed as terminally differentiated exhausted lymphocytes move along this pathway varies between chronic infection and cancer models, as well as between tumour types, with the differences driven by the specific tumour microenvironment and the co-stimulatory signals received during development (42,44,57).

1.3.6.1 Transcription factor control of precursor exhausted and terminally differentiated exhausted lymphocytes. – TCF1 and T-bet

TCF1 plays a number of roles in lymphocyte biology, including a role in the commitment and development of thymic progenitors into double negative thymocytes, as well as in the development and maintenance of central memory T cells (T_{CM}) during and immediately after an acute infection. TCF1 is essential in the establishment and persistence of the precursory exhausted population that are PD-1+, on persistent antigen stimulation and is responsible for their stem-like, self-renewing properties (78,80,84,85). It has been mentioned that initial evidence suggested a development of precursor exhausted lymphocytes from a terminally differentiated effector T cell origin, however the importance of TCF1 as well as other transcription factors important in memory cell differentiation such as Id3 and shared transcriptional profiles has led to a consideration of greater crossover with the memory compartment than initially considered, as depicted in figure 1(80,86).

In addition to positivity for TCF1, the precursor exhausted population has been shown to possess high expression levels of other transcription factors. The T-box transcription factor, T-bet expressed in T cells (T-bet), encoded by *TBX21* gene, is known to play a role in differentiation of lymphocytes and sustain activity of short lived effector cells in acute infection. Within the precursor exhausted population, it acts to maintain survival by repressing expression of PD-1 and

other inhibitory receptors and suppressing the progression to a terminally differentiated exhausted phenotype(71,87). T-bet was much discussed in the early exhaustion literature with regards to its reciprocal relationship with its sister T-box transcription factor Eomesodermin (Eomes). Eomes regulates protein expression needed for memory cell development following acute infection and is responsible for terminally differentiated exhausted lymphocyte development, regulating among other processes, surface inhibitory receptor translation (88). The reciprocal expression pattern of these two T-box transcription factors is well established in chronic infections, in tumour models however there is evidence of reduced T-bet and Eomes expression in TILs as tumours progress. Another example of the difference between the canonical LCMV exhaustion model and the lymphocyte dysfunction experienced in cancer (81).

Additionally the thymocyte selection-associated high mobility group box protein (TOX) has been increasingly identified as a key player in promoting the persistence of precursor exhausted lymphocytes. Expression is elevated in these cells, and is maintained into terminally differentiated exhausted lymphocytes where it is essential to their maintenance and avoiding apoptosis (89,90). Its expression is also necessary for expression of multiple surface markers of exhaustion with PD-1, CD39, TIM3, 2B4 and TIGIT all under expressed in exhausted lymphocytes from chronic LCMV infection on deletion of the TOX gene (89). TOX, expression is induced by high antigen stimulation of the TCR and plays a crucial role in epigenetic remodelling that differentiates this population from memory cell populations, with TOX and TCF1 co-expression differentiating progenitor exhausted lymphocytes from progenitor memory lymphocytes, despite TOX also playing a role in effector memory T cell (T_{EM}) development (85,90).

1.3.7 Cell surface markers of exhaustion and dysfunction

1.3.7.1 PD-1 and its ligands

The programmed cell death receptor 1, known as PD-1 or CD279, has been mentioned extensively with regards to its significance in lymphocyte exhaustion, though without detailed description of its function, control or ligands. A cell surface receptor, PD-1 is a member of the CD28/CTLA-4 family of T cell regulators and consists of an immunoglobulin (Ig) superfamily domain, linked to a transmembrane domain and an intracellular tail. Its intracellular tail contains an immunoreceptor tyrosine-based inhibition motif (ITIM) and an immunoreceptor tyrosine-based switch motif (ITSM), which are phosphorylated on binding to its ligand. First described in 1992 as a gene upregulated in T cell hybridoma cells undergoing programmed cell death, PD-1 knock out mice

Chapter 1

developed profound autoimmunity suggesting an important role in tolerance and immune regulation (91–93).

PD-1 is encoded by the *Pdcd1* gene on chromosome 2 in humans and expressed on T cells, B cells and natural killer T (NKT) cells, as well as being found on activated monocytes and DCs. PD-1 is not expressed on resting T cells but is induced after activation, with effects of its ligation evident within a few hours of TCR stimulation, though this is not always correlated with the degree of expression (93).

In addition to PD-1 expression associated with CTL activation, as discussed above it is a key marker of exhaustion with PD-1 positivity a marker of precursor exhausted lymphocyte populations and high levels of PD-1 positivity associated with a terminally differentiated exhausted population. The presence of high PD-1 expression alone can identify a functionally distinct population of TILs with high levels of tumour antigen engagement and recognition (94).

Engagement of PD-1 with its ligands allows for recruitment of protein tyrosine phosphatases (PTPs), including SHP-2 as well as SHP-1, which allows for downregulation of TCR co-stimulation through de-phosphorylation of key signalling elements including CD3 ζ , ZAP70, PKC θ and PI3K. Additional inhibitory activity can be mediated through reduced AKT activity mediated by loss of PI3K, as well as potential activity through the inhibition of the RAS-MEK-ERK signalling pathway, and reduction in cell cycling proteins, among other mechanisms (reviewed in 91,93).

The ligands for PD-1 are the programmed death-ligand 1 (PD-L1) also termed B7-H1 or CD274, and programmed death-ligand 2 (PD-L2), also called B7-DC or CD273. These transmembrane cell surface proteins are members of the B7 protein family. Expression of both ligands is stimulated by IFN- γ , though type 1 interferons can also upregulate their expression, and GM-CSF and IL-4 also associated with PD-L2 expression. PD-L1 is principally expressed on tumour cells, antigen presenting cells, T lymphocytes, endothelial cells and fibroblasts, whereas PD-L2 is mostly found on dendritic cells, B cells, macrophages and monocytes (93,96).

Inhibiting the PD-1/PD-L1 axis has been discussed in terms of blocking PD-1 with drugs such as nivolumab or pembrolizumab, but there has been advances in inhibiting PD-L1. A handful of anti-PD-L1 inhibitors are in routine clinical use currently and demonstrating strong efficacy in a range of tumours. This includes Atezolizumab, Avelumab and Durvulumab, which between them have been licensed for use in non-small cell and small cell lung cancer, triple negative breast cancer, urothelial, renal cell, merkel cell and hepatocellular carcinomas.

In efforts to improve the efficacy of immune checkpoint blockade therapies and select patients who are most likely to respond, measuring levels of PD-L1 expression, as defined by a variety of

metrics, though all immunohistochemistry based, have been incorporated into trial designs. PD-1/PD-L1 inhibitors are now licensed for use in a number of contexts if PD-L1 expression reaches a pre-defined level, this including oesophageal cancer(97). While immunohistochemistry is utilised in clinical practice for such assessments, there is evidence for equivalent results being obtained from flow cytometry based techniques, allowing quantification of PD-L1 expression on specific cell types such as immune cells or cancer cells (98).

1.3.7.2 CTLA-4

The cytotoxic T-lymphocyte-associated protein 4 (CTLA-4), CD152, is another inhibitory member of the CD28 family. First identified in 1991 as an alternative receptor for the B7 ligands, it was observed that CTLA-4 knock out mice developed a profound autoimmunity suggesting an importance in immune tolerance (99,100).

CTLA-4 is predominantly identified in intracellular vesicles within activated conventional T lymphocytes and FoxP3+ regulatory T lymphocytes (T_{REG}). This occurs due to rapid endocytosis of CTLA-4 from the plasma membrane after its expression, with 90% of the protein being identified as intracellular. The mechanism of action of CTLA-4 remains under debate, however it is expressed on activated T cells following TCR engagement, and out competes CD28 for its targets, binding CD80 and CD86 with greater avidity and affinity. It is hypothesised that CTLA-4 then removes these molecules from the cell surface so they can no longer enhance activity, while also recruiting a phosphatase to the TCR and thus weakening its signalling. An additional mechanism of action is suggested with engagement of PI3K (101,102).

The therapeutic effects of blocking CTLA-4 for anti-cancer effects has already been alluded to, with ipilimumab being the first checkpoint blocking immunotherapy to gain widespread use. It has often been considered that the mechanism of action of this was to inhibit CTLA-4 binding to the ligands of, and out competing, CD28. However other mechanisms have been proposed, including the antibody mediated depletion of T_{REG}, the subgroup of lymphocytes in which CTLA-4 is constitutively expressed, thus removing a mechanism of dampening the anticancer immune response (102).

Regardless of mechanism, what has been observed from use of these treatments, blocking CTLA-4 induces a range of auto-immune like side effects. An immune mediated colitis in particular was identified as being associated with ipilimumab, and its sister drug tremelimumab in early trials, resulting in some treatment related fatalities, prompting a change in practice among oncology services administering these drugs, and almost the cancellation of investigation into this important therapy (65,66).

1.3.7.3 TIM3

The T-cell immunoglobulin and mucin-domain containing-3 (TIM3) or Hepatitis A virus cellular receptor 2 (HAVCR2) is another cell surface protein identified to be expressed by IFN- γ producing lymphocytes and is considered another key surface marker of exhaustion (103). A member of the TIM family of immune-regulatory proteins, TIM3 is encoded by the *HAVCR2* gene in humans on chromosome 5. While initially identified on CD4+ and CD8+ lymphocytes, expression has subsequently be identified on T_{REG}, myeloid cells, NK cells and mast cells (104).

TIM3 is reported to have multiple ligands, including Galectin 9, Phosphatidylserine, HMGB1, and CEACAM1. The mechanism of its inhibitory mechanism is poorly understood, and TIM3 has no known inhibitory signalling motifs in its cytoplasmic tail. When upregulated, TIM3 can be found in lipid rafts at the immunological synapse. In its un-ligated state TIM3 is thought to bind the HLA-B-associated transcript 3 (BAT3) and tyrosine kinase FYN, and once ligated tyrosine residues on its intracellular domain are phosphorylated, causing release of these proteins and subsequent inhibitory signalling (104).

While initially identified in an autoimmune setting, TIM3 has been identified as associated with lymphocyte exhaustion and is a marker of the most dysfunctional lymphocytes in the context of LCMV, as well as human chronic viral infections, HIV, HBV and HCV (104). It also often identifies the most dysfunctional CD8+ tumour infiltrating lymphocytes where it is strongly associated with PD-1. Expression of TIM3 has been identified as being regulated by T-bet, but also the immunosuppressive cytokine CD-27 (105), linking it with other inhibitory receptors such as LAG3 and TIGIT (106). It has also been shown to be expressed on T cells that have lost TCF1 expression and thus moved away from a progenitor like exhausted phenotype and is under the control of TOX (78,89).

TIM3 is differentially expressed in TILs from various tumour types, though is regularly described as expressed on CD8+ TILs from melanoma, head and neck cancer, haematological malignancies and gastric cancer (58,104).

Building on such observations, interest has been ongoing in manipulating TIM3 therapeutically in order to augment the anticancer response of other checkpoint inhibitors. There have been successes in pre-clinical models and human trials of TIM3 inhibitory molecules are ongoing. Of additional note, co-blockade of TIM3 and CD39, molecules with high expression on CD8+ TILs not responsive to anti-PD-1 therapy, has shown promising results in shrinking tumours in a mouse melanoma model (69).

1.3.7.4 LAG3

Lymphocyte-activation gene 3 (LAG3) is another cell surface inhibitory receptor. Encoded in humans by the LAG3 gene and also known by CD233, LAG3 was identified in 1990 in an NK cell line. It has subsequently been identified as another important negative regulator of lymphocyte function and is expressed upon activated T lymphocytes of various subtypes, B lymphocytes and plasmacytoid dendritic cells. Another type 1 transmembrane protein it possesses 4 immunoglobulin like domains on its extracellular fragment, and an intracellular tail (107,108).

The principle ligand of LAG3 is MHC class II, to which it binds with higher affinity than CD4, with whom it bears significant structural differences (107,109). Additionally galectin-3 and the C-type lectin LSECtin have been identified as ligands, as has the fibrinogen-like protein 1 (FGL1) (108,110). Similar to TIM3, LAG3 lacks a specific inhibitory motif on its intracellular domain, but does possess several highly conserved motifs, the precise mechanism for its inhibitory effects remain to be elucidated. Despite this uncertainty, its inhibitory effects appear to be correlated with the degree of LAG3 expression, suggesting a mechanism as a rheostat to limit over activity of lymphocytes (108).

Expression of LAG3 is under the control of numerous transcriptional regulators, including TOX, nuclear factor of activated T cells (NFAT) among others, with T-bet acting to repress its transcription in a manner different to TIM3. LAG3 expression is also shown to be mediated by IL-27 (108,111).

Similarly to early studies into CTLA-4 and TIM3, mice deficient in LAG3 were shown to have a propensity for autoimmunity, including type 1 diabetes. Investigation into lymphocytes infiltrating human tumours followed with its up regulation on dysfunctional lymphocytes noted (112). Inhibition alongside PD-1 in pre-clinical models demonstrated an ability to induce proliferation and cytokine release in dysfunctional lymphocytes and to bring about tumour regression. Findings that have been followed up with in-human studies, though no LAG3 targeting molecules have found their way into routine clinical use (108).

1.3.7.5 TIGIT, 2B4, CD38 and others

Of course PD-1, CTLA-4, TIM3 and LAG3 are not the only inhibitory receptors identified as checkpoints to lymphocyte function, they are just among the most high profile. There is a host of candidate molecules identified through high throughput omics techniques such as transcriptomic assessment using RNA sequencing at a bulk or single cell resolution, epigenetic profiling through techniques such as the Assay for Transposase-Accessible Chromatin using sequencing (ATAC-seq),

Chapter 1

and high dimensional mass cytometry using cytometry by time of flight (CyTOF), among others (41,44,113).

The application of such approaches onto a reproducible murine model, in the LCMV infection has led to the detailed characterisation of lymphocyte dysfunction in this context. Large scale studies utilising RNAseq have identified proteins up or down regulated in this canonical model. This includes sets of transcription factors, genes responsible for cell trafficking and chemotaxis, aberrations in cell metabolism and also distinct patterns of cell membrane proteins (41,43).

By identifying modules of genes and proteins, associated with distinct phenotypes in the LCMV model, an appreciation can be made of similar classes of immune cells within other contexts, including human tumours. It is at this intersection with patients receiving immunotherapy treatments that molecular phenotypes resulting in distinct clinical outcomes can be identified. It has been reproducibly shown in a range of tumour types that the abundance of a precursor exhausted lymphocyte population is associated with improved patient survival (69,70). In some contexts an abundance of the precursor exhausted TIL population is associated with improved responses to immune checkpoint blockade(70) where as in others possession of a high proportion of a terminally differentiated exhausted phenotype is associated with improved responses, highlighting the need to understand precisely the nature of exhaustion and dysfunction in each clinical context (69,114).

Commonly identified among the wider group of potential immune inhibitory receptors over expressed in exhausted and dysfunctional lymphocytes is the T cell immunoglobulin and immunoreceptor tyrosine-base inhibitory motif [ITIM] domain (TIGIT). Present at the surface of some T lymphocytes and NK cells this member of the immunoglobulin superfamily is encoded by the *TIGIT* gene. Similar to other molecules in this class, early results showed a correlation between loss of TIGIT function and autoimmunity (115,116). Expression is upregulated upon T cell activation, when it can bind to its ligand the poliovirus receptor (PVR). This ligand is shared with the co-stimulatory molecule CD266, and it is by out-competing this positive signal that TIGIT's inhibitory function is thought to work, at least in part, though interfering with CD266 dimerization is also considered (115,116).

TIGIT has been demonstrated to be highly expressed upon tumour infiltrating lymphocytes, where it plays a role as a regulator of anti-tumour responses which is considered to be closely associated with PD-1 signalling. Co-blockade of PD-1 and TIGIT has been shown to dramatically increase IFN- γ production in tumour infiltrating CTLs and improve survival in mouse models (117). As the mechanism for action of TIGIT and its precise place within the immune suppressive

microenvironment of cancers are further uncovered, manipulation of this pathway is increasingly being considered a potential avenue for clinical cancer immunotherapy research.

The Natural Killer Cell Receptor 2B4, also known as CD244, is another often discussed additional inhibitory T cell receptor. This Signalling Lymphocyte Activation Molecule (SLAM) family immune-regulatory receptor has been identified on many cell types including NK cells, basophils, monocytes, dendritic cells and CD8+ T cells. Possessing two extracellular Ig-like domains, a transmembrane domain and a cytoplasmic domain consisting of two Immunoreceptor Tyrosine-based Switch Motifs (ITSM) that can interact with a range of inhibitory and activating signals, including SHP1 and SHP2. Its ligand is CD48, a transmembrane receptor found ubiquitously on haematopoietic cells (118,119).

CD244 has been identified as being upregulated on antigen experienced effector and effector memory CD8 T cells, and particularly in lymphocyte exhaustion and is co-expressed with numerous inhibitory receptors including PD-1, TIM3 and LAG3 (44,56). Similarly to TIGIT, blockade of CD244 has been shown to increase production of effector molecules and degranulation by antigen specific T cells, as well as increase proliferation (120).

A final protein to mention is the lymphocyte activation marker CD38, also known as cyclic ADP hydrolase. This glycoprotein is found on numerous immune cells including T and B lymphocytes, monocytes and NK cells. With an ability to act as an enzyme and a receptor, in its receptor capacity CD38 binds CD31 on the surface of T cells and activates them to produce cytokines. On binding its ligands CD38 has been shown to induce intracellular calcium signalling, a key component of T cell activation (121). As mentioned CD38, along with TIGIT and 2B4 are frequently discussed as being surface markers strongly correlated to the exhausted phenotype and have been identified on this subset through high dimensional cytometry, making them potential molecules of interest in this project (44).

Others inhibitory and stimulatory surface receptors have been identified through high dimensional profiling studies but will not be discussed at length here as they are out of the scope of this project. They do however represent a fascinating area of molecular biology, with potential implications for preclinical and clinical research, both in translational cancer science and in the field of chronic viral infection.

1.3.7.6 CD39 and adenosine metabolism

Extracellular accumulation of nucleotides, including adenosine is negligible in healthy tissues, while it is high at sites of inflammation and within tumours. Such observations have led to the hypothesis of a function for extracellular ATP (eATP) in modulating inflammation which has been

gradually uncovered over the past two decades. It is now broadly accepted that while eATP, released by stressed or dying cells, provides pro-inflammatory signals, adenosine broadly has immune inhibitory effects (122). Adenosine signalling occurs through the type 1 purinergic receptors such as A_{2A} inhibiting immune effectors, and has directly contradictory effects to those induced by ATP binding to type 2 purinergic receptors (122,123). T cell activation itself also causes release of eATP, suggesting a necessity for homeostatic control of this process (124).

The majority of eATP in the tumour microenvironment is metabolised into extracellular adenosine by a pair of ecto-enzymes, CD39 and CD73, producing an immune inhibitory milieu. AMP is produced following eATP metabolism by CD39 and then converted to adenosine by CD73. CD39 is typically the processes rate limiting step (123,125).

CD39, also defined as ectonucleoside triphosphate diphosphohydrolase 1, is encoded by ENTPD1, and is a plasma membrane bound enzyme, active at the external cell surface. Expression, along with downstream adenosine receptors, are triggered by a range of factors released by cells under stresses. This includes TNF- α and IL-6 in response to chronic inflammation, as well as TGF- β and HIF1- α , secondary to epithelial-to-mesenchymal transition, and also as a result of chronic antigen stimulation of lymphocytes resulting in exhaustion (122,124,126).

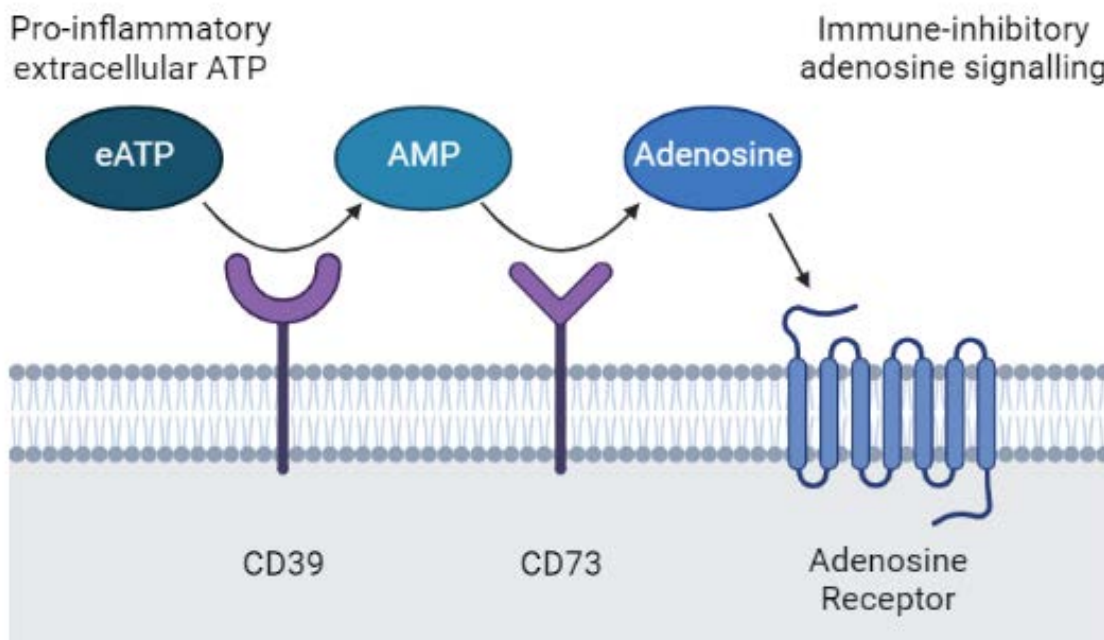


Figure 2 Metabolism of extracellular ATP to Adenosine.

Schematic diagram showing metabolism of extracellular ATP to AMP by CD39, and AMP to immune inhibitory adenosine by CD73(122). Created with BioRender.com.

High levels of CD39 have been identified in numerous solid organ and haematological cancers. The majority of this overexpression of CD39 comes from increases in the cell surface enzyme on non-cancer cells within the tumour microenvironment. This includes vascular endothelial cells, fibroblasts and a number of immune cells, including natural killer cells, macrophages, CD4+CD25+ regulatory T cells, and tumour specific cytotoxic CD8+ lymphocytes (122,127). So important is CD39 to Treg function, that loss of this can nullify their ability to negatively regulate effector T cell functions, while it is present on only a small fraction of CD8+ T lymphocytes in healthy individuals (125,126).

CD73 is itself highly expressed at the cell surface of tumour cells, as well as myeloid cells, fibroblasts and vascular epithelial cells within the tumour microenvironment (127). In addition to CD39 and CD73, the adenosinergic pathway is regulated by a number of membrane channels controlling ATP release, as well as a host of specific ATP and adenosine receptors (24).

On activated CD8+ T lymphocytes, CD39 has been shown to be a marker of keen interest. It is associated with an exhausted phenotype, identified in numerous early studies as being associated with dysfunction, PD-1 expression and a terminal exhaustion phenotype(44). In human chronic infection CD39 has been closely correlated with PD-1 expression and with increasing viral load in both HIV and HCV, presumably as a result of increasing lymphocyte dysfunction (126).

More recently CD39 expression on tumour infiltrating CD8+ lymphocytes has been correlated to an ability to detect TILs with tumour antigen specificity versus bystander lymphocytes (128,129). This has been reproduced across a number of solid tumours, and patients whose tumours contained a high number of CD8+ TILs that were labelled as double positive for CD39 and CD103 had an increased likelihood of survival (129).

In addition, TILs positive for CD39 show an impaired ability to secrete IL-2 and TNF- α , while IFN- γ production is maintained at a reduced level (130,131). CD39 positivity is highly correlated with PD-1 and co-expression in CD8+ TILs is associated with an effector-memory, as well as exhausted phenotypes, and is also associated with a strong tissue resident memory T lymphocyte transcriptomic pattern (130).

It can therefore be hypothesised that CD39 positivity can help identify a population of CD8+ TILs that are tumour reactive, associated with increased survival and associated with an exhausted, tissue resident memory phenotype. There is little, published data of how such a cell type may influence human adenocarcinomas of the upper digestive tract.

1.3.8 Tissue resident memory cells

Throughout the discussion of lymphocyte exhaustion, it is noted that the border is often blurred between the assumed effector T lymphocyte (T_{EFF}) origin of precursor and terminally exhausted lymphocytes, and memory T lymphocytes. Another population with the functionality of both effector and memory lymphocytes that are gaining increasing attention for their important role in tumour biology and immunotherapy responses are tissue resident memory cells (T_{RM}).

T_{RM} cells reside in peripheral tissues, away from secondary lymphoid organs, where they can respond rapidly to alarm signals and counter the effects of viral infection and emerging malignancy (132–134). Peripheral retention is maintained by downregulation of markers of tissue egress such as the chemokine receptor type 7 (CCR7) and the cell adhesion molecule L-selectin (CD62L). T_{RM} also possess increased expression of cell surface proteins that enable their retention, including markers that have become used for their identification, C-type lectin CD69 and the Integrin, alpha-E (ITGAE) commonly referred to as CD103(135). Additionally PD-1, CXCR6 and CD101 are all commonly present on the surface of TRMs and can aid in their identification, though the expression of these markers vary between tissues and organs. CD103 for example is most highly expressed in T_{RM} cells at mucosal sites, though is also found on T_{RM} isolated from cancers, likely a reflection of the epithelial origin of many solid tumours (136).

The differentiation of T_{RM} cells is driven by transcriptomic signatures in common with both memory and effector T cells, reflecting their origin from T memory cells, and their ability to rapidly proliferate and demonstrate effector functions (137–139). Transcriptional signatures, like surface marker expression appears to be tissue specific, reflecting the tissues within which they are retained as well as being specific for the potential pathogens they have encountered, and the potential that some T_{RM} populations may arise from long lived peripheral effector-memory T lymphocytes (T_{EM}). A number of transcription factors have been identified as important in T_{RM} development and maintenance, though no master regulator has been identified for control of T_{RM} development in all scenarios. The transcription factors Blimp-1, Runx3 and Id2 have all been observed to play important roles, while Hobit is involved in murine T_{RM} development and Notch expression is upregulated in human T_{RM} populations (137,138,140).

It is increasingly understood that T_{RM} cells play an important role in cancers. Their presence within tissues means that T_{RM} are intimately associated with developing tumours and can expand rapidly on detection of cognate peptide-MHC, and their abundance has been associated with better clinical outcomes in a range of cancers (134). Tumour associated T_{RM} are increasingly considered to be a heterogeneous population though have been seen to be enriched for tumour reactivity

and appear to have greater capacity to undertake effector functions than PD-1 positive non-T_{RM} CD8+ populations in the same tumours (114,141).

The heterogeneity of the tumour infiltrating T_{RM} populations is increasingly considered, with distinct functional capabilities and surface marker profiles. As there is no definitive marker or transcriptional signature to delineate T_{RM}, it can be challenging to define if these subsets are true T_{RM} cells, T_{RM} cells with exhausted-like features or other PD-1 positive lymphocyte populations such as classically exhausted lymphocytes with phenotypic similarities to T_{RM}. Such difficulties highlight the importance of characterising TILs in specific contexts to understand how they influence the tumour biology. An example these heterogeneous populations would include the Blimp^{high} and Id3^{high} groups described by Milner et al (140), where by the former group described a population that possessed elevated transcripts encoding TIM3 and Granzyme B, and could be interpreted as a terminally exhausted-like populations of TILs with maintained functionality. The latter Id3^{high} group conversely was classified as having high expression of TCF1, high Slamf6 and intermediate PD-1 expression. Such groups with differential functionality and responses to immunotherapy have been identified in other studies of human and murine cancers, heightening the interest in the nature of the heterogeneity in the composition of T_{RM} populations, and the influence this could have on patient outcomes (114,133,142).

An understanding of the complexion of lymphocyte exhaustion and tissue resident memory cell infiltration within cancers of the gastrointestinal tract is gradually developing(143). While there is published data relating exhaustion and T_{RM} infiltration of oesophageal squamous cell carcinomas(144,145), it remains limited and has yet to result in novel approaches to treating this patient cohort. While lymphocyte infiltration, and specifically CD8+ lymphocyte infiltration has been demonstrated as independently prognostic for patients undergoing resection of oesophageal adenocarcinoma(27), the specific composition of this lymphocyte compartment with regards to exhaustion and the abundance and phenotype of T_{RM} remain unexplored.

1.4 Oesophageal cancer

1.4.1 Background demographics and aetiology

Cancer of the oesophagus is the seventh most common malignancy and the sixth most common cause of cancer death worldwide, accounting for over 500,000 deaths globally in 2018 (146). Gastric cancer is the fifth most prevalent cancer globally and fourth on the list of cancer deaths, though it is less prevalent in the UK and western populations than oesophageal cancer (147,148).

Chapter 1

While incidence of distal gastric cancer is falling steeply, malignancy of the distal oesophagus and gastro-oesophageal junction is increasing, with both predominantly adenocarcinomas (147,149).

Oesophageal adenocarcinoma is more prevalent in many Western countries, where incidences are increasing, rising six-fold in the past 40 years, largely as a result of increased obesity, dietary changes, gastro-oesophageal reflux disease and associated Barrett's oesophagus, a recognised precursor lesion(150). These rises in cases of oesophageal adenocarcinoma are seen in the United Kingdom, as in other developed countries, where incidence is currently 6.6 per 100,000, the highest in the world (147). Squamous cell carcinomas represent the majority of cases of oesophageal cancer worldwide and predominates in East Asia and Africa with alcohol consumption and tobacco smoking the principle risk factors as well as dietary consumption of nitrosamines (150). The incidence of oesophageal squamous cell carcinoma is gradually falling.

Sadly, with patients often presenting with advanced disease, less than 40% will be potentially suitable for curative surgery, the principle strategy for long term disease control. Optimal curative outcomes are achieved with a mixed modality approach combining surgery with chemotherapy or chemoradiotherapy, depending upon disease characteristics, though despite such treatment, over 50% of patients will relapse (151,152). It is for these reasons, as well as the difficulties in controlling metastatic disease with current treatments including palliative chemotherapy, radiotherapy and endoscopic interventions, that current 5 year survival for oesophageal cancer is at approximately 17% (148).

1.4.2 Oesophageal Adenocarcinoma and Barrett's oesophagus

As discussed oesophageal adenocarcinoma (OAC) typically occurs in the distal oesophagus and gastro-oesophageal junction (GOJ). As an adenocarcinoma its origin is that of glandular epithelial tissue. The global incidence of OAC is rising, and it can be increasingly viewed as a disease associated with obesity, social deprivation, and advancing age. Obesity is among the greatest risk factor, resulting in increased gastro-oesophageal reflux disease (GORD) driving development of the precursor lesion Barrett's oesophagus. The disease is more common in males, with more than twice as many men than women diagnosed with OAC in the UK annually. Additionally, increasing age is a key factor in disease development, 41% of newly diagnosed patients are over 75. Oesophageal cancer incidence in the UK is 43% higher in women from the most deprived communities compared to the least, and this rises to 50% higher incidence in men. 59% of cases of oesophageal cancer in the UK are considered preventable (148,150,153).

Barrett's oesophagus (BE) is a classical example of a precursor malignant lesion, presenting a mosaic of intestinal and gastric metaplasia with oesophageal squamous epithelia being replaced

by gastric columnar cells, considered to be as a result of GORD. BE is not a single state, but shows progression from squamous epithelium, through a non-dysplastic (NDBE) stage, a low grade dysplasia (LGD) and into high grade dysplasia (HGD) which can eventually transform into an oesophageal adenocarcinoma. As lesions progress through these stages, the annual risk of transformation to OAC increases, from <0.3% per year for NDBE, to 5-10% per year for LGD and >20% for HGD (154–156). At a molecular level, BE shows significant abnormality with rates of tumour mutational burden only slightly lower than that of OAC and high numbers of single-base substitutions, with this increasing with progression to HGD. Predicting which patients will progress to an occult cancer is challenging. While mutations to key OAC driver genes have been observed in BE, as well as loss of heterozygosity of certain chromosomal fragments, 17p and 9p, and mutation of *TP53* and associated with risk of progression in some studies, no molecular pattern has been proven reliable to select patients at highest risk (150,156,157). As such routine endoscopic surveillance remains to gold standard monitoring.

Given the anatomical continuity between the distal oesophagus and the stomach, and the understanding that many oesophageal adenocarcinomas arise from metaplasia of squamous epithelium to a gastric-like columnar epithelium at either the GOJ or distal oesophagus, terminology can become important. Tumours arising at the GOJ can be considered as oesophageal tumours, junctional tumours or further divided based upon the Siewert Classification. Siewert type I tumours are adenocarcinomas of the distal oesophagus from an area of metaplasia which may infiltrate into the GOJ, type II arise from the cardia or short segments of intestinal metaplasia at the junction, and type III tumours arise from the gastric tissue beyond the junction and invade the oesophagus from below (158). For the purposes of this study, oesophageal adenocarcinoma will refer to tumours of the oesophagus and junction (Siewert type I-III) unless otherwise stated. Junctional or GOJ adenocarcinomas include Siewert type I-III. Oesophagogastric tumours will be used to describe adenocarcinomas of the oesophagus and stomach generally. Gastric adenocarcinomas will relate to those tumours arising in the stomach, not involving the junction.

Accurate clinical and pathological staging of cancers is crucial in predicting prognosis for patients and selecting the most appropriate therapeutic options. The most commonly used approach is the TNM (Tumour, Lymph node and Metastasis) scoring detailed by the 8th edition of the American Joint Committee on Cancer (AJCC) staging of epithelial cancers of the oesophagus and oesophagogastric junction (159). Separate scores are allocated based upon the bulk of the primary tumour (T0-T4), the number and distribution of involved lymph nodes (N0-N3) and the presence or absence of distant metastases (M0-M1). There are different scoring systems available for clinical staging, pathological staging and staging after neoadjuvant therapies. Of note a T score

of 0 represents a regressed or undetectable tumour, T1 invades the oesophagus no deeper than the submucosa, with increasing depth allocated higher scores until T4 tumours which are invading structures outside the oesophagus (159). Details of Siewert and TNM classification is detailed in Appendix A.

1.4.3 Curative Treatment – surgery, chemotherapy and radiotherapy

Optimal curative treatment for OAC involves surgical resection of the tumour and regional lymph nodes alongside either pre-operative chemoradiotherapy or peri-operative chemotherapy. Surgery is extensive and most commonly utilises the Ivor Lewis oesophagectomy technique, where by a laparotomy and right thoracotomy are undertaken in order to mobilise the tumour and adjacent organs, perform two-field lymphadenectomy of associated oesophageal and gastric lymph nodes, resection of the tumour and adjacent oesophagus and stomach, followed by intrathoracic anastomosis of the gastric conduit with the proximal oesophagus (160,161). Both open and minimally invasive techniques are used for this procedure and in some health economies there is a drive towards robotic techniques. There is a move to performing oesophagectomies in high through-put centres by experienced operators to improve outcomes, but even with this, surgery typically lasts 6-8 hours, has a significant associated mortality of approximately 2%, and given the nature of the anatomical changes, almost 60% of patients will experience significant morbidity after their surgery, and all will have lifelong nutritional implications (161,162).

There has been a gradual evolution of perioperative chemotherapy and chemoradiotherapy over the past decades since the confirmation in the early 2000s that platinum based combination chemotherapy regimens given either before, or before and after surgery could improve outcomes (163). These early trials importantly proved that there was not a significant increase in perioperative mortality with adding intensity to the treatment as had been feared, and that, in the case of one study of lower oesophagus, GOJ and stomach cancers treated with perioperative chemotherapy, 5 year survival can be extended from 23% to 35% (164). Subsequent studies assessed outcomes in more specific populations, and trialled varying treatment regimes, typically favouring a cisplatin or oxaliplatin backbone, and included radiotherapy. At present, depending on tumour characteristics including location, expected patient fitness and co-morbidities, one of two approaches is typically chosen for optimal perioperative treatment in oesophageal adenocarcinoma. This is either perioperative chemotherapy of docetaxel (50mg/m²), oxaliplatin (85mg/m²), leucovorin (200mg/m²) and fluorouracil (2600mg/m² 24 hour infusion) given in 2 weekly cycles for four cycles before and after surgery as per the FLOT trial(151), or preoperative chemoradiotherapy using the CROSS protocol consisting of carboplatin (AUC 2mg/mL per min)

and paclitaxel (50mg/m²) weekly for 5 cycles with concurrent radiotherapy of 41.5Gy in 23 fractions 5 days per week, followed by surgery (152).

There remain a cohort of patients who for various reasons, proceed directly to surgery after diagnosis without neoadjuvant therapy. This is either due to fitness, contraindications to chemotherapy because of comorbidities or even due to patient choice, though with the understanding that they do so, potentially at the expense of poorer outcomes.

Among the key predictors of success for curative treatment are the achievement of a complete pathological resection, described as R0, where a margin of normal tissue at least 1mm is observed around the tumour, and the degree of tumour regression following preoperative treatment (162). It is observed that CROSS style chemoradiotherapy has superior percentage of tumours achieving a complete pathological response. This is countered by concerns that the less intense systemic chemotherapy given in CROSS undertreats micro-metastatic disease and may be inferior in preventing distant metastases. For these reasons, both treatment regimens are considered appropriate, and are selected based upon patient characteristics (162,165).

The potential for immunotherapy to add benefit to these established neoadjuvant therapies is an area of keen interest and numerous clinical trials. Trials are ongoing assessing the use of anti-PD-1 and PD-L1 antibodies, either alone or with chemotherapy or radiotherapy protocols (165).

Adjuvant therapies, given after surgery have shown little benefit in oesophageal cancer, but the publication of data that nivolumab improved patient disease free survival to 22.4 months compared to 11.0 months, when given to patients who had residual pathological disease at the primary site following chemoradiotherapy and surgery, is of significant interest (165,166). It has led to approval for use in this context by the US FDA in May 2021 (167) and subsequent approval for use by the National Institute for Health and Care Excellence (NICE) in the UK (168). A first immunotherapy treatment to be approved and funded for patients with oesophageal cancer by the National Health Service (NHS).

1.4.4 Treatment of inoperable and metastatic oesophageal adenocarcinoma

As mentioned the majority of patients diagnosed with oesophageal cancer, do so with advanced or inoperable disease. At present, their outlook is poor. A recent population study from Sweden placed median survival in individuals receiving palliative therapy for oesophageal cancer at just 5.5 months. An added insult, is that this patient group experience significant morbidity as a result of their disease, and spent a median of 19% of their life after diagnosis, in hospital (169).

Outcomes for patients in clinical trials appear better, but median survival is typically less than one

Chapter 1

year. The recommendations for palliative treatment is typically with a platinum chemotherapy agent plus a fluoropyrimidine, though sometimes a taxane is added (162,170,171).

Between 7 and 34% of gastric cancers over express the HER2 and some data suggests this group of patients have worse outcomes. Trastuzumab, a monoclonal antibody targeting HER2 can induce antibody induced cell killing, and block stimulatory HER2 signalling and has been shown to be of some benefit in patients with advanced gastric or GOJ cancer, in the ToGA study median survival was improved from 11.1 months to 13.8 months with addition of HER2 therapy to palliative chemotherapy. Trastuzumab is funded for use in the NHS for HER2 overexpressed gastric and oesophageal cancer alongside cisplatin based chemotherapy regimens (153,172).

In the second line setting, responses and survival are even poorer. Second line Docetaxel is commonly used in relapsed disease, though the survival benefit is only 1.6 months, less than 7 weeks (173). With the outcome of several decades of trials improving the management of metastatic oesophagogastric cancer being median survival of less than 1 year, and much shorter than that for many patients, it is clear why there is such a strong appeal to harnessing immunotherapies in this scenario if it were possible to achieve some of the results seen elsewhere.

1.4.5 Rationale for immunotherapy - tumour microenvironment, inflammatory phenotype and TMB

Central to understanding the inherent resistance of OAC to systemic therapies and the difficulties in developing immunotherapeutic strategies based upon biomarkers such as PD-L1 scoring, is the complexity and heterogeneity of this tumour type. On the surface there are many factors that suggest OAC should be a disease primed for response to checkpoint blockade yet early studies have shown a disease largely refractory to such treatments.

Often referred to as oesophageal cancer, the OAC and OSCC subtypes are very divergent with OAC showing a molecular profile in keeping with being on a continuum with chromosomally unstable subtype of gastric adenocarcinoma and OSCC showing resemblance to head and neck SCC(174). OAC possesses a high tumour mutational burden (TMB), with TMB scores of approximately 8.0 mutations/megabase though this varies by study, likely due to its chronic inflammatory GORD-related aetiology. It has been shown to have low prevalence of high microsatellite instability (MSI-high) approximately only 4%, with these almost exclusively among GOJ tumours (174–176).

Based upon the promising results from the Keynote-158 trial the US FDA has approved pembrolizumab for use in patients with any metastatic or unresectable cancer, that displays a

TMB-high (≥ 10 mutations/megabase) (177). Similarly, tumours demonstrating high degrees of microsatellite instability (MSI-high) and deficiency of mismatch repair genes (MMRd) are considered to possess a hyper-mutated state and as such produce high numbers of neoantigens and high CD8+ TIL numbers. Patients with tumours demonstrating these characteristics have also been granted access to pembrolizumab by the FDA as second line therapy in the setting of advanced disease (178). Given this we would expect a good proportion of patients with metastatic OAC to respond to anti-PD-1 checkpoint blockade, however results have often been disappointing, and are lower than would be expected based upon TMB, adding to growing evidence that TMB alone is a poor predictor of ICB response (179,180).

Oesophagogastric cancers are often characterised as being interferon high or inflamed, and lymphocyte rich (181). This is clearly the case in some though there is a group in whom an immune suppressive environment predominates, and in whom lymphocyte exclusion is present.

It is known from histological assessments of resected oesophageal cancers, that patient outcomes are best in those individuals who have tumours possessing high levels of lymphocyte infiltration (182). This association with improved survival following surgery was shown to be true in patients with tumours highly infiltrated with cells positive for CD8 but not the case for the general T cell marker CD3 or for CD4 (27,144,183).

As increasingly detailed understanding of the genetic aberrations underpinning OAC beyond TMB, MSI-high and MMR are uncovered, associations with different immune phenotypes are apparent. The most commonly mutated gene in OAC is *TP53*, and tumours with aberrant *TP53* have been shown to have high frequencies of long interspersed nuclear element-1 (L1) retro-transposons. This is the most common structural genetic abnormality seen in OACs and has a strong negative correlation with immune activation pathways, and is associated with low immune infiltration picture and associated with poor survival (176,184).

Tumours of the chromosomal instable subtype of gastric and oesophageal adenocarcinomas have been shown to be highly inflamed by tumour associated macrophages and in cases exclude CD8+ TILs to the tumour margin. They also display suppression of pro-inflammatory cytokines IL-2, IL-3 and IFN- γ . Conversely the MSI and EBV associated oesophagogastric subtypes demonstrate a high level of CD8+ TIL infiltration, high expression of PD-L1/PD-L2 and are rich in immune activatory cytokines (174,176,185).

Interestingly, one recent study in gastric and OGJ adenocarcinoma has demonstrated that high CD8+ T lymphocyte infiltration is associated with high PD-L1 expression and that this is correlated with a poorer PFS and OS. They also found that high PD-L1 expression on tumour stromal rather

Chapter 1

than cancer cells was associated with the presence of CD8 TILs at the invasive margin of tumours, rather than centrally (186).

Of course CD8+ T lymphocytes are not the only immune cell or stromal tissue relevant to cancer progression. Relevance of tumour associated macrophage (TAM), CD4+ T helper lymphocytes, T_{reg} and cancer associated fibroblasts (CAF) have all been observed in the outcome of oesophageal cancers. Heterogeneity, as for the other themes discussed thus far, is also the case for these components of the immune microenvironment. Between the distinct subsets described earlier, genome stable oesophagogastric cancers enrich for CD4+ T cells, TAMs and B cells, whereas chromosomally unstable tumours show infiltration with CAFs, TAMs and exclusion of CD8+ TILs (174,185).

At present the only biomarker demonstrated as predictive of response to immunotherapy in oesophagogastric adenocarcinoma is PD-L1 expression as defined by either Combined Positive Score (CPS) or Tumour Proportion Score (TPS). The increasing understanding of the characteristics of the mutational landscape of this group of cancers, and their immune infiltration often identified through complex genomic profiling, has yet to make an impact on decision making in the clinic. It is clear that to select the correct therapeutic approach for each patient with oesophageal cancer, knowledge of the tumour immune landscape including potentially the intrinsic capabilities of the CD8+ lymphocytes in this system, would allow optimal deployment of treatments, be they immunotherapy, surgery, chemotherapy or other novel combinations.

1.4.6 Early immunotherapy trials

Following the early successes with immune checkpoint blockade observed in pre-clinical models and in melanoma, and because of the reasons outlined above, such as a relevance of CD8+ TIL numbers to survival and a high tumour mutational burden, trials were designed early to test the effectiveness of PD-1 and CTLA-4 blockade in oesophagogastric adenocarcinoma. Early trials showed mixed results. While there were no responses observed from single agent or doublet immunotherapy comparable to those seen in Melanoma, there was an anti-tumour effect observed in some patients with response rates often comparable to the generally poor responses seen with chemotherapy in this setting.

ATTRACTION-2 was a randomized phase III study undertaken in an Asian population across 49 centres in Japan, South Korea and Taiwan, assessing nivolumab vs placebo in patients who had progressed following, or were intolerant of, two lines of chemotherapy. Median survival was improved to a modest 5.3 months from 4.1 months, but 12 month survival increased from 10.9% in the placebo group to 26.6% in the treatment arm. Additionally while the RECIST evaluated

response rate was 12% with nivolumab, 40% of patients experienced some tumour shrinkage. Responses were observed in both patients with a high and low PD-L1 expression (187).

These results demonstrated the possibility of anti-cancer activity for nivolumab in multiply treated oesophagogastric adenocarcinoma. While median survival benefit was modest, a subgroup were clearly deriving benefit and almost half were seeing some tumour regression, a significant result indeed given how refractory to treatment OG cancers do become. With a large proportion of patients only ever receiving first line therapy, further investigation was needed and in other populations if global use of immune checkpoint inhibitors was to be adopted, this large trial did establish a proof of principle to be followed (187,188).

The CHECKMATE-032 study sought to assess responses to nivolumab vs one of two combinations of ipilimumab and nivolumab in western populations where they had received at least 1, but more usually 2 or more, lines of chemotherapy. Here responses were observed in the nivolumab only group, superior to the combination groups. Again a sizable minority of patients received benefit with 12 month survival 39% with nivolumab compared to 24% in one of the combination arms. There was no placebo group (180). Assessing responses to pembrolizumab in previously treated gastric and junctional adenocarcinomas, similar responses were seen, the KEYNOTE-059 study showed 42.6% experienced a measurable reduction in tumour size (189).

Buoyed by these results the KEYNOTE-061 study assessed pembrolizumab vs paclitaxel as a second line treatment in advanced oesophagogastric cancer, and included PD-L1 positive and negative patients. Results here however were negative with no significant improvement in progression free survival or overall survival, in both PD-L1 positive and negative cohorts (190).

Also unsuccessful were some attempts to move the use of checkpoint blockade earlier in the treatment paradigm of advanced oesophagogastric cancer. The KEYNOTE-062 trial showed that pembrolizumab with or without chemotherapy in the first line setting was not superior to chemotherapy alone in patients with PD-L1 high (CPS>10) or PD-L1 intermediate (CPS>1) tumours (191).

It would appear that there is a place for checkpoint inhibitors in advanced oesophagogastric adenocarcinoma in patients who have been sensitised to respond, either by earlier chemotherapy, through high tumour mutational burden, or by other factors.

Given this, it is perhaps not a surprise that the recent improvements in outcome with anti-PD-1 therapies in oesophageal cancer are seen when this is combined with or after chemotherapy. The Checkmate 649 study showed a statistically significant survival and progression free survival benefit in first line treatment for gastric, GOJ and oesophageal adenocarcinoma with nivolumab

Chapter 1

plus chemotherapy utilising a platinum backbone, such as capecitabine and oxaliplatin or fluorouracil and oxaliplatin, compared to chemotherapy alone. The benefit was most profound in patients with PD-L1 high tumours (CPS >10) but was also seen in intermediate (CPS>1) and negative cohorts (192). Additionally the already discussed Checkmate-577 study has shown a benefit from adjuvant nivolumab given following chemoradiotherapy in high risk resected gastro-oesophageal adenocarcinoma, where there was no evidence of complete pathological response (166).

Oesophageal adenocarcinoma is a complex and heterogeneous disease as has been repeatedly mentioned. On reflection it is no great surprise that a simple approach of utilising first line single agent or combination checkpoint blockade would not be sufficient to bring about meaningful responses in this patient population. The data presented above, demonstrates an importance of CD8+ T lymphocytes in the control of this disease, either following surgery or by systemic treatment of advanced disease. The responses observed in some patients to checkpoint blockade, in many instances regardless of PD-L1 status, a biomarker predictive of CD8 TIL infiltration and a pro-inflammatory microenvironment, are interesting. As too is the suggestion that the use of cytotoxic chemotherapy in some form, has a priming effect on the tumour microenvironment or the CD8+ TILs themselves. As such there must be a more effective way to predict those who will respond to therapies, and when the systems behind these predictions of response are understood, there is potential to exploit them for patient benefit. We should be under no illusion that the positive results of the trials discussed above, still represent at best, a short improvement in disease free survival, reasonable health, and overall survival, much more will have to be achieved if we are to bring about the sea change in 5 year survival that is hoped for when pursuing immunotherapeutic treatments.

The aim of this project was to investigate the phenotype of tumour infiltrating CD8+ T lymphocyte exhaustion in resected human oesophageal adenocarcinomas in order to gain insight into potential mechanisms behind differential responses to immune checkpoint blockade.

Chapter 2 Materials and Methods

2.1 Experimental protocols

2.1.1 Access to samples

Tumour samples were accessed through collaboration with the Academic Surgical department and obtained through the Upper Gastro Intestinal Tumour Ecology Study, led by Professor Tim Underwood (ethical approval in place; REC number 18/NE/0234). Human oesophageal and gastric adenocarcinoma samples were collected from resected tumours at the time of surgery from patients undergoing curative procedures at University Hospitals Southampton NHS trust.

Patients were approached prior to surgery by a member of the clinical trials team and provided with information regarding enrolment into the study, and if in agreement, informed consent was obtained. Study enrolment did not alter the clinical management of the patients, but following tumour resection, samples were obtained for multiple research projects, including this study. Patient and treatment details, as well as clinical outcomes were collected and anonymised by the clinical trials team.

Samples were collected in theatre immediately on completion of tumour resection, and 8mm punch biopsy specimens were removed from the centre of the tumour, with the remainder sent for routine histological assessment. Anonymised specimens were then transferred directly to the research laboratory on ice, where they were received and processed for analysis immediately, ensuring time from resection was at an absolute minimum.

2.1.2 Tumour disaggregation

Oesophageal and Gastric adenocarcinoma samples were washed in sterile Phosphate buffered saline (PBS) (Sigma-Aldrich, Darmstadt, Germany), and minced using a scalpel. Specimens were then transferred into 5ml of RPMI 1640 Medium (Sigma-Aldrich, Darmstadt, Germany) supplemented with Sodium pyruvate solution (Sigma-Aldrich, Darmstadt, Germany) at 1mM, HEPES Buffer (Lonza, Basel, Switzerland) at 10mM, L-Glutamine solution (Sigma-Aldrich, Darmstadt, Germany) at 2mM, Penicillin-Streptomycin (Sigma-Aldrich, Darmstadt, Germany) at 50 units/mL and 50µg/mL, and Amphotericin B (Gibco, Thermo-Fischer Scientific, Waltham, MA, USA) 1.25µg/mL. Specimens incubated at 37°C with continuous agitation in medium containing Collagenase P at 3 IU/mL (Merck, Darmstadt, Germany) and DNase I at 40 IU/mL (Merck, Darmstadt, Germany).

Chapter 2

Disaggregated material was passed through a 70µm Easystrainer™ sterile strainer (Greiner bio-one, Kremsmünster, Austria), centrifuged at 1500rpm for 5 minutes and the supernatant removed. Cells were re-suspended in 1mL of 1X red blood cell lysis buffer (Biolegend, San Diego, CA, USA). Cells further suspended in 10mL of complete RPMI medium and passed through a 40µm sterile strainer (Fisher Scientific, Loughborough, UK). Cell suspension centrifuged at 1500rpm for 5 minutes and supernatant discarded. Cell pellet re-suspended as single cell suspension ready for further use.

2.1.3 Flow cytometry

Monoclonal antibodies used for flow cytometry staining are detailed in Appendix B, and were supplied by BioLegend (San Diego, CA, USA) and Thermo Fisher Scientific (Waltham, MA, USA). All antibodies were titrated prior to first use to identify the optimal concentration for use, using either peripheral blood mononuclear cells (PBMC) from healthy donors or other suitable control cell types expressing the marker of interest.

Staining of cells for extracellular marker was undertaken in U-bottom 96 well plate, in a final volume of 100µL MACS buffer, comprised of PBS supplemented with foetal calf serum (FCS) (GE Healthcare, Chicago, IL, USA) at final concentration of 0.5% and Ethylenediaminetetraacetic acid (EDTA) (Thermo Fisher Scientific, Waltham, MA, USA) at final concentration of 2mM. For intracellular staining 100µL Permeabilization Wash Buffer (Foxp3/Transcription Factor Staining Buffer Set, Thermo Fisher Scientific, Waltham, MA, USA) was used. Antibodies added at final concentration of between 1.25 and 5µL per 100µL dependant on results of antibody titration experiments. All antibody staining was incubated for 30mins at 4°C in dark conditions.

Intracellular staining was performed following fixation and permeabilisation of samples using 200µL Fixation/Permeabilization solution (Foxp3/Transcription Factor Staining Buffer Set, Thermo Fisher Scientific, Waltham, MA, USA), incubated on ice for 45 minutes. Following permeabilisation, antibody staining undertaken in Permeabilization Wash Buffer.

Samples for flow cytometric evaluation only analysed using Beckton Dickinson (BD) FACSCanto II flow cytometer or a BD LSRFortessa flow cytometer. Data was analysed using FlowJo version 10.8.1 software (FlowJo LLC, Beckton Dickinson, Ashland, Oregon).

Fluorescence-activated cell sorting undertaken by staining cell samples in same method as for analysis using the FACSCanto, and samples sorted using a BD FACSAria IIb machine. Extracellular staining only was used prior to cell sorting given need for live cells. Cells sorted into 500µL RPMI

1640 supplemented as above, in sterile nuclease (RNase/DNase) free tubes, or into 500µL of TRIzol™ solution (Zymo Research, Irvine, CA, USA).

2.1.4 Tumour infiltrating lymphocyte culture

Disaggregated samples of resected oesophageal or gastric adenocarcinoma tumour, or sorted lymphocytes (TIL) were cultured in 24-well or 96-well plates containing either 2000µL or 200µL of Human TIL culture medium. Human TIL culture medium was comprised of RPMI 1640 Medium (Sigma-Aldrich, Darmstadt, Germany) supplemented Human AB Serum (Sigma-Aldrich, Darmstadt, Germany) at a final concentration of 10%, Sodium pyruvate solution (Sigma-Aldrich, Darmstadt, Germany) at 1mM, Hepes Buffer (Lonza, Basel, Switzerland) 10mM, L-Glutamine solution (Sigma-Aldrich, Darmstadt, Germany) at 2mM, Penicillin-Streptomycin (Sigma-Aldrich, Darmstadt, Germany) at 50 units/mL and 50µg/mL, and Amphotericin B (Gibco, Thermo-Fischer Scientific, Waltham, MA, USA) 1.25µg/mL.

Medium was supplemented with anti-CD3 pure functional grade anti-human antibody (Thermo-Fischer Scientific, Waltham, MA, USA) up to 1µg/mL, anti-CD28 pure functional grade anti-human antibody (Thermo-Fischer Scientific, Waltham, MA, USA) up to 0.5µg/mL and IL-2 (Proleukin) (Novartis, Basel, Switzerland) 1000/6000 IU/mL. Concentrations varied dependent upon experimental set up. Specimens were incubated at 37°C, and medium supplemented with IL-2 was changed every 48-72 hours if prolonged culture required.

2.1.5 Cell Freezing

Cells for freezing suspended in 500µL of culture medium, RPMI 1640 Medium (Sigma-Aldrich, Darmstadt, Germany) supplemented with Sodium pyruvate solution (Sigma-Aldrich, Darmstadt, Germany) at 1mM, Hepes Buffer (Lonza, Basel, Switzerland) 10mM, L-Glutamine solution (Sigma-Aldrich, Darmstadt, Germany) at 2mM, Penicillin-Streptomycin (Sigma-Aldrich, Darmstadt, Germany) at 50 units/mL and 50µg/mL, and Amphotericin B (Gibco, Thermo-Fischer Scientific, Waltham, MA, USA) 1.25µg/mL.

Samples were then placed in 1mL cryogenic tubes suitable for liquid nitrogen freezing on ice. 500µL freezing mix added, consisting of 80% Foetal Bovine Serum (GE Healthcare, Chicago, IL, USA) and 20% Dimethyl sulfoxide (DMSO) (Sigma-Aldrich, Darmstadt, Germany), and samples transferred immediately to gas phase of liquid nitrogen freezer, being transferred to liquid phase after 24 hours.

Chapter 2

Samples thawed by adding and diluting in 10mL of warmed mixture of 50% Foetal Bovine Serum and 50% culture medium. Rapid thawing to ensure dilution of DMSO to reduce toxicity to cells. Cells centrifuged at 1200rpm for 5 minutes prior to resuspension in 10mL of culture medium. Cells were re-suspended in desired dilution volume after further 5 minute centrifuge at 1200rpm.

2.1.6 RNA extraction

RNA extraction from cultured cell lines, thawed PBMC samples or sorted tumour infiltrating lymphocytes utilised commercially available RNA spin column kits. The kits trialled were the Qiagen RNeasy Plus Micro Kit (Qiagen, Hilden, Germany) (193), Zymo Quick RNA Miniprep Kit (Zymo, Irvine, CA, USA) (194) and Direct-Zol Zymo RNA Microprep Kit (Zymo, Irvine, CA, USA) (195). These products came complete with buffers, RNase/DNase free tubes, and utilised spin column based nucleic acid purification technology.

All RNA extraction procedures were undertaken in a dedicated room for work using nucleic acid techniques, and in a dedicated hood kept sterile by laminar air flow, following sterilisation with UV light and RNase decontamination solution RNaseZap (Invitrogen, Carlsbad, CA, USA).

Dedicated pipettes, pipette tips and containers were used for RNA extraction procedures, all certified as RNase and DNase free. RNA extraction using spin columns were performed as per manufacturers' protocol, with samples and reagents kept on ice except for when otherwise specified. RNA samples were analysed and/or frozen at -80°C immediately on completion of extraction.

RNA extraction using the phenol-chloroform technique was similarly undertaken in a dedicated room and hood kept sterile by laminar flow, UV sterilisation and RNAase decontamination solution. All equipment sterilised and RNase/DNase free. Protocol from Toni et al selected (196). Steps utilising chloroform undertaken in a laboratory fume hood, sterilised with RNase decontamination solution prior to use. RNA samples in 500µL TRIzol™ thawed on ice and kept on ice throughout. 100µL of Chloroform >99% (MP Biomedicals, Thermo Fisher Scientific, Waltham, MA, USA) added and mixed thoroughly by shaking. Sample allowed to rest for 3 minutes before centrifugation at 12,000xg for 15 minutes. The RNA containing upper aqueous phase was transferred to 100µL of Chloroform in a fresh tube, mixed thoroughly by shaking, allowed to rest for 3 minutes and centrifuged at 12,000xg for 15 minutes. RNA precipitated by adding aqueous phase to 250µL of RNase free Isopropanol (Thermo Fisher Scientific, Waltham, MA, USA) in a fresh RNase free tube. Mixed by inverting tube 20 times, and allowed to settle at room temperature for 10 minutes. Centrifuged at 12,000xg for 10 minutes at 4°C. Supernatant discarded, 1mL of freshly prepared 75% ethanol added, centrifuged at 7,500xg for 5 minutes at 4°C. Supernatant discarded

and 75% ethanol wash repeated. Supernatant carefully removed by pipette and precipitated RNA allowed to air dry for 3-5 minutes. RNA solubilized in 20 μ L of nuclease-free water before immediate use or freezing at -80°C.

2.1.7 RNA quantification

RNA quantification was undertaken using Qubit Fluorometric Quantification with a Qubit 4 Fluorometer device (Invitrogen, Carlsbad, CA, USA), utilising the Qubit RNA HS Assay Kit (Invitrogen, Carlsbad, CA, USA) with a defined detection range of 0.25-100ng RNA/ μ L. Samples for analysis and standards were prepared in a sterile hood with sterile, RNase free equipment (as for RNA extraction). Samples were prepared as per manufacturer's protocol, on ice, and analysed immediately.

Quality assessment of RNA product extracted was made using the Agilent 2100 Bioanalyzer with the Agilent RNA 600 nano kit (Agilent Technologies, Waldbronn, Germany) and 1 μ L of sample. This technique had a manufacturer defined detection range of 25-500ng/ μ L. Samples and reagents were prepared and analysed as per manufacturer's instructions.

2.1.8 Smart-seq2 RNA sequencing

RNA sequencing undertaken using the Smart-seq2 protocol as described by Picelli et al (197). Purified RNA samples extracted from sorted tumour infiltrating lymphocytes used as input. Procedure undertaken in a dedicated room and hood kept sterile by laminar air flow, following sterilisation with UV light and RNase decontamination solution RNaseZap (Invitrogen, Carlsbad, CA, USA). Dedicated pipettes, pipette tips and containers were used as for RNA extraction procedures, all certified as nuclease-free. All samples kept on ice unless otherwise stated.

2.1.8.1 Primer preparation

Primers for Smart-seq2 specifically ordered (biomers.net, Ulm, Germany) and subject to HPLC purification. These included the Oligo-dT30VN (5'-AAGCAGTGGTATCAACGCAGAGTACT30VN-3') primer which anneals to all RNAs with a poly(A) tail, contains 30 thymidine bases, 'V' is either A,C or G and 'N' is any base. Template switching oligonucleotide (TSO) (5'-AAGCAGTGGTATCAACGCAGAGTACATrGrG+G-3') containing the common primer sequence at the 5' end, and at the 3' end 2 riboguanosines (rG) and one locked nucleic acid modified guanosine (+G) to facilitate template switching. The final primer ISPCR (5'-AAGCAGTGGTATCAACGCAGAGT-3') acts as a PCR primer for the amplification step post reverse transcription. Primers dissolved in

Chapter 2

TE buffer (10mM Tris, 1mM EDTA) (Sigma-Aldrich, Darmstadt, Germany) to a concentration of 100 μ M solution. Stored at -20°C.

2.1.8.2 Reverse transcription

RNA in 2.3 μ L nuclease-free water added to 1 μ L of oligo-dT30VN primer and 1 μ L of 10mM dNTP mix (Thermo Fisher Scientific, Waltham, MA, USA), in nuclease-free 0.2mL PCR tubes. Mixed by vortexing. Oligo-dT30VN annealing completed by incubating at 72°C in thermal-cycler with heated lid for 3 minutes (Applied Biosystems® Veriti® 96-Well Thermal Cycler, Thermo Fisher Scientific, Waltham, MA, USA), samples immediately returned to ice on completion.

Reverse transcription mixture made as detailed in Appendix C combining SuperScript II reverse transcriptase (200U/ μ L, Invitrogen, Thermo Fisher Scientific, Waltham, MA, USA), SuperScript II first-strand buffer (5x Invitrogen, Thermo Fisher Scientific, Waltham, MA, USA), RNase inhibitor (40U/ μ L, Thermo Fisher Scientific, Waltham, MA, USA), Dithiothreitol (DTT) (100mM, Thermo Fisher Scientific, Waltham, MA, USA), Betaine (5M, Sigma-Aldrich, Darmstadt, Germany), Magnesium Chloride (1M, Sigma-Aldrich, Darmstadt, Germany), the TSO primer and nuclease-free water. 5.7 μ L of mixture added to RNA/oligo-dT30VN/dNTP mixture, and reverse transcription step run on a thermal-cycler with heated lid, as detailed in Appendix C.

2.1.8.3 PCR pre-amplification and cDNA clean up

PCR mixture prepared as detailed in appendix C by combining first-strand reaction produced during reverse transcription stage with KAPA HiFi HotStart ReadyMix (2x, Roche Molecular Systems, Pleasanton, CA, USA) high fidelity DNA polymerase and reaction reagent mixture, the ISPCR primer (10 μ M) and nuclease free water. After mixing, the PCR pre-amplification step is performed on a thermal-cycler with heated lid (Appendix C), though of note 22 cycles of PCR were utilised rather than the 18 in the source publication, following protocol optimisation.

On completion of PCR pre-amplification the cDNA product was purified using magnetic Agencourt AMPure XP beads (Beckman Coulter, Indianapolis, IN, USA). 25 μ L of equilibrated AMPure XP beads are added to the PCR reaction mixture at a 1:1 ratio. After incubating at room temperature for 8 minutes, the PCR tubes were placed on a magnetic stand for 5 minutes. The clear solution was removed carefully, and the beads washed twice with freshly prepared 80% Ethanol. The beads were allowed to air dry before being re-suspended in 17.5 μ L of nuclease-free water off the magnetic stand. The PCR tubes were replaced onto the magnetic stand and 15 μ L of the clear solution containing the cleaned cDNA product was removed and placed in fresh tubes for analysis and storage. This cDNA product was then analysed using the Agilent 2100 Bioanalyzer with the

Agilent High Sensitivity DNA kit (Agilent Technologies, Waldbronn, Germany) as per manufacturer's protocol using 1µL of sample. Purified cDNA was stored at -20°C.

2.1.8.4 Tagmentation and Indexing

Tagmentation using the Illumina Nextera XT DNA sample preparation kit (Illumina, San Diego, CA, USA) was undertaken using 150pg of purified cDNA from each sample. This cDNA, with differing volumes owing to concentration variations was prepared on ice and mixed with nuclease-free water added (volumes varied), Tagment DNA buffer (2x, 10µL, Nextera XT kit), and Amplicon tagment mix (5µL, Nextera XT kit, added last to standardise degradation). The total reaction volume was 20µL. The reagents were then incubated in a thermal-cycler for 5 minutes at 55°C, before being held at 4°C.

The Tn5 transposase was stripped from the tagmented DNA with addition of 5µL NT buffer (Nextera XT kit) prior to incubation at room temperature for 5 minutes. Amplification of adapter-ligated post tagmentation fragments was undertaken by preparation of the enrichment PCR mixture containing the tagmented cDNA (25µL), Nextera PCR master mix (15µL), with 5µL each of Index 1 and Index 2 primers. Total reaction volume 50µL. PCR performed for 12 cycles in a thermal-cycler with heated-lid as detailed in Appendix C.

The tagmented and indexed PCR product purified with Agencourt AMPure XP beads by repeating the process described previously, but with 30µL of beads added to the 50µL reaction mixture, beads at a ratio of 0.6:1, to minimise carryover of primer dimers. Purified DNA analysed using the Agilent 2100 Bioanalyzer with the Agilent High Sensitivity DNA kit (Agilent Technologies, Waldbronn, Germany) as per manufacturers protocol using 1µL of sample. Purified cDNA is stored at -20°C.

2.1.8.5 Library pooling and DNA sequencing

Tagmented and indexed samples were analysed by Bioanalyzer as above to identify average fragment size. Qubit Fluorometric Quantification with a Qubit 4 Fluorometer device (Invitrogen, Carlsbad, CA, USA), and the Qubit dsDNA HS Assay Kit (Invitrogen, Carlsbad, CA, USA) performed on all samples, as per manufacturers protocol, to obtain the DNA concentration for all samples. Sample molarity calculated using the following formula:

$$\text{Picomoles}/\mu\text{l} = \text{DNA Concentration}(\mu\text{g}/\text{ml}) / [0.66 * \text{DNA Size}(\text{bp})]$$

Samples diluted to produce 3nM solution. Equal volumes of each sample for sequencing mixed. DNA concentration, average fragment size and molarity confirmed with Bioanalyzer and Qubit assessment.

Chapter 2

Pooled libraries were sequenced by Illumina next generation sequencing using the Illumina NextSeq550 platform – High output kit v2.5, 75 cycles, 400 million single end reads (Illumina, San Diego, CA, USA). Libraries from 9-12 samples multiplexed to give in excess of the targeted 30 million single end reads per library. Multiplexed libraries were diluted and loaded into sequencing cartridges as per Illumina NextSeq550 protocol.

DNA sequencing using Illumina NextSeq550 system (Illumina, San Diego, CA, USA).

2.1.9 Post-sequencing data processing

Binary Base Call (BCL) files produced by the NextSeq550 system were transferred to the University of Southampton Iridis high performance computer cluster and converted to FASTQ files using the BCL2FASTQ software package version 2.18, completing de-multiplexing and storage as text files. FASTQ were then aligned to the human genome (using hg38) with software package STAR 2.7.6a. Details of script used for the above computational alignment detailed in appendix D. On completion of alignment the number of reads per gene from all samples were transferred to the R software environment version 4.0.2 for collation into a single data frame and for downstream analysis.

Differential gene expression analysis was undertaken using the DESeq2 package version 1.28.1 for R to produce normalized gene expression counts and principle component analysis. Heatmaps generated using Pheatmap package version 1.0.12 and volcano plots using EnhancedVolcano package version 1.6.0. Normalized gene expression counts produced using DESeq2 were used as input for Gene Set Enrichment Analysis using the Broad Institute software version 4.1.0. Gene set variation analysis undertaken in R using the GSVA (version 1.45.0) package. QIAGEN IPA analysis was undertaken using the IPA software (December 2021 version) via their desktop application (Qiagen Digital Insights, Hilden, Germany). Script for downstream analysis displayed in appendix D.

2.1.10 Lymphocyte proliferation assay

Proliferation assays were undertaken on sorted lymphocyte populations. Disaggregated tumour or healthy donor PBMC samples were thawed and stained as described above. Populations of interest were sorted using the BD FACSAria IIb machine into 500µL of RPMI 1640 Medium (Sigma-Aldrich, Darmstadt, Germany) supplemented with Sodium pyruvate solution (Sigma-Aldrich, Darmstadt, Germany) at 1mM, Hepes Buffer (Lonza, Basel, Switzerland) at 10mM, L-Glutamine solution (Sigma-Aldrich, Darmstadt, Germany) at 2mM, Penicillin-Streptomycin (Sigma-Aldrich, Darmstadt, Germany) at 50 units/mL and 50µg/mL, and Amphotericin B (Gibco, Thermo-Fischer Scientific, Waltham, MA, USA) at 1.25µg/mL. No human AB serum or FCS was used given the

propensity of CFSE to bind to albumin. For experiments comparing two populations of interest, an equal number of cells from each group were sorted.

Sorted cells were pelleted by centrifuge at 2500 rpm for 3 minutes and then re-suspended in PBS containing 5 μ M solution of Carboxyfluorescein succinimidyl ester CFSE (CellTrace™, Thermo-Fischer Scientific, Waltham, MA, USA) and incubated at room temperature shielded from any light for 5 minutes. Cells were again pelleted in the 1.5mL tube by centrifuge and washed in 1mL of 50% RPMI 1640 Medium (Sigma-Aldrich, Darmstadt, Germany) and 50% foetal calf serum (FCS) (GE Healthcare, Chicago, IL, USA). This washing process was repeated 3 times before cells were re-suspended in 200 μ L TIL culture medium as described in section 2.4 and supplemented with IL-2 (Proleukin) (Novartis, Basel, Switzerland) at 1000 IU/mL.

Stained lymphocyte populations were transferred to U-bottomed 96-well plates (Costar, Sigma-Aldrich, Darmstadt, Germany) bound with anti-CD3 pure functional grade anti-human antibody (Thermo-Fischer Scientific, Waltham, MA, USA) and anti-CD28 pure functional grade anti-human antibody (Thermo-Fischer Scientific, Waltham, MA, USA), where they were incubated at 37°C for 24 hours.

96-well plates were bound with stimulatory antibodies by adding 200 μ L PBS containing anti-CD3 antibody at 1 μ g/mL and anti-CD28 antibody at 0.5 μ g/mL, to each well planned for use, and incubating for 2 hours at 37°C before aspirating off PBS immediately prior to addition of test sample in TIL culture medium.

Following 24 hour incubation, sample lymphocytes were stained for flow cytometry with APC conjugated anti-CD8a antibody (BioLegend, San Diego, CA, USA), in 100 μ L MACS buffer after washing twice by pelleting cells in the 96-well plate by centrifuge at 1500rpm for 2 minutes and re-suspending in 200 μ L of MACS, as described in section 2.3. Following staining for 30 minutes on ice, shielded from light, lymphocytes were washed and then re-suspended in 200 μ L MACS solution for analysis on the BD LSRFortessa flow cytometer.

2.1.11 Lymphocyte stimulation assay

Stimulation assays were performed on thawed disaggregated tumour samples, and healthy donor PBMCs. Thawed samples were washed and each experimental condition re-suspended in 200 μ L of TIL culture medium prepared as described in section 2.4, with the addition of 5 μ L of PE/Cy7 fluorophore labelled anti-CD107a antibody. Samples were added to U-bottomed 96 well plates with or without prior anti-CD3 and CD28 antibody binding, performed as described in section 2.10.

Samples were incubated at 37°C for 5-6 hours, with Brefeldin A (Golgi-Plug™, Beckton Dickinson, Franklin Lakes, NJ, USA) added at a concentration of 0.1% to each sample after the first hours incubation. On completion of incubation period samples were removed from the incubator, and stained for flow cytometry using both extracellular and intracellular staining, as detailed in section 2.1.3. Samples were subsequently re-suspended in 200µL MACS solution for analysis on the BD LSRFortessa flow cytometer.

2.2 Experimental procedure development and optimisation

2.2.1 RNA sequencing experiment optimisation

2.2.1.1 Assessment of RNA extraction techniques

Cell numbers available for bulk RNA sequencing were expected to be low so the optimal approach for extracting RNA quickly, from small numbers of cells was required. A range of methods for RNA extraction were considered and assessed for their ability to isolate RNA from small numbers of cells. Four methods were assessed including 3 commercially available spin column based protocols (Qiagen RNeasy Plus Micro Kit (193), Zymo *Quick*-RNA™ Miniprep Kit (194), Zymo Direct-zol™ RNA Microprep Kit (195)) and the reliable though more labour intensive phenol-chloroform RNA extraction method (196). The Zymo Direct-zol™ and phenol-chloroform techniques require samples stored in TRIzol™, a trade name for guanidinium thiocyanate.

All RNA extraction experiments were performed by the same operative to minimise bias, and work was undertaken within a hood dedicated for pre-PCR work, sterilised with ultra-violet light, treated with RNase inhibitor and protected by laminar air flow. All samples were kept on ice, apart from when protocols stipulated a specific temperature. RNA was stored at -80 degrees and returned to this temperature immediately when not in use, with freeze-thawing kept to absolute minimums.

Spin column kits were tested as per the manufacturer's recommendations. Multiple phenol-chloroform RNA extraction protocols were reviewed, the protocol published by Toni et al. in 2018 (196) was selected for assessment, given its second clean up step to improve RNA purity.

Initial assessment of RNA yield were derived using Human Embryonic Kidney 293T (HEK 293T) cells. They were counted and diluted to allow RNA extraction to be undertaken on 1000, 3000, 5000 and 10,000 cells in 500µL of either cell culture medium or TRIzol™, according to manufacturer's protocol. This process was repeated at least three times to ensure smooth

application of the technique and consistency of results. The best performing RNA extraction experiments are summarised for each technique below.

The RNA concentration of the extraction product was quantified using Qubit4 flurometer and Qubit High Sensitivity RNA kit. According to the manufacturers of this test the sensitivity is 0.25-100ng/ μ L with an input of 1-20 μ L. To attain the highest sensitivity from this test the whole extraction product would be used for analysis, therefore 2 μ L of sample was used for analysis (198).

# cells for extraction	Mean RNA concentration (ng/ μ L)	Resuspension volume	Yield (ng)	Yield/cell (pg)
Qiagen Rneasy Plus Micro Kit				
1,000	2.10	12 μ L	25.20	25.20
5,000	5.33	12 μ L	63.96	12.79
Zymo Quick-RNA™ Miniprep Kit				
1,000	0.64	50 μ L	32.00	32.00
5,000	2.24	50 μ L	112.00	22.40
Zymo Direct-zol™ RNA Microprep Kit				
1,000	1.15	12 μ L	13.80	13.80
5,000	9.04	12 μ L	108.48	21.70
Phenol-Chloroform RNA extraction technique				
1,000	Not recordable	20 μ L	-	-
5,000	1.79	20 μ L	35.87	7.17

Table 1 RNA extraction technique analysis.

Summary of RNA extraction from HEK 293T cells using Qiagen RNeasy Plus Micro Kit, Zymo Quick-RNA™ Miniprep Kit, Zymo Direct-zol™ RNA Microprep Kit and phenol-chloroform RNA extraction technique. Displayed are results obtained from 1000 and 5000 cells in 500 μ L of solution. Best performing assessment of each technique shown for comparison.

Of the methods assessed all 3 spin column based techniques produced good RNA yields. The Zymo Direct-zol™ RNA Microprep Kit had the benefit of an ability to elute RNA into a small volume of water, and of using cells stored in TRIzol™ as its input, a potent inhibitor of nucleases. TRIzol™ represents a practical medium into which cells can be sorted into, lysed and stored without disruption. The Phenol-chloroform technique did not yield higher RNA output and was

Chapter 2

considerably more labour intensive. For these reasons the Zymo Direct-zol™ RNA Microprep Kit was selected for further assessment.

RNA was isolated from the human PBMCs of healthy donors alongside HEK 293T cells, to allow both quantification and assessment of quality of the extracted RNA product. Cells were counted and diluted in 500µL TRIzol for extraction. RNA quantification was again assessed using the Qubit4 fluorometer and Qubit High Sensitivity RNA kit, while an assessment of RNA quality was made using the Agilent 2100 Bioanalyzer and RNA 6000 Nano Kit with input volume of 1µL and sensitivity range 25-500ng/µL (199). This assessment produces an RNA integrity number, with high quality RNA producing scores close to 10, with figures greater than 8 typically suggesting good quality RNA (200).

RNA was readily extracted from high numbers of cells from both cell lines and PBMCs, 25-50,000 cells in 500µL TRIzol™, with a yield of greater than 0.5pg/cell for the small PBMC cells. However, lower cell numbers 5-10,000 cells did not result in easily quantifiable yields of RNA from PBMCs, though it could recover RNA from larger, cells lines where RNA is known to be more abundant.

# cells for extraction	Mean RNA concentration (ng/µL)	Resuspension volume	Yield (ng)	Yield/cell (pg)	RIN
HEK 293T cell RNA extraction					
1,000	1.45	12uL	17.40	17.40	n/a
5,000	3.9	12uL	46.8	9.36	8
25,000	27.333	12uL	327.996	13.11984	9.1
100,000	40.00	12uL	480.00	4.80	10.00
PBMC RNA extraction					
1,000	Too low	12uL	-	-	n/a
5,000	0.84	12uL	10.08	2.016	n/a
25,000	2.04666	12uL	24.5592	0.982	n/a
100,000	5.84	12uL	70.08	0.7008	6.6
500,000	19.066666	12uL	228.7992	0.4575	7.6

Table 2 Assessment of the Zymo Direct-zol™ RNA Microprep Kit.

Summary of quantification and quality assessment of RNA extraction from HEK 293T cells and human healthy donor PBMCs using the Zymo Direct-zol™ RNA Microprep

Kit. Displayed are results obtained from 1000, 5000, 25,000, 100,000 and 500,000 cells in 500 μ L of TRIzol™.

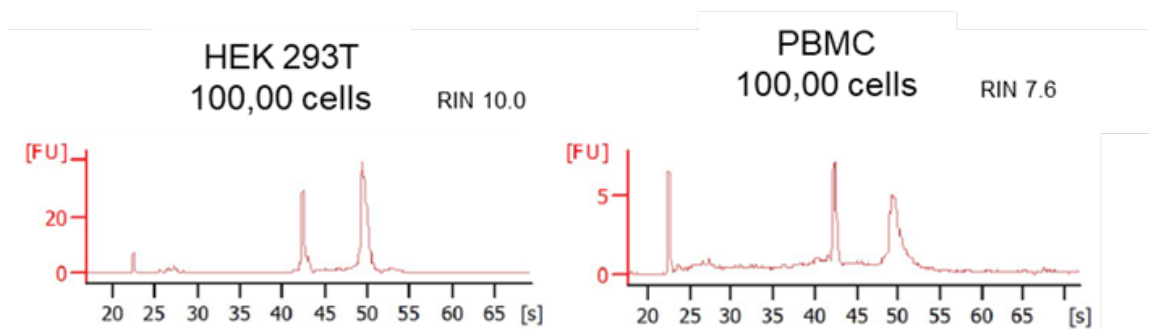


Figure 3 RNA quality assessment using Agilent 2100 Bioanalyzer.

Electropherogram output with RNA integrity number from Agilent 2100 Bioanalyzer and RNA 6000 Nano Kit of RNA extracted from 100,000 HEK 293T cells and human healthy donor PBMCs.

It is possible to use the Zymo Direct-zol™ RNA Microprep Kit to extract high quality RNA from cells stored at -80°C in TRIzol™, though RIN numbers do reduce as concentrations approach the lower end of the Agilent RNA 6000 Nano kit detection range. Yield per cell from human PBMCs are significantly reduced when compared to human immortalised cell lines, though this is to be expected given the differing morphology and transcriptional output of these cells and is consistent with the literature. This technique was shown to extract a high yield of RNA from low numbers of cells down to 1000 cells, and it was expected it would do so from lower numbers of cells, though this may difficult to quantitate.

Given these observations the Zymo Direct-zol™ RNA Microprep Kit was used to extract RNA from sorted OAC TILs sorted into TRIzol™. With the aim for downstream sequencing, ample controls were used to assess the efficiency of the RNA extraction process.

2.2.1.2 Assessment of expected yield of TILs isolated by fluorescence-activated cell sorting (FACS)

In order to assess the feasibility of undertaking bulk RNA sequencing on sorted samples of rare populations of TILs from oesophageal adenocarcinoma specimens, an assessment was made of the potential yield in terms of cell numbers. Initially a total of 7 fresh samples from resection specimens were sorted, using the gating strategy outlined in chapter 4.2.1. 3 populations of CD8+CD44+ TILs were collected in this trial, all expressing PD-1 and CD39 positivity and varying degrees of TIM3 and LAG3 expression. The first population is positive for PD-1 and CD39, but negative for LAG3 and TIM3, and labelled as 'Double Positive' (DP). A second population was PD-

Chapter 2

1, CD39 and LAG3 positive, but TIM3 negative and labelled 'Early Exhausted' (EExh), and a final population was positive for PD-1, CD39, LAG3 and TIM3 and provisionally labelled 'Late Exhausted' (LExh). TILs from these populations were sorted into 400µL of ice cold TRIzol™ solution, and on completion of sorting, were transferred on ice directly to storage on -80 freezer for storage.

Additionally a population labelled P4 was also sorted comprising of cells not gated as morphologically lymphocytes, which presumably includes cancer cells from the tumour. These cells were sorted into 500µL of ice cold complete RPMI and were frozen utilising the technique described in section 2.1.5 in case of need in future experiments.

As was expected the greatest number of cells was recovered for the Double Positive (DP) population 1, ranging from 66,000 from a progressing tumour treated with chemotherapy, to 189 in a responding tumour treated with chemoradiotherapy, median 6,900. The lowest number of cells were recovered from the Early Exhausted (EExh) population 2 with a range from 14,000 cells in a treatment naive tumour to 1 cell from a regressing chemoradiotherapy treated tumour. The median was 201 cells recovered. Given the potentially low yield of TILs from sorting using FACS a high sensitivity technique was needed for isolation of RNA and generation of cDNA library.

Sample sort number	Pretreatment modality	Degree of tumour regression	Population 1	Population 2	Population 3
1	No pre-treatment	N/A	59,000	14,596	2,402
2	No pre-treatment	N/A	3,221	30	18,507
3	CRT	TRG2	189	1	485
4	Chemo (FLOT)	TRG5	6,967	97	2324
5	CRT	TRG1	41,226	1,132	1,643
6	Chemo (FLOT)	TRG1	5,773	201	50
7	Chemo (FLOT)	TRG5	66,929	2,178	403

Table 3 Cells recovered from trial FACS sorts of human oesophageal adenocarcinoma specimens.

Number of tumour infiltrating lymphocytes from populations defined above recovered by FACS from the first 7 tumours sorted using the BD FACS Aria IIa. Table

includes details of patient pre-treatment regimen and where applicable, histological response.

2.2.1.3 Assessment of feasibility of RNA sequencing using SmartSeq2 protocol

Given the challenges described, a sensitive RNA sequencing protocol was sought for use in this project. While keen to exploit the depth of sequencing that bulk RNA sequencing of a homogenous population allows, many standardised approaches to bulk RNA sequencing would require concentrations of RNA not feasible for this project. An example of this being the Illumina TruSeq platform, a standardised process for performing RNA sequencing which would be attractive, though requires a minimum input of 100ng RNA (201). Estimates based upon earlier work would suggest that a potential yield from 1000 sorted lymphocytes may only equate to approximately 2ng, thus a more sensitive process is required. As such the SmartSeq2 RNA sequencing protocol was considered adaptable to this purpose (197). Initially developed as a full-length single cell RNA sequencing technique utilising single sorted cells, it can also be adapted to use several picograms of purified RNA as its input genomic material. As such it can be used for bulk RNA sequencing of low concentrations of RNA. This has been used increasingly in studies investigating the transcriptional profile of lymphocytes from human tissues, given its flexibility and sensitivity (94,114,202).

As a first step towards adopting the Smart-Seq2 protocol for this project, purified RNA, extracted during assessment of the Zymo Direct-zol™ RNA Microprep Kit, was used for a trial of cDNA production. The concentration of the purified RNA input was measured using the Qubit4 fluorometer and Qubit High Sensitivity RNA kit immediately prior to starting, and this was added directly to the primers and di-nucleotide mix prior to the reverse transcription step. Template switching and PCR pre-amplification steps were performed prior to clean-up of cDNA using Agencourt AMPure XP beads, as detailed in section 2.1.8. Purified cDNA was then stored at -20°C.

An assessment of the cDNA produced was made using the Agilent 2100 Bioanalyzer with the Agilent High Sensitivity DNA kit. Similar to the kits for RNA assessment, this produces an electropherogram detailing the distribution of DNA by fragment length, including two standardised markers. Additionally it provides estimates of DNA concentration and molarity (203).

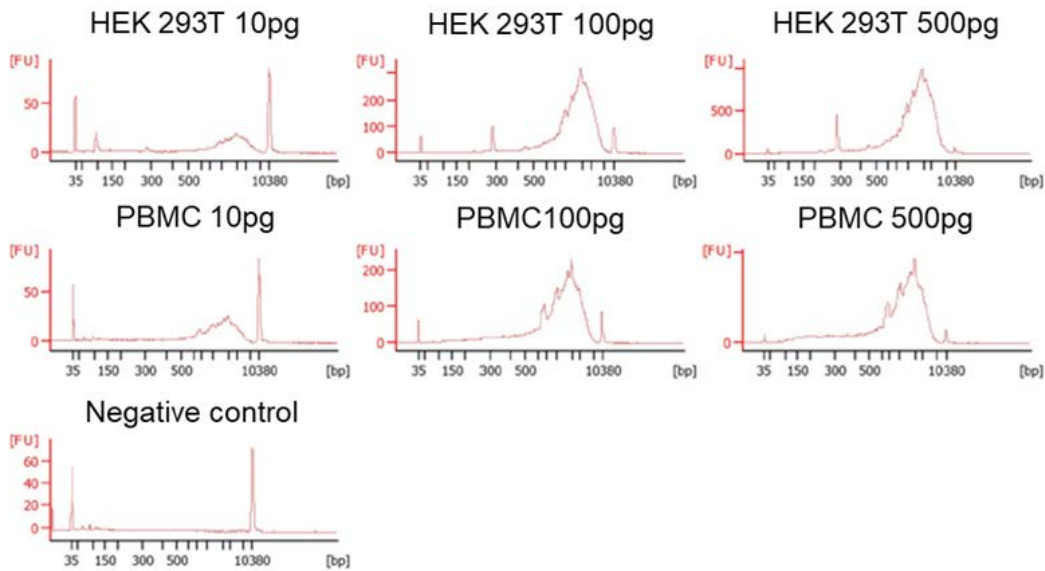


Figure 4 Trial library preparation using SmartSeq2 protocol.

Electropherogram output from Agilent 2100 Bioanalyzer and Agilent High Sensitivity DNA kit of cDNA produced using SmartSeq2 protocol from RNA extracted from HEK293T cells and healthy donor PBMCs. Amount of RNA input at 10, 100 and 500pg.

This trial demonstrated an ability to utilise the SmartSeq2 protocol to produce a cDNA library from low volumes of RNA, from 500pg down to as little as 10pg, extracted from cells, including PBMCs, stored in and extracted from TRIzol™, using the Zymo Direct-zol™ RNA Microprep Kit.

2.2.1.4 cDNA production and indexing of sequencing library from RNA extracted from oesophageal adenocarcinoma TILs

To test further the feasibility of utilising the SmartSeq2 protocol, library preparation was attempted on populations of lymphocytes extracted from human oesophageal adenocarcinomas. As detailed above the first 7 patient samples sorted for this project yielded differing numbers of cells. Samples unlikely to be used for final sequencing analysis due to low collection yields in one or more population were used for the initial trials.

RNA was extracted as previously using the Zymo Direct-zol™ RNA Microprep Kit and eluted into 12µL of RNase/DNase free water. A positive control of RNA extracted from 500,000 PBMCs extracted simultaneously produced highly concentrated, high quality RNA (RNA concentration 67ng/µL, RIN 8.2 Agilent 2100 Bioanalyzer with the Agilent High Sensitivity DNA kit). RNA from the most abundant sorted population from the trial sample was diluted with nuclease free water and an equivalent of 100, 500 and 1200 cells RNA was inputted into the process, an estimated 0.2, 1 and 2.4pg of RNA respectively. On analysis by the Agilent 2100 Bioanalyzer with the Agilent High

Sensitivity DNA kit, a peak representing cDNA was visible at all 3 levels of RNA input after cDNA production.

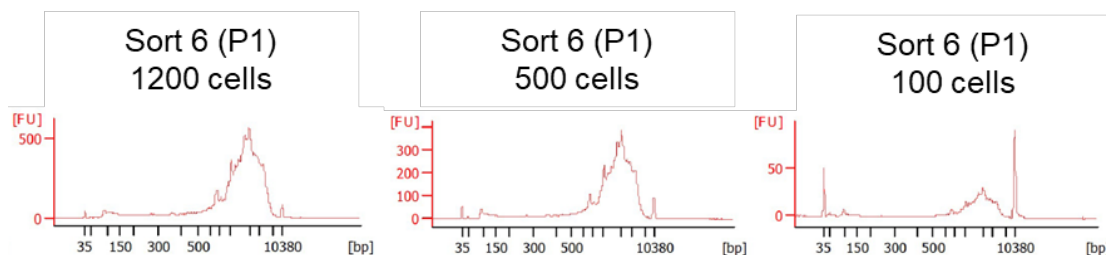


Figure 5 Successful cDNA production from oesophageal adenocarcinoma TILs using SmartSeq2 protocol.

Electropherogram output from Agilent 2100 Bioanalyzer and Agilent High Sensitivity DNA kit of cDNA produced using SmartSeq2 protocol from RNA extracted from sorted exhausted tumour infiltrating lymphocytes. Electropherograms show cDNA from Sort 6 samples population 1 with equivalent of 1200, 500 and 100 cells of RNA input.

Successful cDNA production utilising the proposed experimental pipeline in samples of approximately 5000 sorted cells and as little as approximately 1pg of purified RNA input, gave confidence to move forward with RNA sequencing of further samples, and in doing so further refine this process.

2.2.1.5 RNA sequencing of sorted TILs from human oesophageal adenocarcinoma

To confirm the efficacy of the RNA sequencing pipeline developed, RNA was extracted from sorted TILs (Double positive, Early Exhausted and Late Exhausted groups, Populations 1, 2 and 3 respectively) isolated from the tumours of three patients collected during the development phase of this work. This included one treatment naïve patient, 1 post chemotherapy and 1 post CRT. The tumours had not only received varying pre-treatment regimens, but also experienced differential responses. The treatment naïve tumour could not be graded for regression, though the chemotherapy treated tumour showed progressing cancer (TRG5) while the CRT treated tumour showed a complete pathological response (TRG1).

RNA was recovered from TRIzol™, using the Zymo Direct-zol™ RNA Microprep Kit, and given the expected difficulties in quantifying RNA yield a control of 50,000 PBMC in an identical volume of TRIzol™ was used and extracted concurrently. Once extraction success was confirmed in the control sample, the SmartSeq2 protocol was initiated using eluted RNA equating to approximately 100-150 cells. 22 cycles of PCR used for PCR pre-amplification step, see materials and methods. On completion of clean up steps, a cDNA library for each population from all 3 patients was obtained.

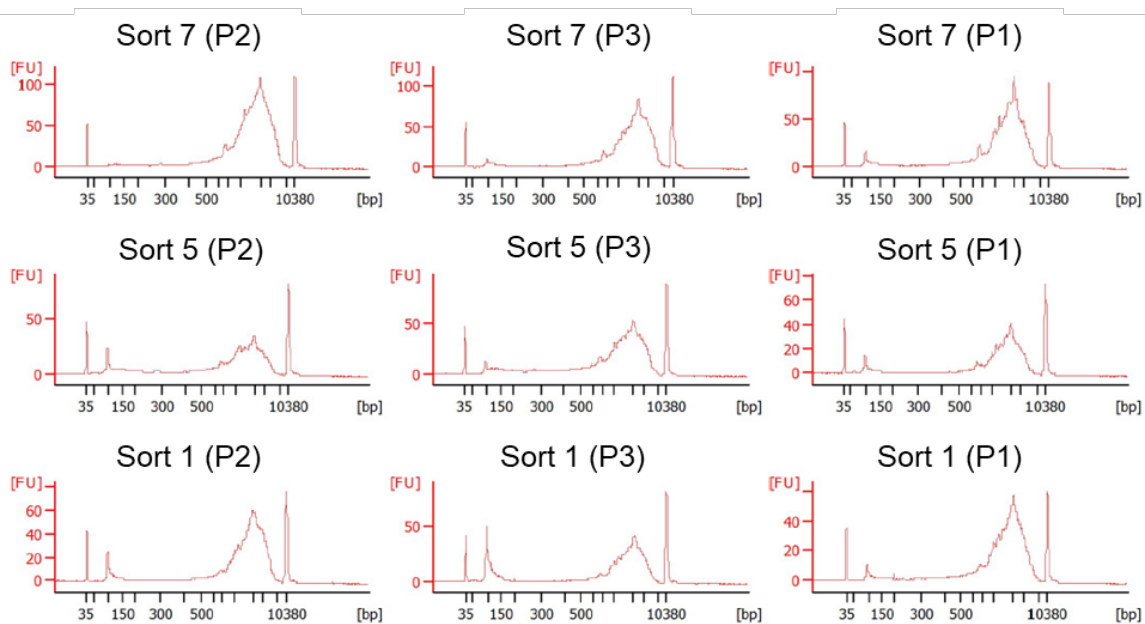


Figure 6 cDNA from 3 populations of TILs extracted from 3 oesophageal adenocarcinomas.

Electropherogram output from Agilent 2100 Bioanalyzer and Agilent High Sensitivity DNA kit of cDNA produced using SmartSeq2 protocol from RNA extracted from sorted exhausted tumour infiltrating lymphocytes. Electropherograms show cDNA from Sort 7, 5 and 1, populations 1,2 and 3.

On completion of the cDNA production from all sample populations, the remaining stages of the SmartSeq2 protocol were undertaken, including sample tagmentation and indexing, followed by further DNA clean-up steps. This was undertaken using the Illumina Nextera XT indexing and sample preparation kits as per the SmartSeq2 protocol. This process results in the cDNA being fragmented into portions the appropriate length for the Illumina sequencing platform with a combination of indexed labels at each end, unique for each sample. On completion samples were again analysed using the Agilent 2100 Bioanalyzer and Agilent High Sensitivity DNA kit to ensure appropriate fragmentation of cDNA for onward sequencing.

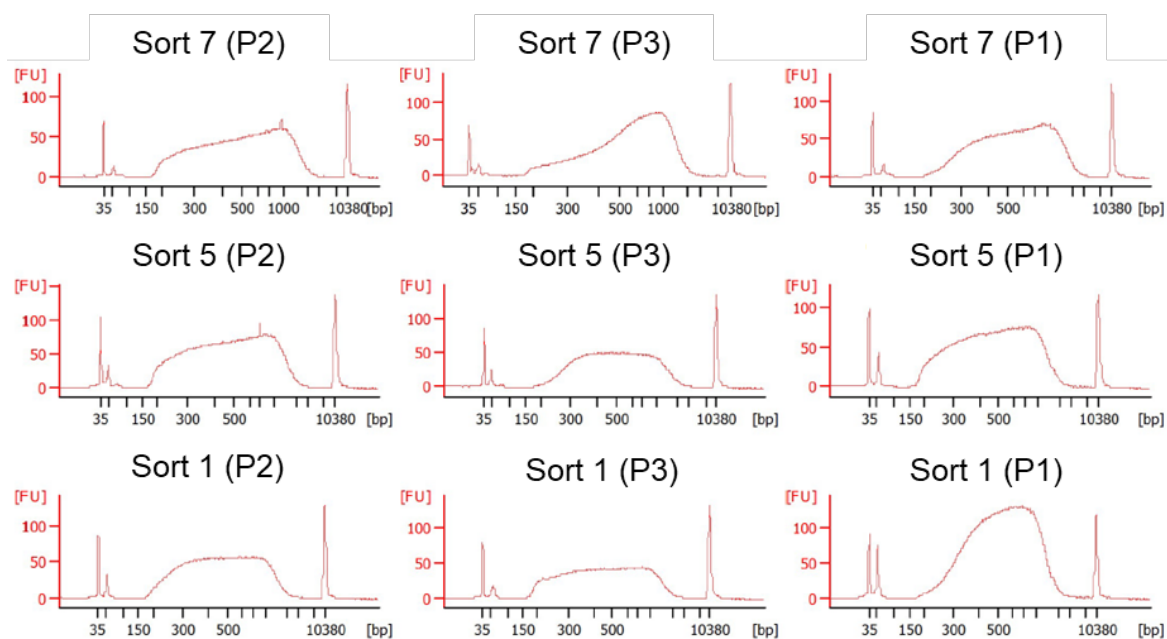


Figure 7 Analysis of tagged and indexed cDNA from first 3 oesophageal adenocarcinomas.

Electropherogram output from Agilent 2100 Bioanalyzer and Agilent High Sensitivity DNA kit of cDNA libraries produced from sorted exhausted tumour infiltrating lymphocytes, following tagmentation and indexing. Electropherograms show cDNA from Sort 7, 5 and 1, populations 1, 2 and 3.

Illumina next generation sequencing using the Illumina NextSeq550 platform was accessed on the same site as clinical treatment of patients and experimental work in this project. In order to allow at least 30 million single end reads per sample, a NextSeq 500/550 High Output Cartridge v2.5 (75 cycles) was purchased and used for sequencing. The molarity of all indexed samples was calculated to ensure equal amounts of indexed DNA from each sample was included in multiplexing and loaded into the sequencing cartridge. cDNA sequencing was run and raw data transferred to the University of Southampton High Performance Computing System, Iridis.

2.2.1.6 Processing of transcriptomic data

On completion of the NextSeq550 sequencing run, Binary Base Call (BCL) files were converted to FASTQ files using the BCL2FASTQ software package version 2.18, completing de-multiplexing and storage as text files. FASTQ files were next transferred to the Iridis system and aligned to the human genome (using hg38) with the STAR 2.7.6a. On completion of alignment data from all samples was transferred to the R software environment for collation into a single data frame allowing downstream data analysis. Initial analysis of data produced demonstrated an ability to calculate differentially expressed genes and normalised and transformed counts to allow gene set based assessment techniques, gene set enrichment analysis and gene set variation analysis.

2.2.2 CD8+ proliferation assay development and testing

An assay for assessing proliferative potential among recovered TILs from human tumour samples was sought in order to compare populations of interest. Several strategies for assessing lymphocyte proliferation were considered and an assay utilising the carboxyfluorescein succinimidyl ester (CFSE) dye was chosen. The fluorescent molecule CFSE binds covalently with intracellular lysine residues and is maintained in stained cells, such that on cellular division the concentration of CFSE is halved in each subsequent daughter cell, with concentrations measurable by flow cytometry. A degree of toxicity is observed at high concentrations, limiting this process to allow observation of up to approximately 8 cycles of proliferation (204).

Experimental development and validation used healthy donor PBMCs, initially counted and then FACS sorted into TIL culture medium. A protocol utilising staining with 5 μ M CFSE and subsequent washes in an FCS rich medium was chosen and decreasing numbers of cells were assessed following culture in a range of conditions and differing incubation lengths between 1 and 6 days. Lymphocytes were cultured in TIL culture medium enriched with IL-2 and human AB serum in 96 well plates bound with anti-CD3 and anti-CD28 antibody. At the end of the incubation period cultured cells were stained with an APC conjugated anti-CD8a antibody prior to flow cytometric assessment, aiming for detection of CD8+ lymphocyte progeny with minimal spectral overlap between antibody and CFSE staining.

With an ability to detect proliferation in low number of sorted cells a priority for this experimental plan, 50,000 down to as few as 500 sorted PBMCs were used for initial analyses and it was possible to identify peaks of proliferating cells from as little as 1,000 sorted cells. It has been possible to observe peaks of events on histograms displaying CFSE staining as detected by the FITC channel of a standard flow cytometer, with this most obvious when only CFSE positive cells were gated. Gates were defined using CFSE and anti-CD8a antibody unstained PBMCs.

The intention of this assay was to identify proliferative potential in the populations of interest, so sorted cells were cultured with IL-2 as well as stimulatory antibodies binding CD3 and CD28. As a result, a high degree of proliferation is observed, with small peaks for the various CFSE positive populations when compared to the CFSE negative peak and the un-cultured CFSE stained control. Given additional experimental time, the assay would have been optimised further with the stimulatory molecules titrated downwards to give a less intense activation of proliferation and clearer delineation of generations of daughter cells of the sorted TILs.

Given it would not be possible to reach the 100,000 lymphocytes it is possible to culture in a 96 well plate from the limited sample sizes available for this project, it was proposed to collect as

many cells as possible for each experimental group, while attempting to roughly match the number of cells collected in paired samples. This would allow direct comparison of paired DN and DP samples.

Utilising this technique it is possible to identify lymphocyte populations undergoing cell proliferation with clear peaks visible for each generation of daughter cell. The protocol developed was taken forward for use on oesophageal adenocarcinoma TILs.

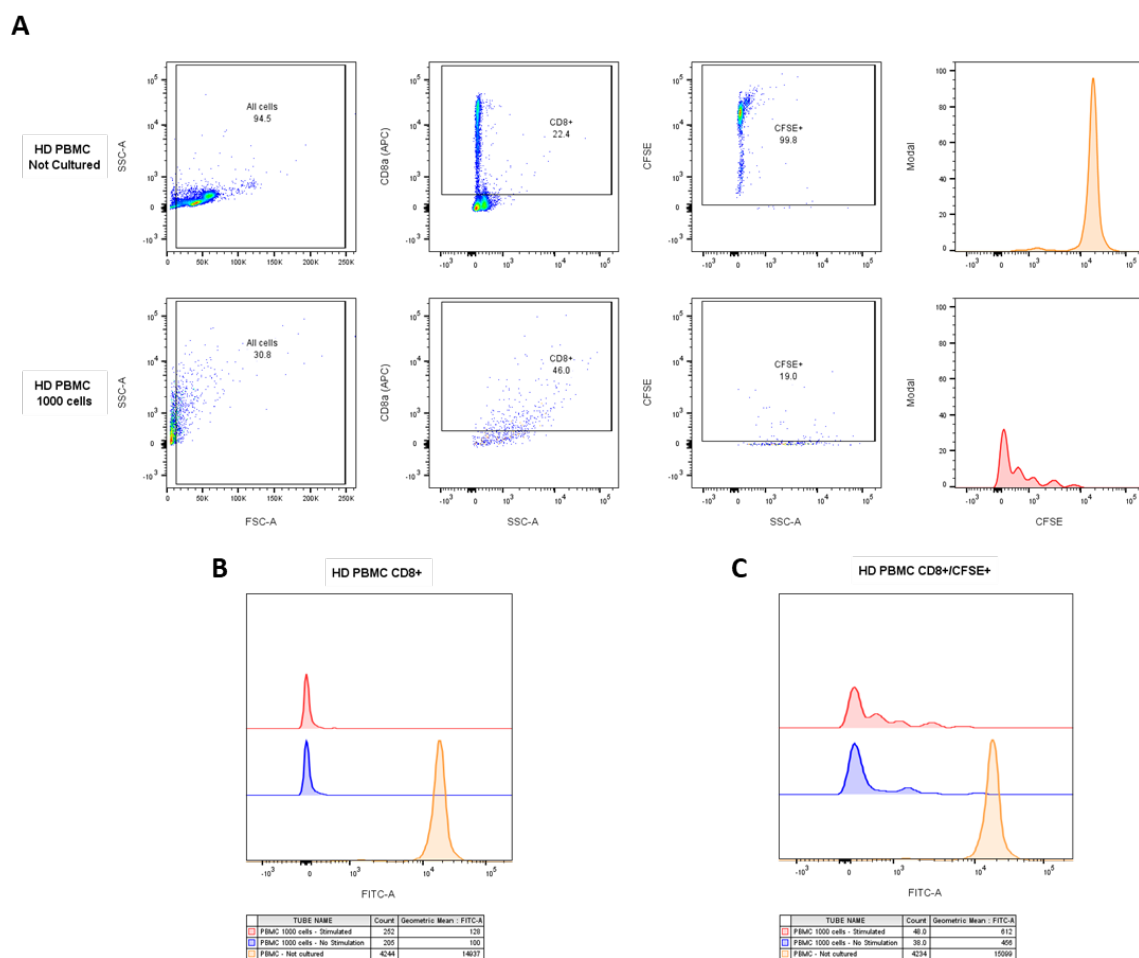


Figure 8 CFSE proliferation assay development utilising HD PBMC samples.

A) Gating strategy identifying CD8+ cells, and subsequent CFSE+ population. Gates set using unstained populations (not shown). Far right graphs display histograms for CFSE staining (as measured by FITC flow cytometer channel) of CD8+CFSE+ cells. Top row shows anti-CD8a stained and CFSE stained cells analysed immediately and not cultured. Bottom row shows results of 1,000 sorted CD8+ CD44+ PD-1- CD39- PBMCs cultured for 24 hours. B and C) Histograms showing CFSE staining of CD8+ cells on left, and CD8+ CFSE+ cells on right. Results from 1,000 sorted CD8+ CD44+ PD-1- CD39- HD PBMCs cultured for 24 hours in the presence (red line) or absence (blue

Chapter 2

line) of stimulatory anti-CD3 and anti-CD28 antibodies. Control population (orange line) of non-cultured HD PBMCs.

Chapter 3 Immunophenotyping of exhausted CD8+ T lymphocytes in human oesophageal adenocarcinoma

3.1 Introduction

Successful control and elimination of a cancer by the immune system requires the trafficking and infiltration of activated tumour antigen specific cytotoxic T lymphocytes into tumours, followed by recognition and killing of cancer cells as described in the cancer-immunity cycle (22). This process can be interrupted at multiple points leading to breakdown and prevention of effective lymphocyte driven destruction of cancer.

In the context of human oesophageal and oesophagogastric junctional adenocarcinomas a pro-inflammatory microenvironment has been described, with a high burden of genomic mutations within the malignant cells, and active infiltration with CD8+ T lymphocytes, a factor known to correlate with survival (27,181,205). Despite this, occult cancers are observed, which are often highly resistant to conventional treatments utilising a mixed modality approach of surgery, radiotherapy and chemotherapy. Trials evaluating the use of immune checkpoint blockade, either as monotherapy or alongside other approaches has led to modest benefits in some groups (166,192,206).

While adenocarcinomas of the oesophagus are grouped together due to their shared aetiology and clinical presentation, they can be extremely heterogeneous in their degrees of immune cell infiltration (205) and their behaviour following immune modulating therapies. It is understood that CD8+ T lymphocyte infiltrates in oesophageal adenocarcinoma express variable amounts of PD-1 and it is hypothesised here that the numbers of exhausted lymphocytes and the proportion of these demonstrating precursor or terminally differentiated exhausted lymphocyte characteristics, may be a contributing factor to responses to therapy, and patient outcomes.

Additionally, the composition of these various CD8+ TIL subtypes within the tumour immune microenvironment may also be a factor in the differential responses observed of tumours to checkpoint blockade before and after neoadjuvant therapies, or first line cytotoxic chemotherapy in the context of metastatic disease (180,192,206).

Immunohistochemistry based approaches have been used extensively to calculate the numbers and broad subgroups of the immune infiltrates in these cancers, with a view to guiding prognosis,

particularly around curative interventions. There are limits to the number of antibody stains that can be utilised in such approaches, impacting the granularity of the data collected, and while high dimensional IHC techniques are increasingly available they are complex. To gain a fuller picture of the CD8+ lymphocyte infiltrates and understand their composition in terms of degrees of exhaustion, a flow cytometric based approach has been adopted here. This has focussed upon antigen experienced CD8+ TILs, and their cell surface expression of hallmarks of the exhausted phenotype, including PD-1 and other key markers as well as crucial intracellular transcription factors. Primary oesophageal and oesophagogastric junctional adenocarcinoma samples resected at the time of curative surgery were used for analysis along with longitudinal data related to disease relapse and patient survival.

The aim of this chapter was to investigate for the presence of an exhausted phenotype among antigen experienced CD8+ tumour infiltrating lymphocytes from resected oesophageal adenocarcinomas, to characterise this population with regards to key surface markers and transcription factors, and to assess if such populations have a bearing on patient outcomes.

3.2 Results

3.2.1 Patient Characteristics

Between October 2018 and November 2021 a total of 45 oesophageal adenocarcinoma and 7 gastric adenocarcinoma samples were accessed through the Upper Gastro-Intestinal Tumour Ecology Study at University Hospitals Southampton. The majority of tissue was sampled at the time of resection surgery with curative intent, 41 oesophageal and all 7 gastric cancer specimens. The remaining 4 oesophageal cancer specimens were obtained during staging laparoscopic assessment prior to initiation of curative treatment and as such were labelled as treatment naïve. These 4 samples were analysed for phenotypic and functional information and were included as treatment naïve samples for this analysis as they were treatment naïve at the time of analysis, despite all 4 proceeding to neoadjuvant chemotherapy. Data related to these patients were not included in survival analysis given sampling was prior to neoadjuvant chemotherapy for all patients and at a different time point in their treatment pathway to the remainder of study participants.

Patients analysed in the oesophageal cancer group were predominantly male (82.2%) with a median age of 67 (range 38-82). Tumours were mostly in the distal oesophagus (66.6%) or gastro-oesophageal junction (31.1%), with all except one of pure adenocarcinoma histology. The non-

adenocarcinoma specimen was labelled an adenosquamous carcinoma of gastro-oesophageal junction on assessment following resection, due to residual squamous cell carcinoma fragments on regression of primary tumour, having initially been classified as an adenocarcinoma on diagnosis. This sample was included for analysis given the initial adenocarcinoma histology (Table 4).

The majority of patients whose tissue was sampled underwent neo-adjuvant treatment prior to surgical resection and tumour sampling, either with chemotherapy (40%), 88% of whom received the FLOT regimen (151), or with chemoradiotherapy (35.5%) (152). Two patients whose tumours were sampled at resection, had undergone additional neoadjuvant therapy with ant-PD-L1 immunotherapy durvalumab as part of the LUD2015-005 study, in addition to CROSS chemoradiotherapy (1 patient) and FLOT chemotherapy (1 patient). Data captured for these patients was used in for flow cytometric phenotyping, but not in RNA sequencing studies or functional assays given the unknown impact such therapies could have on long term T cell function (Table 4).

Characteristic	No. (%)
Median age (range) – yr	67 (38-82)
Male sex	37 (82.2%)
Pre-treatment modality (All patients)	(Total 45)
No pre-treatment	11 (24.4%)
Chemotherapy	18 (40%)
Chemoradiotherapy	16 (35.5%)
Tumour Location (All patients)	(Total 45)
Mid Oesophagus	1 (2.2%)
Distal Oesophagus	30 (66.6%)
GOJ	14 (31.1%)
Tumour Histology (All patients)	(Total 45)
Adenocarcinoma	44 (97.7%)
Adenosquamous	1 (2.2%)
Tumour Differentiation at resection (All patients)	(Total 45)
Well	6 (13.3%)
Moderate	11 (24.4%)
Poor	16 (35.6%)
NA	12 (26.7%)
Response to pre-treatment at resection (Neoadjuvant treated resection samples only)	(Total 30)
TRG1	9 (30.0%)
TRG2	6 (20.0%)
TRG3-5	15 (50.0%)
Pathological tumour staging at resection (All patients)	(Total 45)
pT0	10 (22.2%)
pT1	9 (20.0%)

pT2	7 (15.5%)
pT3	18 (40.0%)
pT4	1 (2.2%)
Pathological lymph node staging at resection (All patients)	(Total 45)
pN0	25 (55.5%)
pN1	13 (28.8%)
pN2	4 (8.8%)
pN3	3 (6.6%)

Table 4 Patient demographics and clinical characteristics of individuals with oesophageal tumours included in the study.

Alongside the label for each group in brackets is detailed which group of patients and how many are included in the analysis. The total number and percentage for each subgroup is detailed.

The intention of neoadjuvant treatment is to improve survival by treating both localised and systemic disease prior to definitive surgery. Differing immune responses were observed with regards to the nature of immune infiltrates following this. Post-operative routine histological assessment assigned each tumour undergoing pre-treatment a regression score using the Mandard tumour regression scoring system (207), a five-point scale with TRG1 representing complete tumour regression, and TRG5 no evidence of tumour regression (Appendix A). Patients with all tumour regression grades were sampled, though a higher proportion of tumour regression was noted in patients undergoing chemoradiotherapy.

The sample population is typical of those undergoing surgical resection of localised oesophageal adenocarcinomas, a disease we know to occur more frequently in males and with increasing incidence into the 7th decade of life (149,208). A mix of pathological staging and differentiation subtypes are observed which is reflective of tumours resected generally. Approximately 25% of tumour samples received, had experienced no exposure to neoadjuvant therapy, either due to lack of patient fitness for such treatment, patient choice, or samples being accessed during staging laparoscopy. A similar number of patients received chemotherapy and chemoradiotherapy (40 and 35.5% respectively). This is not entirely within keeping of practice at the study centre where there is a preference towards chemoradiotherapy, but a reflection of preferential sampling of patients undergoing chemotherapy or no pre-treatment, during the latter stages of this project. Therefore assumptions about the demographics and neoadjuvant therapies of patients undergoing resection surgery should not be taken from this small, though broadly representative sample size.

3.2.2 Flow Cytometry assessment

Flow cytometric phenotypic assessment of the CD8 T lymphocyte component of resected tumours was planned for the sample specimens. Tumour samples were received on ice directly from the theatre where surgical resection was taking place on the same site as all onward analysis ensuring ischaemic time on ice was kept to a minimum.

Tissue was immediately disaggregated into a single cell suspension utilising a protocol previously optimised by the academic surgery group and collaborators within the School of Cancer Sciences (209). Using a combination of enzymatic and mechanical disaggregation, the protocol has been shown to improve the release of a variety of cell types prior to high throughput single cell sequencing. This technique is comparable to other commonly used tumour disaggregation techniques (210).

All antibodies used for flow cytometry in this project were titrated using either peripheral blood mononuclear cells (PBMC) from healthy donors or other suitable control cell types expressing the marker of interest. This was undertaken to allow maximum discrimination between positive and negative staining, without antibody oversaturation resulting in false positives. This also avoids the financial cost of excess antibody use where not necessary. Samples were stained with varying concentrations of antibodies, (0.25, 0.5, 1, 1.5 and 2 times the manufacturer recommended concentration) and analysed using the flow cytometry equipment intended for use in the final experiment. The optimal antibody concentration was selected and taken forward for future experimental work.

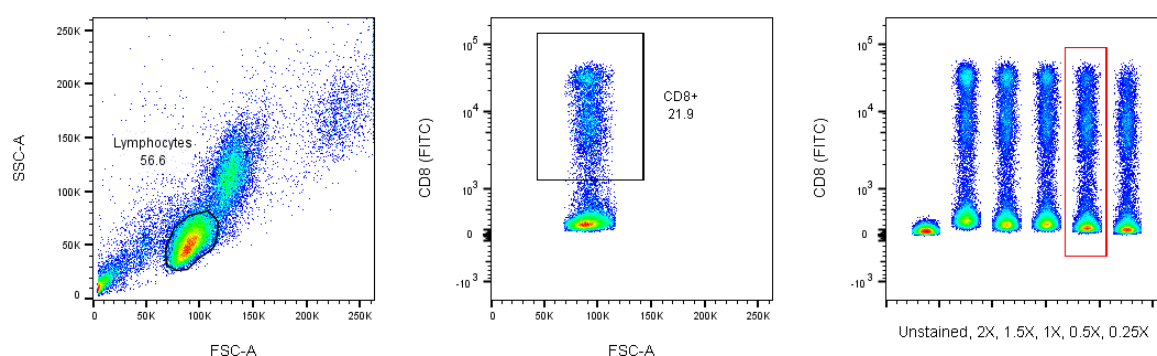


Figure 9 Exemplar antibody titration experiment showing anti-CD8a FITC antibody.

PBMC from healthy donor stained with increasing concentrations of antibody of interest (0X, 0.25X, 0.5X, 1X, 1.5X and 2X manufacturers recommended concentration) and then analysed on flow cytometer intended for use in final experiment. Lymphocytes gated and antibody positive population identified. Samples

concatenated and optimal concentration identified, 0.5X recommended, in this instance (highlighted in red).

PBMC from 6 healthy donors were collected from a leukocyte reduction system chamber (LRS cone) produced as a by-product of plateletpheresis and obtained from the NHS Blood and Transplant service. These cells were collected for use as controls to be used in experimental work and for assay optimisation. LRS cones were collected immediately following plateletpheresis and PBMC extracted using density gradient centrifugation with Ficoll Paque®. Recovered cells were counted and frozen in liquid nitrogen in a controlled freezing solution containing 10% DMSO, to allow thawing when needed.

Consideration was made to the suitability of storing disaggregated tumour for later analysis and comparisons were made between flow cytometric analysis on day of resection and at a later date after freezing. Attempts were made at disaggregating tumour samples snap frozen in liquid nitrogen immediately after resection, utilising mechanical or enzymatic techniques, though poor cell yields were obtained. Instead samples were disaggregated on receipt and then frozen in liquid nitrogen storage in a controlled freezing solution containing 10% DMSO.

Frozen samples were analysed by flow cytometry and comparisons made with matched samples that were analysed on the day of resection. It was observed that while some variation in the percentage of events gated as lymphocytes was observed, higher in frozen samples, the proportions of cells gated as positive for CD8, PD-1 and CD39 remained constant with no significant difference (Figure 10).

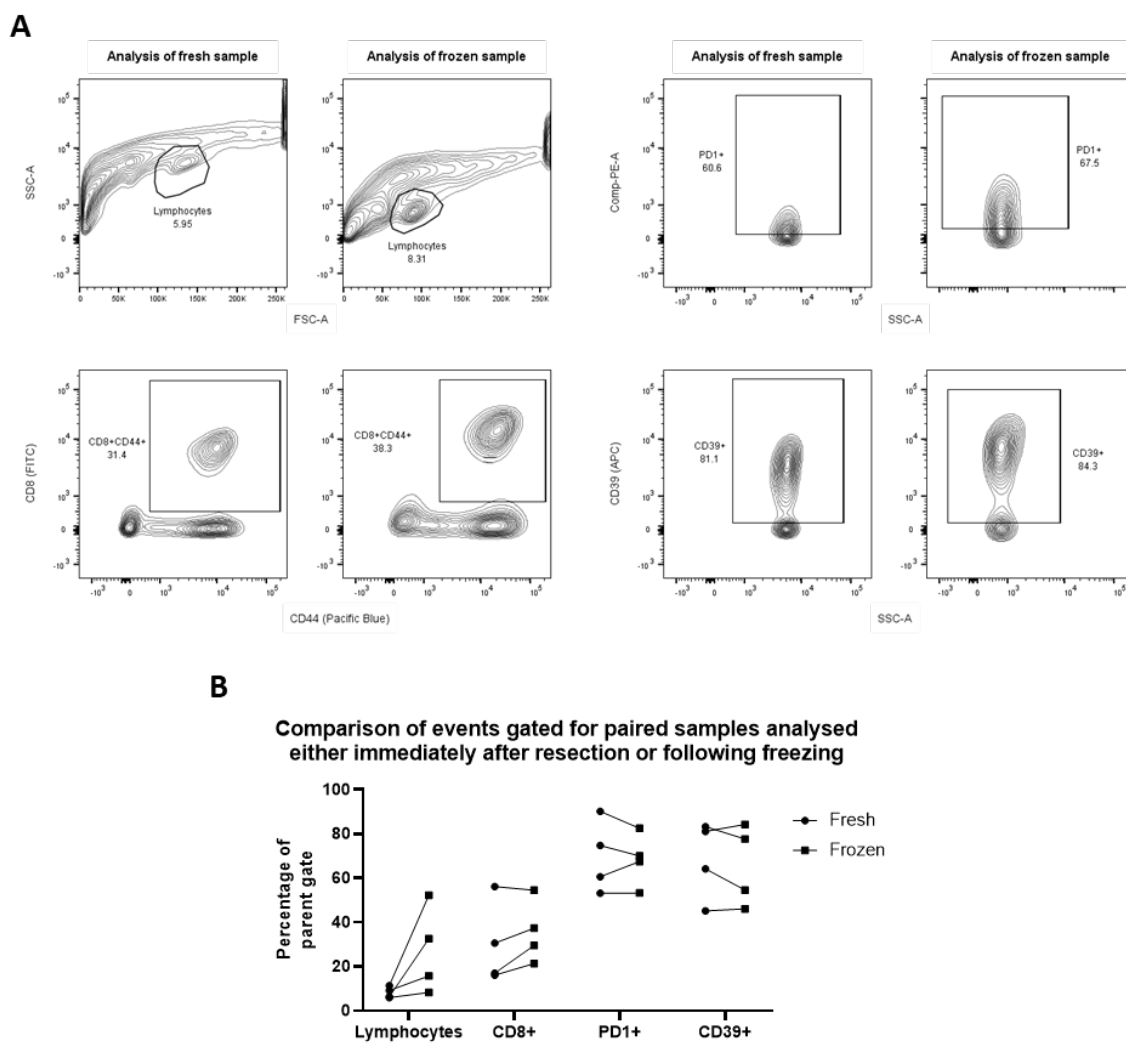


Figure 10 Comparison of fresh vs freeze-thawed sample analysis.

A) Exemplar flow cytometry plots comparing paired samples analysed immediately after resection and following freezing in 10% DMSO containing solution. Plots show percentage of all events gated morphologically as lymphocytes, percentage of lymphocytes gated as CD8+CD44+ and percentages of CD8+CD44+ lymphocytes gated as positive for PD-1 and CD39. B) Percentage of parent gate positive for specific markers, with paired samples analysed on the day of resection and disaggregation, and frozen samples analysed later. Lymphocytes are percent of all events gated morphologically as lymphocytes, CD8+ are percentage of single cell lymphocytes, PD-1+ and CD39+ are percentage of CD8+CD44+ lymphocytes gated positive for these markers.

The differences in the number of events gated as lymphocytes with a higher percentage seen post freezing, may well represent increased fragility and death of cancer cells during the freezing and thawing process skewing this percentage. The maintenance of the proportions of lymphocytes

gated as positive for CD8, PD-1 and CD39 is very encouraging, suggesting a robustness of this group of cells to the freezing and thawing process. These encouraging results allowed ongoing utilisation of freezing disaggregated tumour samples in 10% DMSO solution for analysis and future work in this project.

3.2.3 Lymphocyte infiltration

3.2.3.1 Immunohistochemistry analysis

An association between the degree of tumour lymphocyte infiltration and the speed of cancer progression has been observed over many decades in a range of cancers. The use of immunohistochemistry techniques has allowed the analysis of resected specimens and estimation of the effect the degree of infiltration of immune cells possessing specific lymphocyte markers has on tumour progression and patient survival. Increased infiltration by cells bearing the general lymphocyte marker CD3 as well as CD8, specific for cytotoxic T lymphocytes, have been associated with increased patient survival in numerous studies across a host of malignancies (211). The degree of T helper cell infiltration as defined by CD4, and regulatory T cell infiltration identified by FOXP3, have also been widely discussed and observed to be associated with superior and poorer prognosis respectively.

The picture in oesophageal cancer, and more specifically oesophageal adenocarcinoma, has been less clear. Early studies analysing the lymphocyte infiltration of oesophageal tumours found an independent correlation between increased intratumoural lymphocyte infiltration and survival in both oesophageal squamous cell carcinoma and adenocarcinoma (182). Further studies have confirmed the association between generalised T lymphocyte and CD8+ T lymphocyte infiltration and patient survival (27), though mixed results were observed for CD4+ T lymphocytes, and FOXP3+ regulatory T lymphocytes where not associated with survival (212). More recent and comprehensive meta-analysis of 30 studies including in excess of 5000 patients has found an association with better over-all survival with generalised lymphocyte infiltration, high CD8+ lymphocyte infiltration and CD4+ lymphocyte infiltration, though not with FOXP3 or CD3+ lymphocytes (205).

Immunohistochemistry allows the analysis of tissue samples fixed in formalin at the time of tumour resection and has great diagnostic value as well as research potential, including opening up historic specimens to research analysis. This technique allows spatial assessment of samples and the proximity of cells of interest to each other and their distribution throughout tumours. There are limits to these techniques however, particularly in the number of antibodies that can reasonably be incorporated into analysis. When investigating a highly heterogeneous cell

population such as cytotoxic T lymphocytes, more than a small handful of cellular markers are required for accurate classification. While multi-parametric immunohistochemistry techniques are increasingly available, to recreate the granularity achieved with flow cytometry is highly complex and expensive.

Currently work is ongoing by collaborators to utilise multidimensional immunohistochemistry approaches to build upon results obtained from traditional immunohistochemistry, and analyse oesophageal adenocarcinoma samples in a tissue microarray in order to explore factors related to antigen processing and lymphocyte function. While results from these experiments are in their infancy they have demonstrated high degrees of CD8+ lymphocyte infiltration deep into the tumour samples analysed and not excluded to the periphery. While the tissue microarray analysed is historic and not from samples shared with this study, they were collected at an identical patient time point to those used for this project. This adds confidence to the assumption that immune cells interrogated in this project are tumour infiltrating, and not from outside the area of interest, though this is not proven.

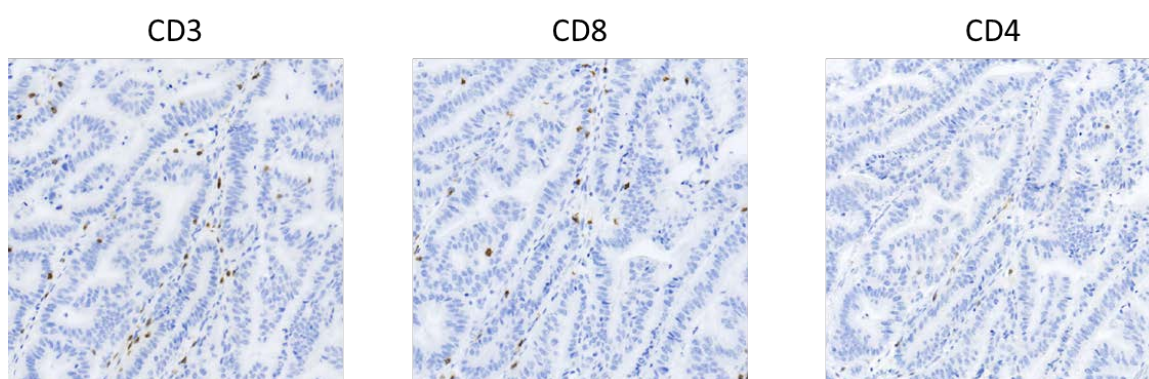


Figure 11 Immunohistochemistry staining of resected oesophageal adenocarcinoma specimen for lymphocyte markers.

Staining of tissue microarray oesophageal adenocarcinoma samples for the T lymphocyte proteins CD3, CD8 and CD4. Image prepared by and courtesy of William Pratt.

3.2.3.2 Flow cytometry analysis

Flow cytometric analysis of disaggregated oesophageal adenocarcinoma samples was undertaken and lymphocyte populations were identified using simultaneously analysed healthy donor PBMC samples with forward scatter and side scatter parameters discriminating them based upon cell size and granularity respectively.

Chapter 3

A lower percentage of events were gated as lymphocytes by flow cytometry in samples obtained from patients who have undergone neo-adjuvant chemoradiotherapy (mean 16.46) when compared to treatment naïve sample or those treated with chemotherapy (20.9 and 20.29 respectively) (Figure 12). A reduction in lymphocyte infiltrates post chemoradiotherapy has been observed elsewhere based upon analysis of pathological specimens, notably with a trend towards reduction of all lymphocyte subsets in the centre of oesophageal adenocarcinoma tumours when compared to the periphery following chemoradiotherapy pre-treatment, and significant reduction in FOXP3+ Tregs (212). Samples in this project are also samples from the centre of the resected tumours, potentially making the similarities more relevant. While the differences observed here did not reach statistical significance given the small sample size, they do fit with previously published results.

No significant difference in the number lymphocytes was observed when tumour stage or the degree of tumour regression to pre-treatment is considered. pT0 tumours and TRG1 groups overlap with no active cancer cells observed and as such could be expected to have a higher number of immune cells as a proportion of all events, and there is a suggestion of this, with a trend in the number of lymphocytes heading down with increasing stage and reduction in treatment response, though this is by no means clear or conclusive (Figure 12).

Several limitations must be taken into account when interpreting this flow cytometry data. Firstly a degree of selection bias is inevitable. Samples were collected from a varied group of patients who had undergone a mix of pre-treatment regimens, though this is not inclusive of the full range of patients who undergo resectional surgery. It was at times challenging to sample tumours that had undergone a good or complete response to pre-treatment due to the limited malignant material remaining. In such cases, a lack of tumour cells will mean a relative increased number of immune cells and other stromal cells, affecting the ratio of events calculated as lymphocytes. Additionally, as discussed earlier, the freeze-thaw process appears to increase the percentage of events gated as lymphocytes so the pre-processing techniques used will also have a bearing. Therefore any conclusions reached from this data must be taken as purely indicative. A clear demonstration of the need for this is the lack of difference in patient over-all survival and PFS among patients above or below the medium number of lymphocyte infiltrates identified by flow cytometry (Figure 12), when it is known that lymphocyte infiltration identified by immunohistochemistry can predict survival(205).

The advantage of flow cytometric analysis is that it allows extensive division of lymphocytes beyond the markers accessible with IHC, to gain greater understanding of the function and activity of the CD8+ compartment.

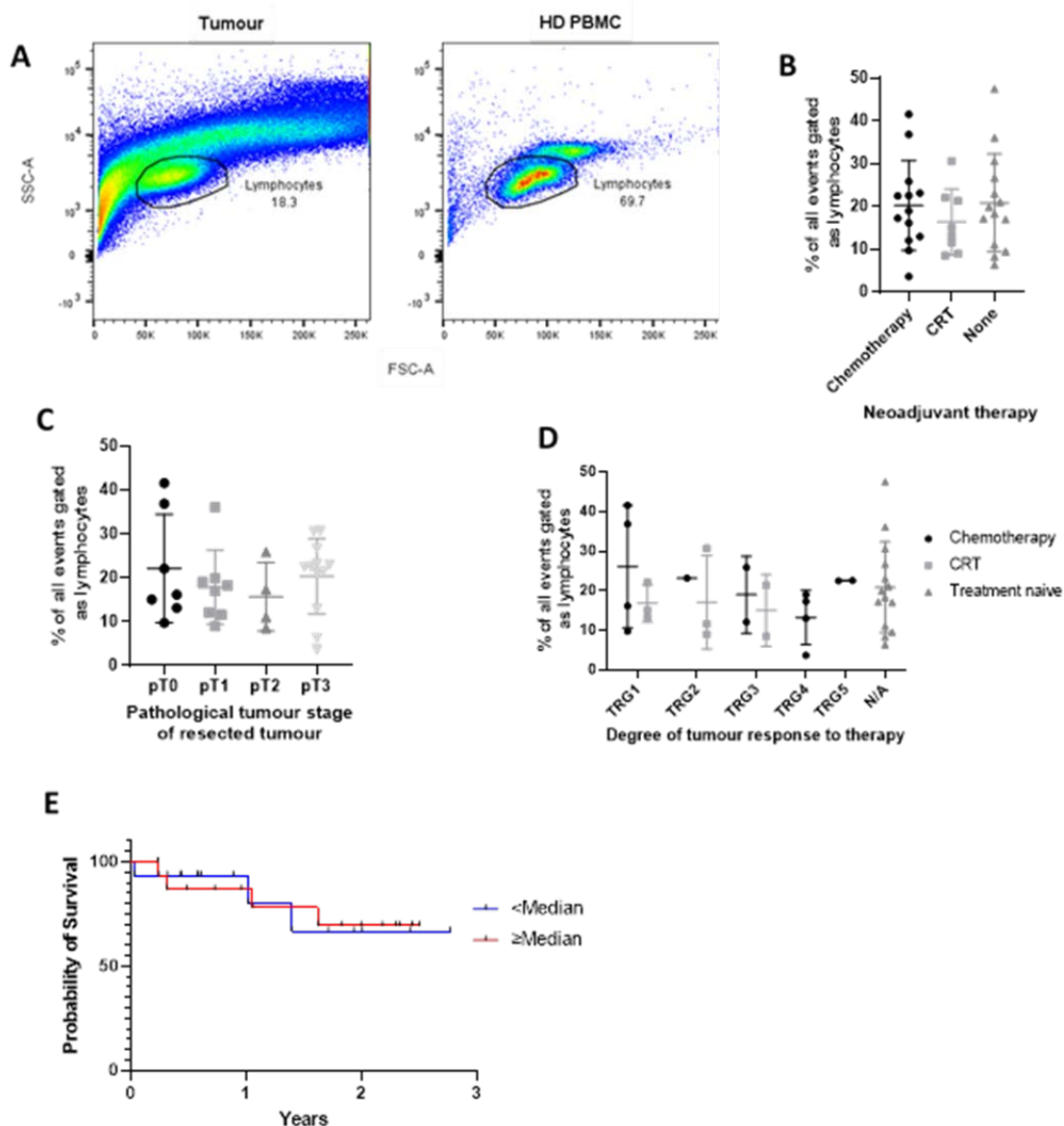


Figure 12 Lymphocyte infiltration in human oesophageal adenocarcinoma.

A) Exemplar flow cytometry plot showing gating of lymphocytes in human oesophageal adenocarcinoma and healthy donor peripheral blood mononuclear cells (HD PBMC). B) Percent of all events gated as lymphocytes from OAC samples analysed by flow cytometry by pre-treatment modality. C) Percent of all events gated as lymphocytes from OAC samples analysed by flow cytometry, by tumour pathological stage. D) Percent of all events gated as lymphocytes from OAC by pre-treatment regimen and degree of tumour response. E) Kaplan-Meier survival curves demonstrating overall survival of patients by degree of lymphocyte infiltration relative to the median percentage of events gated as lymphocytes. Hazard ratio (95% confidence interval) for \geq Median group 1.01 (0.22-4.49). All hazard ratios for Kaplan-Meier graphs in this chapter are calculated using the logrank test unless otherwise stated.

3.2.4 Antigen experienced CD8+ lymphocyte infiltration

Flow cytometric analysis was undertaken to analyse the CD8+ lymphocyte component of resected oesophageal adenocarcinomas. Fluorophore labelled antibodies were selected for use on the BD FACS Canto II flow cytometer, allowing identification of up to 6 antigens.

All samples were stained with antibodies for CD8a, the alpha isoform of the TCR co-receptor expressed on cytotoxic T lymphocytes, and CD44, a cell-surface glycoprotein found on numerous cell types including activated lymphocytes. Positivity for both markers allows identification of cytotoxic CD8+ lymphocytes that are activated and have thus experienced MHC class I bound antigen.

Lymphocytes were identified based upon size and granularity as described above, and single cells selected by removing doublets identified based upon measurement of forward scatter width and area measurements. A clearly definable population positive for both CD8a and CD44 was measured in both PBMC samples obtained from healthy donors, and lymphocytes infiltrating into oesophageal adenocarcinoma samples. The number of double positive, antigen experienced CD8+ T lymphocytes within the tumours can be calculated as a percentage of cells gated as lymphocytes and singlets.

The percentage of antigen experienced CD8+ T lymphocytes is highest in patients pre-treated with chemotherapy (mean 33.8%), and lowest within treatment naïve tumours (25.5%), with those treated with chemoradiotherapy at an intermediate level (30.7%). This picture of variation in CD8, CD44 double positive TILs based on pre-treatment regimen is lost when calculated as a proportion of all flow cytometry events, though as discussed previously this figure is a lot more prone to confounding variability compared to percentages of events gated as lymphocytes (Figure 13).

When analysed by pathological tumour stage at time of resection the percentage of lymphocytes positive for CD8 and CD44 increases in a statistically significant manner with increasing pathological stage from pT1 to pT3 (unpaired t test $p=0.0083$). pT0 tumours, the group containing no viable tumour cells was higher than pT1, as discussed previously there are challenges in taking specimens from regressed tumours so samples are likely to be of the tumour bed with fibrosis associated with necrotic tumour, rather than tumour seen in resected pT1-3 specimens. A higher percentage of immune cells may not be unexpected given this microenvironment (Figure 13).

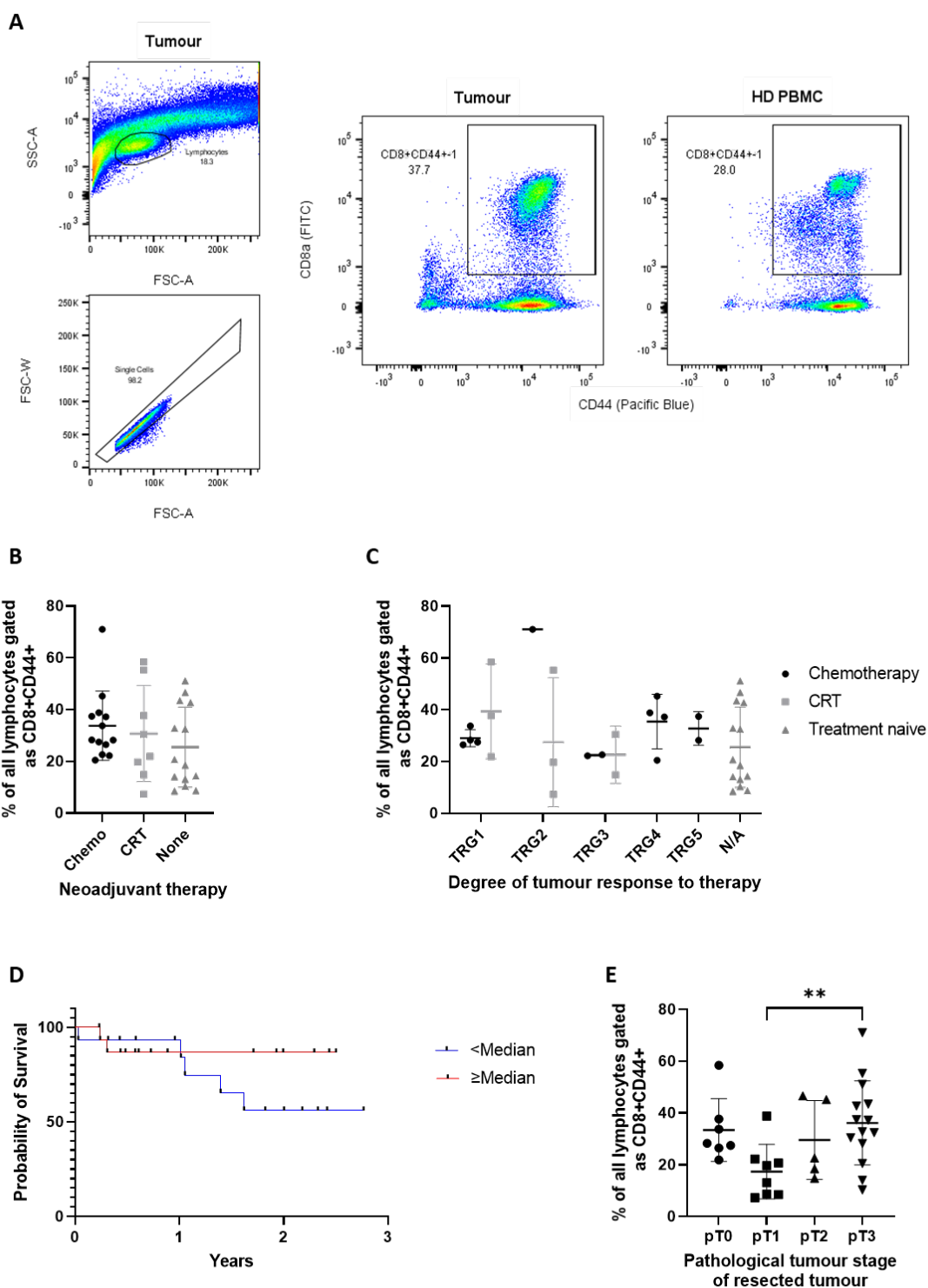


Figure 13 CD8+CD44+ tumour infiltrating lymphocytes from human oesophageal adenocarcinoma.

A) Exemplar flow cytometry plots showing gating of CD8+CD44+ lymphocytes in human oesophageal adenocarcinoma and healthy donor peripheral blood mononuclear cells. Lymphocyte population identified, singlets selected and CD8 and CD44 dual positive population selected. B) Percent of lymphocyte singlets gated as

CD8 and CD44 dual positive from OAC samples analysed by flow cytometry by pre-treatment modality. C) Percent of lymphocyte singlets gated as CD8 and CD44 dual positive by pre-treatment regimen and degree of tumour response. D) Kaplan-Meier graph demonstrating overall survival of patients by percentage lymphocytes gated as CD8 and CD44 dual positive, with respect to the median. Hazard ratio (95% confidence interval) for \geq Median group 0.44 (0.10-1.92). E) Percent of all events gated as CD8 and CD44 dual positive lymphocytes from OAC samples analysed by pathological staging of tumour at time of resection. Statistical significance of difference calculated using unpaired t-test. * denotes p value <0.05 , ** <0.01 , *** <0.001 , **** <0.0001 . Statistical significance will be calculated and labelled as such throughout this chapter unless otherwise stated.

No clear pattern is observed for percentage of CD8 and CD44 positivity by degree of tumour regression, either when observed by pre-treatment regimen or as a whole cohort.

Analysis of patient overall survival (OS) and progression free survival can be undertaken separating individuals into those with high or low percentages of CD8+CD44+ lymphocytes when compared to the median. The median is chosen for division of patients into groups not for any pre-specified biological reason, but to allow unbiased explorative analysis. It is observed that those with a high percentage of antigen experienced CD8+ TILs among lymphocyte infiltrates show increased survival, with 2 year OS of 86% for those with greater than or equal the median and 56% for less than median. Median follow-up of all individuals was 1.93 years (Figure 13).

There is no clear data within the literature on the effects of antigen experience among CD8+ infiltrates on disease control or survival in oesophageal cancer. CD44 is commonly used as a marker to identify antigen experienced effector/memory lymphocytes compared to naïve lymphocytes, often in combination with a marker like CD62 Ligand/L-selectin which is reciprocally expressed, though given the limited antibody panel used this was not included.

From a mechanistic perspective, such a finding is intuitive, as for immune control of progressing cancers activated antigen specific cytotoxic T lymphocytes that have capacity to undertake killing of tumour cells are required within the tumour microenvironment. This data does not provide information about the ratio of such potentially cytotoxic lymphocytes, with inhibitory immune cells, or their position within the tumour microenvironment with regard to the cancer cells, but a correlation with percentage of lymphocytes does appear apparent with survival.

3.2.5 PD-1 and CD39

3.2.5.1 PD-1

In addition to markers to identify antigen experienced CD8 T lymphocytes all patient samples were stained with antibodies specific for PD-1 and CD39.

The activation and exhaustion marker PD-1 has been a key surface marker to understanding lymphocyte dysfunction and exhaustion in response to chronic antigen exposure. PD-1 is expressed to a moderate degree at the cell surface on CTL activation, and at a higher concentration on chronic stimulation associated with exhaustion (94). The discovery that blocking its activity through antagonistic antibodies, could reverse this dysfunction and cause meaningful immune mediated tumour control, culminating in the widespread adoption of anti-PD-1 monoclonal antibody therapies has led to significant interest and research.

After numerous clinical studies investigating the benefit of PD-1/PD-L1 antagonism in oesophageal adenocarcinoma, a place for immunotherapy is being elicited by using biomarker based approaches to select patients. Studies such as the Checkmate 649 study which demonstrated a benefit from first line chemo-immunotherapy in metastatic disease(192), and Checkmate 577 (166), which showed a place for adjuvant nivolumab in resected tumours without optimal response to neoadjuvant chemoradiotherapy, have highlighted the potential for immunotherapy in this disease. These studies have shown reasonable responses, but even when selecting patients with high PD-L1 expression, expected to have high lymphocyte infiltration, over half of patients will show no response.

Disaggregated oesophageal adenocarcinoma samples were analysed by flow cytometry and lymphocyte singlets were identified as previously stated. CD8+CD44+ lymphocytes were then assessed for degree of PD-1 positivity, defined using PBMCs from healthy donors and FMO controls. Analysis of this population showed a significant increase in PD-1 expression in antigen experienced CD8 TILs when compared to PBMCs from healthy donors.

Compared to chemoradiotherapy and treatment naïve tumours, samples post chemotherapy possessed a higher percentage of total lymphocytes that are CD8+CD44+PD-1+ (means 23.9% vs 14.7% and 18.8% respectively). Conversely, the percentage of CD8+/CD44+ lymphocytes positive for PD-1 was highest for treatment naïve specimens (mean 66.8%), when compared with those treated with CRT (48.9%) and chemotherapy(66.1%). A low percentage of CD8+CD44+ lymphocytes from healthy donor PBMCs were positive for PD-1 (mean 8.5% of 4 donors) (Figure 14).

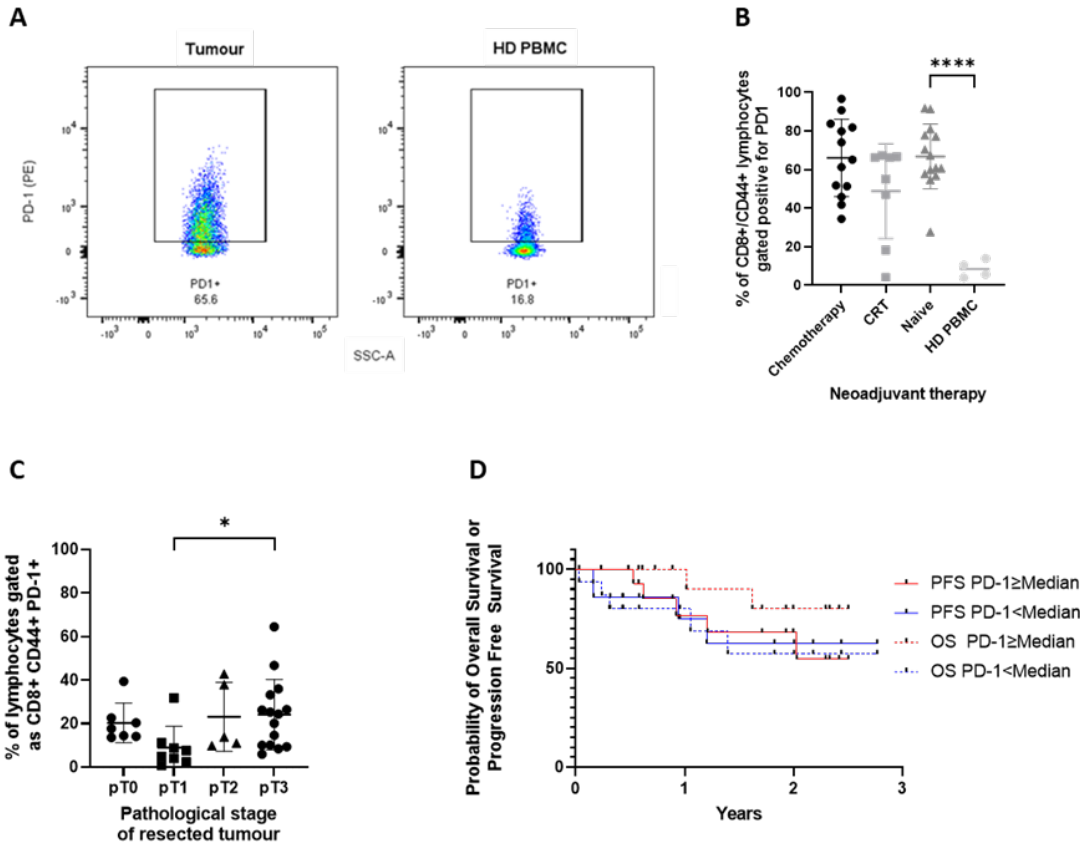


Figure 14 PD-1 expression on CD8+CD44+ tumour infiltrating lymphocytes from human oesophageal adenocarcinoma.

A) Exemplar flow cytometry plot of showing gating of PD-1 positivity among CD8+CD44+ lymphocyte singlets from human oesophageal adenocarcinoma and healthy donor peripheral blood mononuclear cells. Gating for CD8+CD44+ lymphocyte singlets as described above. B) Percent of CD8+CD44+ lymphocyte singlets gated as positive for PD-1 from OAC samples analysed by flow cytometry by pre-treatment modality and from PBMC collected from healthy donors. Significant difference between percentage positive in treatment naïve TILs vs HD PBMC ($p < 0.0001$). C) Percent of lymphocyte singlets gated as CD8+CD44+PD-1+ by pathological tumour stage at resection. D) Kaplan-Meier graph demonstrating overall survival and progression free survival of patients by percentage CD8+CD44+ lymphocyte singlets gated as PD-1 positive with respect to the median result. Hazard ratio (95% confidence interval) for \geq Median group in overall survival analysis 0.31 (0.06-1.37) and for \geq Median group in progression free survival analysis 0.89 (0.24-3.36).

The intensity of staining for PD-1 was higher on TILs from tumour samples than that seen on PD-1 positive lymphocytes from healthy donors. It has been mentioned that PD-1 is expressed on T cell

activation, but is expressed at a higher frequency on lymphocytes undergoing dysfunction due to chronic antigen exposure. Additionally it has been noted in NSCLC that CD8+ TILs expressing high levels of PD-1, can be considered a population enriched for tumour reactive lymphocytes, associated with a distinct transcriptional and functional profile in keeping with impaired effector functions, while also associated with increased response to immune checkpoint blockade(94), an observation that may be relevant in OAC.

There is a trend towards higher PD-1 expression with increasing tumour stage from T1 to T3 at resection. T0 tumours showed an intermediate level of PD-1 positive CD8+ TILs and only one T4 tumour was analysed. This trend was a suggestion when the PD-1 positivity was calculated as a percentage of CD8+CD44+ TILs but became statistically significant for T1 compared to T3 tumours when CD8+CD44+PD-1+ TILs were calculated as a percentage of all lymphocytes (mean 8.96% vs 25.1%, $p=0.0198$). No discernible trend was observed when PD-1 positivity among CD8+CD44+ lymphocytes, all lymphocytes or total events were analysed in the context of degree of tumour regression (Figure 14).

Patient overall survival and progression free survival was assessed in the context of PD-1 expression either above or below the median value for CD8+CD44+ lymphocytes. It is observed that overall survival is increased among patients with a higher percentage of PD-1 positivity (2-year OS 80%) compared to those with a PD-1 positivity percentage below the median (2-year OS 62.5%). This is in spite of the findings described above where PD-1 expression was highest in bulkier tumours, which we might expect to indicate more lymphocyte dysfunction, larger mass of cancer and higher risk of negative patient outcomes. This could suggest a biological advantage to higher numbers of PD-1 positive TILs rather than it being representative of advancing cancer (Figure 14).

3.2.5.2 CD39

The ectonucleoside triphosphate diphosphohydrolase 1, CD39, is encoded by the *ENTPD-1* gene and is expressed by various immune and non-immune cells. This extracellular enzyme, in combination with CD73, acts to bind and hydrolyse extracellular ATP (eATP) and convert this into adenosine. As discussed it acts to promote an immune inhibitory environment, and its expression on cytotoxic T lymphocytes has been associated with an exhausted phenotype, as well as enriching for tumour reactive and tissue resident memory cell populations (122,129).

Antigen experienced CD8+ TILs from oesophageal adenocarcinomas display a clearly definable population of CD39+ cells, not present in a corresponding population from healthy donor PBMCs and defined using FMO samples. This population is present across samples regardless of pre-

Chapter 3

treatment, but is of highest frequency in treatment naïve specimens (mean 60.1% of CD8+CD44+ lymphocytes positive for CD39), with those undergoing chemotherapy (mean 50.4%) also expressing high levels of CD39 positivity, and CRT treated specimens the lowest (mean 40.1%). A very low percentage of CD8+CD44+ lymphocytes from healthy donor PBMCs were positive for CD39 (mean 1.99% from 4 separate donors). This is in keeping with results observed elsewhere where estimates have ranged up to approximately 6% of CD8+ lymphocytes from HD PBMCs, a number far below those seen in tumour infiltrating lymphocytes (129,131). There is unsurprisingly a strongly statistically significant difference between these healthy donor PBMCs and treatment naïve TILs ($p=0.0001$) (Figure 15).

There is no clearly significant association with degree of tumour regression, though potentially fewer CD39+ TILs are observed in progressing tumours. As with PD-1 positivity, there is a trend towards higher CD8+CD44+CD39+ TILs as a percentage of all lymphocytes, with increasing pathological tumour stage. This is not statistically significant based upon the current sample but is distinct and is again in keeping with a potentially more dysfunctional TIL population within bulkier tumours (Figure 15).

Overall survival and progression free survival are observed to be higher in patients whose resection specimens contained a percentage of CD39+ cells among antigen experienced CD8+ lymphocyte infiltrates that was greater than the mean (2 year OS 93.8% and PFS 72.7% vs 48.1% and 45% respectively), this is in a similar manner to the increased survival seen in PD-1 positivity among this TIL population (Figure 15).

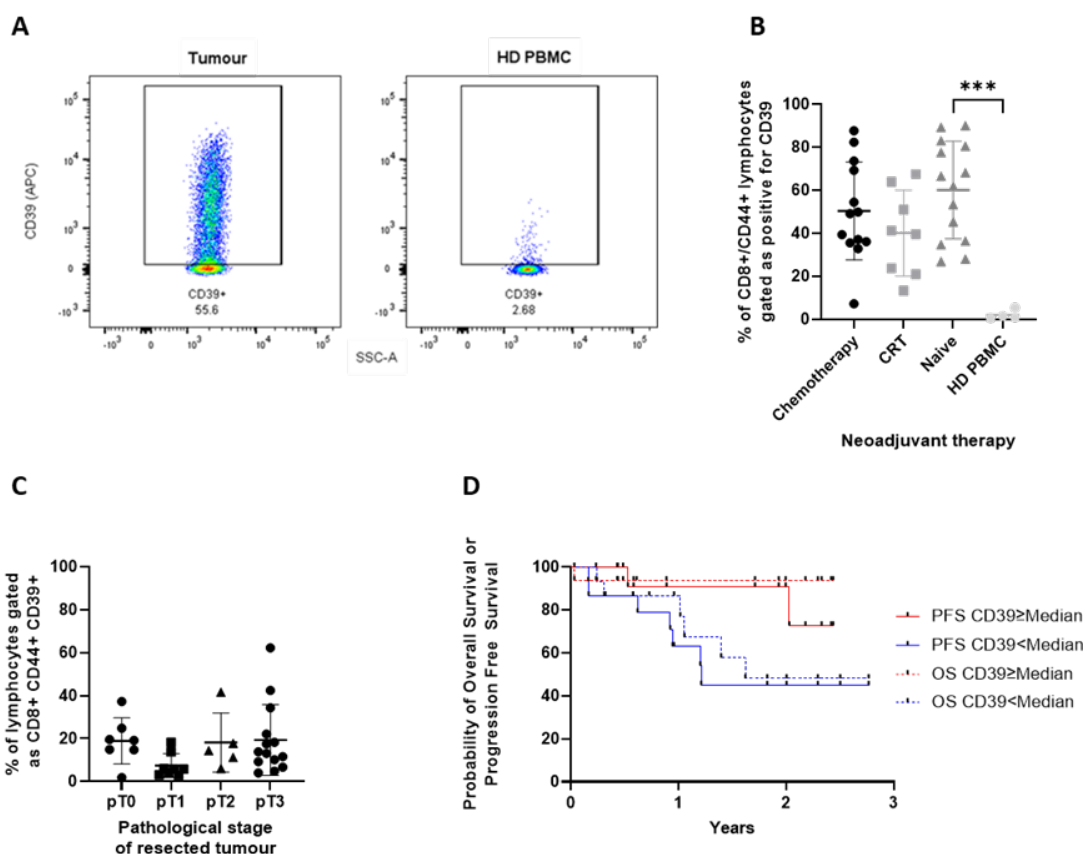


Figure 15 CD39 expression on CD8+CD44+ tumour infiltrating lymphocytes from human oesophageal adenocarcinoma.

A) Exemplar flow cytometry plot showing gating of CD39 positivity among CD8+CD44+ lymphocyte singlets from human oesophageal adenocarcinoma and healthy donor peripheral blood mononuclear cells. Gating for CD8+CD44+ lymphocyte singlets as described above. B) Percent of CD8+CD44+ lymphocyte singlets gated as positive for CD39 from OAC samples analysed by flow cytometry by pre-treatment modality and from PBMC collected from healthy donor. C) Percent of lymphocyte singlets gated as CD8+CD44+CD39+ by pathological tumour stage at resection. D) Kaplan-Meier graph demonstrating overall survival and progression free survival of patients by percentage CD8+CD44+ lymphocyte singlets gated as CD39 positive with respect to the median percentage positive. Hazard ratio (95% confidence interval) for \geq Median group in overall survival analysis 0.16 (0.04-0.70) and for \geq Median group in progression free survival analysis 0.27 (0.07-1.01).

Given the potential features that CD39 positivity can be associated with, there could be numerous hypotheses for improved survival. It is plausible that more tumour specific T lymphocytes would equate to better control of tumours, tissue resident memory cells have been associated with

responses to immunotherapies and tumour control, and potential association with PD-1 and subsequently PD-L1 could suggest increased infiltration and less immune exclusion. Additionally the propensity for some larger tumours to possess high numbers of CD39+ TILs suggests differences in survival is not solely related to tumour stage at the time of surgery.

3.2.5.3 PD-1 and CD39 dual positivity

The presence of clearly defined PD-1 positive and CD39 positive populations among antigen experienced CD8 TILs from oesophageal adenocarcinoma raises the question of whether these populations overlap. With both markers being associated with lymphocyte activation, progressing dysfunction and exhaustion an association between these groups was expected.

Analysis of early samples in this study revealed a clearly definable double positive population in the majority of specimens which was sizable and often in excess of 25% of all antigen experienced CD8+ TILs. By collating data from all samples collected it can be observed that the PD-1, CD39 double positive population accounts for a greater proportion of CD8+CD44+ TILs from tumours naïve to pre-treatment (mean 47.1%) and those exposed to chemotherapy (mean 37.2%) compared to those treated with chemoradiotherapy (mean 26.8%). Conversely the chemoradiotherapy group has the highest percentage of PD-1 and CD39 double negatives among antigen experienced CD8+ TILs (mean 37.8%) (Figure 16). When PBMCs from healthy donors are analysed, a mean of 0.6% of CD8+CD44+ lymphocytes were double positive for PD-1 and CD39 (from 4 separate donors).

There is a clear survival advantage among patients with high percentage of PD-1+CD39+ lymphocytes among their antigen experienced TILs and when calculated as a percentage of total lymphocyte infiltrates. The advantage is less clear when progression free survival is calculated but still appreciable (Figure 16).

It is difficult to see a clear association between the degree of tumour regression and the percentage of PD-1 CD39 double positive TILs, though TRG1 samples, demonstrating a complete pathological response do appear to have a higher than average number of this phenotype. It is difficult to make a clear assessment given the limited data points in some groups, with a range of percentages of DP lymphocytes observed across tumour regression scores. On further analysis of the data a clear association between degree of regression and survival is demonstrated, not displayed, as would be expected given historic data, with no relapses or deaths in individuals achieving a complete pathological response to neoadjuvant therapy, and the worst PFS and OS is observed in patients with signs of tumour progression after treatment and T3 or T4 tumours at

time of surgery.

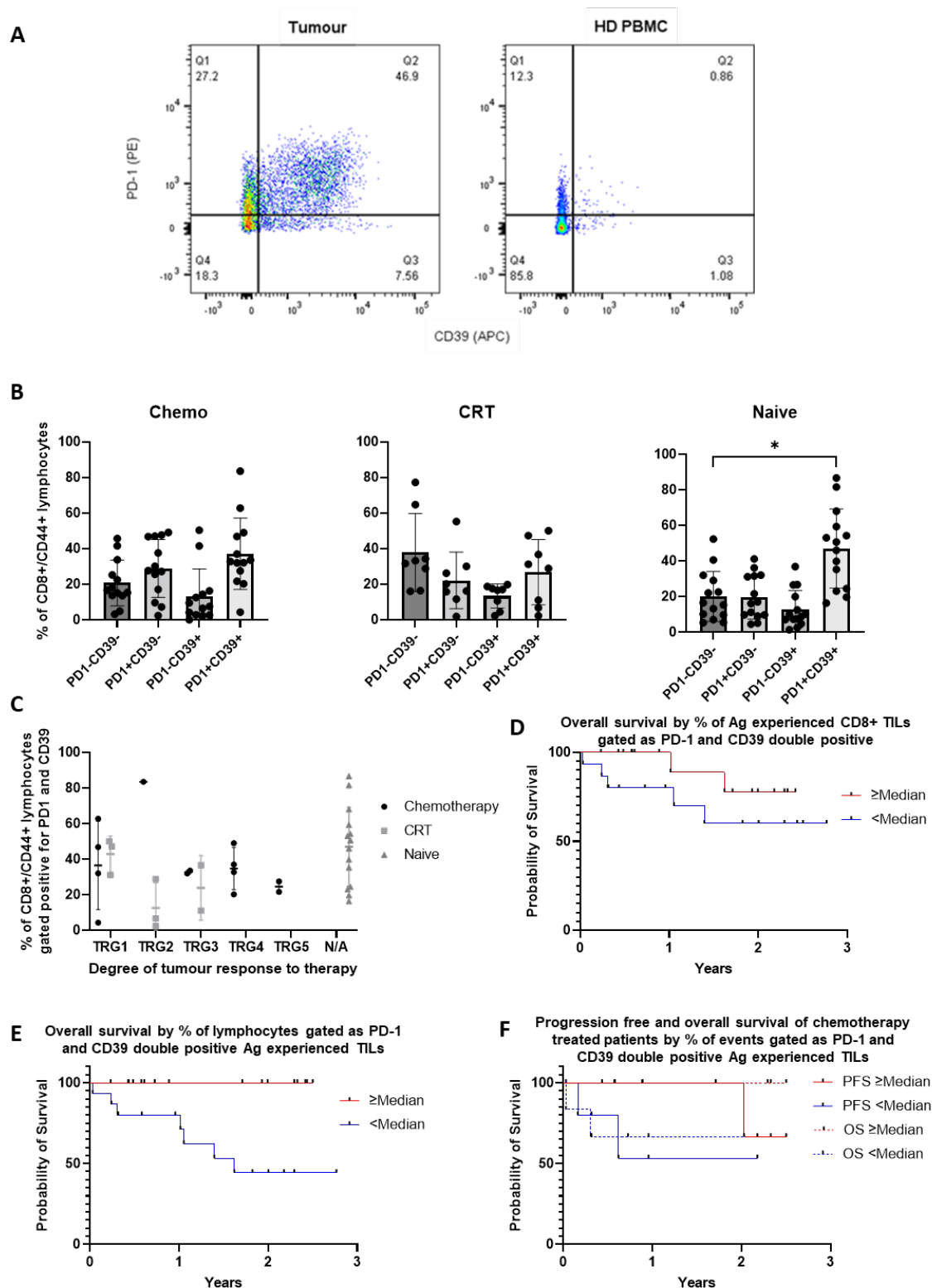


Figure 16 PD-1 and CD39 dual expression on CD8+CD44+ tumour infiltrating lymphocytes from human oesophageal adenocarcinoma.

A) Exemplar flow cytometry plots showing gating of PD-1 and CD39 dual positivity among CD8+CD44+ lymphocyte singlets from human oesophageal adenocarcinoma

and healthy donor peripheral blood mononuclear cells. Gating for CD8+CD44+ lymphocyte singlets as described above. B) Percent of CD8+CD44+ lymphocyte singlets gated as positive or negative for PD-1 and CD39 from OAC samples analysed by flow cytometry. Separate graphs for specimens from patients that have received neoadjuvant chemotherapy, chemoradiotherapy or were treatment naïve. C) Percent of CD8+CD44+ lymphocyte singlets gated as positive for PD-1 and CD39 by pre-treatment regimen and degree of tumour response. D) Kaplan-Meier graph demonstrating overall survival of patients by percentage CD8+CD44+ lymphocyte singlets, double positive for PD-1 and CD39, with respect to the median percentage positive. Hazard ration (95% confidence interval) for \geq Median group 0.36 (0.08-1.57). E) Overall survival of patients by percentage of all events gated as lymphocyte singlets, double positive for PD-1 and CD39, with respect to the median percentage positive. Hazard ration (95% confidence interval) for \geq Median group 0.12 (0.02-0.54) (Calculated using Mantel-Haenszel method). F) Progression free survival and overall survival of patients by percentage of all events gated as lymphocyte singlets double positive for PD-1 and CD39 with respect to the median percentage positive for patients pre-treated with chemotherapy alone. Hazard ration (95% confidence interval) for \geq Median group in overall survival analysis 0.10 (0.006-1.67) (Calculated using Mantel-Haenszel method) and for \geq Median group in progression free survival analysis 0.26 (0.02-2.87).

Given the relatively small sample cohort here it can be difficult to elucidate if the survival benefit seen is due to pre-treatment strategy, degree of response to therapy, pathological T stage at surgery, among other patient factors. What can be observed however, is that analysis of the chemotherapy treated group alone, the largest cohort available for survival analysis, shows that individuals with a percentage of DP TILs greater than or equal to the median, had a greater PFS and OS than those below the median. OS at 2 years was 100% with greater than or equal to the median and 66.6% below the median. PFS at 2 years was similarly 100% and 53.3% respectively. Similar trends are observed when chemoradiotherapy pre-treated patients and treatment naïve patient samples are analysed, though the number included for analysis is lower (Figure 16).

The differences in overall and progression free survival detailed here are of real interest with a high percentage of PD-1 CD39 double positive lymphocytes associated with improved patient outcomes across all pre-treatment groups. The observation that this phenotype was abundant in some treatment naïve samples, a group we may expect to fare poorly given their suboptimal therapy pre-surgery, but is still associated with better outcomes, also adds weight to this association.

In order to better understand the nature of this double positive group, further flow cytometric analysis has been undertaken to characterise these cells further. Given the weight of evidence delineating the role of PD-1 principally, but also CD39, in lymphocyte exhaustion, a focus has been directed into the expression of surface markers of exhaustion, as well as the crucial T-box transcription factors T-bet and eomesodemin (Eomes) which play important roles in regulating cellular processes of early and late lymphocyte exhaustion respectively. It remains important to note however that PD-1, CD39 and CD44 are all known to be expressed in effector, memory and tissue resident memory CD8+ phenotypes, and while lymphocyte exhaustion is a widely studied phenomenon observed among tumour infiltrating lymphocytes, it is not necessarily the only process at play in this population.

3.2.6 Tbet and Eomes

To shed light onto the composition of the PD-1+CD39+ double positive (DP) population of antigen experienced CD8+ lymphocytes, and in particular to compare them with the corresponding PD-1-CD39- double negative population (DN), T-bet and Eomes were selected for assessment by flow cytometry alongside the combination of extracellular markers discussed above, CD8a, CD44, PD-1 and CD39.

As discussed previously, T-bet controls normal effector cell differentiation in CD8+ and CD4+ lymphocytes as well as regulating the progenitor-exhausted phenotype by suppressing PD-1 and other inhibitory co-receptors. Eomes conversely, has a role to play in facilitating memory cell formation, and in exhaustion has been shown to signal transcription of the inhibitory receptors suppressed by T-bet in the LCMV model of exhaustion (29). Observations in cancer have been mixed, and highlighted a context specificity. In a murine cancer model described by Schietinger et al. increased Eomes expression is not observed with a progressive exhausted phenotype, but rather loss of T-bet and Eomes is observed(81).

Given that the DN population are all antigen experienced CD8+ lymphocytes we would expect this population to be high in T-bet, but low in Eomes. The DP group however could display a range of expression profiles of the transcription factors depending on the degree of exhaustion, and the reciprocity of T-bet and Eomes in oesophageal cancer.

PBMC from healthy donors stained with the intracellular antibodies and FMO samples were used to identify populations as T-bet high or low, and Eomes high or low. This is typically reported in the literature rather than positive or negative, as particularly with T-bet, there is no definable negative population. Given the reciprocal relationship of the two T-box transcription factors, T-bet^{High} Eomes^{Low} and a T-bet^{Low} Eomes^{High} populations were outlined as detailed below. It would be

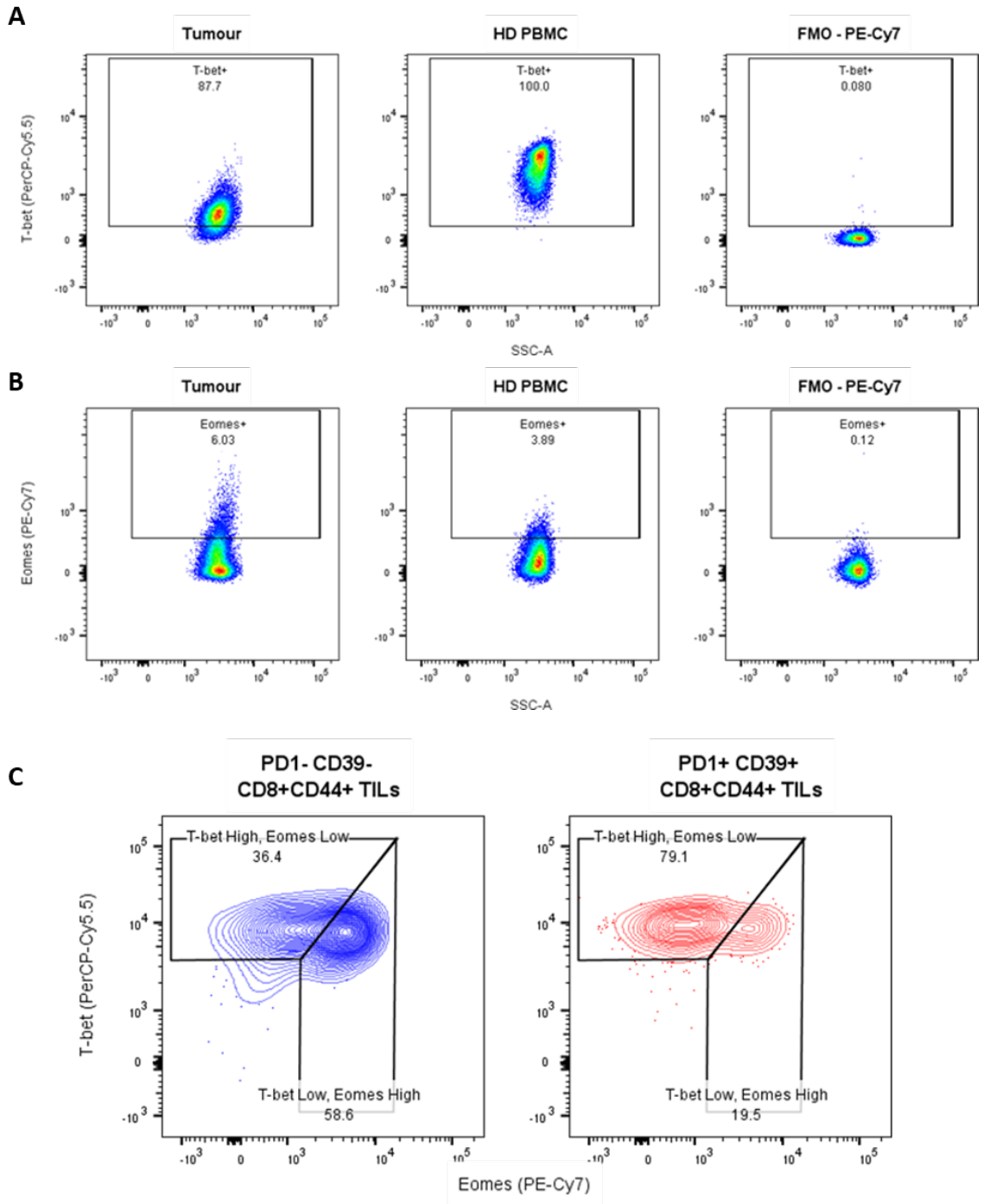
Chapter 3

expected that if the DP population were terminally exhausted due to their continued antigen engagement, then this group may enrich for the T-bet^{Low} Eomes^{High} phenotype.

It was observed however, that the PD-1+ CD39+ DP group (mean 22.15%), along with the PD-1- CD39+ group (mean 17.85%) possessed a low abundance of T-bet^{Low} Eomes^{High} lymphocytes. A higher frequency of this group was observed in the PD-1- CD39- DN group (mean 37.84%) and the PD-1+ CD39- group (47.36%) (Figure 17).

The DP group demonstrated a high proportion of T-bet^{High} Eomes^{Low} (mean 64.2%), higher than the other groups including the DN population (mean 40.6%).

Direct comparisons of the DP and DN populations shows a statistically significant difference in the proportion of CD8+CD44+ TILs shown to be Tbet^{High}Eomes^{Low} with a higher percentage among the DP group (p=0.0048). Based upon the literature of lymphocyte exhaustion, the possession of this combination of T-box transcription factors would indicate early exhaustion, and counters a hypothesis that the DP group is composed predominantly of a terminally differentiated exhausted lymphocyte population. This is further reinforced with comparison of Tbet^{Low}Eomes^{High} events between groups, where the DP group has a lower abundance (p=0.0193) (Figure 17).



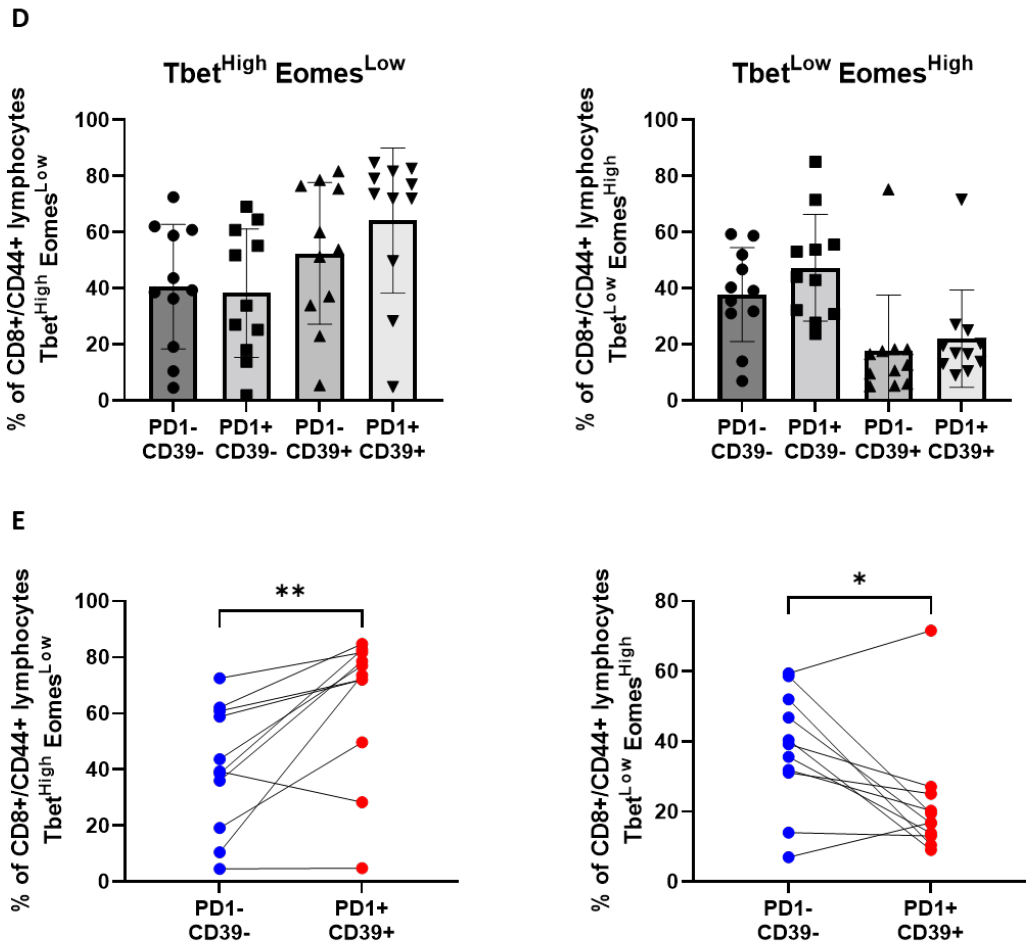


Figure 17 T-bet and Eomes expression by CD8+CD44+ tumour infiltrating lymphocytes from human oesophageal adenocarcinoma.

A and B) Exemplar flow cytometry plots showing gating of T-bet (A) and Eomes (B) positivity among CD8+CD44+ lymphocyte singlets from human oesophageal adenocarcinoma and healthy donor peripheral blood mononuclear cells on full staining and utilising an FMO. Gating for CD8+CD44+ lymphocyte singlets as described above. C) Flow cytometry plots demonstrating difference in staining of T-bet and Eomes among antigen experienced CD8+ T lymphocytes that are either PD-1 and CD39 DP or DN. Difference in proportion of events gated as Tbet^{High}Eomes^{Low} and Tbet^{Low}Eomes^{High} displayed. D) Flow cytometry results of human oesophageal adenocarcinoma samples showing percentage of CD8+CD44+ TILs either gated as Tbet^{High}Eomes^{Low} (left) or Tbet^{Low}Eomes^{High} (right) for different groups depending on positivity for PD-1 and CD39. E) Comparison made of percentage of CD8+CD44+ TILs that are Tbet^{High}Eomes^{Low} or Tbet^{Low}Eomes^{High} among PD-1 and CD39 DN and DP populations. Statistical significance of difference in percentage of test group between

DN and DP populations calculated using a paired t-test, (Tbet^{High}Eomes^{Low} $p=0.0048$, Tbet^{Low}Eomes^{High} $p=0.0193$).

3.2.7 Cell surface markers of exhaustion

Further flow cytometry panels were developed for use on the same equipment to assess surface markers of exhaustion. The core markers of anti CD8a, CD44, PD-1 and CD39 antibodies were maintained, with an additional 2 antibodies included in each panel. When selecting further markers, particular note was made of the work by Bengsh et al. who undertook high dimensional cytometry using CyTOF profiling of lymphocyte exhaustion from various contexts as well as RNA seq and epigenetic analysis. A large number of clusters of exhausted lymphocytes were identified using these single cell techniques, allowing detail about the various stages of dysfunction to be appreciated, with the results then mapped onto data related to lymphocytes in human disease including HIV, CMV and lung cancer (44). Surface markers were selected for investigation based upon those most differentially expressed in severe viral illness and cancer, including the archetypal exhaustion markers TIM3 and LAG3, as well as a panel adding TIGIT to TIM3, and a final panel including CD38 and CD244 (2B4).

All antibodies were titrated as previously discussed to identify the optimal concentrations for staining. Human oesophageal adenocarcinoma samples in liquid nitrogen were thawed and analysed alongside HD PBMCs as previously described. Samples of PBMC from healthy donors labelled with all antibodies but the marker of interest were used (FMO), to identify cells positive for the marker of interest and allow calculation of the percentage positive (Figure 18).

3.2.7.1 TIM3 and LAG3

The T-cell immunoglobulin and mucin-domain containing-3 (TIM3) or Hepatitis A virus cellular receptor 2 (HAVCR2) has been discussed as a marker of dysfunction, and for its inhibitory mechanism on activated CTLs. TIM3 has been identified as being expressed on oesophageal cancers previously, as well as being identified on the most exhausted TILs in other malignancies (144).

TIM3 showed a generally low level of expression on antigen experienced CD8+ TILs from oesophageal adenocarcinoma specimens (mean 5.1%). This was higher than that seen among healthy donor controls, though not by a large margin (mean 3.6%), and given the small number of different healthy donors analysed not of statistical significance using the unpaired t test (Figure 18).

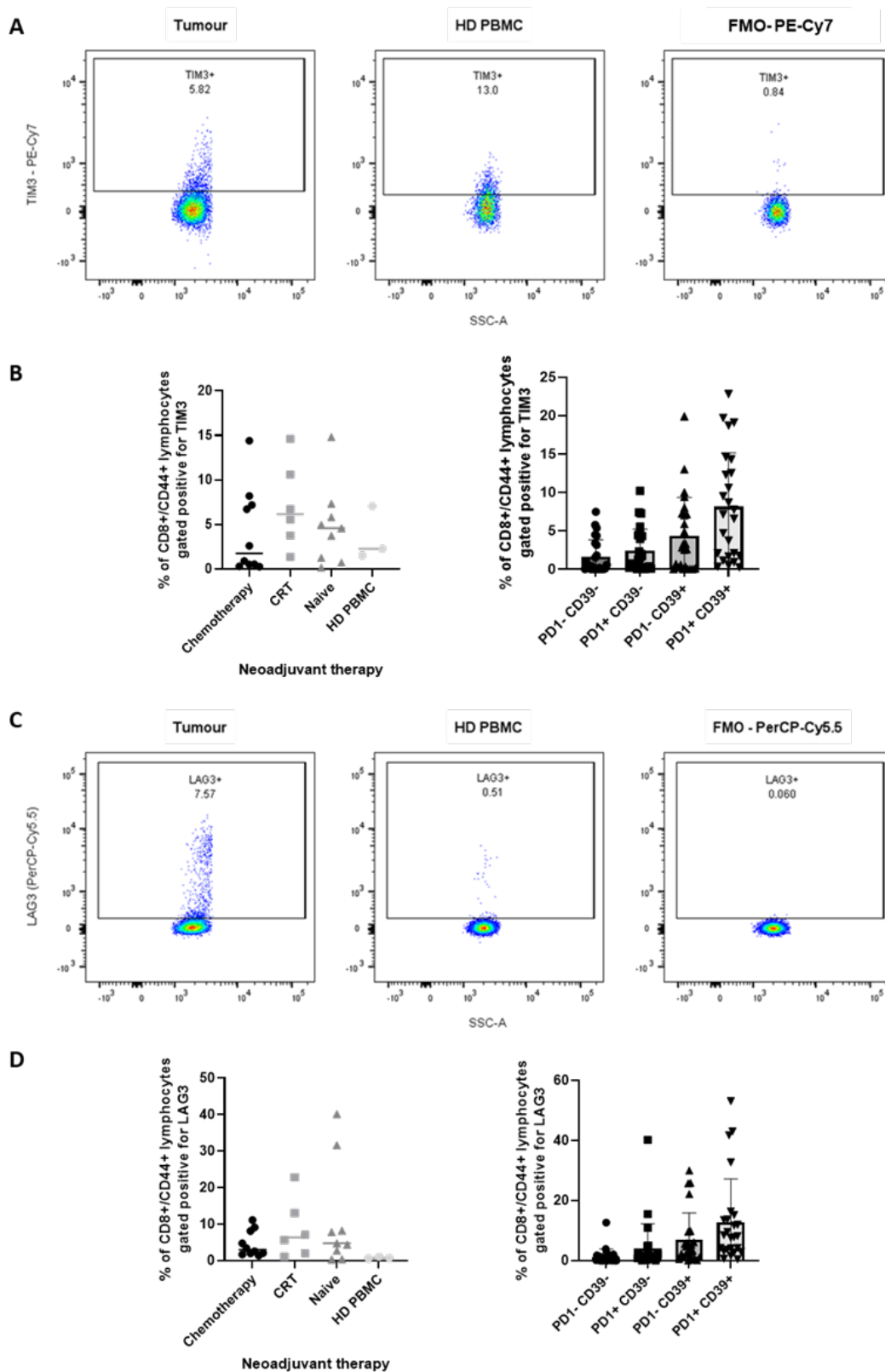


Figure 18 TIM3 and LAG3 expression by CD8+CD44+ tumour infiltrating lymphocytes from human oesophageal adenocarcinoma.

A and C) Exemplar flow cytometry plots showing gating of TIM3 and LAG3 positivity among CD8+CD44+ lymphocyte singlets from human oesophageal adenocarcinoma

and HD PBMCs on full staining and utilising an FMO. Gating for CD8+CD44+ lymphocyte singlets as described above. B and D)) Flow cytometry results of human oesophageal adenocarcinoma samples showing percentage of CD8+CD44+ TILs either gated as positive for TIM3 or LAG3, results divided by neoadjuvant treatment or HD PBMC control (left) and by different groups depending on positivity for PD-1 and CD39 (right).

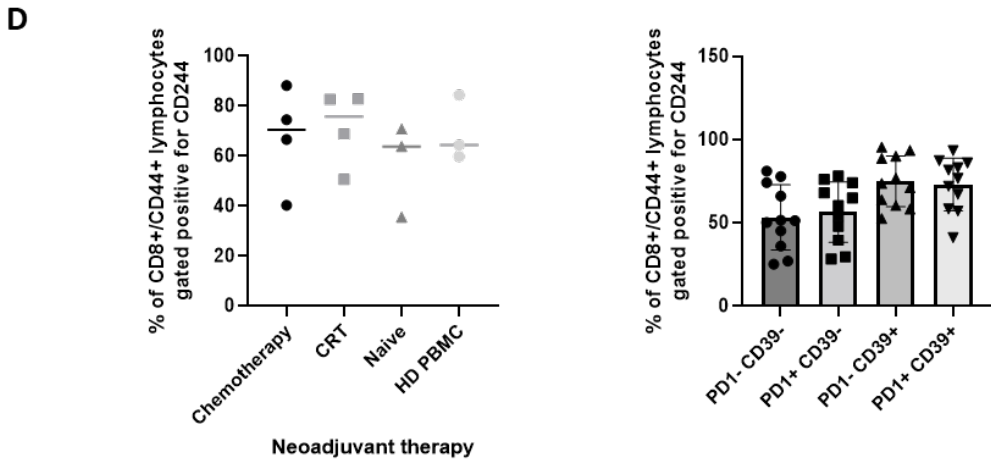
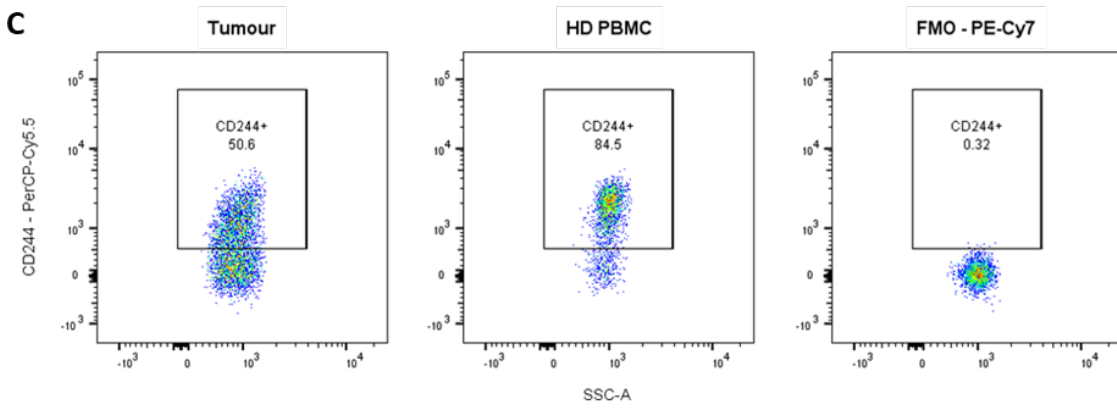
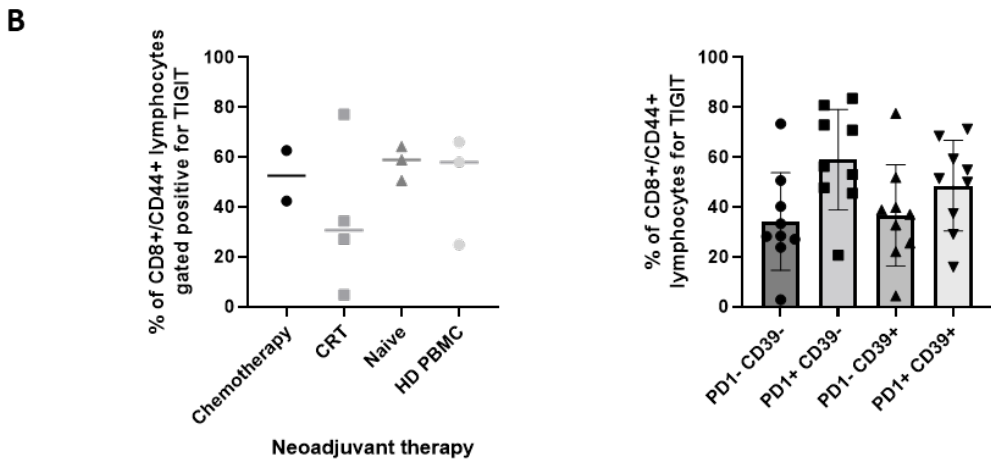
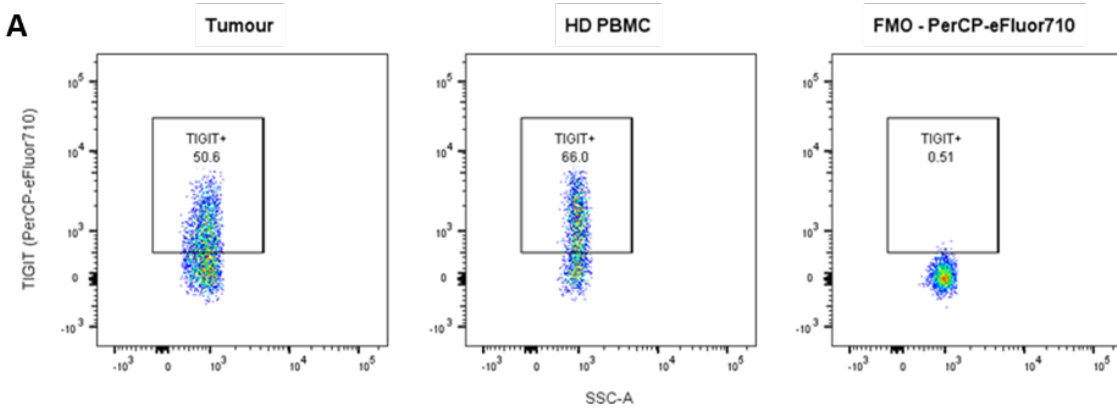
The percentage of CD8+CD44+ TILs positive for TIM3 was highest among individuals who had received CRT (mean 7.1%) and lower among treatment naïve patients (mean 4.8%), and tumours of patients treated with chemotherapy (4.2%) (Figure 18).

As may be expected given the nature of PD-1 and CD39 as being markers of activation and exhaustion, TIM3 was expressed most upon the surface of cells in the DP group (mean 8.13%) and lowest among the DN group (mean 1.61%). The difference here is of a high degree of statistical significance, $p < 0.0001$ (Figure 18).

Lymphocyte-activation gene 3 (LAG3), is another inhibitory receptor strongly associated with lymphocyte dysfunction and exhaustion in multiple contexts. A higher degree of expression for LAG3 (mean 7.9% of CD8+CD44+ TILs) was identified on tumour samples than for TIM3, and this contrasted with a lower expression level on a corresponding HD PBMC samples (mean 0.75%). Similarly the highest percentages were observed in patients who had received neoadjuvant CRT (mean 8.6%) or were treatment naïve (mean 11.1%) compared to those who had received chemotherapy (mean 4.6%). Again, as might be expected, the highest percentage of CD8+CD44+ TILs positive for LAG3 in the DP group (mean 12.8%) when compared to the DN group (mean 1.28%), with a high degree of statistical significance $p = 0.0003$, calculated with the paired t test (Figure 18).

3.2.7.2 TIGIT, CD244 and CD38

As described above TIGIT, CD38 and CD244 cell surface expression was also assessed in the sample population. Cells positive for these proteins were identified as previously with the use of PBMC FMOs to gate a true positive and negative group.



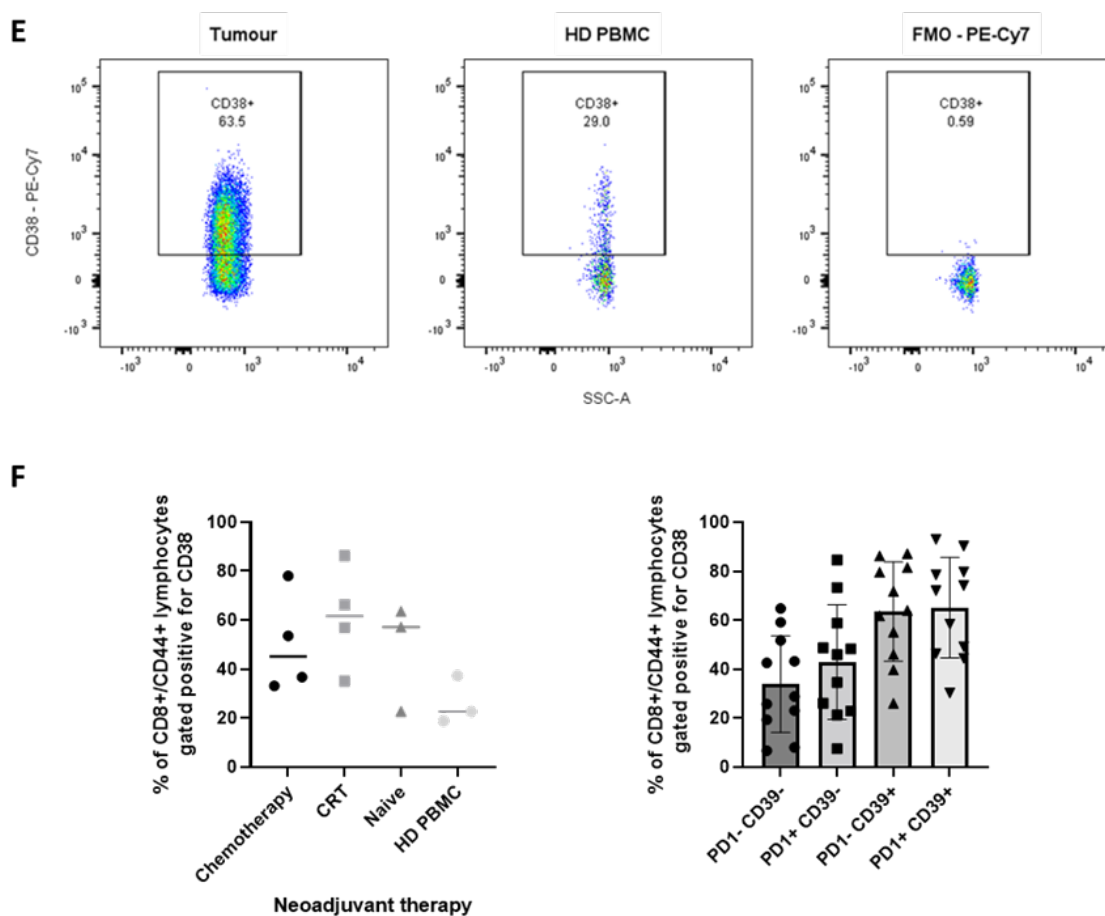


Figure 19 TIGIT, CD244 and CD38 expression by CD8+CD44+ tumour infiltrating lymphocytes from human oesophageal adenocarcinoma.

A, C and E) Exemplar flow cytometry plots showing gating of TIGIT, CD244 and CD38 positivity respectively, among CD8+CD44+ lymphocyte singlets from human oesophageal adenocarcinoma, and HD PBMCs on full staining and utilising an FMO. Gating for CD8+CD44+ lymphocyte singlets as described above. B, D and F) Flow cytometry results of human oesophageal adenocarcinoma samples showing percentage of CD8+CD44+ TILs gated as positive for TIGIT, CD244 or CD38 respectively, results divided by neoadjuvant treatment or HD PBMC control (left) and by different groups depending on positivity for PD-1 and CD39 (right).

T cell immunoglobulin and immunoreceptor tyrosine-base inhibitory motif [ITIM] domain (TIGIT) expression was assessed on a number of tumour resection samples. TIGIT was expressed on a large proportion of CD8+CD44+ TILs and HD PBMC (mean 46.9% and 49.6% respectively). Based upon a small sample size, the highest percentage was among treatment naïve (mean 57.9%) and chemotherapy (mean 52.5%) pre-treated individuals, though with only 2 patients treated with chemotherapy included in analysis this must be interpreted cautiously. It would appear that the

Chapter 3

lowest percentage of TIGIT positive is among CRT pre-treated CD8+CD44+ TILs (mean 35.8%) (Figure 19).

The PD-1+ CD39- TIL group appeared to have the highest percentage of TIGIT positive CD8+CD44+ TILs (mean 59.0%) and the PD-1- CD39- DN group the lowest (mean 34.2%) (Figure 19). When comparing the DP (mean 48.6%) with the DN group there is a statistically significant difference, with a p value of 0.012 when assessed using the paired t test (Figure 20).

CD244, also known as Natural Killer Cell Receptor 2B4 is another marker of activation, often highlighted as being of interest in lymphocyte dysfunction and exhaustion(44). CD244 is shown to be highly expressed among CD8+ CD44+ TILs as well as HD PBMC (mean 65.9% and 69.5% respectively). There are similarly high levels of expression across all pre-treatment regimens, ranging from mean 56.7% in treatment naïve to 71.3% for CRT treated patients, though again there must be caveats about sample size (Figure 19). There is a high frequency of events positive among all PD-1 and CD39 subgroups with only a small increase between DN and DP, from mean 53.3% to 73.0%, though this is statistically significant according to the paired t test ($p=0.0019$) due to the larger sample size for this data set (Figure 20).

CD38 is a cell surface glycoprotein also known as cyclic ADP ribose hydrolase, and is found on the cell surface of CD4 and CD8 lymphocytes and NK cells. It is a marker of activation as well as being found to be enriched in exhausted lymphocytes (44).

This too is highly expressed among CD8+CD44+ TILs from oesophageal cancer (mean 53.6%), and is demonstrated at moderate levels on HD PBMC (mean 26.3%). Similar expression levels are observed across all pre-treatment regimens (means ranging from 47.8 to 61.1), though again this is based upon relatively small sample set. The highest percentage positive for CD38 among the PD-1/CD39 subsets was among the PD-1- CD39+ group (mean 63.5%) and the DP group (mean 65.1%) (Figure 19). A comparison between the DP and DN (mean 33.9%) CD8+CD44+ TILs reveals a highly statistically significant difference ($p<0.0001$ paired t test) with the DP group revealing the higher expression levels (Figure 20).

All 5 surface markers described here showed increased expression among PD-1 CD39 double positive compared to double negative TILs. The increase in TIM3 and LAG3 suggests the possibility of an increasingly terminally differentiated exhausted population in the DP group, though the fact that they contributed a minority of TILs in this group would imply that this may be a minority population. Relatively high levels of TIGIT, CD244 and CD38 were observed among corresponding populations of HD PBMCs, raising questions about the validity of these markers for discriminating tumour reactive lymphocyte populations. CD38 shows a highly significant variation between the

DP and DN groups, and while this may be a reflection of the increased lymphocyte exhaustion here, is likely to be a reflection of increased lymphocyte activation in the PD-1+ CD39+ DP population (Figure 20).

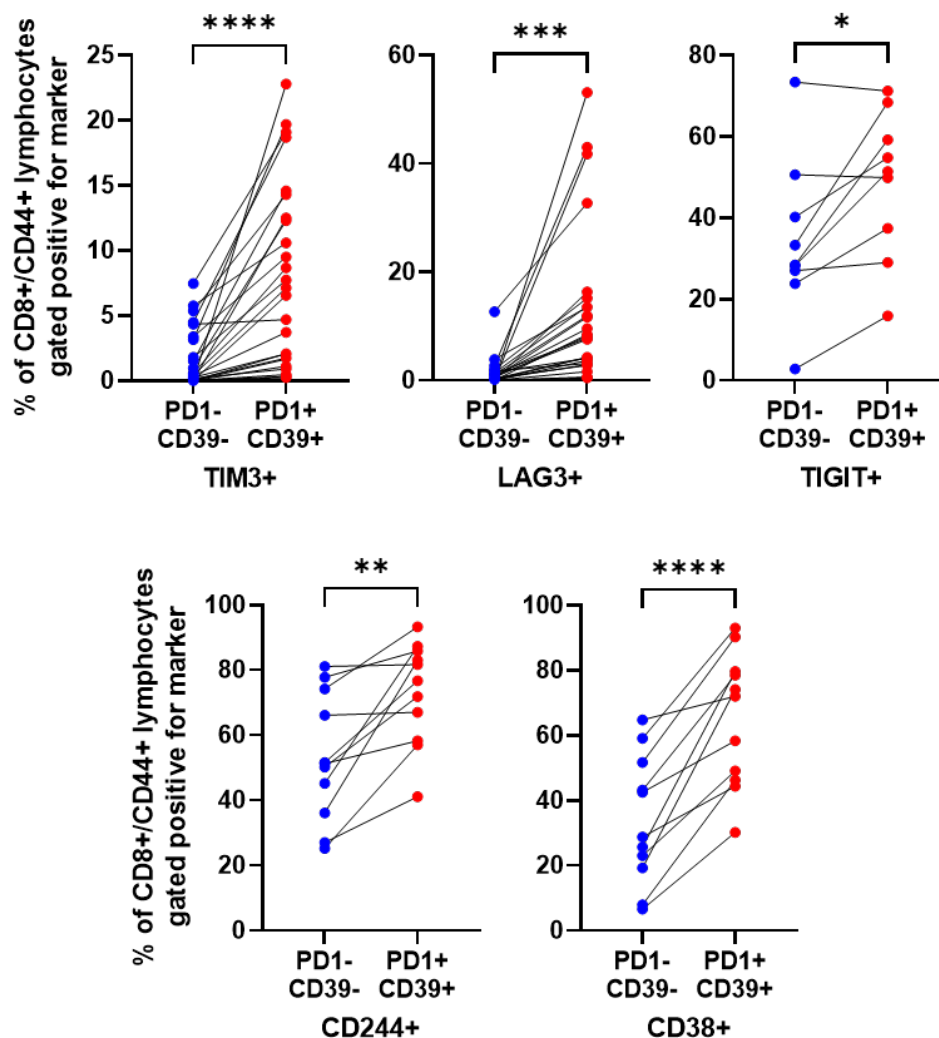


Figure 20 Exhaustion marker expression on DN and DP TILs in human oesophageal adenocarcinoma.

Linked percentage of CD8+CD44+ tumour infiltrating lymphocytes from human oesophageal adenocarcinoma specimens positive for surface markers associated with dysfunctional phenotypes that are either PD-1 and CD39 double positive or double negative. Comparisons between groups made using paired t-test.

3.2.8 Exhaustion marker expression and degree of PD-1 expression

It has been discussed that PD-1 expression is observed on TCR signalling and T cell activation. This is typically at a low expression level of PD-1, and it is only after persistent TCR stimulation that

Chapter 3

high levels of PD-1 expression are seen, which are associated with the dysfunctional phenotype. PD-1 high lymphocytes in chronic infection are associated with high levels of the transcription factor Eomes, a terminally differentiated exhausted phenotype, poor responsiveness to immune checkpoint blockade and reduced survival in some cohorts (57,68,88).

Daniela Thommen et al. described a PD-1 high population in human non-small cell lung cancer specimens, as being functionally and transcriptionally distinct from PD-1 intermediate TILs as well as PD-1 high CTLs from chronic infection. PD-1 high TILs were shown to possess increased expression of surface markers of exhaustion, increased tumour reactivity, and decreased ability to produce effector molecules such as IFN- γ and IL-2. There was no correlation between the amount of PD-1 expression and expression of T-bet and Eomes within these tumour infiltrating lymphocytes. A high abundance of PD-1 high TILs also correlated with improved patient survival and predicted response to immune checkpoint blockade (94).

A similar approach was adopted utilising the samples from the oesophageal adenocarcinoma cohort to investigate the impact increasing PD-1 expression would have on exhaustion marker expression. A gating strategy was designed to allow reproducible graduated level of PD-1 expression, and this was applied to the first 17 patient samples analysed. Degree of PD-1 expression was labelled from PD-1 + to PD-1 6+, and the percentage of events in each of these gates positive for the different surface markers of exhaustion was calculated, provided there were at least 10 events in the gate.

An increase in marker expression with increasing PD-1 expression was observed for CD39, TIM3, LAG3 and TIGIT. This is as is to be expected given what is known about expression patterns for these markers with PD-1 expression. There was no clear correlation for CD244 or CD38 in this patient cohort. It had been expected they would rise too with increasing PD-1 expression given the correlation seen with CD244 and CD38 and terminally exhausted phenotypes, but as already discussed these markers are principally T lymphocyte activation markers rather than specific for exhaustion (Figure 21).

Of note, the degree of expression of TIM3 and LAG3 at the higher levels of PD-1 expression, is much lower than that seen in the NSCLC cohort. For example, in the highest PD-1 expression level, TIM3 was expressed on an average of 9.642% of cells in the oesophageal cancer cohort, compared to a mean of approximately 75% of cells in NSCLC, LAG3 was present on an average of 21.97% in the oesophageal cancer patients compared to 50% in NSCLC (Figure 21) (94). While results between studies cannot be accurately compared, this does demonstrate an example of the heterogeneity that exists in lymphocyte dysfunction between cancers, likely due to the effects of complex and dynamic tumour microenvironments. It also hints at a less significant role for

terminally differentiated exhausted lymphocytes in oesophageal cancer, where the evidence displayed in this chapter increasingly points to a small minority population.

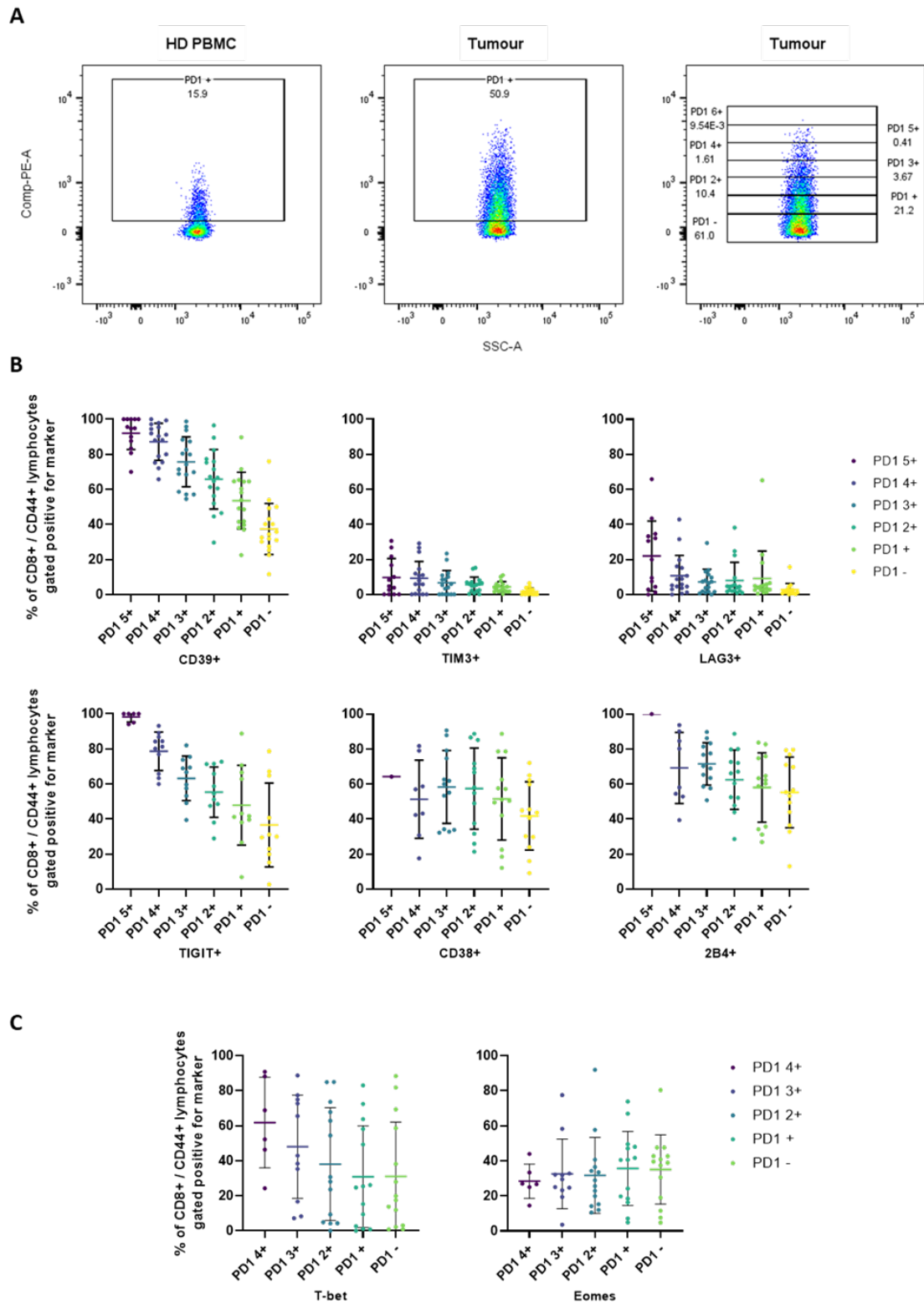


Figure 21 Cell surface exhaustion marker and T-box transcription factor expression in human oesophageal adenocarcinoma by degree of PD-1 expression.

A) Exemplar flow cytometry plots showing gating strategy used to identify degree of PD-1 expression. The first positive gate is defined based upon PD-1 expression in healthy donor PBMC analysed at the same time as tumour, and these measurements used for subsequent gates. B) Percentage of events in each gate of PD-1 expression level positive for cell surface markers of exhaustion. C) Percentage of events in each gate of PD-1 expression level positive for T-bet (left) and Eomes (right).

Similar analysis of T-bet and Eomes expression in OAC CD8+ TILs graduated by the level of PD-1 expression does not show any significant change as we progress through the groups. This would sit against the perceived wisdom of increasing PD-1 expression signifying an increasingly terminally differentiated exhausted population, but as mentioned already, is in keeping with the observations by Thommen et al. who have also reported a lack of correlation of both transcription factors with degree of PD-1 expression in human TILs. This is in contrast to results obtained from the chronic murine LCMV infection model, and implies processes apart from the classical model of lymphocyte exhaustion at play in both NSCLC and the oesophageal adenocarcinomas analysed here.

3.3 Discussion

It has been possible to utilise a flow cytometric approach to analyse the phenotype of the CD8+ T lymphocyte compartment of immune infiltrates from human oesophageal adenocarcinoma. By adopting an enzymatic and mechanical disaggregation technique followed by controlled freezing, samples can be frozen, thawed and analysed at later time-points, without compromising the lymphocyte surface marker expression profiles. Changes in the percentage of events identified as lymphocytes morphologically can be considered to be secondary to cell death among the fragile cancer or stromal cell populations rather than the immune cells of interest, the composition of which appears stable.

Within the lymphocyte compartment, is a significant population that stains positively for CD8a and CD44, representing a presumed cytotoxic T cell population that has experienced antigen alongside appropriate co-stimulatory signals and is activated. This is highest in samples from patients who have undergone pre-treatment with chemotherapy and radiotherapy. A higher than median percentage of these antigen experienced CD8+ TILs is associated with improved overall survival, though this could well be as a result of this group containing a higher number of patients from the optimally pre-treated cohorts, rather than the treatment naïve patients. An association of high CD8+CD44+ lymphocyte infiltrates with improved survival is intuitive and would suggest

infiltration with activated, rather than bystander TILs that have potential for sustained tumour killing.

A high percentage of CD8+CD44+ TILs from the oesophageal adenocarcinoma cohort were positive for PD-1. This was highest in the tumours of patients pre-treated with chemotherapy as well as treatment naïve individuals, and a high proportion of CD8+ TILs positive for PD-1 was positively correlated with survival. CD39 expression is similarly elevated in antigen experienced CD8+ TILs compared to corresponding populations from healthy donors, was highest in treatment naïve and chemotherapy pre-treated individuals, and is also associated with improved survival.

Of particular note co-expression of PD-1 and CD39 was highest in tumours of treatment naïve individuals, and possession of a higher percentage of CD8+CD44+ lymphocytes displaying this phenotype was associated with a marked increase in patient overall survival and progression free survival. Tumours possessing high percentage of PD-1+CD39+ DP TILs were observed in each pre-treatment regimen, including a significant number in tumours of patients not treated with neoadjuvant therapies. An abundance of DP TILs was associated with improved PFS and OS in all groups including the potentially sub-optimally treated naïve individuals.

While it would be unwise to infer a causal relationship, it is attractive to consider the link between an abundant population that may well be enriched for tumour reactive clones (129), and patient survival. PD-1 and CD39 co-expression is observed in examples of terminal exhaustion, and while this implies a dysfunctional CTL pool with impaired effector function, it also suggests that to get to this point, the CD8+ TILs have achieved appropriate TCR signalling and engagement with cognate MHC-peptide in the context of productive co-stimulation, very possibly in response to tumour associated antigens or neoantigens.

Closer inspection of the PD-1 and CD39 double positive (DP) population reveals a measurable cohort of TILs expressing multiple exhaustion markers, significantly more so than is seen in the double negative (DN) population. This could suggest a terminally differentiated exhausted phenotype, in a portion of the DP group. TIM3 and LAG3 is expressed at modest levels in the DP group, and while higher than in the DN group or HD PBMC controls, it is less than may be expected if the DP group is comprised of a dominant terminally differentiated exhausted TIL population.

Adding to the evidence that the DP group is not comprised solely of terminally differentiated exhausted TILs is the flow cytometric assessment of the expression levels of the T-box transcription factors T-bet and Eomes in this context. Here we observe a DP population enriched for a T-bet^{high} Eomes^{low} phenotype with low abundance of T-bet^{low} Eomes^{high} when compared to

Chapter 3

the DN group. It is also observed that the percentage of these T-bet and Eomes groups does not change significantly with increasing PD-1 expression, as might be expected if the population of interest were behaving in line with the classical LCMV model of lymphocyte exhaustion. Instead we see reasonably static proportions of TILs are T-bet^{high} or Eomes^{high}, even potentially a fall in Eomes and rise in T-bet with increasing PD-1 expression, a finding mirroring observations seen in NSCLC (94).

So how to define the DP population? The data presented would suggest a heterogeneous population, and could be explained by a dominant precursor exhausted population with a minority terminally differentiated exhausted lymphocyte population, though this would not account for the static transcription factor profiles observed with increasing PD-1 expression. It may be that this population is principally comprised of other lymphocyte populations known to express PD-1 and CD39, namely activated effector CD8⁺ lymphocytes, or tissue resident memory (T_{RM}) CD8⁺ lymphocytes. Mouse models of cancer and assessment of tumours from patients are increasingly demonstrating a key role for T_{RM} lymphocytes in tumour control, and patient survival, as well as in augmenting responses to immune checkpoint blockade therapies (114,129,130).

In conclusion, human oesophageal adenocarcinomas demonstrate infiltration with a definable population of PD-1 and CD39 double positive TILs that correlate with improved progression free and overall survival. This population appears heterogeneous and while it may possess a small minority population of terminally differentiated exhausted lymphocytes characterised by possession of multiple surface markers of exhaustion, it would appear to be comprised predominantly of a less exhausted cell type. This dominant group may conform to a precursor exhausted lymphocyte phenotype as defined by chronic LCMV infection model, but may also be a non-traditionally exhausted TIL population analogous to the tumour reactive TILs described by Thommen et al, or the TRM phenotype described by de Lara et al, Clarke et al and many others as being potentially so important in containing progressing cancers (94,114,129,130).

To further characterise this PD-1⁺ CD39⁺ phenotype, a transcriptomic based approach has been adopted as well as further utilisation of multi-parametric flow cytometry to allow multidimensional assessment of this TIL population, in a bid to greater understand its composition and factors that influence patient response to therapy and ultimately survival in oesophageal adenocarcinoma.

Chapter 4 Transcriptomic assessment of exhausted CD8+ T lymphocyte populations in human oesophageal adenocarcinoma

4.1 Introduction

A high abundance of the PD-1 CD39 double positive (DP) antigen experienced CD8+ TILs has been demonstrated to be associated with superior progression free and overall survival in the cohort of resected oesophageal adenocarcinomas assessed in this study. Data presented thus far has utilised a 6-fluorophore flow cytometry approach and has alluded to the DP population being a heterogeneous collection of CD8+ T lymphocytes, comprising a majority portion of precursor exhausted, CD8+ effector or tissue resident memory CD8+ lymphocytes as well as a minority terminally differentiated exhausted population.

To characterise this group further a transcriptomic based approach was proposed allowing multidimensional analysis to a degree not possible through flow cytometric analysis. Various RNA sequencing approaches were considered including single cell and bulk sequencing techniques, as well as different options for the material sequenced which could include whole tissues or sorted cell populations. Ultimately a bulk RNA sequencing approach for FACS sorted populations of TILs was selected, in order to take advantage of the depth of sequencing available to bulk techniques with the ability to examine specific, defined populations of lymphocytes extracted from human tumour samples. In order to understand the character of this DP population, it was decided that it should be sequenced alongside the PD-1 CD39 double negative (DN) population, as well as the minority population of potentially terminally differentiated exhausted lymphocytes, in order to allow for comparison and appreciation of differentially expressed genes in each group, and enriched gene sets generated from previously published data.

To successfully complete analysis on these target populations from primary patient tissues a sensitive technique was required and an RNA sequencing pipeline was developed and tested before being applied to oesophageal adenocarcinoma samples.

Described here are the results obtained from successful transcriptomic assessment of sorted populations of OAC TILs, analysed with the intention of undertaking deep phenotypic characterisation of PD-1+ CD39+ antigen experienced CD8+ TILs from primary patient samples.

Chapter 4

The aim of this phase of the project was to use a bulk RNA sequencing approach to assess the transcriptomic phenotype of the PD-1 and CD39 double positive population of antigen experienced CD8+ tumour infiltrating lymphocytes. The transcriptomic profile of this population was to be compared with the PD-1 and CD39 double negative group as well as a similarly PD-1 and CD39 positive group, which is also expressing the exhaustion markers TIM3 and LAG3. It was planned to use this information to characterise this population of interest using gene set enrichment analysis techniques, with regards to lymphocyte exhaustion and other dysfunctional lymphocyte populations. It is hoped the insights gained into the functionality of this population will aid understanding as to how and why it can influence patient outcomes in this difficult to treat cancer.

4.2 Results

To understand the characteristics of the PD-1 and CD39 double positive group of tumour infiltrating lymphocytes from human oesophageal adenocarcinoma further, transcriptomic assessment was planned using RNA sequencing. The principle output was intended to be analysis of differential gene expression (DGE) with a secondary target of undertaking gene set enrichment analysis to compare the expression profile of the population of interest, with gene sets published in the literature describing known phenotypes. Given this a bulk RNA sequencing technique would be appropriate to gather sufficient depth of sequencing, with the population of interest being collected via FACS sorting. A target of 30 million reads per sample was the intended output. As comparators for the population of interest, sequencing data was gathered for the double negative population, as well as potentially terminally exhausted populations containing multiple co-inhibitory receptors, to allow comparison up and down the gradient of dysfunction and exhaustion.

With this in mind preliminary work was planned to assess potential methods for acquiring this sequencing data. A key consideration at the outset of this experimental work stream, was the fact that analysis will be undertaken using small numbers of cells collected via FACS. The samples received from surgery are small, and the nature of their collection means that larger volumes cannot be obtained. A high sensitivity approach would need to be adopted and methods were assessed and optimised prior to utilising patient derived tissue.

4.2.1 RNA sequencing pipeline optimisation

A cell sorting strategy was developed, identifying and isolating the cell populations of interest, utilising FACS sorting with the core antibodies detailed in chapter 3, targeting CD8a, CD44, PD-1

and CD39, and additionally antibodies specific for TIM3 and LAG3. This allowed collection of key cell populations into appropriate medium for storage prior to RNA extraction. The populations collected included a PD-1 CD39 double positive population (DP) which was also TIM3 and LAG3 negative, a population we denoted as an early terminally exhausted PD-1+ CD39+ LAG3+ TIM3- population (EExh), a population denoted as a late terminally exhausted PD-1+ CD39+ LAG3+ TIM3+ population (LExh), and a PD-1- CD39- double negative population (DN). Additionally, a sample of the non-lymphocyte cellular material was collected (population 5) and stored in controlled freezing solution in liquid nitrogen. Given the open ended nature of this project, it was considered prudent at the outset to collect a sample of the tumour cells, should they be needed as a source of patient specific tumour antigens for future experimental work. Cell sorting and storage techniques were optimised prior to their use on clinical samples of interest, and calculations of expected yields for each cell population was estimated. It was noted that for the most infrequent populations, the EExh and LExh groups, potentially very few cells were likely to be recovered, numbering into the several hundred, and this influenced decision making regarding further RNA sequencing techniques. Details of the yields for each experimental group sorted in the preliminary experiments are detailed in chapter 2.

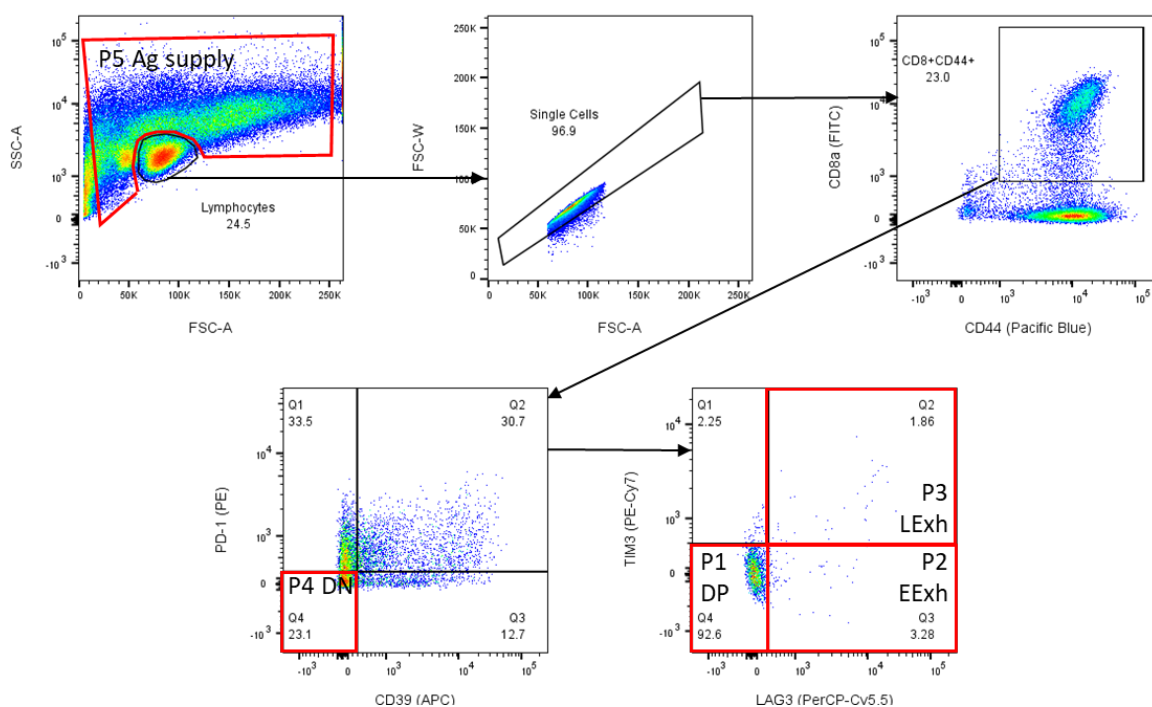


Figure 22 Gating strategy for FACS sorting of lymphocyte populations of interest.

Depiction of gating strategy for Fluorescence-activated cell sorting using BD FACS Aria. Exemplar oesophageal adenocarcinoma sample displayed. Populations 1-3 (P1-3) all singlet lymphocyte populations CD8,CD44,PD-1,CD39 positive and then LAG3-TIM3- (DP), LAG3+ TIM3- (EExh) and LAG3+ TIM3+ (LExh) respectively. Population 4 is

Chapter 4

CD8 and CD44 positive, but PD-1 and CD39 negative. Population 5 (P5) non-lymphocyte tumour cells stored for future experimental work to be used as potential antigen supply.

With a need to extract sufficient RNA for sequencing from small numbers of sorted lymphocytes in mind, a range of sensitive RNA extraction techniques were evaluated, including a number of commercially available spin column based kits as well as a phenol-chloroform RNA extraction method. The results of these experiments are detailed in chapter 2. Ultimately the Zymo Direct-zol™ RNA Microprep Kit (213) was selected for use, given the relatively high yields achieved, and the ease of storing sorted cells in TRIzol™, a trade name for guanidinium thiocyanate, prior to RNA extraction.

In order to produce complementary DNA (cDNA) of sufficient quality for RNA sequencing from the low concentrations of RNA available, a highly sensitive sequencing technique was required. The single cell RNA sequencing SmartSeq2 protocol was selected (197), with extracted RNA used as input material rather than whole cells, to allow for bulk cDNA library production from low numbers of cells. This technique was optimised using RNA extracted from counted and then sorted HD PBMCs, with high quality cDNA produced. Trials using sorted OAC TILs were then undertaken before cDNA was produced from sorted TIL populations of interest extracted from resected human OAC samples. The details of this experimental set up and analysis is detailed in chapter 2.

Sample cDNA was cleaved and labelled utilising the NexteraXT tagmentation reaction from Illumina and final multiplexed libraries were sequenced using the Illumina NextSeq550 platform. Data output from this process was transferred to the high-performance computing facility for data alignment and de-multiplexing, before further transfer to the R software environment for downstream analysis. Details in chapter 2 and Appendix D.

The culmination of the RNA sequencing pathway development and optimisation, was the sequencing of three groups of sorted TILs from 3 separate patients as a preliminary analysis, to test the process and develop downstream analysis skills and strategies.

4.2.2 Preliminary data analysis

Analysis of the data generated from the first RNA sequencing assessment was completed allowing development of a bioinformatics pipeline and to demonstrate feasibility of the procedure from resection of tumour sample through to data processing. The data analysis pipeline will be

discussed here and the same process was deployed on subsequently collected samples. Exemplar script for all analysis is included in Appendix D.

The number of DNA fragments aligned to each gene for every sample were collated into a single data matrix and loaded into the statistical environment R for analysis alongside a table containing metadata required for analysis. An example of the read count matrix and metadata sheet are included in Appendix E.

The primary output for this RNA sequencing experiment was to undertake differential gene expression analysis and use this information to look at specific genes of interest as well as to undertake pathway and gene ontology analysis. The second primary output from the data generated was to facilitate gene set enrichment analysis, in order to investigate if differences in gene expression between the populations of interest are similar to those seen in published series of lymphocyte exhaustion and dysfunction, and to aid in detailed identification of key populations.

The first stage of analysis utilised the DESeq2 package, a statistical tool developed for use within the R environment to test for differential gene expression in RNAseq experiments and other high dimensional data techniques, through use of negative binomial generalised linear models (214).

The matrix containing the read count information is transformed into a DESeqDataSet and the factor for comparison is defined, the population type (DN, DP, EExh or LExh) and any batch effects can be factored into the experimental design, for instance the sequencing run. Following this unless specifically stated, as in the case of data processed for GSEA, pre-filtering is undertaken removing genes from the data set with low expression levels. Assessment of the strictness of filtering required for optimal results has been undertaken and it has been decided to remove genes where there are less than 5 normalised counts in 5 separate samples for full datasets, and 5 normalised counts in 3 separate samples for the initial trial dataset. Pre-filtering acts to remove rows with very few reads and thus reduce memory size of the object being analysed and the computing power required for this. In doing so it also limits the number of analyses undertaken, reducing the false discovery rate of results incorrectly deemed significant, improving accuracy and significance of estimations made.

Differential expression analysis was completed using the *DESeq2* function in the DESeq2 package. This function uses negative binomial generalized linear models to estimate dispersion and logarithmic fold changes incorporating data-driven prior distributions (214). A results table can be produced from this output by defining the groups intended for comparison, for example to compare DN to DP populations. Here Log fold change shrinkage is undertaken for ease of

Chapter 4

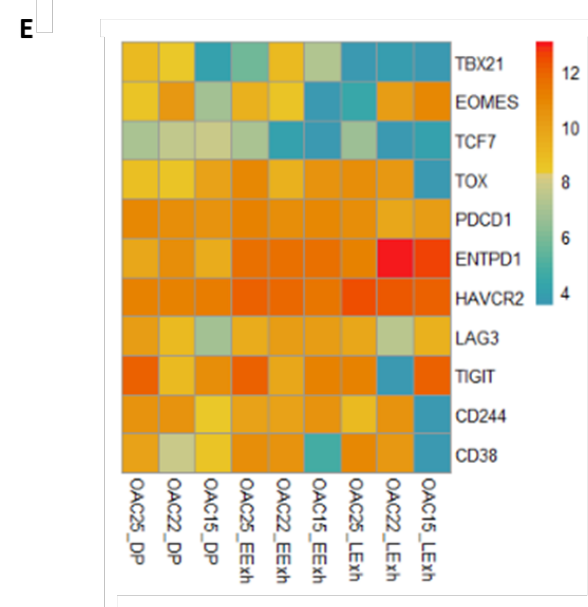
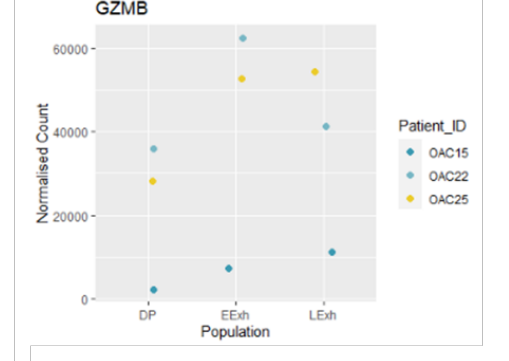
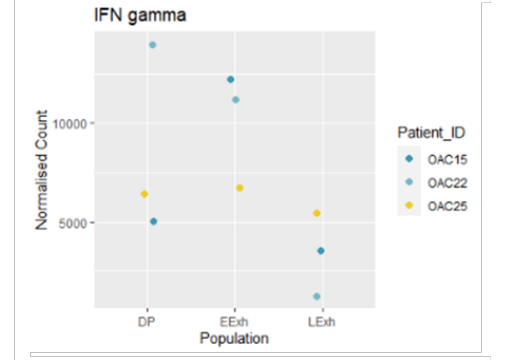
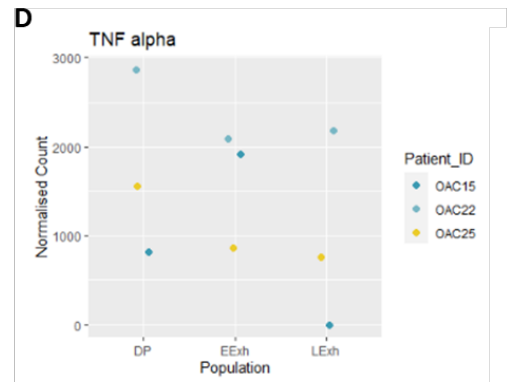
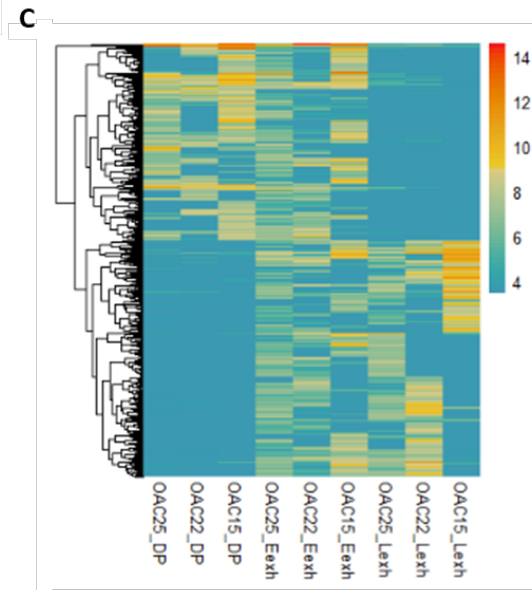
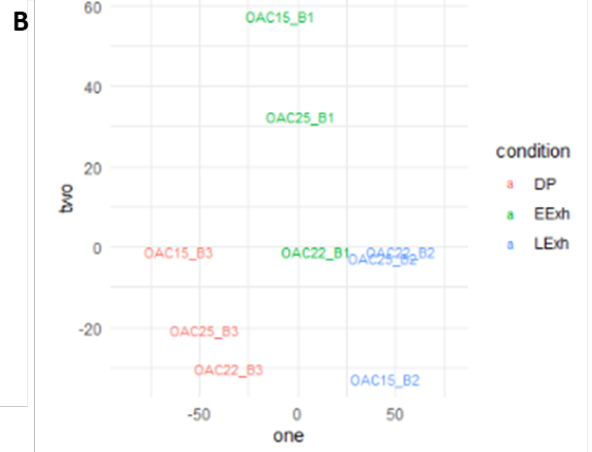
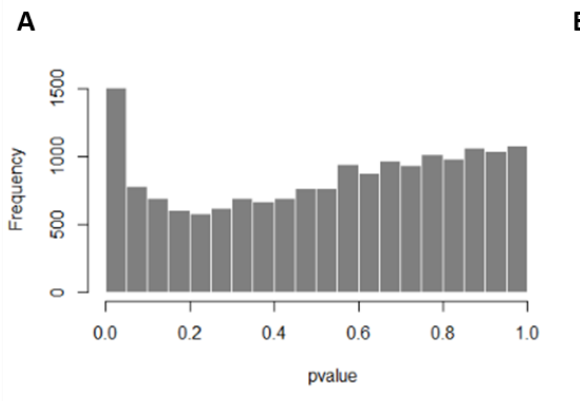
visualisation and ranking, and the *ashr* method has been used for this project (215). The results tables produced at this point will produce Log2 fold change calculations, Wald test p values and adjusted p values. This can be used for identification of significantly differentially expressed genes, or utilised for further analysis such as enrichment of gene ontology labels, pathway analysis, or with packages such as the QIAGEN Ingenuity pathway analysis software.

Additionally at this point in the analysis pathway, a matrix can be produced displaying normalised counts for all genes listed for each sample, using the DESeq2 package. This is the basis of input into the Broad Institute software to allow completion of gene set enrichment analysis, a technique for assessing if an *a priori* defined set of genes are enriched in a specific group compared to another, and an intended primary output for the data collected (216,217).

Finally read count data can be transformed to remove dependence of the variance on the mean. Here *variance stabilizing transformation (VST)* (218) is undertaken as is *regularized logarithm (rlog)* calculation (214). These transformations both produce transformed data on the log2 scale which has been normalised with respect to library size. It can be of use to visualise this transformed data as PCA plots or heatmaps.

This analysis pipeline was used to undertake assessment of the read count data collected following sequencing of the cDNA libraries produced from the first 3 patients. Filtering of poorly expressed genes, produced an appropriate number of genes differentially expressed with a p value <0.05, as shown in the histogram of p values (Figure 23.A), suggesting an acceptable false discovery rate.

Differences in terms of gene expression between the samples was visualised using a principle component analysis (PCA) plot, which showed that the samples broadly clustered according to phenotype, rather than patient ID. This is reassuring, even with a degree of heterogeneity in the samples in terms of pre-treatment regimen and response to therapy. This would suggest differences in phenotype based upon the markers used for sorting, is greater than any differences seen as a result of neoadjuvant therapy or inter-patient variability (Figure 23.B).



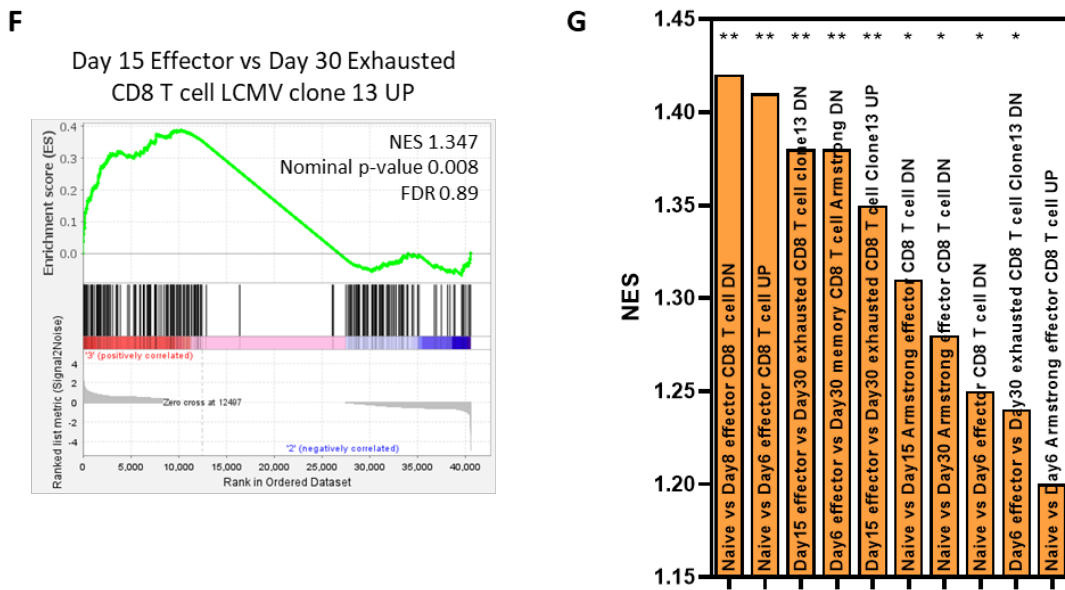


Figure 23 Analysis of preliminary dataset showing DEG profiling and GSEA.

A) Histogram of the range of p values for differential gene expression analysis using DESeq2. Frequency is the number of genes with each p value. B) Principle Component Analysis (PCA) plot for gene expression by condition, with Double Positive (DP) group labelled red, Early Exhausted (EExh) in green and Late Exhausted (LExh) in blue. C) Heatmap showing 467 differentially expressed genes between DP and LEExh phenotypes in trial dataset, 212 show increased expression in DP and 255 show reduced expression. EExh population show intermediate expression pattern. Data normalised and transformed with variance stabilizing transformation (VST) and displayed on a log2 scale. Each row represents a gene, and order has been determined by unsupervised clustering. D) Gene expression plots for selected genes showing normalised counts for each sample from the trial sequencing experiment in each phenotype. Genes selected are CD8 T lymphocyte effector molecules tumour necrosis factor alpha (TNF alpha), interferon gamma (IFN gamma) and granzyme B (GZMB). E) Heatmap showing expression of genes of interest to lymphocyte exhaustion in samples from trial sequencing. Data normalised and transformed with VST and displayed on a log2 scale. F) Example gene set enrichment plot for assessing enrichment of a gene set detailing genes with increased expression in Day 15 Effector vs Day 30 Exhausted CD8T cells from Clone 13 LCMV infection enrichment, in the LEExh vs DP groups. Gene set published in the assessment of lymphocyte exhaustion gene expression profiles by Doering et al. G) Histogram showing Normalised Enrichment Score (NES) for top 10 enriched gene sets when GSEA is undertaken comparing LEExh phenotype vs DP, with regards to the lymphocyte exhaustion gene

sets detailed by Doering et al (43). Asterisks represent calculation of nominal p value.

* = $p < 0.05$, ** = $p < 0.01$, *** = $p < 0.001$.

A total of 467 genes were identified as being significantly differentially expressed when the LExh group was compared to the DP group, defined by possessing a wald test p value < 0.05 . 212 genes showed increased expression in the DP group and 255 in the LExh group. This included a host of genes involved in immunological processes and included the *Tbx21* gene encoding T-bet, with reduced expression in the LExh group. These significantly differentially expressed genes can be visualised as a heatmap (Figure 23.C), individually with expression counts for each sample observed (Figure 23.C), or as a heatmap showing pre-defined genes (Figure 23.E).

Successful normalisation of counts and completion of GSEA, utilising software and techniques developed by the Broad Institute, was an important test for this process. This was highlighted as a key output prior to starting this investigation. The successful comparison of the samples sequenced using a collection of gene sets of a comparable phenotype, exhausted lymphocytes analysed by Doering et al, provided a proof of principle for this final and crucial step. The results of this GSEA showed enrichment of gene sets related to LCMV mediated lymphocyte exhaustion in the LExh when compared to the DP groups (Figure 23.F and G). This result, in keeping with what may be expected based on published data elsewhere gave confidence in the decision to invest into expansion of this data set.

4.2.3 Expansion of data set

Following the success of the trial RNAseq experiment, a power calculation was undertaken to identify the optimal number of replicates to generate reliable and meaningful results. The Scotty web based power calculation tool (219), developed by researchers at the University of Utah, was used, modelling the number of samples required for to detect at least 50% of the expressed genes that are differentially expressed by a 2 fold change with a p value < 0.01 , based on the trial data set produced in this project. This predicted that the minimal sample size required was 6 replicates, though 10 replicates would produce optimal results. It was aimed to multiplex samples for sequencing allowing approximately 30 million reads per sample, with a target for an excess of 5 million mapped reads per sample, and ideally around 5-15 million mapped reads per sample to allow differential gene expression analysis of highly expressed genes and downstream analysis approaches such as GSEA and GO analysis.

Initial plans were to sequence 8 collections of all 4 sample groups from treatment naïve patients and 8 sets from patients treated with chemotherapy. This would allow a detailed analysis and characterisation of the TIL groups in the treatment naïve setting as well as following

Chapter 4

chemotherapy, and could thus potentially shed light on to the differential responses to immunotherapy observed in oesophageal cancer following pre-treatment with cytotoxic chemotherapy.

Difficulties were experienced on upscaling the sample number, however, and despite success in cDNA library preparation previously from a similarly low number of sorted cell, persistent low cDNA yields were obtained. During the trial RNAseq experiment, cDNA libraries had been prepared from as few as 125 sorted cells, and this approach was initially adopted in the expanded sample collection phase, in order to increase the potential number of tumour samples available for analysis. Inconsistent quantities of cDNA were obtained from the numbers of cells sorted, despite successful cDNA production from positive controls.

Troubleshooting was undertaken, with assessment from sample preparation, FACS sorting, sample storage, RNA extraction, RNA storage and cDNA production using SmartSeq2 all investigated. Particular note was made to the sort efficiency of the BD FACS Aria II machines used for the sorting of sample TIL populations with analysis of sort efficiency of the machines measured and alternatives used, RNA extraction methods with new reagents and spin columns used, as well as additional positive and negative controls, and the assessment of the SmartSeq2 process where fresh reagents were used.

By increasing the number of cells sorted a sufficient number of samples were obtained to expect successful downstream analysis in order to produce DEGs via DESeq2 and GSEA, though these issues did limit the number of samples available for analysis. A final target was set for at least 6 samples in each analysis group, though in total more than this were collected for all except the LExh group.

4.2.4 Data analysis of full data set

Analysis of the full data set included read counts for 6 treatment naïve patients and 3 chemotherapy pre-treated patients. The treatment naïve samples include 5 DN samples, 6 DP samples, 5 EExh samples and 4 LExh samples. The Chemotherapy group included 2 DN samples, 3 DP samples, 2 EExh and 2 LExh samples. Significant difficulties were experienced in increasing the number of samples but the final numbers are expected to allow a sufficiently detailed analysis with a degree of statistical robustness.

A total of 230,579,845 reads were mapped to gene identifiers, with an average of 7,951,029 mapped reads per sample and a range from 2,492,780 – 23,261,804 mapped reads per sample. This was above the absolute minimum acceptable read number of 5 million reads per sample, but

below 10-15 million mapped reads per sample that had been hoped for. Quality control metrics for sequencing runs was considered satisfactory to proceed to downstream analysis. Given these outcomes, all samples sequenced were used for analysis.

The results obtained from analysis of these samples will be collated into 2 datasets. The first includes only the treatment naïve samples and is used for initial analysis. The second will include all samples, naïve and chemotherapy pre-treated and look for concordance with the initial findings. The data from the CRT pre-treated patient is being excluded from the final analysis in order to maintain a degree of patient homogeneity.

4.2.5 Comparison of treatment naïve and chemotherapy treated samples from expanded data set

It had been described that sequencing data has been collected for a small number of patient samples pre-treated with chemotherapy and a larger group that are treatment naïve. By combining these data sets we can increase the number of samples included, and if they are phenotypically identical potentially increase the potential to find, and the power of, significant results.

It is hypothesised, that the characteristics of the cell populations of interest in this project, are conserved between pre-treatment regimes, though the abundance of each group varies with treatment.

As described above, read count data for all treatment samples was uploaded into the statistical environment R for analysis. This data underwent pre-filtering, normalisation, transformation and differential expression analysis for comparison of the DP with the DN group. This was undertaken for treatment naïve samples alone, chemotherapy exposed samples alone, and as a combined cohort, allowing comparison for similarities and differences in the results obtained.

Analysis of treatment naïve samples alone revealed a total of 261 significantly differentially expressed genes (DEGs) defined by an adjusted p value of less than 0.05. 18 genes were shown to have significantly over expressed by the same metric, and 243 had reduced expression in the DP group compared to the DN. This can be visualised in the volcano plot (Figure 24). While the heatmap shows a high degree of heterogeneity between samples in terms of gene expression and read depth, some of this is accounted for with normalisation and transformation techniques. Identical calculation of DEGs for chemotherapy pre-treated samples revealed a far larger number of DEGs, likely including many false positives, making direct comparison challenging.

Chapter 4

Downstream analysis was undertaken to assess for GO term enrichment both using a list based approach to via the web based portal for assessment gene ontology and pathway enrichment, available at Toppgene, and with a GSEA based approach utilising the technology developed by the Broad Institute. Additionally, Log₂fold change figures calculated by DESeq2 were inputted into the QIAGEN Ingenuity Pathway Analysis (IPA) software. By compiling information on relative differential expression levels of numerous genes, not just those labelled as significant by the wald testing in DESeq2, it can be observed if this information coalesces around certain pathways related to upstream regulators, specific biological pathways or downstream functions and phenotypes. Finally GSEA was undertaken to assess GO term and Reactome pathway enrichment between the populations of interest.

The results of this analysis showed a high degree of similarity between the results obtained using treatment naïve samples and those previously exposed to chemotherapy. As an example, of the top 20 enriched GO terms in DP vs DN analysis among treatment naïve samples (Figure 24.D), 18 were enriched in the DP group of the small cohort of chemotherapy treated samples, which included just 2 DN and 3 DP samples. The majority of these top 20 results were enriched in the top 200 results in the chemotherapy only group, and those not included in this crossover were gene sets related to cardiac muscle development and myeloid dendritic cell activation, likely false positive results. Similarly, all of the top 20 enriched reactome pathways in the DP group among naïve samples (Figure 24.E), were found enriched in the DP group in chemotherapy pre-treated samples only. Similar correlations between results obtained from comparisons between DP and DN populations in both treatment groups using the other data analysis techniques outlined above.

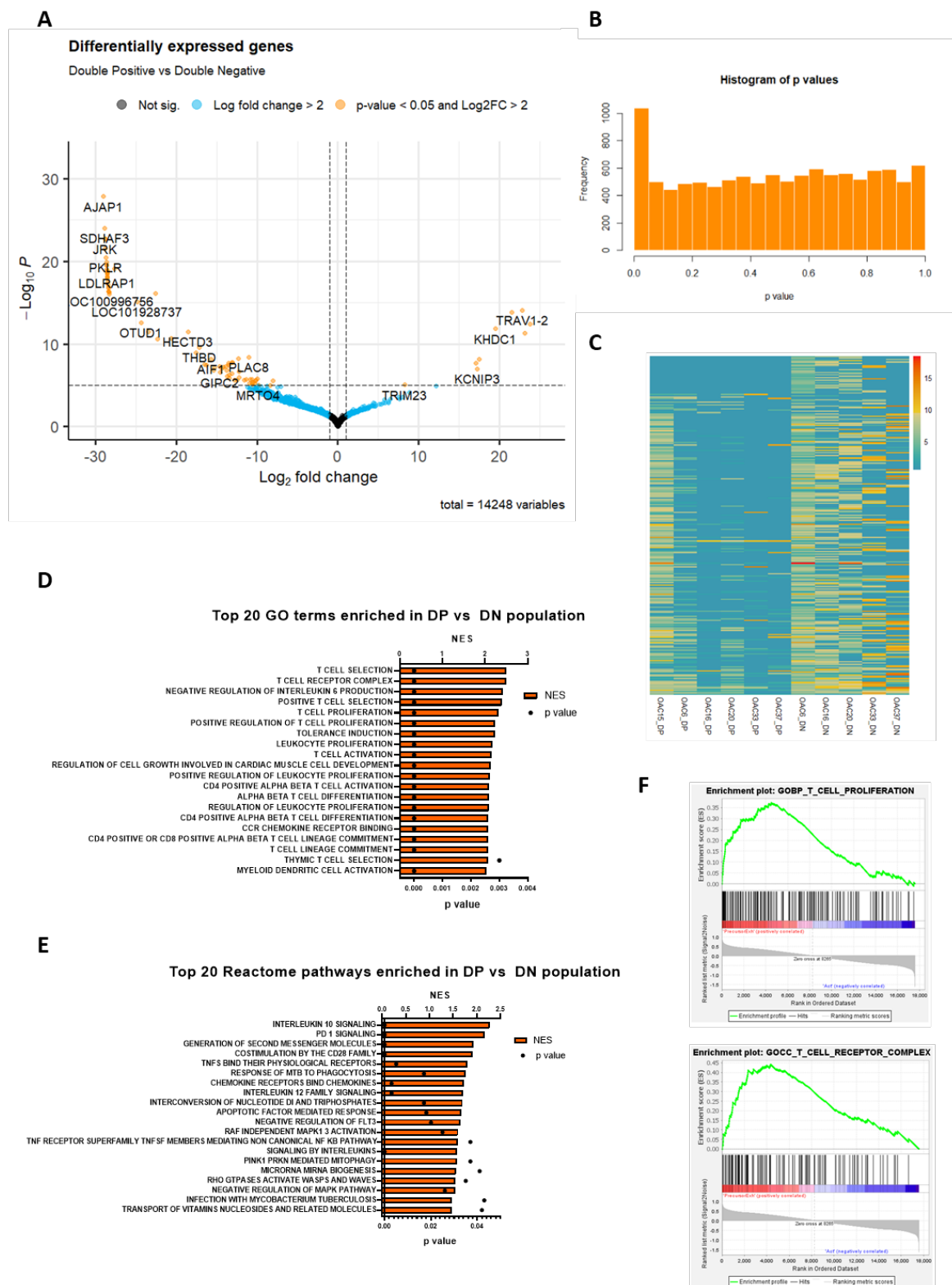


Figure 24 Differential gene expression analysis and GSEA comparing DP with DN populations in treatment naïve samples.

A) Volcano plot displaying 261 differentially expressed genes with a p value < 0.05, 28 with increased expression in the DP group and 243 increased in the DN group. B) Histogram showing the range of p values for differential gene expression analysis

using DESeq2 comparing DP and DN treatment naïve samples. Frequency is the number of genes with each p value. C) Heatmap showing VST normalised gene counts of 263 differentially expressed genes. D) Top 20 GO terms enriched in the DP vs DN group on analysis by GSEA using the Broad Institute software. Bars related to Normalised Enrichment Score (NES) and points related to nominal p value. All results showed FDR <25%. E) Top 20 Reactome pathways enriched in the DP vs DN group on analysis by GSEA using the Broad Institute software. Bars related to Normalised Enrichment Score (NES) and points related to nominal p value. The top four results showed FDR <25%. F) Exemplar GSEA enrichment plots for GO terms related to T cell activation and T cell receptor complex expression.

The high degree of overlap with the naïve samples observed when analysing results from the chemotherapy pre-treated samples alone provided confidence that the populations isolated are comparable regardless of pre-treatment and that combining read counts from these two groups can add power to the results, without confounding the outcomes.

4.2.6 Comparison of DP and DN populations from all treatment naïve and chemotherapy pre-treated samples.

4.2.6.1 Gene ontology term and Reactome pathway analysis with GSEA

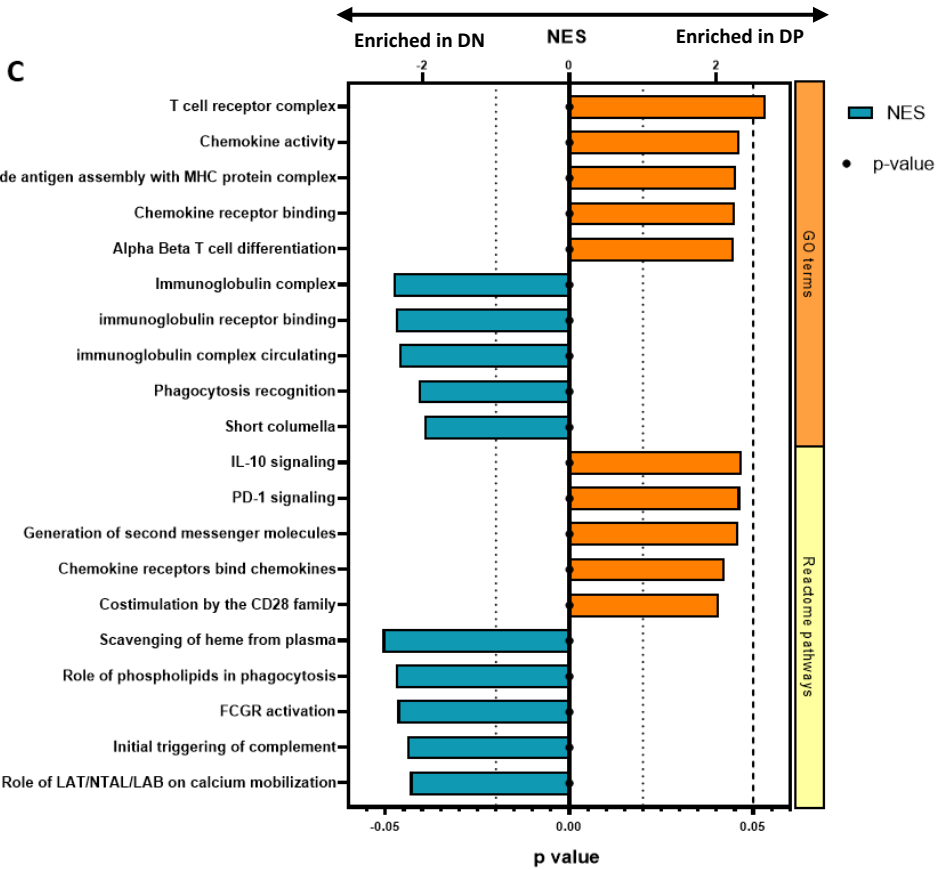
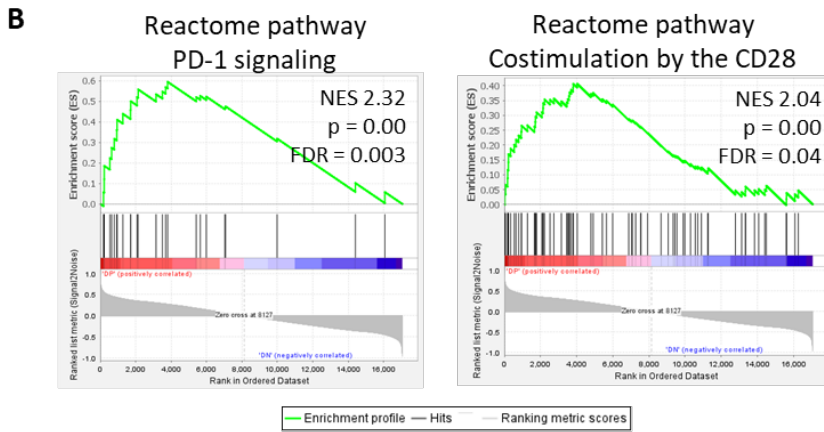
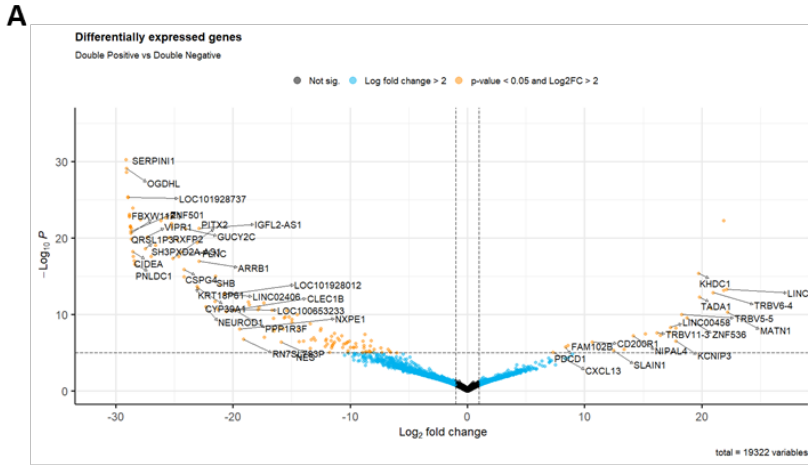
Read counts obtained for all treatment naïve and chemotherapy treated samples were combined and DGE analysis was undertaken as previously described. A total of 485 significantly DEGs with an adjusted p value of less than 0.05 were identified, 66 genes showed increased expression in the DP group, and 419 in the DN group. Assessment of these differentially expressed genes, reassuringly showed *PDCD1*, the gene encoding PD-1 over expressed in the DP group. Over expressed in the DN group were a number of immune active molecules including *NFKB1*, encoding a subunit of the NFKB transcription factor. As described already, while assessing individually differentially expressed genes is interesting, it is difficult to gain an impression of function in doing so. Normalised read counts for each sample, and Log2fold change results for each gene were calculated using the DESeq2 package and used for GSEA and IPA assessment.

GSEA was utilised to assess for enrichment of GO terms and Reactome pathways in all samples and showed results comparable to the analysis of just treatment naïve patients. GO analysis revealed 432 of the 3126 gene sets enriched in the DP group did so with a p value of <0.05. 228 had a p value <0.01 and 225 a FDR < 25%. This total was a greater number of statistically significant results than when just the naïve patient samples were used, around double the number, not a larger order of magnitude. The higher number with a significant FDR suggests that

the increased number of samples is reducing the likelihood that significant results are false positives. Among the top 10 most enriched gene sets were those related to TCR complex molecules, chemokine activity, alpha/beta T cell differentiation, T cell activation and positive regulation of T cell activation, lymphocyte chemotaxis and positive regulation of leukocyte cell-cell adhesion. Other high ranking gene sets include numerous results for leukocyte and T cell proliferation, chemotaxis, adhesion, positive selection and migration signals. Also among those with a low FDR and high enrichment were gene sets related to production of IL-2, IL-10, IL-12 and IFN- γ (Figure 25.C).

These GO results were supported by GSEA analysing enrichment of gene sets describing Reactome pathways when all DP and DN samples are compared. 483 gene sets enriched in the DP group, 54 with a p value <0.05 and 25 with a p value <0.01. 9 gene sets had an FDR <25%. Within the 20 most significantly enriched gene sets were pathways related to PD-1 signalling and CD28 co-stimulatory signalling and chemokine receptors binding chemokines. Also included in this list are IL-10, IL-12, and IFN gamma signalling pathways, as well as downstream TCR signalling (Figure 25.C).

Combining these GSEA results suggests a DP population enriched for lymphocyte activation, proliferation and migration, with regards to the DN group, as well as showing evidence of increased TCR and CD28 signalling as well as PD-1 signalling.



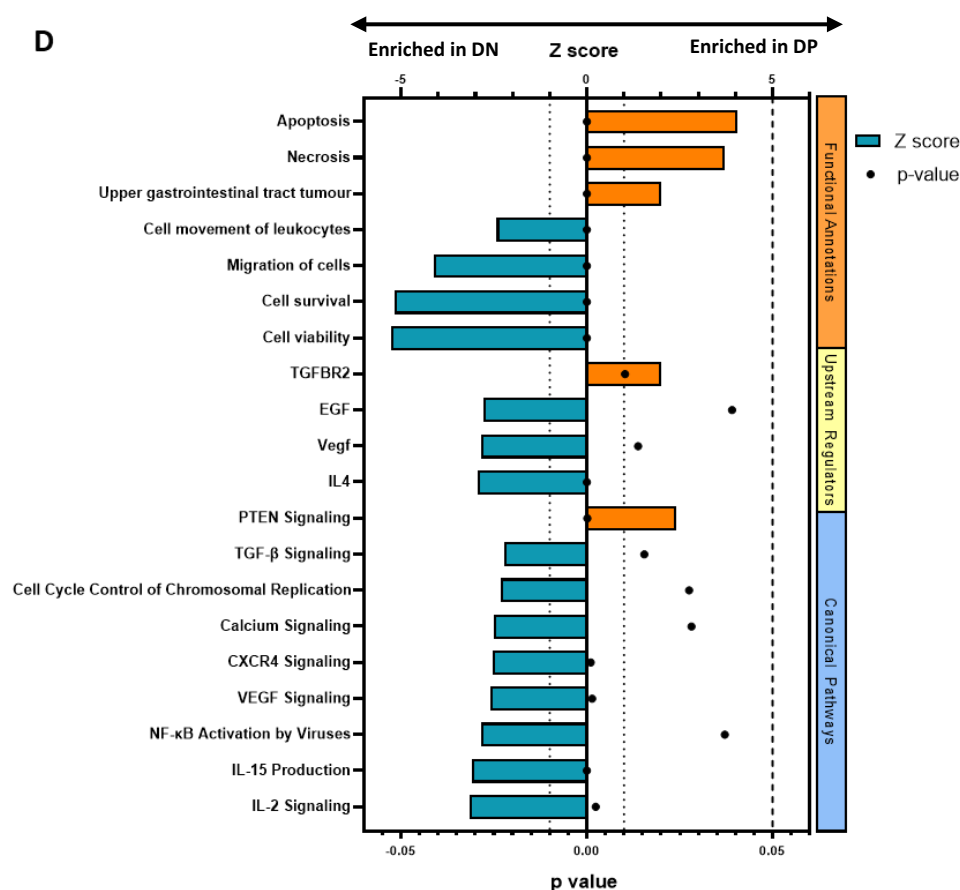


Figure 25 Comparison of DP and DN populations from all post chemotherapy and treatment naïve patient samples.

A) Volcano plot displaying 485 differentially expressed genes with a p value <0.05, 66 with increased expression in the DP group and 419 increased in the DN group. B) Gene set enrichment plots assessing enrichment of PD-1 signalling and co-stimulation by the CD28 family in the DP vs DN populations. C) Summary of GSEA of top enriched GO terms and Reactome pathways in DP vs DN populations. Normalised enrichment score (NES) (bars) show degree of enrichment and p value <0.05 suggest statistical significance (points). Positive NES indicates enrichment in DP population with negative value indicating enrichment in DN population. First 10 results related to Gene ontology terms, with first 5 the most enriched in the DP group and the next 5 the maximally enriched in the DN group. The next 10 are related to Reactome pathways with the first 5 the maximally enriched gene sets in the DP and the next 5 the most enriched pathways in the DN group. D) Selected IPA analysis showing most relevant significantly enriched pathways related to cellular functional processes, upstream regulatory molecules and canonical pathways. Functions with a Z-score greater than 2 (orange bars) show enrichment in the DP phenotype, whereas those with a score less than -2 (blue bars) show enrichment in the DN group. Significant Z-

scores demonstrated by bars crossing of the dotted line (Z-score >2 or <-2) and p value below the dashed line ($p<0.05$).

When the GO gene sets enriched in the DN group compared to the DP group are scrutinised, the picture is less clear cut. This may well be a result of a more heterogeneous population here. 4571 gene sets were enriched in the DN group, 303 had a p value of < 0.05 and 80 a p value of <0.01 , with 4 showing an FDR $<25\%$. The top 20 enriched GO terms represented a greater variety of systems than those in the DP group and is likely affected by false positives. While gene sets related to immunoglobulin receptor signalling were observed, there was also gene sets related to diseases of impaired glucose tolerance, supraventricular tachycardia and muscular dystrophy. It is difficult to see clear reproducible patterns. This is similar to the results seen in analysis of the treatment naïve patients only, but more marked here. Reactome pathway based GSEA showed a similar picture with 44 of 458 enriched gene sets possessing a p value <0.05 , 23 with a p value <0.01 , and 18 an FDR $<25\%$. Within the most enriched gene sets are pathways related to FC γ receptor immunoglobulin binding, but also those related to the complement cascade, and multiple pathways related to the extracellular matrix and molecules such as keratin and collagen (Figure 25.C).

Of note, when similar techniques have been used to evaluate GO term enrichment in CD39- vs CD39+ in chronic infection, it was not possible to classify the CD39 negative group while the positive group enriched for gene sets related to mitosis and cell cycle processes (126).

4.2.6.2 Ingenuity Pathway Analysis

Log₂fold change data was calculated for a combined chemotherapy pre-treated and naïve data set with regards to comparison of DP and DN groups, calculated using the DESeq2 package, and was inputted into the IPA software. Results were analogous with those observed for the treatment naïve group alone, with significant enrichment of functional annotations related to apoptosis and necrosis in the DP group, and cell survival and viability in the DN group. Analysis of upstream regulatory and canonical pathways demonstrated upregulation of TGF beta receptor 2 effects and PTEN signalling in the DP group. VEGF and IL-4 dependent pathways are again over expressed in the DN group as are canonical VEGF and IL-15 signalling gene sets, as well as CXCR4 and IL-2 signalling pathways. Considering the upstream regulators identified as enriched through IPA analysis and GSEA in the DP group, a combination of TGF- β , IL-2 and IL-15 signalling does not necessarily point towards activated effector CD8+ function, however as has already been alluded to, when viewed through the lens of a tissue resident memory cell phenotype these cytokines all play a role in TRM development and maintenance (134,220) (Figure 25.D). In addition, enriched in the DP group though not considered significant due to a Z-scores of 1.8 and 1.2 respectively, were

signatures related to signalling of RUNX3 and Id3, key transcription factors in TRM development and maintenance in peripheral tissues (134).

There is some discord between the results from IPA analysis with those Reactome and GO term analysis derived from GSEA, particularly regarding cell cycling, survival and proliferation, which were observed in the initial analysis of treatment naïve samples and remains in this expanded dataset. The IPA analysis suggests an increase in general cell survival signatures in the DP group and apoptosis in the DN group (Figure 25.D), while GSEA shows increased leukocyte and lymphocyte specific survival and proliferation signatures in the DP group (Figure 25.D). This may not necessarily be cause for concern, and may be a reflection of the heterogeneity of the DN population compared to the DP population producing a wider variety of cell signals, and the more general survival signatures observed in the DN group with IPA compared to the more specific lymphocyte survival signatures seen in the DP population with GSEA.

4.2.6.3 GSEA phenotypic assessment indicating tissue resident memory lymphocyte phenotype and potential immunotherapy resistance

Further GSEA analysis using gene sets curated from published data was undertaken.

Given that these populations of interest are defined by their expression, or lack of, cell surface PD-1 and CD39, GSEA was undertaken to assess for enrichment of signatures related to lymphocyte exhaustion. The DP and DN groups were compared using gene sets derived from LCMV models and also from tumour infiltrating lymphocytes detailed in a range of publications. Of particular interest, when using gene sets describing exhausted and activated human TILs derived from large single cell data atlases described by Andreatta et al, the DP group enriched for effector memory, terminally exhausted and precursor exhausted phenotypes, when compared to the DN group. The strongest enrichment was for the precursor exhausted phenotype (NES 2.59, $p=0.0$) (221). Interpretation of this is not easy, but could suggest populations of all of these subsets of lymphocytes at levels greater than that seen in the comparator group.

Data from work by Paulino Tallón de Lara et al, examining the ability of a population of PD-1+ CD39+CD8+ lymphocytes to control breast cancer metastases in a mouse model, showed enrichment of gene sets related to effector CD8+ T cells and tissue-resident memory CD8+ T cell activity (130) The experimental populations compared were a PD-1+CD39+ double positive population of CD44+CD8+ lymphocytes when compared to the rest of the CD44+CD8+ T cells, a highly analogous if not identical experimental model to this study. The DP and DN OAC TIL samples were analysed using the same gene sets as those used by Tallón de Lara et al, and a similar pattern of enrichment was observed. The DP group was enriched for the effector vs memory

CD8+ upregulated gene set published by Goldrath et al. (NES 1.697 p=0.00) and for a gene set comprising genes upregulated in a tissue resident memory cell population described by Savas et al. (NES 1.759, p=0.00) (141,222).

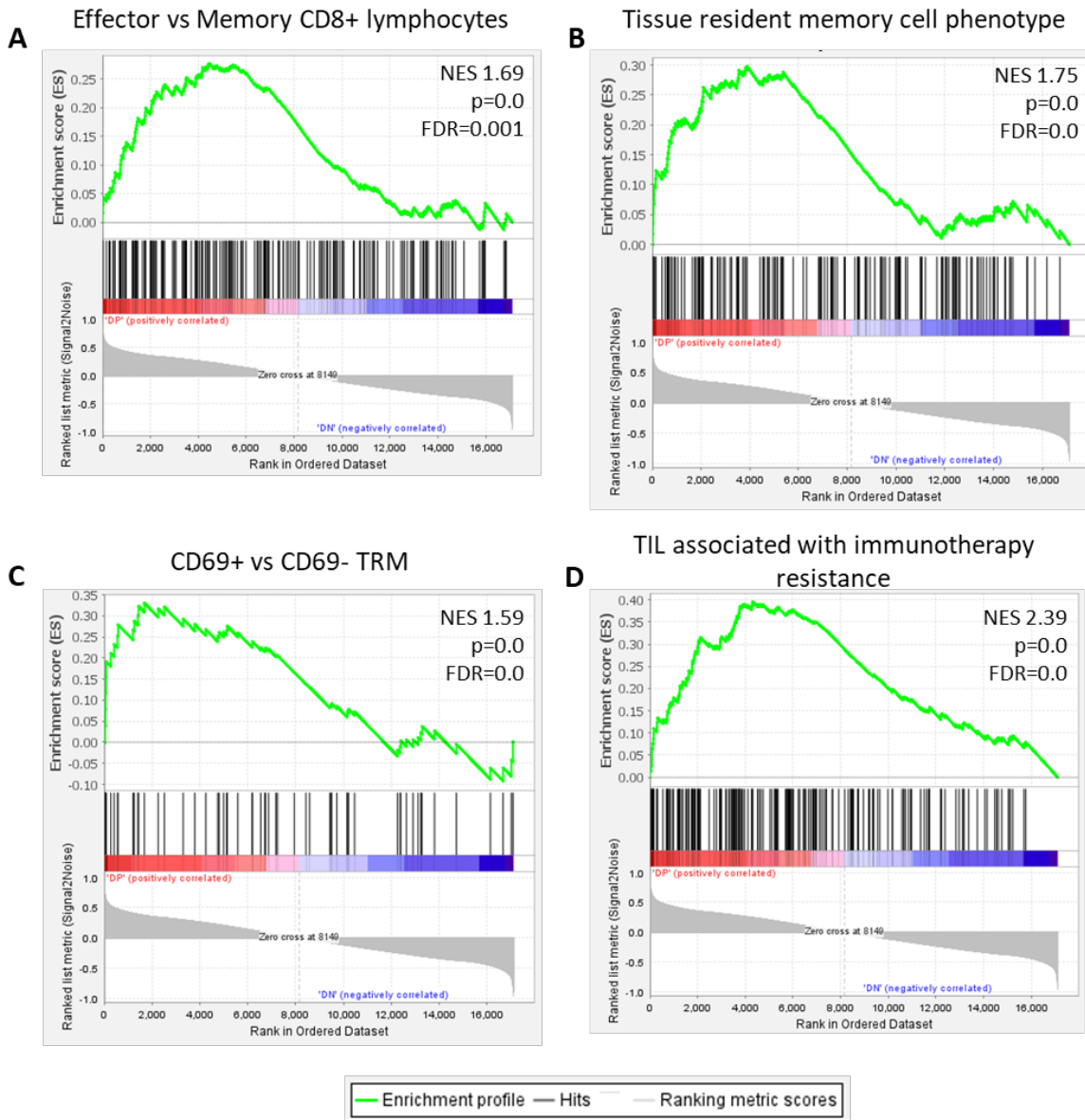


Figure 26 GSEA comparison of DP and DN phenotypes

GSEA enrichment plots displaying enrichment of gene sets describing key CD8+ T lymphocyte phenotypes in the PD-1 and CD39 double positive group of antigen experienced TILs when compared to the double negative group. A) Enrichment for Effector CD8+ T lymphocyte gene set as described by Goldrath et al.(222) B) Enrichment for the tissue resident memory CD8+ T lymphocyte gene set as described by Savas et al.(141) C). Enrichment for the CD69+ tissue resident memory phenotype as described by Kumar et al.(136) D) Enrichment for the CD8_B phenotype described

by Sade-Feldman et al. as being associated with markers of exhaustion and resistance to treatment with immune checkpoint blockade(69).

To further confirm the picture that the DP group is composed of cells of an effector-memory or TRM phenotype, using data from a more recently published analysis of the core transcriptional signature of CD69+ TRM cells, a gene set was produced from the 250 most differentially expressed genes in lung TRM cells. This gene set was also shown to be significantly enriched in the DP group when compared to DN (NES 1.592, p=0.00) (136).

Additionally by utilising gene sets produced from published data related to responses to immune checkpoint blockade, it was observed that the DP group was strongly enriched in gene sets from single-cell expression clusters associated with reduced responses to these therapies in melanoma. In their paper Moshe Sade-Feldman et al. identified the population of CD8 TILs, labelled CD8_B, as being associated with increased cellular markers of exhaustion, including PD-1 and CD39 and also associated with reduced response to checkpoint blockade (69). This gene set was strongly enriched in the oesophageal adenocarcinoma TIL DP population when compared to the DN group (NES 2.398, p=0.00).

These attempts to clarify the phenotype of the DP population with respect to the DN group, suggests mixed population, potentially composed of portions of precursor exhausted lymphocytes and terminally differentially exhausted lymphocytes, though also containing a significant population of effector-memory lineage cells including TRMs. Comparing this DP population to samples further along the lymphocyte exhaustion gradient will allow further clarity to be obtained.

4.2.7 Comparing the LExh and DP phenotype from all analysed samples.

4.2.7.1 Ingenuity Pathway Analysis

An identical data analysis pipeline to that described above, was implemented for assessing the relative differences between the transcriptomic profiles of the LExh population and the DP population in treatment naïve samples alone and then in the combined naïve and chemotherapy pre-treated samples. The purpose of undertaking this was to investigate if the LExh population, in possession of multiple surface markers of exhaustion did indeed possess a transcriptomic profile in keeping with that of a terminally differentiated exhausted phenotype, to confirm if this is shared with the DP group, or is the DP group more in keeping with a precursor exhausted or other non-exhausted phenotype.

Chapter 4

Gene counts were subject to the same pre-filtering as for the DP vs DN comparison and DGE counts created. As for previous analyses, the treatment naïve cohort was investigated for trends and themes, and then analysis was repeated using the full data set to add power and confidence to results obtained through increased sample numbers.

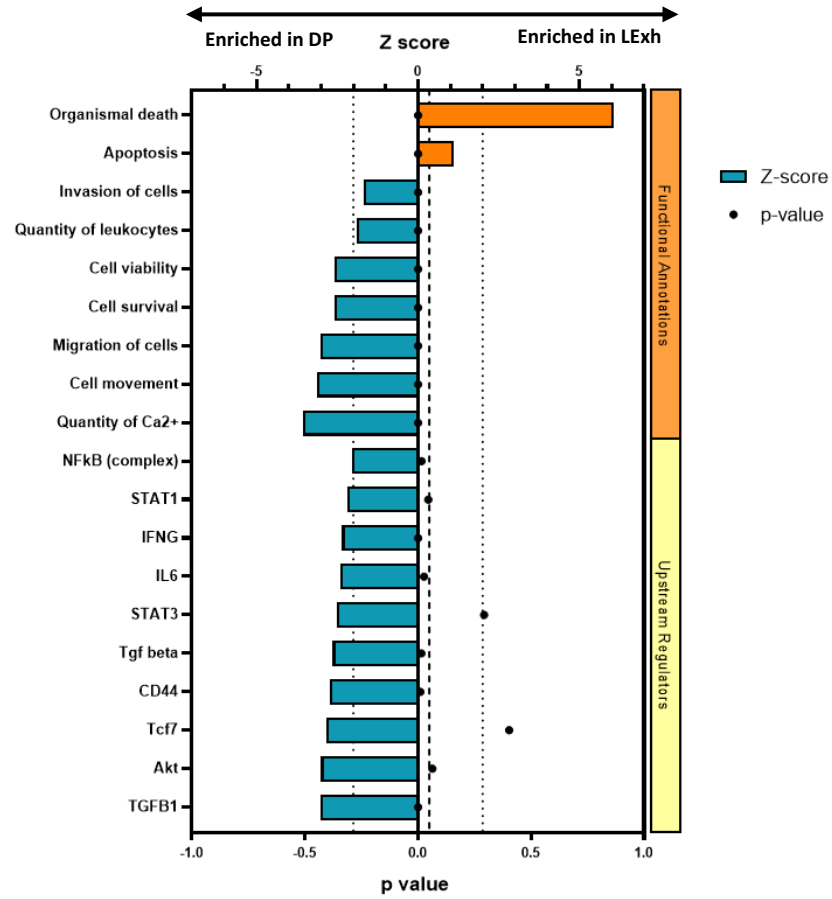
For the treatment naïve samples alone, when comparing the LExh with DP groups a total of 429 genes were significantly differentially expressed with a p-value <0.05 , with 100 showing increased expression in the LExh group and 329 in the DP group. A similar number of DEGs were identified using all samples with 578 showing a p-value <0.05 , 386 over expressed in the DP group and 192 in the LExh group, with a high degree of overlap between groups, with over 30% of the DEGs from the analysis of naïve samples, seen in the combined analysis.

The list of genes significantly differentially expressed were again used to identify GO terms with increased or decreased expression. As previously, given the limitations of assessing for GO term enrichment using lists of differentially expressed genes, there were no clear patterns that emerged from this analysis.

Log₂fold change data was inputted into the IPA software to assess canonical states, functions and upstream regulators that are enriched in each test group. By using the same experimental conditions as previously discussed, a log₂fold change of greater than 0.5 or less than -0.5 required for gene inclusion, 1699 genes were included for analysis. Signatures related to cell survival, viability, movement and migration, were enriched towards the DP group. Within the LExh group there was a corresponding trend towards signatures related to cell death and organismal death, though enrichment of apoptotic markers was not of statistical significance (Figure 26).

Canonical pathway analysis revealed a similarly small number of significantly enriched results, however of interest, the T cell exhaustion pathway was enriched towards the LExh group, though not significantly so, as was the T cell receptor signalling pathway. This could well suggest a more exhausted group occurring as a result of increased TCR signalling, fitting with the overarching hypothesis of the LExh group representing a terminally differentiated exhausted phenotype. CXCR4 and CDK5 signalling were increased in the DP group. As was Notch and Integrin signalling which could be highly relevant given the suggestion in earlier analysis that the DP group may contain a significant TRM population (Figure 26). Notch is a key transcription factor in TRM establishment and CD103 a key integrin often defining TRM populations (134).

A



B

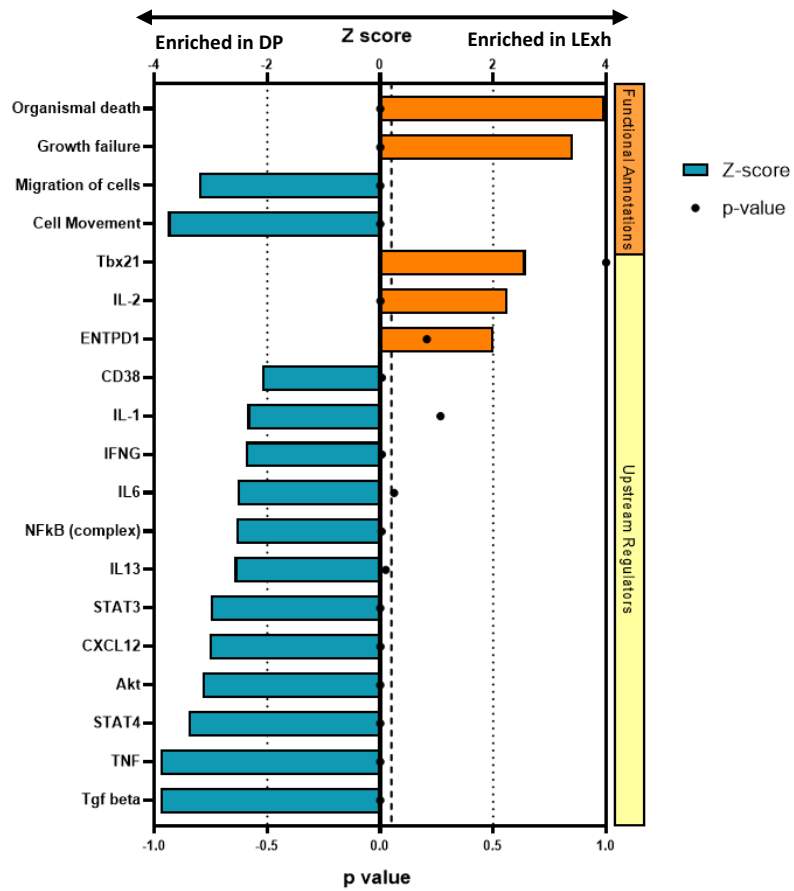


Figure 27 Comparison of the LExh and DP populations with Qiagen IPA analysis.

A) Selected results of analysis of treatment naïve samples with the QIAGEN IPA analysis software showing most relevant significantly enriched pathways related to cellular functional processes and upstream regulatory molecules. Functions with a Z-score greater than 2 (orange bars) show enrichment in the LExh phenotype, whereas those with a score less than -2 (blue bars) show enrichment in the DP group. Significant Z-scores demonstrated by bars crossing of the dotted line (Z-score >2 or <-2) and p value below the dashed line ($p < 0.05$). B) Selected results of analysis of the combined group of treatment naïve and chemotherapy pre-treated samples with the QIAGEN IPA analysis software showing most relevant significantly enriched pathways related to cellular functional processes and upstream regulatory molecules.

Potentially the most interesting method for interrogating the IPA results is the effects of upstream regulators that is observed. In this analysis a number of key transcription factors are enriched in the DP group, including a collection that provide proliferative signalling to CD8+ lymphocytes including the NF κ B complex and NFAT. Additionally, in keeping with comments related to TRM populations, downstream effects of the STAT3 and STAT4 molecules are shown to be enriched in the DP group, transcription factors shown to play key roles in differentiation and maintenance of populations of T memory cells(134,140) (Figure 26).

Of real interest is the effects of *TCF7*, the gene that encodes for the key transcription factor in the precursor exhausted lymphocyte phenotype, TCF-1, which is enriched in the DP population (Figure 26). Additionally, by amending the experimental parameters and including more genes for analysis, downstream effects of Eomes and TOX transcription factors can be observed significantly enriched in the LExh group, again, canonical transcription factors for terminally differentiated exhausted phenotype (34,89).

By expanding the data set to include the samples from patients pre-treated with chemotherapy, broadly similar results are observed from IPA analysis. By using a cut-off of plus or minus 1.5 log2fold change for inclusion allowed optimal parameters for analysis, it is observed that processes associated with cell death and apoptosis are again enriched in the LExh population, as were transcriptional profiles in keeping with signalling by *ENTPD1*, the CD39 gene, unsurprising given increased CD39 expression is associated with the presence of multiple exhaustion markers, as well IL-2 signalling (Figure 26). A surprise inclusion among upstream regulators enriched in the LExh group is the t-box transcription factor T-bet, labelled by its gene name *Tbx21* (Figure 26). On the surface this appears at odds with a description of the LExh group as a more terminally differentiated exhausted population, where we would expect Eomes to dominate at the expense

of reduced T-bet. However this is in keeping with observations of dysfunctional TILs in lung cancer as well as other tumour models, where both T-bet and Eomes are maintained with progression to a more exhausted-like state (94).

Enriched in the DP group on IPA analysis of the combined naïve and chemotherapy treated group, are features related to cell movement and migration which are shared with the results from analysis of treatment naïve samples only. Also shared between the two analyses are effects of upstream regulators including, IFN- γ and TGF- β signalling, and the regulators of transcription AKT, NF κ B and STAT3 (Figure 26).

4.2.7.2 Gene ontology term and Reactome pathway analysis with GSEA

Further comparisons were made between these two groups using GSEA. Again GO term and Reactome pathway enrichment was examined in comparisons of the LExh and DP groups. Assessing all GO terms in the MSigDM collection, of the 15,473 gene sets, 8,562 remained after filtering and 3,945 were enriched in the LExh population with 4,617 in the DP group. In the LExh group 127 gene sets were enriched with a nominal p value <0.05 and 28 <0.01. No gene sets had a FDR<25%. Among these significant results were terms related to negative control of cell cycling, particularly negative regulation of G1 to S phase, though positive regulation of G2 to M phase was noted. Additionally negative regulation of TNF signalling was observed (Figure 27.A). Repeating this analysis including all samples for analysis revealed 7697 gene sets that passed filtering, 4028 enriched in the LExh group, 319 of these had a p value <0.05 and 114 a p value <0.01. This again included a large number of gene sets related to cell cycle checkpoints, particularly negative regulation of cell cycling, though positive regulation was also observed (Figure 27.B).

GSEA assessment of GO terms enriched in the DP group revealed, 149 had a nominal p value <0.05, 47 with <0.01 and 6 gene sets had an FDR<25% when treatment naïve samples alone were assessed. Here there was enrichment of terms related to chemotaxis and cell migration, as well as positive effects of type 1 interferon signalling (Figure 27.A). Analysis of the full data set showed that among the 3669 gene sets enriched in the DP group, 424 possessed a p value <0.05 and 169 a p value <0.01. Among the most enriched, processes related to immunoglobulin signalling are again represented, as are gene sets related to chemotaxis and migration of cells generally as well as immune cells and leukocytes specifically (Figure 27.B).

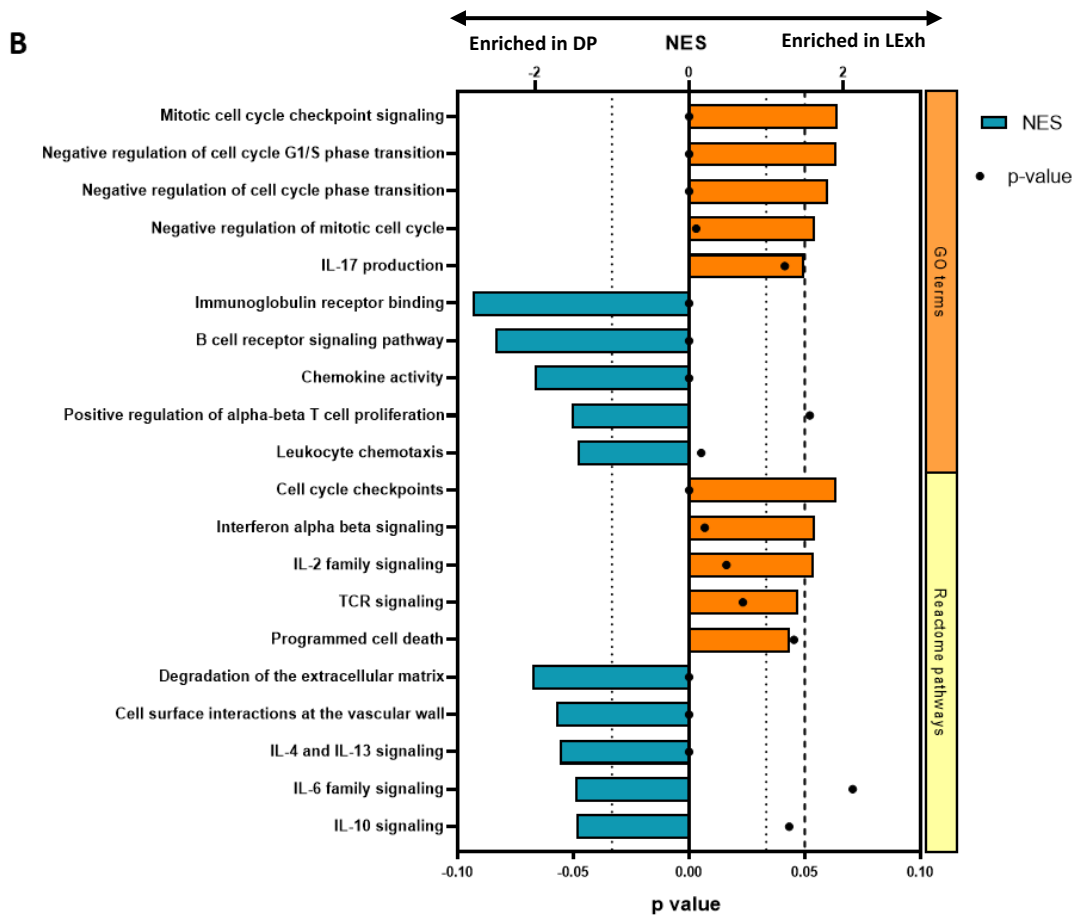
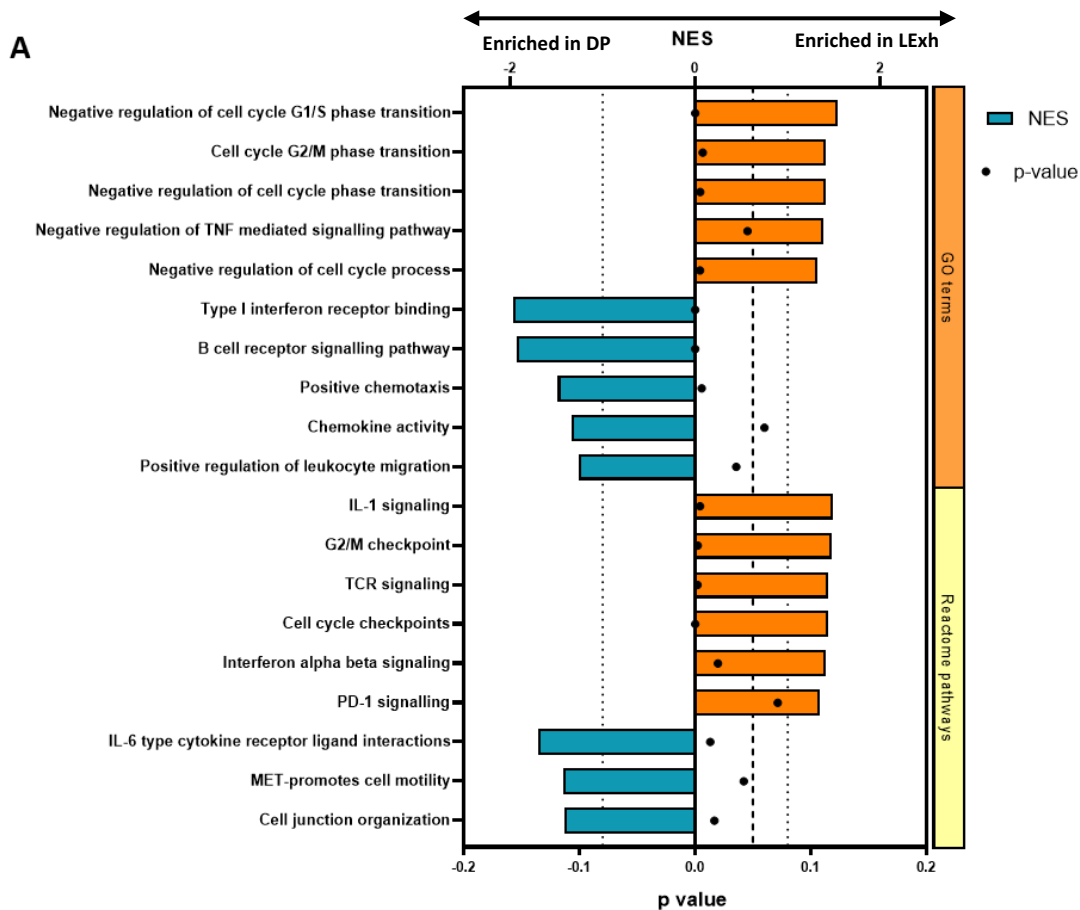


Figure 28 GSEA comparing the LExh and DP populations using GO terms and Reactome pathways.

A) Selected results from analysis of treatment naïve samples comparing LExh and DP groups with respect to GO terms and Reactome pathways from the MSigDB using GSEA. Functions with a normalised enrichment score (NES) greater than 1 (orange bars) show enrichment in the LExh phenotype, whereas those with a score less than -1 (blue bars) show enrichment in the DP group. Significant NES demonstrated by bars crossing of the dotted line (Z-score >1 or <-1) and p value below the dashed line ($p < 0.05$). B) Selected results of analysis of the combined group of treatment naïve and chemotherapy pre-treated samples for enrichment of GO terms and Reactome pathways when LExh and DP groups were compared by GSEA.

The analysis of Reactome pathway enrichment in naïve samples revealed 1036 gene sets passing filtering, with 633 being enriched in the LExh group, 73 with a p value < 0.05 , 20 < 0.01 and none with a FDR $< 25\%$. The significantly enriched group included pathways related to cell cycle checkpoints, again pointing to a degree of restraint of mitosis, and in contrast to the GO assessments of the same population, type 1 interferon signalling (Figure 27.A). Downstream TCR signalling gene sets were enriched, potentially implying increased antigen exposure and signalling, as were PD-1 signalling, suggesting increased PD-1 engagement in the terminally differentiated exhausted group, though this final result did not reach statistical significance. This correlates with the IPA analysis of the same data set which demonstrated evidence of increased TCR signalling and lymphocyte exhaustion pathways in the LExh group. Reactome pathway enrichment analysis of the full data set revealed 595 gene sets are enriched in the LExh group, 142 with a p value < 0.05 and 65 with p value < 0.01 . Significant enrichment was observed for elements related to mitotic cell cycling, particularly M phase and S phase, as well as cell cycle checkpoints. Additionally, the LExh group enriched for gene sets related to type 1 interferon signalling, PTEN regulation, IL-1, IL-2, IL-17 and IL-37 signalling as well. TCR signalling showed significant enrichment in the LExh group, as did gene sets related to programmed cell death (Figure 27.B).

The DP group from naïve samples was enriched for 403 Reactome pathway gene sets, of which 41 were significantly so with a p value < 0.05 , and 20 with $p < 0.01$. 9 had an FDR less than 25%. This included terms related to IL-6 signalling, in keeping with the IPA analysis of the same groups, as well as pathways related to cell motility and cell to cell interactions (Figure 27.A). 346 Reactome gene sets were enriched in the DP group of the full data set, on comparison with all LExh groups. This included 70 with a p value < 0.05 and 49 with p value < 0.01 . The most statistically significant results related to interaction with the extracellular matrix, IL-4, IL-6, IL-10 and IL-12 signalling as well as TGF- β signalling (Figure 27.A).

4.2.7.3 GSEA phenotypic assessment

As described previously GSEA can also be used to assess for enrichment of gene sets describing specific phenotypes in experimental populations. This has been completed with regards to comparison of the LExh and DP groups using gene sets derived from various CD8+ lymphocyte exhaustion models, as well as CD8+ effector, memory and T_{RM} phenotypes.

Gene sets produced detailing the transcriptional differences between the canonical exhaustion model of LCMV clone 13 infection were used to interrogate differences between the LExh and DP groups, as were gene sets derived from the transcriptomic profiles of exhausted TILs derived from large single cell atlases (41,43,221).

Highly enriched in the LExh group was the gene set detailing the terminally exhausted group described by Andreatta et al (221) (NES 1.805 and p=0.013) which was identified through analysis of TILs from human cancers, predominantly melanomas. Also highly enriched in this group was the precursor exhausted population (NES 1.58 and p=0.026) from the same source publication. This may represent the strong crossover of genes shared between these gene sets, though may also suggest that the DP group is not dominated by TILs of a precursor exhausted phenotype, but in fact is formed of a dominant population lymphocytes of an alternative lineage. As has been shown, the evidence has increasingly suggested a T_{RM} dominant DP group.

Alongside this, also highly enriched in the LExh group were gene sets related to an effector vs memory phenotype described by Goldrath et al(222) (NES 1.7 and p=0.0) and Wherry et al (41) (NES 1.62 p=0.0) (Figure 28). This could be in keeping with the LExh population being a terminally differentiated exhausted population arising from persistently stimulated effector lymphocytes, with the DP population a T_{RM} population arising from memory cells. Alternatively, both DP and LExh populations could be T_{RM} lymphocytes, the later in keeping with a T_{RM} population with a phenotype more analogous with exhausted lymphocytes with possession of multiple inhibitory receptors such as TIM3, but not functionally exhausted. Such PD-1 high, TIM3+ T_{RM} cells have been described in a variety of tumour types now including in lung cancer by Clarke et al, where they have been associated with reactivity to immune checkpoint blockade (114).

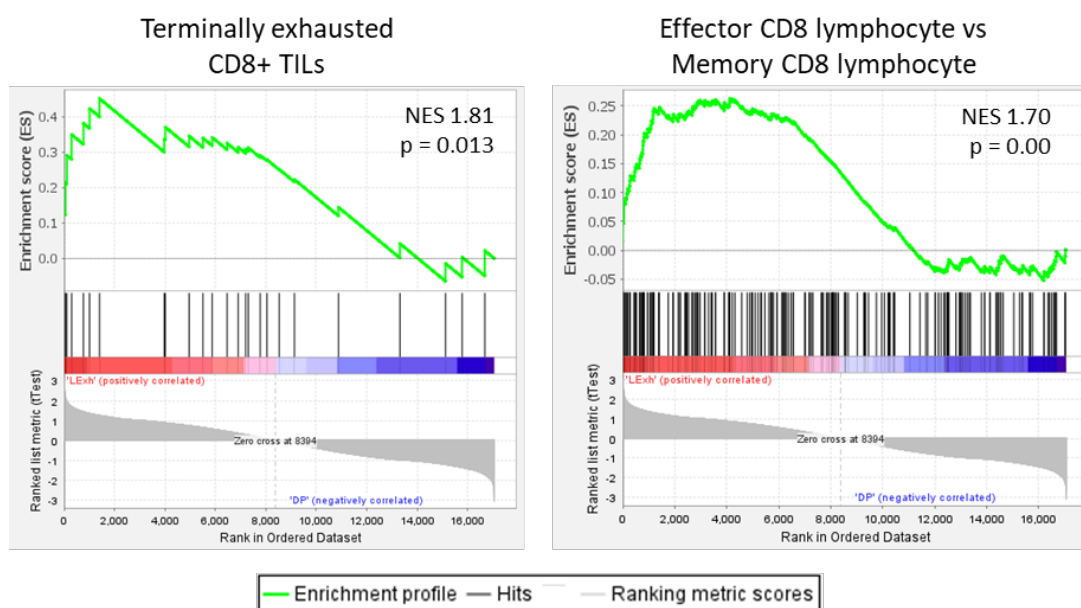


Figure 29 GSEA comparison of LExh and DP phenotypes.

GSEA enrichment plots detailing enrichment of gene sets detailing differentially expressed genes in terminally exhausted CD8+ TILs derived from human tumours (41) and effector vs memory CD8+ lymphocytes (222) when LExh samples were compared with DP samples from a combined data set comprising all treatment naïve and chemotherapy pre-treated patient samples.

4.2.8 Comparison of all experimental phenotypes from combined treatment naïve and chemotherapy pre-treated samples.

4.2.8.1 Gene set variation analysis

The benefits of utilising a GSEA based strategy for comparing two phenotypes with respect to gene sets of interest has been demonstrated thus far, though this does not allow comparison of more than two groups. Gene set variation analysis (GSVA) is a related approach that allows unsupervised estimation of the relative enrichment of a gene set of interest across all samples of a data set, not just between two populations (223). Each sample is apportioned an enrichment score for each gene set analysed, which can then be incorporated into downstream analysis.

Utilising this approach for analysis of data collected in this project made it possible to compare all 4 experimental phenotypes. Gene sets including those detailing GO terms, Reactome pathways, and phenotype descriptions, were selected for use in GSVA based upon their significance in GSEA assessment of two phenotypes earlier in the experimental work stream. Gene sets were divided into those describing cell states and activated signalling pathways, as well as specific cellular phenotypes.

The first group of gene sets investigated related to cellular states that were shown to be significantly enriched in earlier GSEA. These were mostly GO terms and we see interesting trends among gene sets related to T cell processes. These are not wholly clear when results from individual samples are visualised, but come to clarity when mean enrichment scores are calculated for each sample group. Specifically it is observed that for T cell proliferation, migration and chemotaxis signatures have the most positive enrichment in the DP group, with lesser positive enrichment in the EExh and LExh groups, and negative enrichment in the DN group (Figure 29.B). T cell activation also follows a similar pattern but with a neutral enrichment in the DP group, a slightly negative enrichment in EExh and LExh groups and strong negative enrichment in the DN group (Figure 29.B). These results are in keeping with earlier GSEA results where the DP group is enriched for T cell activation and proliferation signatures when compared to the DN group, and enriched for migration signatures when compared to the LExh group.

Reactome pathways related to cytokine signalling demonstrated as having significant enrichment in earlier analyses were also explored by the same method. Here we have seen a gradient from negative enrichment in the DN group, through neutral enrichment scores in the DP group to positive enrichment in EExh and LExh groups for PD-1 signalling, TCR signalling, IL-2 family signalling and IL-12 signalling (Figure 29.C). This is not surprising for PD-1 signalling, given that the DN is defined by the absence of PD-1 by flow cytometry, and we know that PD-1 expression is increased with expression of multiple markers of exhaustion. The increase in TCR signalling is of interest and fits with a hypothesis of increased TCR interaction with cognate peptide-MHC complexes driving progression towards lymphocyte exhaustion and dysfunction. IL-2 and IL-12 both act to mediate increased cytotoxicity in CD8⁺ T lymphocytes and this result suggests that while the LExh groups are becoming dysfunctional, they remain exposed to these stimulatory signals.

A high level of enrichment for IL-10 signalling gene sets is observed in the DP, with lesser enrichment in the EExh and LExh groups and negative enrichment in the DN group (Figure 29.C). This anti-inflammatory cytokine is known to play a role in priming tissue resident memory cells, with reduced exposure resulting in lower numbers of functional CD103⁺ T_{RM} cells in vitro and in animal models, both directly and through the effects of increase TGF- β (134,224). Combined IL-4 and IL-13 signalling was observed as similarly maximally enriched in the DP group (Figure 29.C). This result is somewhat difficult to interpret with IL-4 and IL-13 key mediators of type 2 inflammation, playing key roles in Thelper-2 and eosinophil activation. These cytokines may play a role in CD4⁺ T_{RM} function, but there is no clear association with CD8⁺ T_{RM} function. This gene set is least enriched in the LExh group, as might be expected given the lack of role for IL-4 and IL-13 in mediation of an exhausted phenotype.

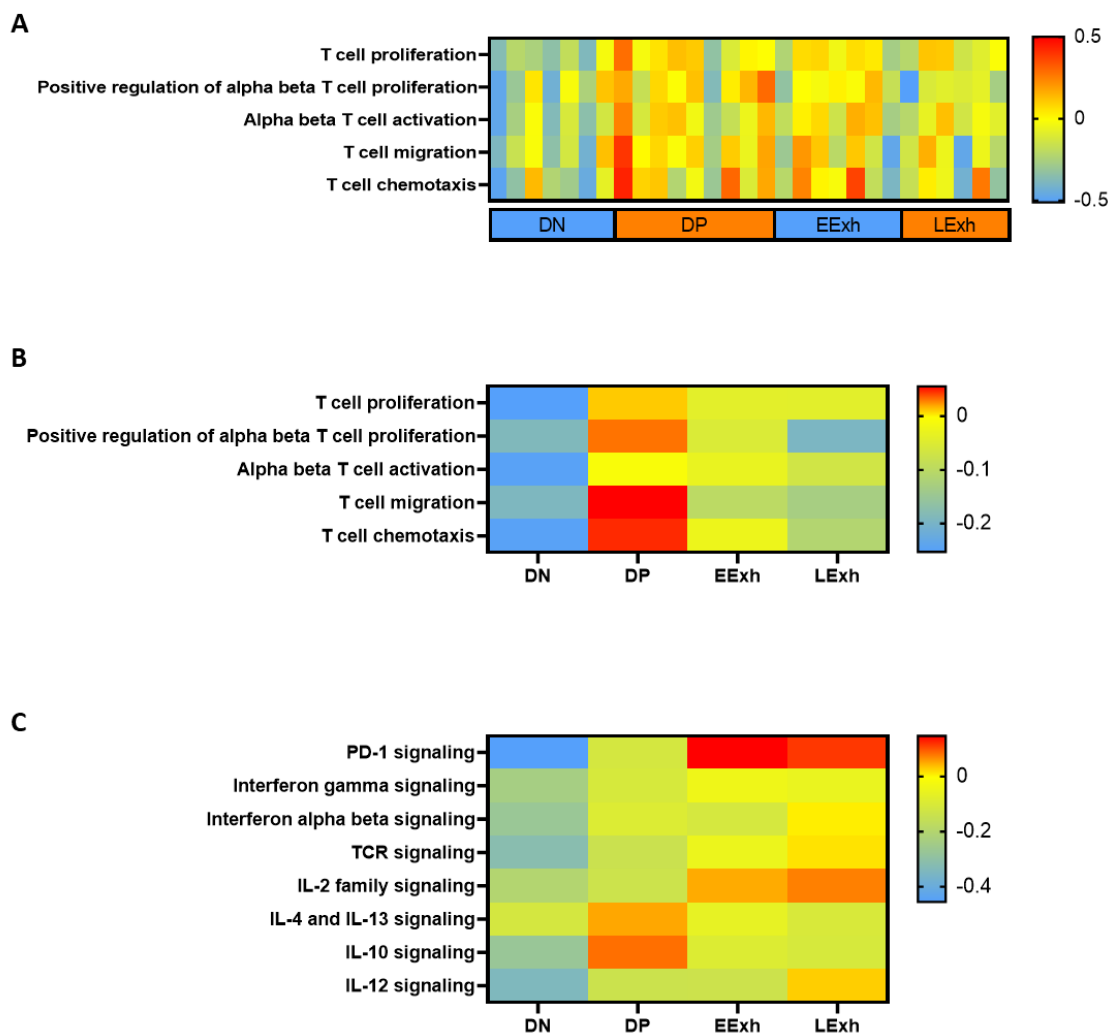


Figure 30 GSVAs analysis of GO terms and Reactome pathways of interest.

A) GSVAs enrichment score for each chemotherapy pre-treated and naïve sample following normalisation using DESeq2 pathway and VST. Selected GO terms displayed related to lymphocyte cellular states. B) Mean GSVAs enrichment scores for each sample population described in A. C) Mean GSVAs enrichment scores for each sample population relating to Reactome pathways describing signalling pathways of interest for all chemotherapy pre-treated and naïve samples.

GSVAs based analysis has also been undertaken using gene sets related the specific phenotypes, derived from published data sets that were shown to be significantly enriched in sorted TIL populations through earlier GSEA assessment.

The study groups were initially designated based upon the assumption that they would show increasing terminal differentiated exhausted phenotype, and assessment of gene sets describing a terminally exhausted gene expression signature, as detailed by Miller et al and Andreatta et al (70,221) were most enriched in the LExh and EExh groups, decreasing to show negative

enrichment in the DN group (Figure 30). Surprisingly, while the precursor exhausted gene set from the first of these publications demonstrated maximal enrichment in the DP group, the latter showed similar enrichment pattern to the terminally exhausted phenotype, though to a lesser degree. This could be explained by the hypothesis increasingly demonstrated, that the DP group is predominantly composed of TILs of a T_{RM} lineage, rather than those aligning with the classical exhausted phenotype first described in LCMV model.

A similar progressive enrichment through the study groups towards a terminally exhausted phenotype was demonstrated with a gene set defined by Sade-Feldman et al in their exploration of transcriptomic profiles in keeping with response or resistance to immune checkpoint blockade in human cancers (69) (Figure 30). Labelled as CD8_B, this expression profile is associated with an increased expression of markers of exhaustion and resistance to immunotherapy.

In earlier analyses it has been demonstrated that the DP population is enriched in signatures related to a tissue resident memory (T_{RM}) phenotype when compared to the DN population. This pattern is demonstrated again here, but continues with higher degrees of enrichment still observed in the EExh and LExh populations (Figure 30). This may suggest that all PD-1 and CD39 positive TIL populations contain a significant T_{RM} derived component, with those that go on to form the LExh group predominantly derived from this fraction. Such an assumption would be in keeping with previously described data Clarke et al. and others showing the importance of a TIM3 and PD-1 positive T_{RM} population which is functionally active and associated with, in this instance, an improved responses to immune checkpoint blockade (114).

Finally, all PD-1 and CD39 positive populations appear enriched for gene signatures relating to an effector vs memory phenotype. Though the effector transcriptional profile described by Miller et al(70) does not significantly differentially enrich, the effector vs memory (221,222) phenotypes showed increased enrichment in all of these groups, and increased with expression of multiple surface markers of exhaustion, demonstrating a potential developmental origin in the effector compartment for these populations of interest (Figure 30). Similar to some earlier results, these mixed findings for groups maximally enriched in an effector phenotype demonstrate the difficulty in deploying these analyses, and again point to a degree of heterogeneity in the composition of these experimental groups with a mix of lymphocytes derived from effector and memory CD8+ lineages.

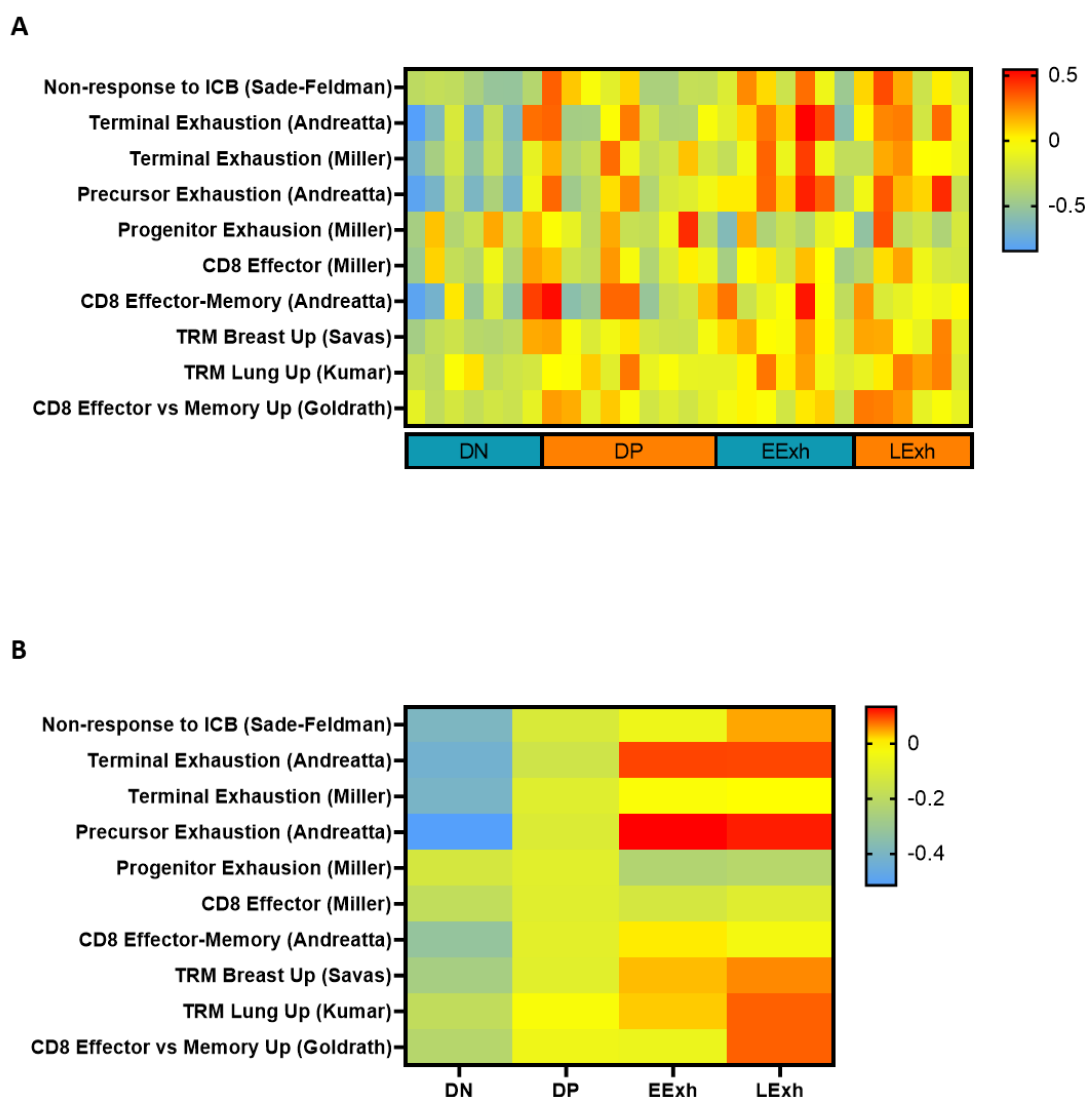


Figure 31 GSVA analysis using gene sets for phenotypes of interest.

A) GSVA enrichment score for each chemotherapy pre-treated and naïve sample following normalisation using DESeq2 pathway and VST. Selected gene sets chosen based upon significance in earlier GSEA analysis. Highlighted in brackets are the source publication for each gene set (69,70,136,141,221,222). B) Mean GSVA enrichment scores for each sample population described in A.

4.2.8.2 Key effector molecule and transcription factor expression

There was a hesitancy early in the RNA sequencing analysis to look closely at individual gene expression levels given the relatively small number of biological replicates, the moderate number of read counts planned for this experiment, and the principle outcome prior to starting was to allow GSEA. However with a body of analysis suggesting a dominant TRM population within the

DP group it is possible to look at normalised gene counts for key transcripts, in order to see if they could shed further light on the identity of this population.

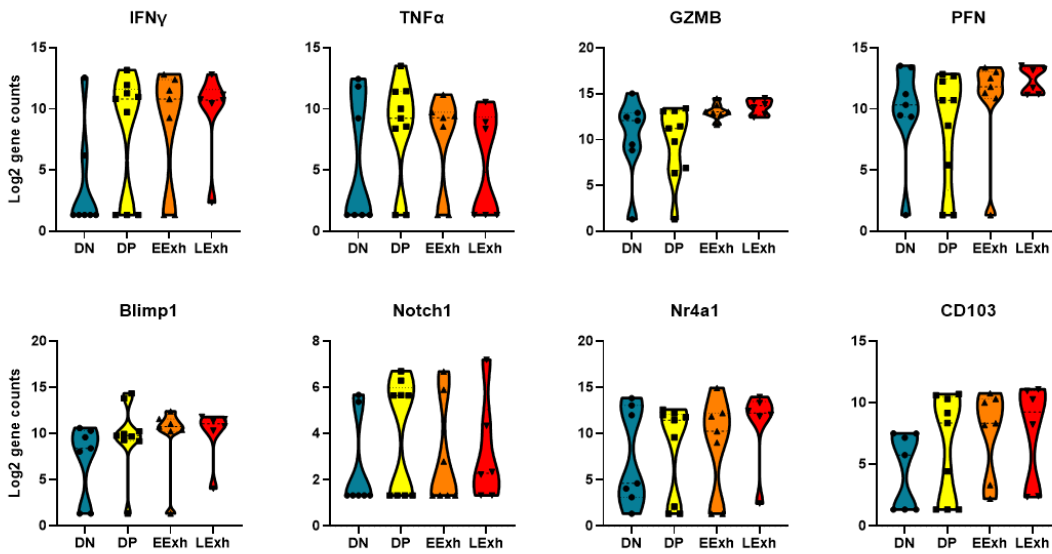


Figure 32 Normalised gene expression for effector molecules and TRM associated markers.

Log₂ variance stabilised distributed gene expression for core CD8⁺ lymphocyte effector molecules IFN- γ , TNF- α , Granzyme B and Perforin, as well as transcription factors Blimp1, Notch1, Nr4a1 and TRM surface marker CD103.

Normalised gene counts were calculated using the DESeq2 package and variance stabilizing transformation, which have then displayed as Log₂ values (Figure 31). It can be seen that IFN- γ and TNF- α transcription is highest in the DP group and while IFN- γ remains high in the EExh and LExh groups, TNF- α transcription does fall off somewhat with increased surface markers of exhaustion. Granzyme B and Perforin transcription appears to increase with progression through the study groups, potentially suggesting increased secretory activity into the immunological synapse (Figure 31). These findings support T_{RM} cells being a key component of both the DP and EExh/LExh populations, with expression of these molecules observed in the literature in T_{RM} both at the mRNA and at the protein level (134,202), where they behave more in keeping with an effector phenotype, rather than as a traditionally dysfunctional exhausted lymphocyte.

A closer assessment of transcription levels of other molecules crucial to T_{RM} development and maintenance was undertaken. The transcription factors Blimp-1 and Notch are required for T_{RM} differentiation, while Nr4a1 is necessary for T_{RM} and T central memory cell maintenance (138,140). The surface marker CD103, encoded for by the *ITGAE* gene is a key marker of TRMs and it is demonstrated here that transcription is increased in the DP, EExh and LExh groups, compared to the DN group.

Statistical significance has not been calculated for these experiments due to the small sample sizes here and the effects of transformation on the absolute numbers calculated. Such calculations however do provide a guide for what may be expected from future experiments to assess protein level expression of some of these molecules of interest.

4.3 Discussion

Data presented here demonstrates it is feasible to undertake bulk RNA sequencing on TIL populations of low abundance sorted from disaggregated human oesophageal adenocarcinoma, and that functional and phenotypic assessments can be made from this. It has been demonstrated that FACS can be used to sort as few as several hundred lymphocytes into a preservative TRIzol solution, the RNA of which can be extracted using commercially available spin columns and cDNA libraries can be produced from this inevitably low yield using the highly sensitive single cell RNA sequencing protocol SmartSeq2.

The results produced from samples processed in the initial trial of RNA sequencing showed clustering on PCA analysis by phenotype, and not by patient or by random distribution, providing confidence that the technique described has successfully captured the transcriptome of the cells of interest. Results of GSEA completed on this trial cohort were broadly in keeping with published data describing analogous populations to those sorted also adding confidence that these results are descriptive of the cell group of interest.

While experimental difficulties hampered progress in expanding the number of sorted samples available for analysis, the final number collected, particularly when chemotherapy pre-treated and naïve samples were combined, exceeded the pre-defined number of biological replicates required to explore phenotypic profiles with confidence.

Analysis of the full data set has shown the DP group, PD-1+CD39+ and TIM3-LAG3- antigen experienced CD8 TILs, to be enriched in signatures indicating T cell activation, proliferation and differentiation with regards to the DN PD-1-CD39- lymphocytes. It is also enriched for these processes on comparison to PD-1+ CD39+ TILs bearing multiple surface markers of exhaustion.

Progression from a DN, through DP to the EExh and LExh groups was associated with increasing enrichment for PD-1 signalling as might be expected, as well as TCR signalling, suggesting elevated levels of TCR engagement with cognate peptide-MHC in these groups. Increasing enrichment for IFN- γ , IL-2 and IL-12 signalling is observed in the same distribution suggesting increased stimulation towards activated CD8+ T lymphocyte behaviour.

Chapter 4

Gene sets describing specific CD8⁺ lymphocyte phenotypes have been used to compare the experimental groups sequenced and there is a suggestion that T_{RM} lymphocytes may comprise a dominant proportion of not only the DP group, but also the EExh and LExh groups. This would fit with an emerging view of CD8⁺ T_{RM} TILs as a heterogeneous population including lymphocytes more in keeping with an effector phenotype and others which may appear to have more in common with terminally differentiated exhausted lymphocytes.

A DP T_{RM} population that is functional and tumour reactive would fit with a hypothesis that an abundance of this population would be associated with improved progression free and overall survival.

Additionally, a population of PD-1⁺ TIM3⁺ CD103⁺ CD8⁺ TILs has been described in some cancers as being highly functional and tumour reactive, an abundance of which is associated with improved response to immune checkpoint blockade (114). Such a population would map closely onto what is known about the LExh group, a population we know to be in low abundance in these human tumours. It could well be that the relative lack of this group, is responsible for the generally poor responses to PD-1 blockade that patients with oesophageal cancers experience in the clinic.

Chapter 5 Functional assessment of exhausted CD8+ T lymphocyte populations in human oesophageal adenocarcinoma

5.1 Introduction

A population of antigen experienced CD8+ TILs possessing positivity for PD-1 and CD39 has been identified infiltrating human adenocarcinoma, an abundance of which may be associated with improved progression free and overall survival. With comparison to the PD-1 and CD39 negative population, this group has been characterised, through flow cytometry, as possessing a heterogeneous transcription factor profile with both T-bet^{Low} Eomes^{High} and T-bet^{High} Eomes^{Low} cells present, and is strongly associated with expression of multiple other cell surface markers of activation and exhaustion.

This DP group is shown through transcriptomic assessment to be enriched for gene sets associated with lymphocyte migration and chemotaxis, as well as increased proliferation, when compared to the LExh group, and even greater enrichment when compared to the DN population. There is a suggestion of increased IFN- γ transcription by the DP group compared to the DN group as well as increased production of other cytokines.

With regards to functional phenotypes the DP group enriches for gene sets related to precursor exhausted phenotype, but is also strongly enriched for tissue resident memory cell gene sets, as are the EExh and LExh groups.

Taken as a whole this could suggest that the DP population is formed of a heterogeneous population of TILs, potentially containing a dominant group of precursor exhausted lymphocytes or T_{RM}, and a minority population of terminally differentiated lymphocytes or T_{RM} possessing a terminally exhausted like phenotype. There are also likely to be a number of bystander lymphocytes, though this is difficult to prove in the absence of information regarding their target antigens.

This chapter describes the results of further flow cytometry based assays to answer questions related to the functionality of the DP population. Multi-parametric flow cytometry utilising up to 12 fluorophores has been undertaken to combine the antibody panels utilised in chapter 1 and explore the double positive population with regards to the T-bet and Eomes transcription factors

alongside additional surface markers of exhaustion and intracellular staining for effector molecules, in an attempt to tease out the heterogeneity of the DP population.

Stimulation assays, culturing the TIL populations in autologous tumour digest, with or without additional stimulation by either CD3 and CD28 stimulating antibodies or the mitogens PMA and Ionomycin, have been undertaken. This aims to investigate the ability of these populations to produce effector molecules including IFN- γ , TNF- α , Granzyme B and Perforin.

Similarly, assays utilising sorted populations of DP and DN TILs to assess proliferation using the intracellular stain CFSE have been undertaken to assess possession of an ability to proliferate in a conducive environment.

Finally, and with a view on future work, flow cytometry has also been undertaken on a limited sample of OAC tumours, to assess expression of CD3 and CD4 to ensure that the population defined as antigen experienced CD8⁺ lymphocytes is indeed this, and not another cell type such as a CD4⁺ lymphocyte or NK cell, both of which can express CD8 positivity. Expression of PD-1 and CD39 on non-CD8⁺ lymphocytes is also assessed to guide future evaluation of the DP group in human tumours. In addition the expression of the canonical marker for tissue resident memory cells (T_{RM}) CD103 has been assessed, as has the CD57 an NK and T cell marker frequently observed in some T_{RM} populations, in order to clarify the nature of the dominant cell type in the DP population of interest.

The aim of this chapter was to assess the functional capacity of the PD-1 and CD39 double positive population of antigen experienced CD8⁺ TILs from human oesophageal adenocarcinoma in order to corroborate transcriptomic results obtained in chapter 4. Additionally this chapter has aimed to draw together results relating to the phenotype of this population of interest, including those regarding, key transcription factors, cell surface markers of exhaustion and tissue residency as well as CD3 and CD4.

5.2 Results

5.2.1 Multi-parametric flow cytometric assessment of the DP population

An antibody panel containing 12 fluorophore labelled antibodies was developed for use on a 4 laser BD Fortessa flow cytometer, with the aim to combine the data presented in chapter 3. This was tested and antibody concentrations were titrated. The panel included the core antibodies used in earlier work, targeting CD8a, CD44, PD-1 and CD39, alongside antibodies staining the

transcription factors T-bet and Eomes as well as the markers of exhaustion TIM3 and LAG3. Additionally, intracellular staining for IFN- γ , TNF- α , Granzyme B and Perforin was included.

A representative collection of samples analysed previously were assessed, including 6 treatment naïve samples and 3 chemotherapy pre-treated samples. A similar number of events were morphologically classed as lymphocytes, through similarity with concurrently assessed HD PBMC samples, in this cohort as was observed in the full sample cohort analysed using the 6 colour flow cytometry panel (means 26.4% vs 19.7%, range 16.2-44.5% vs 3.6-47.5% respectively). Likewise a similar number of this lymphocyte population was identified as CD8+ CD44+ as identified in the full data set (means 23.4 vs 29.8%, range 2.8-44.7% vs 7.3-71% respectively). As expected from a predominantly chemotherapy naïve cohort based upon earlier findings, the antigen experienced CD8 TILs assessed showed varying degrees of PD-1 and CD39 positivity, with the largest group being the PD-1+ CD39+ DP population. Results from the chemotherapy treated samples were distributed throughout the samples, and not clustered together.

5.2.1.1 T-bet and Eomes expression

It has been suggested that the DP group is comprised of a heterogeneous population of CD8 TILs and may be comprised of both precursor exhausted and terminally differentiated exhausted lymphocytes as shown by the mix of T-bet^{High} Eomes^{Low} and T-bet^{Low} Eomes^{High} lymphocytes in earlier analysis.

Multi-parametric flow cytometry data displayed here, shows the proportions of lymphocytes with these transcription factor profiles varied based upon the degree of expression of surface markers of exhaustion TIM3 and LAG3. The CD8+ CD44+ populations defined and described in earlier chapters labelled Double Negative (DN, PD-1- CD39-), Double Positive (DP, PD-1+ CD39+ LAG3- TIM3-), Early Exhausted (EExh, PD-1+ CD39+ LAG3+ TIM3-), and Late Exhausted (LExh, PD-1+ CD39+ LAG3+ TIM3+) were utilised again in this evaluation.

Upon this analysis a clearly dominant population suggestive of precursor exhausted or terminally differentiated exhausted lymphocytes based upon T-box transcription factor profile and the exhaustion markers TIM3 and LAG3 was not seen (Figure 32).

The DN group showed a similar proportion of cells gated as T-bet^{High} Eomes^{Low} in this analysis as in the initial analysis (mean 39 vs 40.6%), though a higher proportion were labelled as Tbet^{Low} Eomes^{High} (mean 59.8 vs 37.9%) (Figure 32. E and D respectively).

The use of the extended flow cytometry panel allows the division of the PD-1+ CD39+ group into sub populations based upon TIM3 and LAG3 expression. Assessing the levels of the two T-box

transcription factors of interest across these populations, it is observed that there is a fall in the percentage T-bet^{High} Eomes^{Low} with progression through these groups (mean percentage DP 60.04%, EEExh 36.41%, LExh 31.96%) (Figure 32.D), a picture that could be in keeping with a falling proportion of precursor exhausted lymphocytes and a move towards a terminally exhausted phenotype. This reinforces the gene set variation analysis results presented in chapter 4 where by the population most enriched for the progenitor exhausted gene set described by Miller et al was the DP population and the population most enriched for the terminal exhaustion gene sets described by Miller et al and Andreatta et al was the LExh group (70,221).

T-bet^{High} Eomes^{Low} TILs were low in the DN group (mean 39.0%) (Figure 32.D) which would suggest an absence of precursor exhausted TILs, though this does not necessarily imply an abundance of terminally differentiated exhausted lymphocytes, given the complex mechanisms by which these T-box transcription factors are involved in lymphocyte development.

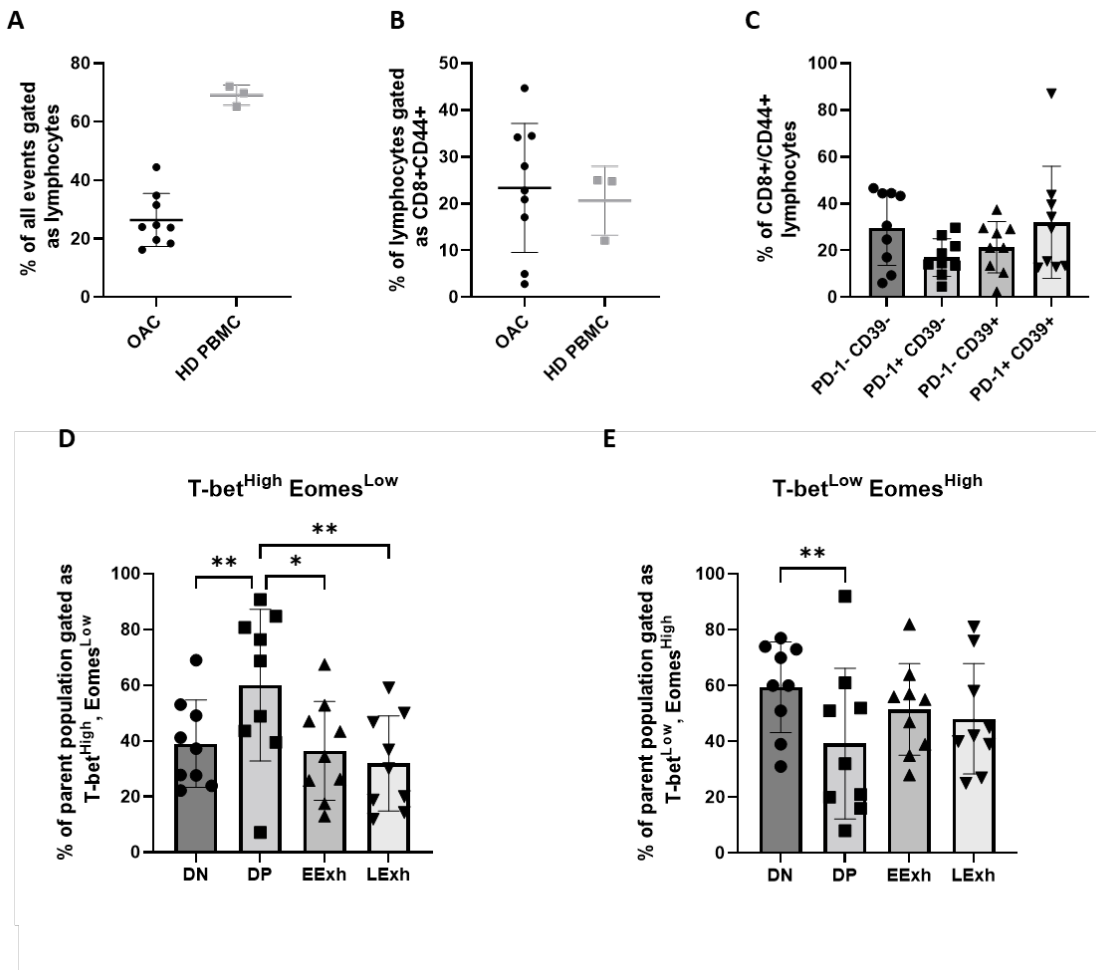


Figure 33 Expression of T-bet and Eomes in PD-1 and CD39 expressing antigen experienced lymphocyte populations.

Results obtained from 9 OAC samples, 6 treatment naïve and 3 chemotherapy pre-treated. All gating strategies as detailed in chapters 3 and 4. Mean value and standard deviation displayed for all figures. A) Percentage of all recorded events gated a lymphocytes based on morphology from OAC samples, and HD PBMC samples used as controls. B) Percentage of CD8+CD44+ cells among events gated as lymphocytes in both OAC samples and HD PBMC. C) Percentage of CD8+CD44+ lymphocytes gated as positive or negative for PD-1 and CD39. D and E) Percentage of populations of interest gated as either Tbet^{High} Eomes^{Low} or Tbet^{Low} Eomes^{High}. Parent populations are all CD8+ CD44+, DN group is PD-1- CD39- TIM3- LAG3-. DP, EExh and LExh groups are all PD-1+ CD39+, and TIM3- LAG3-, TIM3- LAG3+ and TIM3+ LAG3+ respectively. This labelling will be applied throughout this chapter. Statistical significance of difference calculated using paired t-test. * denotes p value <0.05, **<0.01, ***<0.001, ****<0.0001. Significance of all figures in this chapter is calculated as such unless otherwise specified.

The differences in percentage of Tbet^{High} Eomes^{Low} TILs between the DP group and all other experimental groups were considered statistically significant as defined by a p value<0.05 calculated with the paired t test (DN vs DP p= 0.0094, DP vs EExh p= 0.0253, DP vs LExh p= 0.0079) (Figure 32.D). All statistical evaluations of statistical significance in this chapter will be calculated using the paired t test unless otherwise specified.

A Tbet^{Low} Eomes^{High} profile in keeping with terminally differentiated exhausted lymphocytes, was identified in all experimental groups (means DN 59.44%, DP 39.22%, EExh 51.44%, LExh 48.11%), but was lowest in the DP group (Figure 32.E). This could potentially suggest a lack of terminally exhausted lymphocytes in this group, with increasing degrees of dysfunction with progress to the EExh and LExh populations.

Statistically significant differences were observed between the DN and DP groups, p=0.0098 (Figure 32.E). While this is of interest, the contrast in Tbet and Eomes expression between the DP and LExh groups is not as clear as may be expected if these groups were to contain homogenous populations of precursor exhausted and terminally differentiated exhausted lymphocytes as defined by the classical LCMV model (88). This lack of concordance to the classical transcription factor profile of lymphocyte exhaustion could well suggest a degree of heterogeneity within these groups.

5.2.1.2 Characterisation of T-bet^{High} Eomes^{Low} and T-bet^{Low} Eomes^{High} populations

To further dissect the DP populations heterogeneity, expression of TIM3 and LAG3 as well as the important CD8+ lymphocyte effector molecules, IFN- γ , TNF- α , Granzyme B and Perforin was assessed in antigen experienced PD-1+ CD39+ CD8+ lymphocytes gated as T-bet^{High} Eomes^{Low} and T-bet^{Low} Eomes^{High}. It has been speculated that the DP group may be comprised of a majority precursor exhausted population and a minority terminally exhausted population. Such phenotypes are canonically described through the profile of T-box transcription factors as well as differential expression of surface markers of exhaustion. Here we observed an increased TIM3 and LAG3 staining in the T-bet^{Low} Eomes^{High} vs T-bet^{High} Eomes^{Low} (means, TIM3 20.44 vs 13.04 p value = 0.0096, LAG3 33.51 vs 21.67 p value = 0.046), with the differences reaching a degree of statistical significance (Figure 33). The observation that there were a measurable number of cells positive for TIM3 and LAG3 in the T-bet^{High} Eomes^{Low} group and a majority negative for these surface markers in the T-bet^{Low} Eomes^{High} group would suggest that using T-bet and Eomes expression cannot be used to describe the OAC TIL populations of interest along the lines of classical lymphocyte exhaustion.

Assessment of staining for IFN- γ and TNF- α in the different T-bet and Eomes populations showed no statistically significant difference though there was a suggestion of an increase expression in T-bet^{Low} Eomes^{High} vs T-bet^{High} Eomes^{Low} (means, IFN- γ 0.57% vs 0.26%, TNF- α 7.11% vs 2.43%) (Figure 33). Perforin staining also showed no significant difference between the groups of interest, though a suggestion of higher expression in the T-bet^{Low} Eomes^{High} group (means 15.11% vs 12.20%) was observed. Granzyme B however did show significantly different expression between the T-bet^{Low} Eomes^{High} vs T-bet^{High} Eomes^{Low} populations (means 55.36% vs 37.20 p value = 0.026) (Figure 33). The similarities between groups defined by T-bet and Eomes supports the notion that this is not the optimal means of further identifying the nature of the DP population.

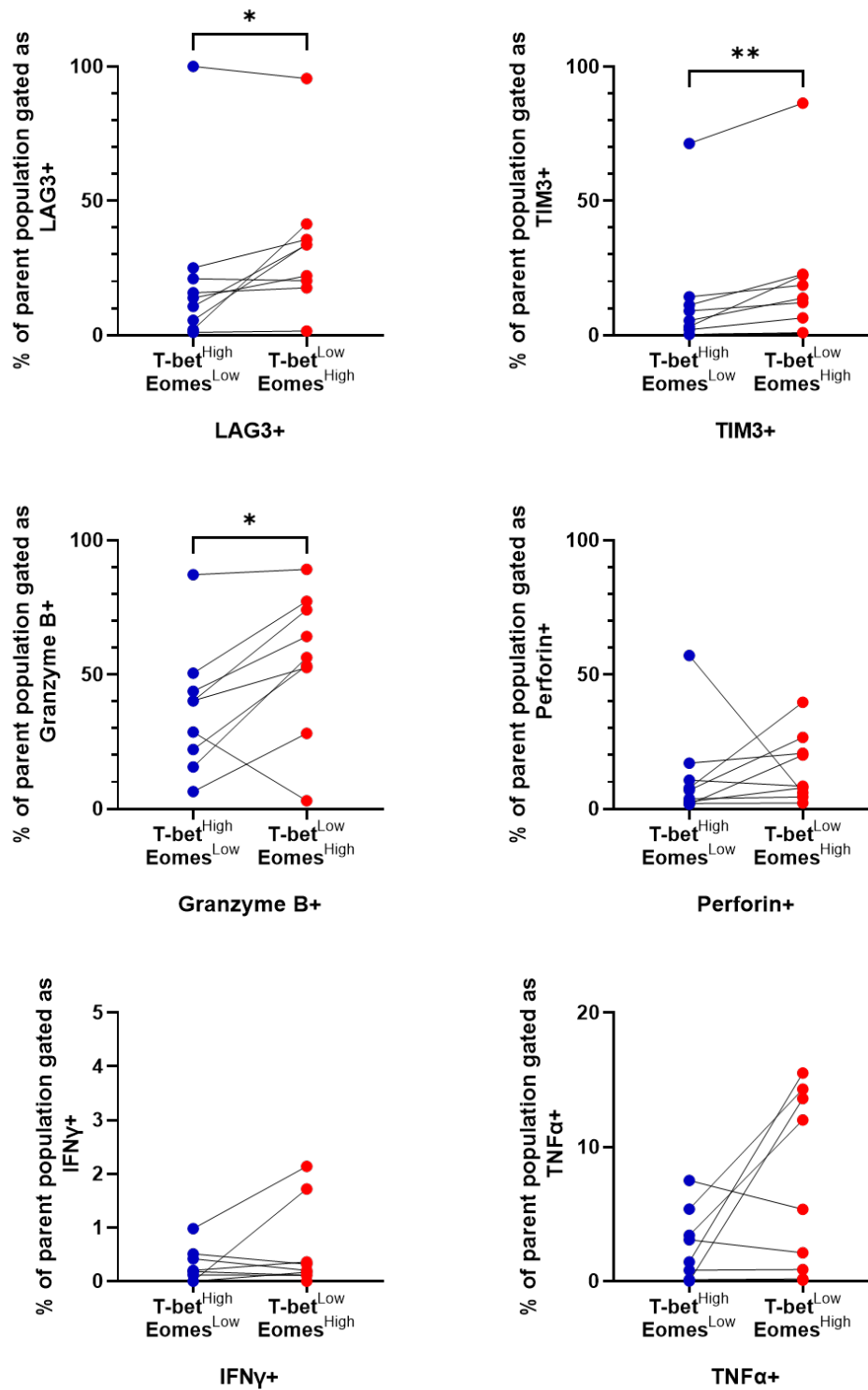


Figure 34 Differential expression of markers of exhaustion and effector molecules between T-bet^{High} Eomes^{Low} and T-bet^{Low} Eomes^{High} populations.

Parent populations are antigen experienced CD8⁺ TILs defined as CD8⁺ CD44⁺, PD-1⁺ and CD39⁺, with percentage of T-bet^{High} Eomes^{Low} cells labelled in blue and the T-bet^{Low} Eomes^{High} labelled in red. Percentage of each group positive for cell surface

TIM3 and LAG3 displayed, as well as intracellular staining for Granzyme B, Perforin, IFN- γ and TNF- α .

5.2.1.3 Expression of CD8+ lymphocyte effector molecules

The populations of interest, DN, DP, EExh and LExh were further evaluated using this extended antibody panel to assess expression of effector molecules, IFN- γ , TNF- α , Granzyme B and Perforin. Increased levels of IFN- γ , TNF- α and Perforin were identified in EExh and LExh groups when compared to the DP group, with Granzyme B expressed at high levels in all groups (Figure 34).

Generally low levels of IFN- γ and TNF- α were observed in the DP populations with increasing percentages positive for the cytokines with progression through the EExh to LExh phenotypes. The differences between the DP groups and the EExh and LExh groups were statistically significant for both IFN- γ and TNF- α (means, IFN- γ DP vs EExh 0.25 vs 2.77% $p=0.017$, DP vs LExh 0.25 vs 5.83% $p=0.014$. TNF- α DP vs EExh 0.91 vs 16.92% $p=0.0034$, DP vs LExh 0.91 vs 20.81% $p=0.002$). Low levels of TNF- α staining were observed in the DN group (mean 0.72%), similar to the DP group, while higher levels of IFN- γ staining was observed in the DN group (mean 2.89%), a similar level to the EExh group (Figure 34).

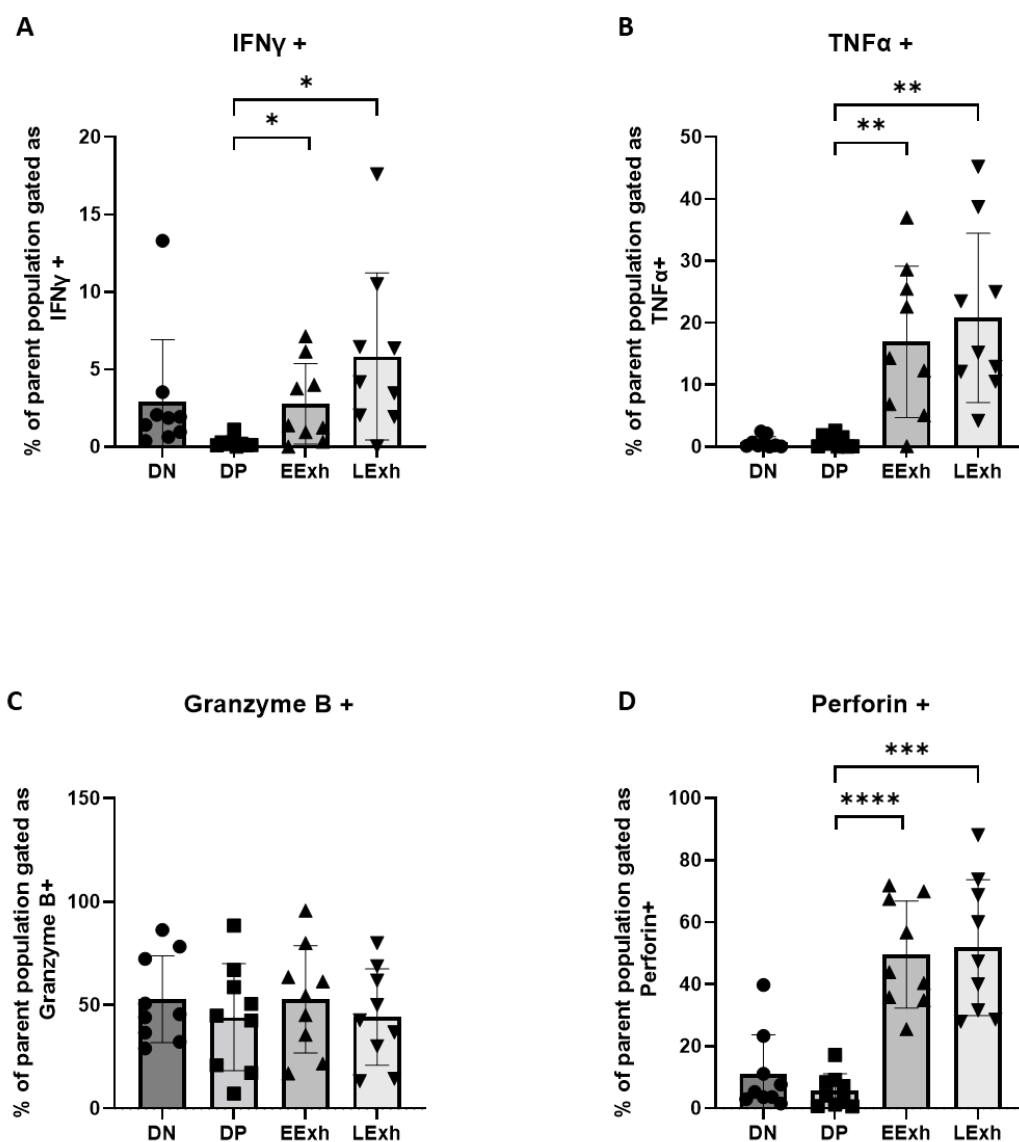


Figure 35 Effector molecule expression by populations of interest from antigen experienced CD8+ lymphocytes.

Results obtained from 9 OAC samples, 6 treatment naïve and 3 chemotherapy pre-treated. All gating strategies as detailed in chapters 1 and 2. Mean value and standard deviation displayed for all figures. A-D) Percentage of populations of interest gated as IFN γ , TNF α , Granzyme B and Perforin respectively. Parent populations are all CD8+ CD44.

Uniform staining for Granzyme B was observed across all experimental populations (means DN 52.83%, DP 44.13%, EEExh 52.73% and LExh 44.19%). This result was unexpected as it is not in keeping with the transcriptomic data displayed in chapter 4 where an increase in Granzyme B expression is observed with progression through these experimental groups, mirroring results described by de Lara et al(130). In addition the terminally differentiated exhausted T_{RM} subgroups

described are associated with increasing Granzyme B expression when compared to more precursor exhausted T_{RM} and other non-T_{RM} populations(114,141). The reason for the uniformly high Granzyme B staining shown here are unclear, but may well relate to the concentration of antibody used in this experiment. While positive gating was determined using fluorescence minus one (FMO) controls, the high levels of staining across all experimental groups may suggest over saturation with antibody. As such these results must be interpreted with caution.

Perforin positivity was highest for the EExh and LExh groups (means 49.61% and 51.80% respectively), with both DN and DP groups showing low levels of staining (means 10.97% and 5.64% respectively). Statistically significant differences were observed between the DP groups and both the EExh and LExh groups (p value <0.0001 and 0.0002 respectively) for Perforin staining (Figure 34).

Taken collectively these results demonstrate maintained levels of Granzyme B across all experimental groups, while Perforin, IFN- γ and TNF- α are all observed at higher levels in EExh and LExh groups compared to DP groups. This does not wholly correlate with RNA sequencing data described in chapter 4 where, for example IFN- γ production is highest in the DP, Exh and LExh groups. The reasons for this could be as result of experimental errors or issues, but given correlations observed between the transcriptomic data and flow cytometry data elsewhere, this could also represent the difference between transcriptional activity and the amount of protein within a cell of interest, either due to being retained in a cellular compartment such as a granule, or due to post translational regulatory processes.

Returning to the question of the composition of the PD-1+ CD39+ TIL populations identified in this study. A terminally differentiated exhausted population would be expected to demonstrate reduced ability to produce IFN- γ and TNF- α (39,41,88) and the persistence of this as defined here by flow cytometry and also by transcriptomic assessment, suggests maintained function. Such an observation is a hallmark of some T_{RM} populations that possess TIM3 and PD-1 positivity but also remain highly functional and able to engage and kill cancer cells (114). This adds greater weight to the assumption that the DP, EExh and LExh are comprised predominantly of T_{RM} subsets

5.2.2 CD8+ Lymphocyte stimulation assays

A protocol was developed to allow for assessment of the ability of CD8+ lymphocyte populations of interest to produce cytokines or cytolytic granule products on stimulation either by autologous tumour, by stimulatory anti-CD3 and CD28 antibodies or the mitogens Phorbol 12-myristate 13-acetate (PMA) and Ionomycin. Staining for CD107a was also undertaken simultaneously to assess for evidence of degranulation.

OAC TILs in disaggregated tumour were stimulated for 4 hours in medium in the presence of the protein transport inhibitor Brefeldin A (BFA) and anti-CD107a antibodies. Cultures were then fixed, permeabilized and stained for core lymphocyte surface markers and intracellular effector molecules.

These experiments were repeated on 6 samples, 3 treatment naïve and 3 pre-treated with chemotherapy. It was observed that the proportions of PD-1 and CD39 positive TILs in this experimental cohort was representative of the full data set, and that the proportions of CD8+ CD44+ TILs positive for these markers was not altered by culture with stimulatory antibodies or PMA/Ionomycin when compared to cells incubated in culture medium alone (Figure 35.B and C).

5.2.2.1 Stimulation of degranulation

Samples were incubated with anti-CD107a antibody, to allow identification of immune cell activation and degranulation. This protein is usually present within the lipid bilayer of lytic granules and moves to the cell surface on fusion of the granules with the cytoplasmic membrane (225,226). CD107a staining was observed at higher concentrations in stimulated TILs and HD PBMC samples than in unstimulated controls. A distinctly higher level of staining was observed in a subpopulation of TILs cultured in tumour, presumably representing ongoing degranulation in the presence of cognate peptide-MHC exposure. It was observed that among antigen experienced CD8+ T lymphocytes, surface CD107a expression was higher in PD-1+ CD39+ and PD-1+ CD39- groups compared to the PD-1- CD39+ and PD-1- CD39- groups. This was the case for samples stimulated by autologous tumour alone, CD3 and CD28 antibodies, and PMA/Ionomycin (Figure 35.D and E). A high percentage of CD107a positive TILs in the PMA/Ionomycin stimulated PD-1+CD39+ suggests a maintained ability to degranulate in this population and a lack of total lymphocyte dysfunction. Increased positivity among TILs stimulated through co-culture with autologous tumour alone suggests preserved functionality within the tumour microenvironment and potentially, tumour reactivity.

CD107a has been widely used as a surrogate marker for lymphocyte degranulation and from analysis of CD8+ TILs from mouse models it has been observed that degranulation increases with progression from CD39 negative populations through intermediate to high levels of CD39 expression and associated increases in PD-1 expression (131). Such findings reinforce observations in this project that PD-1+ CD39+ OAC TIL populations maintain cytolytic capabilities and can engage and kill tumour cells and potentially impact patient survival.

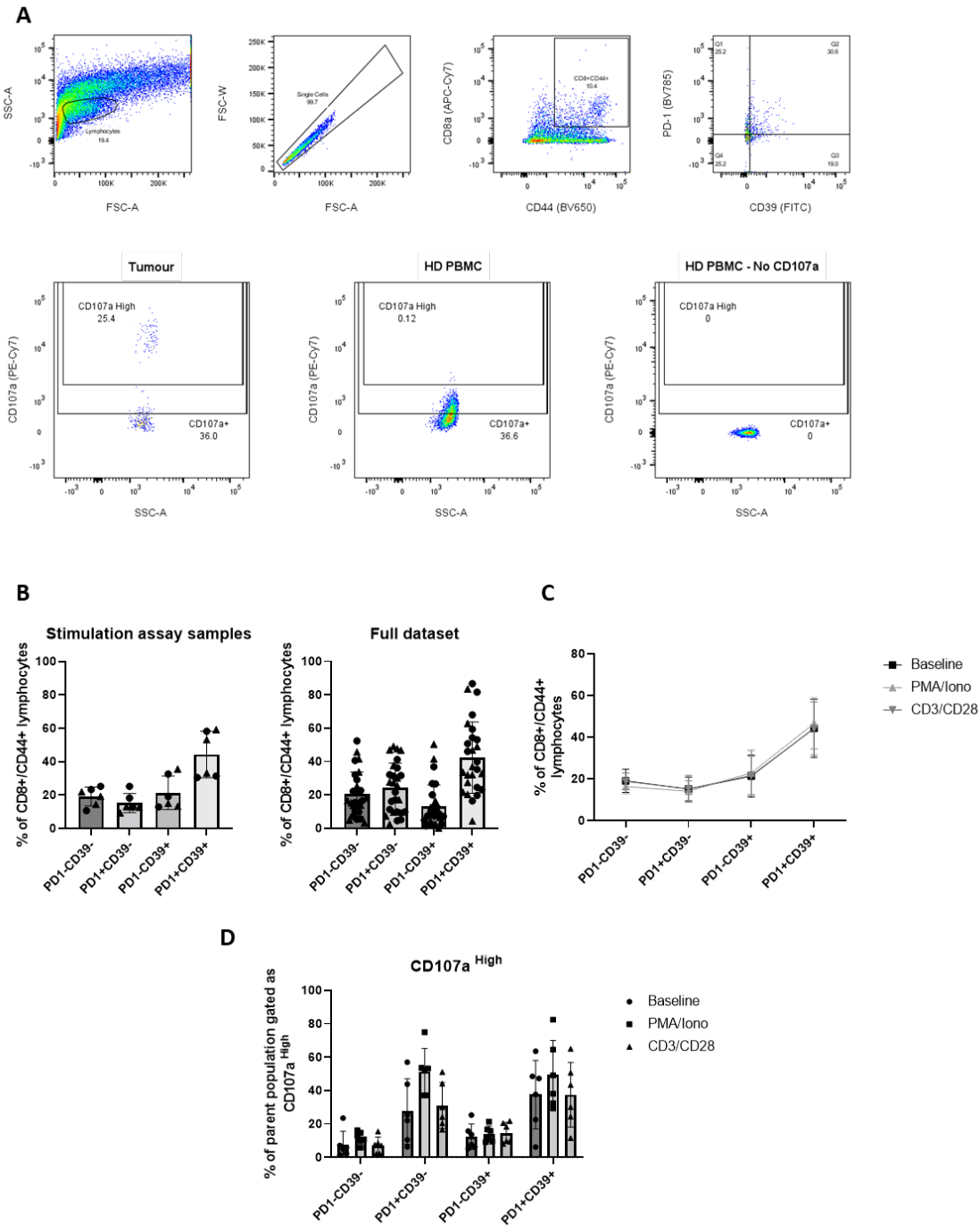


Figure 36 Degranulation of CD8+ lymphocyte populations on stimulation by autologous tumour alone, anti-CD3/CD28 antibodies or PMA/Ionomycin.

A) Exemplar flow cytometry plots showing gating strategy for degranulation assay with top row showing results from an OAC tumour with the lymphocyte population identified using a PBMC sample, then singlets selected using FSC-A and FSC-W, CD8+ CD44+ population identified and then subdivided based upon PD-1 and CD39 positivity. Second row shows the degree of CD107a staining and gates for a PD-1-CD39- population of OAC TIL (left) and HD PBMC with (centre) and without (right)

addition of staining antibody. B) Percentage of CD8+ CD44+ OAC TILs gated as positive for PD-1 and CD39 in baseline degranulation assays, stimulated with autologous tumour alone. Circles represent treatment naïve samples and triangles chemotherapy pre-treated. Comparison made with all samples from 6 colour flow cytometry dataset described in chapter 3. C) Mean and standard deviation for percentages of CD8+ CD44+ OAC TILs at baseline after incubation in culture medium with autologous tumour alone, and after stimulation with anti-CD3 and CD28 antibodies or PMA/Ionomycin. Limited variability between proportions of each group based upon treatment. D) Mean and standard deviation for percentage of CD8+ CD44+ OAC TILs of varying PD-1 and CD39 expression, that are gated as highly positive for CD107a.

5.2.2.2 Stimulation of effector molecule production

Concurrent to assessment of degranulation in the OAC samples, intracellular staining for the cytokines IFN- γ and TNF- α as well as the granule products Granzyme B and Perforin was undertaken. Unlike in the earlier multi-parametric flow cytometry assessment describing these molecules, analysis here was undertaken following culture in the presence of Brefeldin A in order to block export of molecules through the cell surface, and allow detection of these typically secreted cellular products.

Low levels of IFN- γ and TNF- α staining was observed in all categories of PD-1 and CD39 positivity after culture with autologous tumour cells alone and in the presence of anti-CD3 and CD28 antibodies. Expression of both of these molecules is increased in samples incubated in the presence of PMA and Ionomycin, and is highest in the PD-1- CD39- and PD-1+ CD39- groups (Figure 36.B). This chemical stimulation, which leads to activation of intracellular signalling pathways bypassing the TCR, suggests that these phenotypes, and especially the double negative and PD-1+ only groups, do maintain an ability to produce IFN- γ and TNF- α cytokines, but do not do so freely within the tumour microenvironment when stimulated by tumour and presumably their target peptides, a process which is ongoing as demonstrated by the presence of degranulation. The fall in ability to produce cytokines with increasing CD39 expression may well represent a degree of dysfunction creeping into these lymphocyte populations as may be expected with the presence of increasing expression of surface markers of exhaustion and exhausted transcriptomic profiles as already discussed, though this may not necessarily be expected in exhausted-like T_{RM} populations.

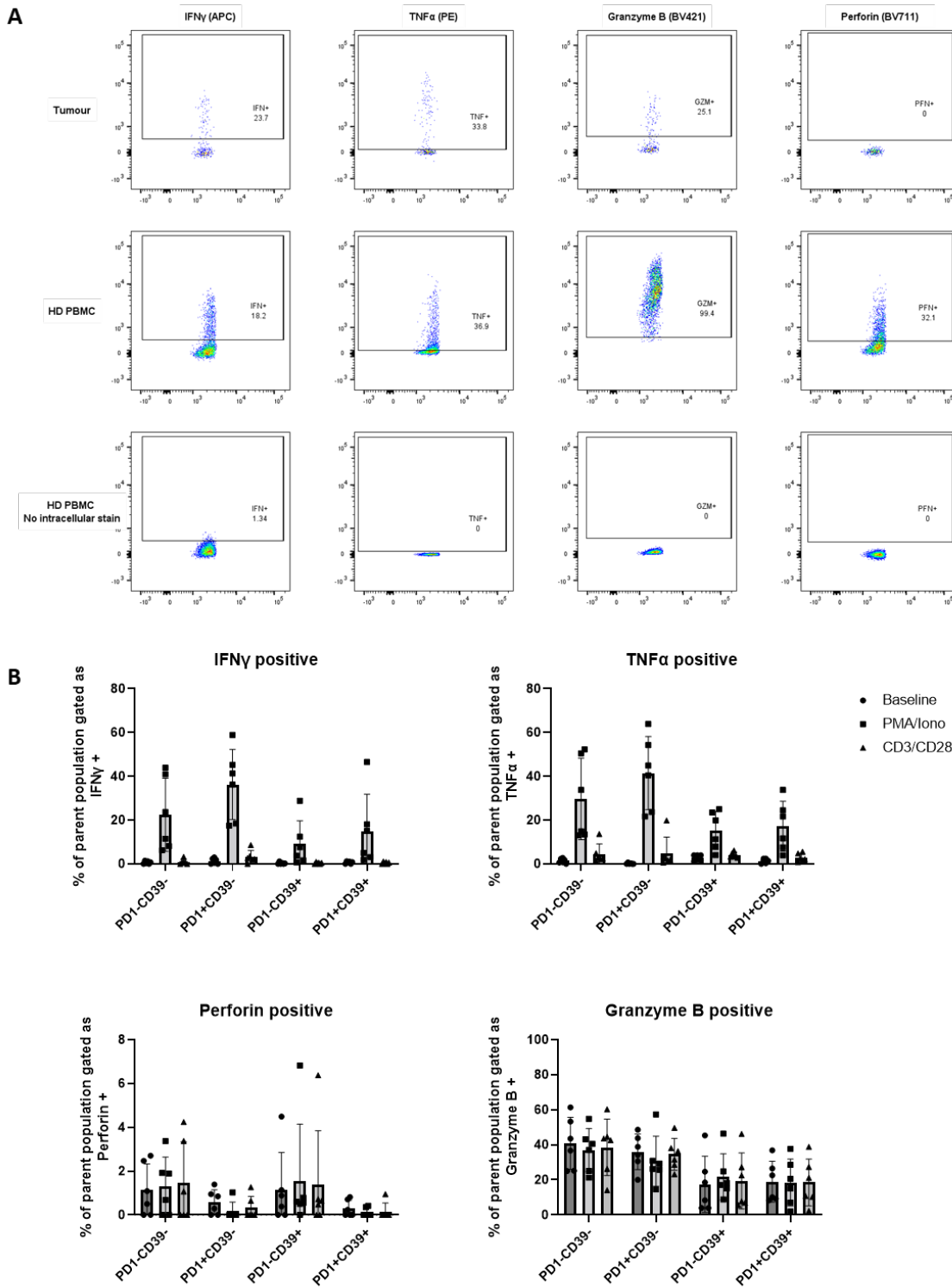


Figure 37 Production of key cytokines and cytolytic granule products by CD8⁺ lymphocyte populations on stimulation by autologous tumour, anti-CD3/CD28 antibodies or PMA/Ionomycin.

A) Exemplar flow cytometry plots showing gating for positivity of IFN- γ , TNF- α , Granzyme B and Perforin by PD-1- CD39⁻, CD8⁺ CD44⁺ lymphocytes from OAC tumours stimulated by PMA/Ionomycin (top row) and HD PBMCs with (middle row)

or without (bottom row) intracellular staining antibodies. B) Mean and standard deviation for percentage of CD8+ CD44+ OAC TILs of varying PD-1 and CD39 expression, that are gated as positive for IFN- γ , TNF- α , Granzyme B and Perforin following stimulation at baseline by autologous tumour cells only, anti-CD3 and CD28 antibodies or PMA/Ionomycin.

Similar to the results observed for active degranulation, this decreasing ability to produce cytokines in CD39+ CD8+ TILs is consistent with published data in mouse models where IFN- γ and TNF- α expression correlates inversely with CD39 expression by TILs (131).

The cytolytic granule products Granzyme B and Perforin were similarly assessed for expression on stimulation, and consistent levels of both of these proteins were observed regardless of stimulation technique. Perforin staining showed highest levels in PD-1- CD39- and PD-1- CD39+ groups with lower levels in the PD-1+ CD39- group and negligible numbers of PD-1+ CD39+ TILs positive. It must be commented that the percentage of all groups positive was low with all means less than 2%.

Granzyme B staining revealed higher percentages of TILs positive across all groups with means typically from 20-40% of CD8+CD44+ TILs. Here, the lowest percentages positive for Granzyme B staining were observed in PD-1+ CD39+ as well as PD-1- CD39+ TILs, with higher expression in CD39- groups. The limited variability between baseline stimulation and PMA/Ionomycin stimulation suggests each group is producing these effector molecules to the best of their functional capacity, rather than being limited by adequate TCR stimulation. This is not to suggest that all groups are receiving optimal TCR stimulation, rather that cytolytic granules are being readily produced in populations, though potentially to lesser degree in CD39 expressing TILs.

5.2.3 CD8+ lymphocyte proliferation assay

Transcriptomic analysis in this project has suggested a differential picture of proliferative processes among the PD-1 and CD39 positive compared to negative CD8+ lymphocyte populations in oesophageal adenocarcinoma. The DP group was enriched for gene signatures related to lymphocyte proliferation compared to the DN, with the EExh and LExh populations a more intermediate picture (Figure 29). Such observations would suggest increased cell division and proliferative potential in the activated T_{RM} or potentially precursor exhausted dominant population in the DP group, with this tailing off in the more terminally exhausted populations.

To investigate this further a lymphocyte proliferation assay was developed, with the aim to compare the DP and DN populations of TILs collected from OAC tumour specimens. Given the

small numbers of the EExh and LExh populations, these were not factored into this experimental work stream. Shown here is provisional data suggesting maintained proliferative potential in PD-1 and CD39 positive OAC TILs.

5.2.3.1 CD8+ proliferation assay development and testing

Several strategies for assessing lymphocyte proliferation were considered and an assay utilising the carboxyfluorescein succinimidyl ester (CFSE) dye was chosen. CFSE is a fluorescent molecule that binds covalently with intracellular lysine residues and is not readily transferred out of stained cells into neighbours. As stained cells undergo proliferation the concentration CFSE is approximately halved in each daughter cell and this can be assessed through standard flow cytometric analysis. Up to 7-8 cycles of proliferation can be observed with this process, a number limited by the toxicity to cells of high concentrations of CFSE and the sensitivity of flow cytometry equipment to detect low concentrations (204).

PBMC samples from healthy donors were used for experimental set up and validation. Decreasing numbers of counted and then FACS sorted lymphocytes were stained with varying concentrations of CFSE and cultured for between 1 and 6 days until conditions were optimised. Lymphocytes were cultured using a protocol for TIL culture optimised by collaborators, in a medium containing IL-2 as well as plate bound anti-CD3 antibody and anti-CD28 antibody plus human AB serum. CD8+ lymphocytes were identified through staining with an anti-CD8a antibody conjugated to an APC fluorophore, selected for its minimal spectral overlap with CFSE detected through the FIT-C channel. The protocol was optimised, as detailed in chapter 2, to detect proliferating cells from a little as 1,000 sorted lymphocytes.

5.2.3.2 Proliferation assay of sorted OAC TILs

Disaggregated OAC tumours were thawed and prepared for FACS as previously optimised for sorting prior to transcriptomic assessment. Antigen experienced CD8+ TILs of the DN or DP groups were sorted into culture medium, of note the DP group was gated as TIM3 and LAG3 negative, to allow direct comparison with earlier transcriptomic assessment. Alongside the OAC TILs collected through FACS sorting, HD PBMC lymphocytes gated as CD8+, CD44+, PD-1- and CD39- were also retrieved. This population was used as controls and also to act as a comparison with regards to the degree of proliferation of the populations of interest. After staining and the allotted 24hours incubation, a further sample of HD PBMCs were stained with antibodies and CFSE to act as control CFSE positive cells prior to incubation and proliferation to indicate maximum staining.

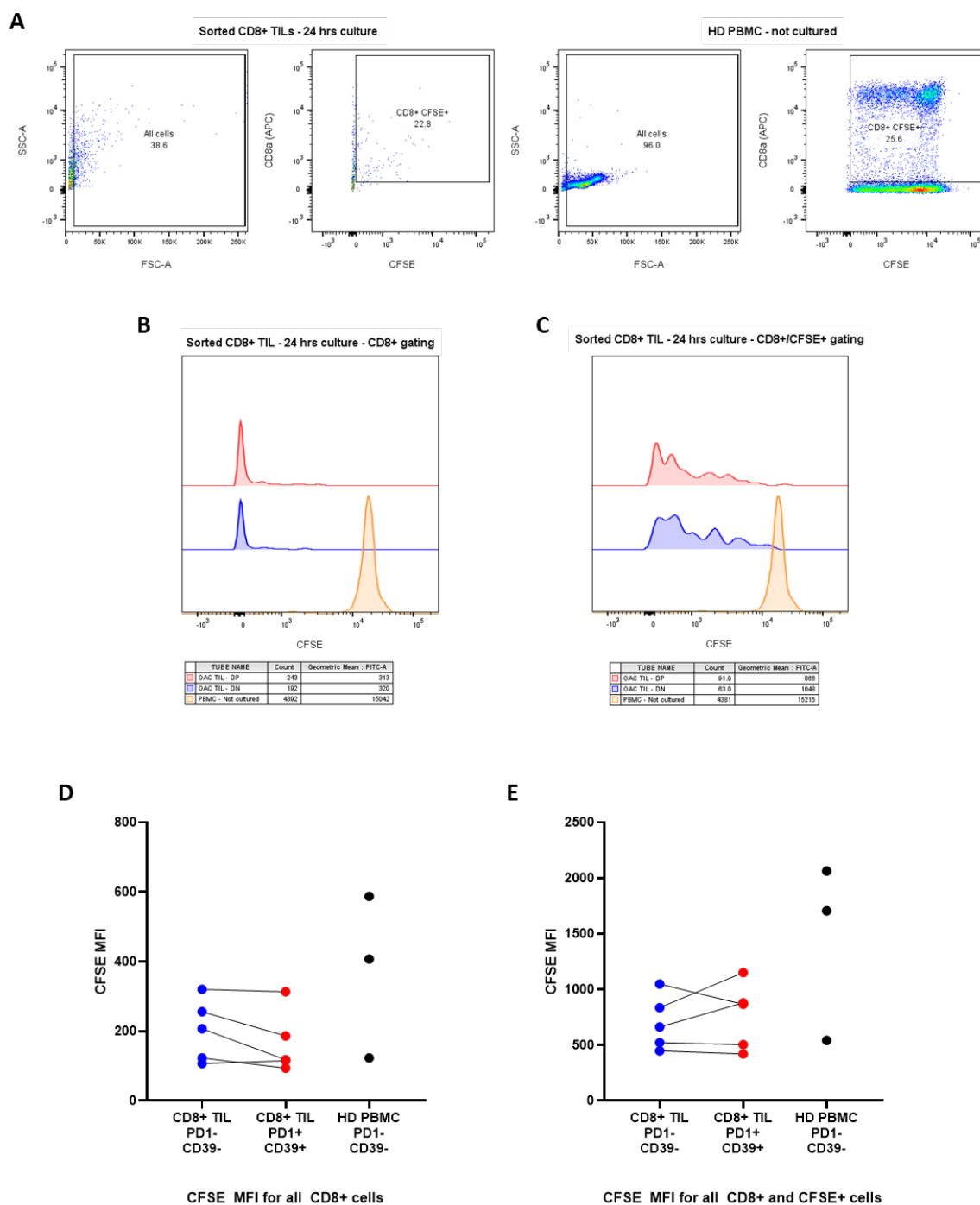


Figure 38 CFSE assay examining proliferative capacity of OAC TIL populations of interest.

A) Exemplar flow cytometry plots showing sorted DN OAC TIL population cultured for 24 hours after CFSE staining (left), and HD PBMC samples stained with CFSE and analysed immediately, not cultured (right). B and C) Exemplar histograms showing CFSE staining of CD8⁺ cells (B), and CD8⁺ CFSE⁺ cells (C) following 24 hours culture of sorted OAC TILs from a treatment naïve patient. Results from culture of PD-1⁺ CD39⁺ (DP) population (red line), PD-1⁻ CD39⁻ (DN) population (blue line) and control population (orange line) of non-cultured HD PBMCs. Legend displays cell count for

each group and geometric mean FIT-C describing the mean fluorescence intensity for CFSE staining. D and E) Mean Fluorescence Intensity (MFI) of CFSE staining for CD8+ (D) and CD8+ CFSE+ (E) cells from DP (red) and DN (blue) populations sorted from human OAC samples and HD PBMC DN cells (black).

A total of 5 samples were thawed and sorted, with recovered TILs cultured and analysed for proliferative capacity, 4 samples were treatment naïve, and 1 had been pre-treated with combination chemotherapy prior to resection. A mean of 3,101 cells were recovered from each population, and after culturing, staining and preparation for flow cytometric assessment a mean of 143.1 CD8+ events were recorded. Median fluorescence intensity for each sample was calculated to give an indication of the degree of proliferation observed, with lower figures suggesting more proliferation. These figures were compared with MFI readings for simultaneously sorted, stained and cultured HD PBMCs and also with freshly stained, non-cultured PBMCs.

No statistically significant differences were observed between the DP and DN groups, though from an admittedly small sample size. Analysis of all CD8+ events was used for these calculations as it was likely more indicative of proliferation as a whole than following removal of CFSE- cells. A similar mean MFI was observed between the DP and DN groups, with 202.6 and 165.1 respectively for the CD8+ cells, and 703.4 and 764.0 respectively for the CD8+ CFSE+ cells (Figure 37).

There was no statistically significant difference between the MFI figures for the DP or DN groups when compared to those of the HD PBMC DN cells cultured concurrently, though there was an appreciable reduction in MFI figures in the OAC TILs compared to controls, which recorded averaged MFI values of 372.3 for the all CD8+ (Figure 37).

These observations describe the proliferative capacity of our populations of interest and do suggest that this is highly maintained in both the DP and DN OAC TIL groups. While there are limitations in terms of the number of TILs available for sorting, and subsequent staining, culture and flow cytometric analysis, assessment of cultures using higher numbers of sorted PBMCs showed efficacy for the assay. It must be stressed that these results do not imply that the DP and DN populations are proliferating equally within the tumour, rather that when stimulated by likely supra-physiological concentrations of IL-2 and antibody stimulation of CD3 and CD28 these populations are able to divide rapidly. This is a scenario that would not be expected to be the case in a terminally differentiated exhausted population which is regularly described as lacking proliferative potential(37), though proliferative ability would be expected in a precursor exhausted population. Unfortunately due to the constraints of the limited number of cells

available from the EExh and LExh groups within the human OAC tumours available, similar assessment of a presumed terminally differentiated exhausted population has not been possible.

What can be inferred from this experiment, when trying to explain a potential survival benefit from having high numbers of PD-1+ CD39+ antigen experienced CD8+ TILs within a tumour, is that this potentially tumour reactive population have the ability to rapidly expand under conducive conditions and possibly enact active anti-cancer responses.

5.2.4 Assessment of the CD4+ compartment of the OAC TILs

Thus far the CD4+ compartment of human OAC TILs has only been alluded to in this project, and has been considered out of its remit. However, it must be acknowledged that these lymphocytes are of real importance in mediating effective anti-cancer effects, both in terms of the co-stimulatory support provided by CD4+ T helper cells and the inhibitory effects of FOXP3+ regulatory T cells.

To gain a clearer impression of the degree of CD4+ lymphocyte infiltration in the study sample population, and to gauge how this compares to published data sets, the multi-parametric flow cytometry panel utilised in earlier experiments was modified to include staining antibodies for CD3 and CD4. In addition to gaining information on the absolute numbers of CD4+ T lymphocytes within the tumours studied, this data was also intended to confirm that the CD8a+ CD44+ positive population that have been labelled as antigen experienced CD8+ T lymphocytes, are in fact cytotoxic T lymphocytes, and not CD8+CD4+ lymphocyte precursors or certain Natural Killer cell populations which are known to express CD8 but not CD3.

A total of 7 OAC digest samples were analysed using a modified 10 antibody flow cytometry panel. This consisted of 5 treatment naïve patient samples, and tumours from 2 patients pre-treated with chemotherapy. As per previous experiments the optimum concentrations of all antibodies used were titrated prior to use, and positivity for each marker was identified through use of FMO samples. Lymphocytes were identified morphologically as previously discussed, and a clearly identifiable CD3+ population was identifiable from this population (Figure 38.A).

The presence of CD3 is a hallmark of T lymphocytes, not expressed by B lymphocytes, and the CD3 positive events identified have been assessed with regards to CD8 and CD4 positivity. It has been shown that in the OAC TILs assessed, there were, as might be expected, dominant populations that were either CD8 or CD4 positive, indicating classical cytotoxic T lymphocytes and T helper cells respectively. There was a mean of 39.16% of CD3+ cells positive for CD8 with a range of 14.9-64.2% in this cohort, with CD4+ lymphocytes a mean of 54.46% of CD3+ events and a range of

28.1-80.5% (Figure 38.B). In previous studies of OAC TILs it has been documented that T helper lymphocytes outnumber cytotoxic lymphocytes, and these findings are broadly in keeping with this(205).

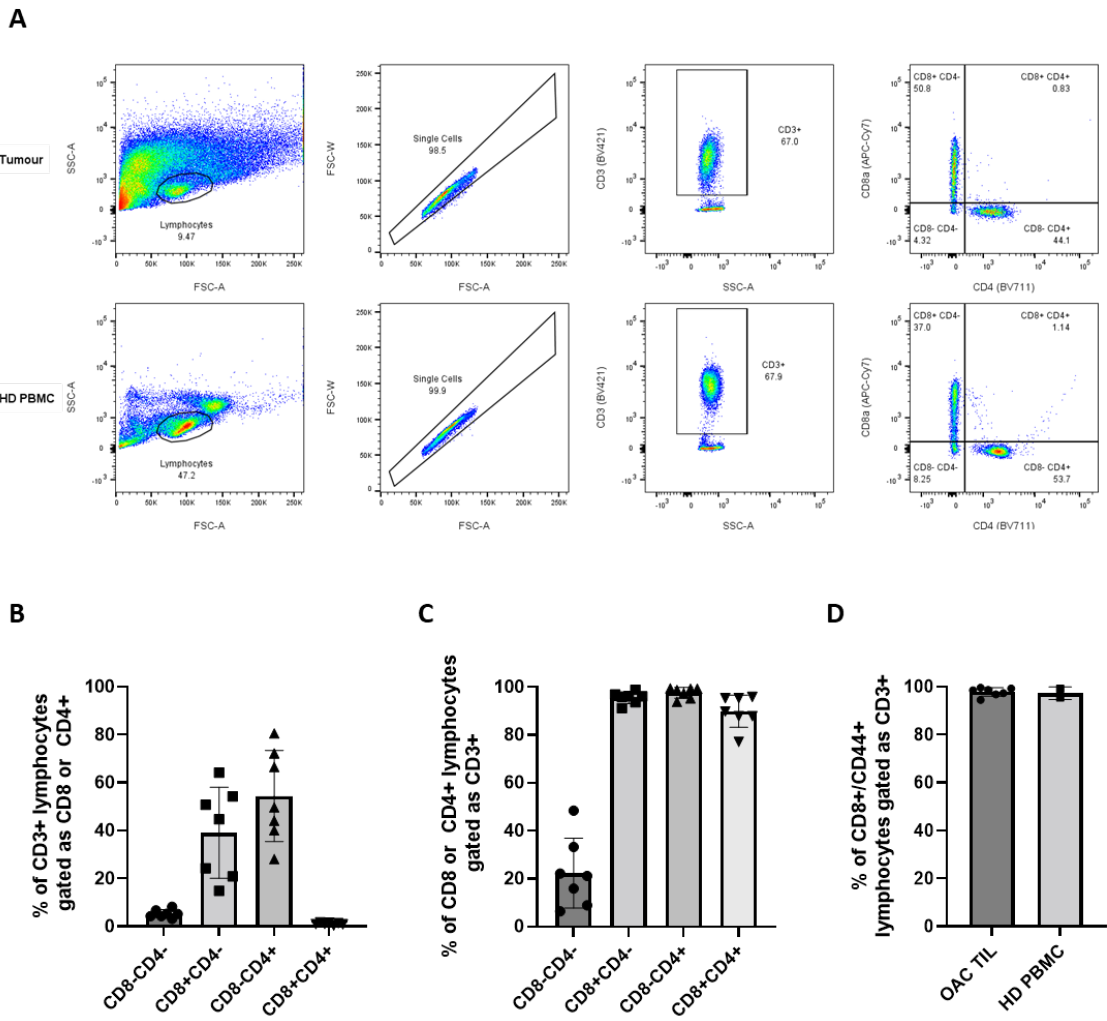


Figure 39 CD3, CD4 and CD8 positivity of OAC TILs.

A) Exemplar flow cytometry plots showing gating strategy for identifying CD3+, CD4+ and CD8+ lymphocytes. Top row is analysis of an OAC tumour, bottom row is analysis from a healthy donor PBMC sample. Lymphocytes identified morphologically with FSC-A and SSC-A (far left), and singlets identified using FSC-A and FSC-W (left). CD3+ cells gated (right) and CD4+ or CD8+ lymphocytes gated (far right). B) Percentage of cells gated as lymphocytes base on morphology and CD3 positivity, classified as either CD8-CD4-, CD8+CD4-, CD8-CD4+ or CD8+CD4+, from 7 human OAC samples. C) Percentage of cells identified as lymphocytes based on morphology gated as either CD8-CD4-, CD8+CD4-, CD8-CD4+ or CD8+CD4+, that are CD3+. D) Percentage of cells identified as lymphocytes based on morphology gated as CD8+ CD44+ that are CD3+

from human OAC samples and HD PBMCs. Mean and standard deviation represented for each group in graphs B-D.

This analysis also reveals a minority population of CD8-CD4- events gated as CD3+, with mean of 5.3% and range of 3.1-8.23% (Figure 38). This population represents a potentially heterogeneous population comprised of NKT cells, mucosal-associated T cells, and $\gamma\delta$ T cells. There were almost no CD3+ cells gated as CD8+ and CD4+ in the samples analysed (mean 1.12% and range 0.39-1.7%) (Figure 38), a frequency in keeping with the proportion of such cells in peripheral blood of healthy individuals, a population that remains incompletely characterised(227).

This data suggests that the cells identified as morphologically in keeping with lymphocytes and also CD3+ positive, are principally CD8+ or CD4+ with a minority population not conforming to these classical populations.

By analysing this data using the same gates but in a different order, it can be seen that almost all the CD8+CD4-, CD8-CD4+ and CD8+CD4+ cells gated as lymphocytes, are positive for CD3 (means 95.46%, 97.56% and 89.81% respectively). A minority of CD8-CD4- cells with lymphocyte morphology, mean 22.28%, were CD3+ (Figure 38). This suggests that the three populations with positivity for CD8 and CD4 are composed almost exclusively of cells of lymphocyte origin. Of those gated as CD8 and CD4 negative, some are likely of T lymphocyte origin as demonstrated by their CD3 positivity, the rest are likely to include other immune cells that share size and shape with T lymphocytes, including B lymphocytes, but presumably also tumour and stromal cells which show morphological overlap with lymphocytes but possess no additional immune cell markers or functions.

This data has been used to allay any concerns that the cells described regularly in earlier chapters as antigen experienced CD8+ lymphocytes, based on CD8a and CD44 staining, are in fact lymphocytes. Analysis of all events gated as lymphocytes based on size and granularity, and showing CD8 and CD44 positivity showed a population almost exclusively comprised of CD3+ cells with mean of 97.8% and 97.35% in the human OAC samples analysed and in HD PBMC samples respectively. This adds confidence to the assumptions made throughout this project that the TILs identified as antigen experienced CD8+ are in fact predominantly cytotoxic lymphocytes and that this population is not a more heterogeneous group comprising multiple other immune cell subtypes.

When considering how the data collected during this project could be expanded and incorporated into clinical decision making, techniques for readily identifying populations of CD8+, PD-1+, CD39+ lymphocytes would be required. As discussed previously, CD39 is not solely expressed on CD8+

lymphocytes, and is often described as being expressed at higher concentrations on CD4+ lymphocytes. This would suggest that techniques such as using immunohistochemistry single staining for CD39 would be insufficient to gain an impression of the number of antigen experienced CD8+ TILs of the DP phenotype, for use in a manner analogous with PD-1/PD-L1 staining currently used in clinical practice.

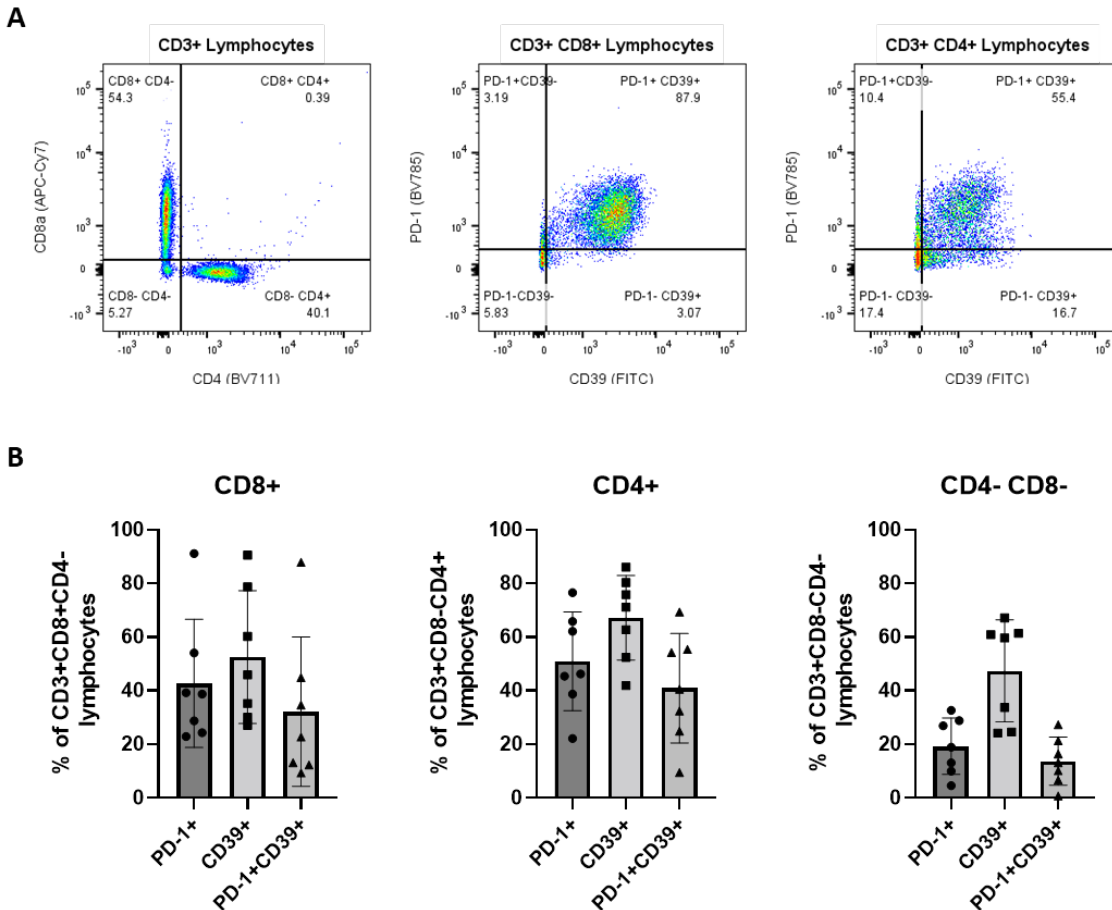


Figure 40 Positivity for PD-1 and CD39 among CD3+ lymphocytes of either CD8+, CD4+ or CD8- CD4- subgroup.

A) Exemplar flow cytometry plot showing gating strategy. CD3+ lymphocytes are separated based upon CD8 and CD4 positivity (left), with CD8+CD4- population (centre) and CD4+CD8- populations (right) gated depending upon PD-1 and CD39 positivity. B) Mean and standard deviation of percentages of CD3+CD8+CD4- (left), CD3+CD8-CD4+ (centre) and CD3+CD8-CD4- (right) TILs that are gated as positive for PD-1, CD39 or PD-1 and CD39. Data based upon observations from analysis of 7 OAC tumour samples.

This expectation was investigated further by assessing the proportion of cells positive for PD-1 and CD39 among CD3+CD8+ and CD3+CD4+ TILs. Significant proportions of the CD8+ and CD4+

lymphocytes stained positively for CD39 (CD8+ mean 52.5 range 27.0-90.0%, CD4+ mean 67.17% range 41.9-86.0%). In this sample the minority CD4-CD8- TIL population also express high CD39 expression (mean 47.33% and range 24.1-67.1%) (Figure 39). These observations rule out the use of CD39 staining as a single assessment to provide information on the character of CD8+ TIL infiltration.

PD-1 and CD39 dual positivity is similarly highly observed in the CD3+CD4+ and the CD3+CD8-CD4- TIL populations (means 40.88% and 13.65% respectively with ranges 9.48-69.3% and 0.72-27.3%) compared to the CD3+CD8+ population (mean 32.12% and range 9.33-87.90%) (Figure 39).

5.2.5 Assessment for expression of markers of tissue resident memory phenotype

One telling observation from the transcriptomic assessment of the TIL populations of interest detailed in chapter 4 is the presence of enrichment for a tissue resident memory phenotype. Tissue resident memory (T_{RM}) cells arise from the memory T lymphocyte compartment and are characterised as non-circulating immune cells that reside within peripheral, non-lymphoid tissues, and play a key role in anti-infection and anti-tumour immune responses (143).

T_{RM} cells within tumours often show an exhausted like phenotype, though they can derive from a variety of lymphocyte origins including naïve T cells, memory T lymphocytes and also T effector cells suggesting a possibly different developmental pathway to classical exhausted lymphocytes from chronic viral infections (133,139,202). Experiments in murine models have previously shown PD-1+ CD39+ TILs to be enriched for T_{RM} transcriptional profiles, an assumption supported in this project (130). To confirm if the PD-1+ CD39+ (DP) TIL population in human OAC is of T_{RM} origin, the subset of samples analysed for CD4 and CD3 expression, was also stained for CD103, a classical T_{RM} marker. These samples were also stained with an anti-CD57 antibody, selected due to recent data suggesting the relevance of CD57 in tumour specific epithelial derived T_{RM} groups (142). CD57 has also been shown to have an association with positive outcomes after resectional surgery for OAC when identified at high levels within the tumour by immunohistochemistry (183).

The differences in CD103 expression between the PD-1- CD39- population and the PD-1+ CD39+ population within the antigen experienced TILs was clear. The PD-1- CD39- (DN) group showed a low percentage of CD103 staining (mean 27.47% range 12.3-80.1) while the PD-1+ CD39+ group showed repeatedly high CD103 positivity (mean 90.91% range 75.2-98.8%) (Figure 40). The difference between these two groups was highly statistically significant when assessed by the paired t test ($p=0.0007$). The PD-1+ CD39- and PD-1- CD39+ groups demonstrated a stepwise increase in the percentage positive for CD103 (means 53.51% and 72.66% respectively) (Figure 40.B).

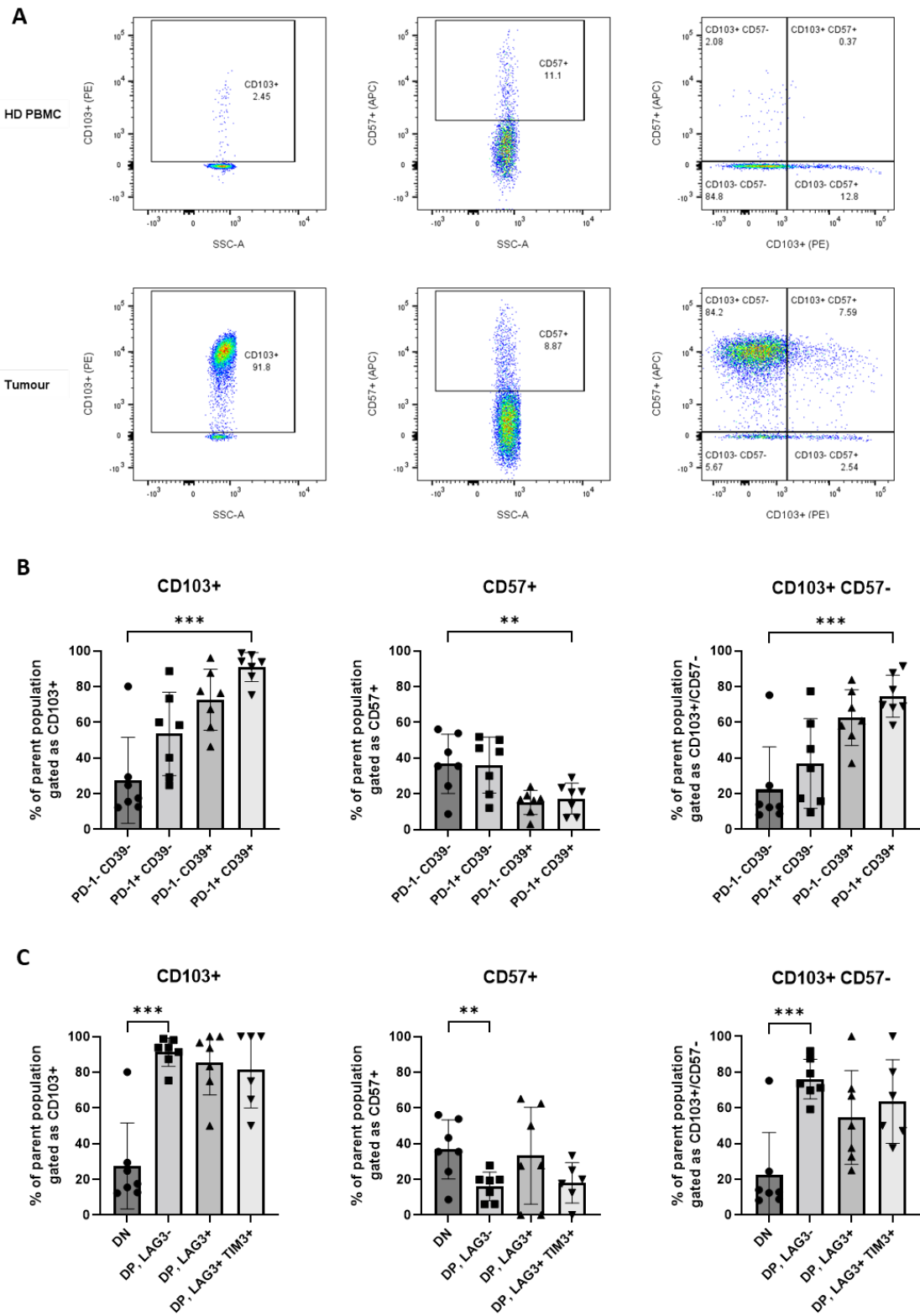


Figure 41 CD103 and CD57 positivity in human OAC TILs.

A) Exemplar flow cytometry plots showing gating for CD103 positivity (left), CD57 positivity (centre) and CD103/CD57 dual positivity. Samples shown are both antigen experienced CD8+ lymphocytes, with top row PD-1-CD39- lymphocytes from HD PBMC, and bottom row PD-1+ CD39+ OAC TILs. B) Mean and standard deviation for

percentage of parent gate positive for CD103 (left), CD57 (centre) or CD103+CD57- (right). Parent populations are all CD8+CD44+ lymphocytes and either PD-1- CD39-, PD-1+ CD39-, PD-1- CD39+ or PD-1+ CD39+. C) Mean and standard deviation for percentage of parent gate positive for CD103 (left), CD57 (centre) or CD103+CD57- (right). Parent populations were all CD8+CD44+ lymphocytes and either PD-1- CD39- (DN), PD-1+ CD39+ LAG3- TIM3- (DP), PD-1+ CD39+ LAG3+ TIM3- (EExh) or PD-1+ CD39+ LAG3+ TIM3+ (LExh).

Examining the same parent populations with regards to CD57 staining, an opposite picture was observed, with stepwise decrease in percentage positive from PD-1- CD39- to PD-1+ CD39+ populations (means 36.77% and 17.33% respectively, with ranges 8.7-56.1 and 6.5-29.0%) (Figure 40.B).

This suggests a CD103+CD57- dominant group within the PD-1+ CD39+ DP population. By assessing the percentage of parent groups that are positive for this phenotype it is observed that this steadily increases to a mean of 74.63% in the DP group (Figure 40.B).

With a slight modification of this gating strategy, by including TIM3 and LAG3 positivity, CD103 expression among the DN, DP, EExh and LEExh populations sorted and sequenced in experiments described in chapter 4, was assessed. A largely analogous picture can be observed as when gating for PD-1 and CD39 alone. CD103 increases significantly from DN to DP groups, but then falls somewhat with progression from DP to the EExh and then LEExh groups (means 91.23%, 85.49% and 81.62% respectively) (Figure 40.C). Similarly, with CD57 positivity in these experimental groups, a drop in percentage positivity is observed between the DN and DP group with followed by a rise in the EExh and then further drop in the LEExh group (means 36.77%, 16.03%, 33.3% and 18.07% respectively). The CD103+ CD57- population was highest in the DP group but remained high in the EExh and LEExh groups too (means 22.6%, 76.09%, 54.64% and 63.55% respectively) (Figure 40.C).

The results from the flow cytometry assessment of this limited cohort of tumour samples suggests that the DP population as defined previously, is highly enriched for CD103+CD57- lymphocytes, suggesting a tissue resident memory cell population that may correspond to populations of T_{RM} cells observed in other cancer models to exert enhanced functional capacity and bring about disease control (142). It also adds weight to the assumption that the EExh and LEExh populations assessed are also dominated by exhausted-like TRM lymphocytes arising from a memory origin, rather than classically terminally exhausted T lymphocytes.

5.3 Discussion

This chapter presents additional flow cytometric and functional data further examining the PD-1+ CD39+ DP population identified in chapter 3 as being associated with improved disease free survival, adding to the transcriptomic profiling undertaken in chapter 4.

The DP population has been shown to possess a transcriptional profile enriched for a T_{RM} phenotype, and data presented here shows this group to be highly comprised of CD8 TILs bearing the canonical T_{RM} surface marker CD103. This group is predominantly CD57 negative, suggesting shared phenotype with the CD103+CD57- CD8 T_{RM} cell type described in hepatocellular carcinoma (HCC) as being associated with high functional capacity and improved tumour control(142). The T_{RM} cells studied in this investigation are all HBV specific, though chosen for their ability to recognise pathogenic peptides, be they infection or cancer, ensuring the investigation did not focus on bystander TILs. It can be assumed that they correspond with TILs targeting neoantigens in this context. Interestingly, the investigation into these T_{RM} subsets in HCC observed relatively low abundance of PD-1^{high} CD39+ TIM3+ T_{RM} cells displaying a terminally exhausted-like character, an observation mirrored here in assessment of OAC tumours.

Further examination of the DP group reveals cells of varying t-box transcription factor profiles. The majority are T-bet^{high} Eomes^{low}, which could suggest dominance of a precursor exhausted phenotype. With progression to the EExh and LExh groups reduced T-bet^{high} Eomes^{low} and increased percentages of T-bet^{low} Eomes^{high} are observed indicating a move towards more terminally differentiated exhausted phenotype in these groups. Such findings support data collected in chapter 4 where transcriptomic analysis demonstrated enrichment for these terminally exhausted gene sets in these groups. The percentages T-bet^{high} Eomes^{low} and T-bet^{low} Eomes^{high} do not appear to come anywhere close to comprising of the entirety of the DP or LExh groups, suggesting these populations are not comprised solely of precursor exhausted or terminally differentiated exhausted lymphocytes, leaving room for the TRM populations described above.

Examination of the differences between TILs gated as T-bet^{high} Eomes^{low} and T-bet^{low} Eomes^{high} has shown that the latter group does possess an increased percentage of lymphocytes positive for the markers of terminal exhaustion LAG3 and TIM3, though the increment is modest and not what may have been expected were this transcription factor profile characteristic of terminal exhaustion, as may have been expected. This T-bet^{low} Eomes^{high} population also demonstrated an increased percentage of Granzyme B positive lymphocytes and a suggestion of increased Perforin positive cells, though IFN- γ and TNF- α positivity was not significantly different.

Assessment of the concentrations of these effector molecules in the various lymphocyte groups examined elsewhere in this study revealed low levels of IFN- γ , TNF- α and Perforin in the DP group with higher levels of all three of these molecules observed in the EExh and LExh groups. This is contrary to the gene count data produced in chapter 4 where IFN- γ production was maintained in the DP group, and could represent reduced secretion in this group. It has been described in the literature that T_{RM} cells, including those expressing TIM3 that would correspond to the LEXh group, maintain cytokine production and cytolytic granule formation, explaining these observations.

Considering the functional ability of the DP population, data presented here suggests that this group maintains an ability to proliferate rapidly if provided with the appropriate environment and signalling. The conditions provided to TILs in this chapters proliferation assay were clearly supra-physiological in terms of IL-2 and stimulation of CD3 and CD28, but have shown that there is capacity for cellular division, something that may not have been the case in a population comprised completely of dysfunctional exhausted lymphocytes.

Additionally, this population has been demonstrated to possess an ability to produce IFN- γ and TNF- α under mitogen stimulation, though to a lesser extent than observed for the DN population. This was more than the number of DP TILs staining positive for IFN- γ and TNF- α on stimulation via CD3 and CD28 or autologous tumour alone which were minimal. From the same experimental results it is observed that there is reduced Granzyme B and Perforin staining, with Perforin staining almost completely absent in the DP group when cultured with protein transport blocked, and this does not appear to vary greatly with the stimulatory signalling the cells are exposed to.

The observations regarding effector molecule production and maintained proliferative capacity overlap further with known T_{RM} characteristics and would fit with the DP population being comprised mostly of this class of TILs. CD8+ T_{RM} are known to maintain relatively stable populations in normal tissue but possess an ability to expand rapidly on activation. They are also characterised by high numbers of transcripts for IFN- γ and TNF- α as well as high protein expression of Granzyme B, all observations made in chapter 4 and chapter 5 of this study (228,229).

In summary the results described in this chapter further reinforce the hypothesis that some human OAC tumours possess an abundance of infiltrating PD-1 and CD39 positive antigen experienced CD8 lymphocytes, which are associated with increased progression free and overall survival, and are predominantly of T_{RM} subtype, while also possessing features in keeping with precursor exhausted lymphocytes.

Chapter 6 Discussion

6.1 Oesophageal adenocarcinoma – an area of unmet need

Oesophageal adenocarcinoma represents an area of significant unmet need in terms of improved treatment options for early stage and advanced disease. The incidence of distal oesophageal and gastro-oesophageal cancers has risen rapidly in Western populations in recent decades (149). With a minority of patients candidates for curative surgery at diagnosis, and more than half of these destined to relapse later, strategies to improve outcomes here and in the setting of metastatic disease are greatly needed (208). Adoption of immune checkpoint inhibitors, which have shown such significant improvements in survival in advanced melanoma and non-small cell lung cancer, is starting to have an influence in oesophageal cancer. This is both in the curative and the palliative settings, though improvements in outcomes remain modest with a only a minority of patients benefiting (166,192). OAC often possess a tumour microenvironment potentially receptive to immune activation by checkpoint blockade, this includes the presence of a high tumour mutational burden, frequent high degrees of immune cell infiltration and enrichment of immune cell gene signatures (230). Despite these factors responses remain poor, with the lack of CD8+ T lymphocytes receptive to such manipulation a potentially crucial factor.

By understanding the composition and nature of the CD8+ T lymphocyte compartment it is hoped that it will be possible to predict those individuals whose tumours are more likely to relapse and as such should be treated with more aggressive therapeutic approaches, and those which are more receptive to manipulation by immune checkpoint blockade. Additionally by assessing the differences in the composition of these populations of immune cells in the tumours of patients exposed to neoadjuvant therapies and those not, it may be possible to understand further the mechanisms behind the differential responses to immunotherapy seen in the first and second line setting for metastatic disease.

An understanding of the nature of CD8+ lymphocyte dysfunction in cancer has evolved over recent years with persistent antigen exposure resulting in lymphocyte exhaustion becoming a dominant hypothesis to explain the lack of effective anticancer responses observed in highly infiltrated tumours. Lymphocyte exhaustion has been understood in the context of data accrued from the murine viral infection LCMV and subsequent cancer models, where activated CD8+ lymphocytes circulate from secondary lymphoid organs to the site of a tumour, are subject to persistent antigen exposure leading to a loss of proliferative capacity, ability to secrete cytokines and cytolytic granules and eventual cell death (39,44). More recent investigation has pointed

towards populations of tissue resident memory cells, maintained in peripheries and arising from a memory lineage, as being key effectors of anti-tumour immune responses, and particularly important in immune responses initiated as a result of immune checkpoint blockade (134,202).

The precise features of both of these models of lymphocyte responses to cancer and immunotherapy are described as being tissue context specific, with different characteristics observed between human and murine cancers as well as varying between the organs and histologies involved. There is evolving evidence of a T_{RM} population observed in oesophageal squamous cell carcinomas and associated with improved survival (145), but characterisation of lymphocyte dysfunction, and T_{RM} positivity, in oesophageal adenocarcinomas remains incomplete.

This work has aimed to investigate the CD8+ T lymphocyte compartment of resected human oesophageal adenocarcinoma with respect to the presence of features of lymphocyte exhaustion and dysfunction with a view to building upon our understanding of the mechanisms behind the resistance of many such cancers to treatment, particularly with immune checkpoint blockade.

On identification of an often abundant antigen experienced PD-1 and CD39 positive T lymphocyte population within these resected cancers, this project aimed to characterise this group and assess their effector functions.

6.2 Key Findings

The results described here demonstrate that human oesophageal adenocarcinoma is variably infiltrated with a population of PD-1 and CD39 positive antigen experienced T lymphocytes that conform to a tissue resident memory cell phenotype and their abundance may correlate with improved disease control and survival.

It has been shown using flow cytometry based approaches, that CD8+ cells are present in tumour digests across a range of tumour stages and degrees of responses to neoadjuvant therapies. Higher percentages of events corresponding morphologically to lymphocytes are CD8+ and CD44+ in higher stage T3 tumours and those previously exposed to neoadjuvant chemotherapy, though not enough data points were available to comment upon variation related to degree of tumour regression. This population represents a group we can confidently ascribe to being comprised overwhelmingly of antigen experienced CD8+ T lymphocytes based upon the high degree of CD3 positivity and the negligible numbers of CD8+CD4+ lymphocytes observed in OAC tumour digests.

The presence of these antigen experienced CD8+ lymphocytes appears to be associated with increased survival, but this observation is far more marked when abundance of PD-1+ and CD39+ antigen experienced TILs is assessed. PD-1 is highly expressed here in CD8+ TILs from OAC

tumours, particularly in treatment naïve and chemotherapy pre-treated specimens, as is CD39 positivity in similar patients. A frequency of this PD-1 or CD39 positive phenotype above the median is associated with better progression free survival in this cohort.

Of note, when PD-1 and CD39 double positive (DP) cells are calculated as a percentage of antigen experienced CD8+ TILs, they are in highest abundance in tumours of patients who are treatment naïve at surgery, suggesting an impact on the numbers of this lymphocyte compartment from cytotoxic chemotherapies. Overall survival is markedly improved when high frequencies of this DP group are observed with respect to total numbers of antigen experienced CD8+ lymphocytes, and particularly when calculated as a proportion of all lymphocytes. This is especially surprising as this DP population, while of variable frequency across individuals, is highest in treatment naïve samples, a group we would consider sub-optimally prepared for surgery when we are considering curative therapies, yet is also associated with improved outcomes. Such an observation raises several important questions, firstly is this reproducible in a larger patient cohort or an artefact caused by the limited sample population available in this study? Secondly, if a high abundance of DP TILs is associated with improved survival and they are reduced by chemotherapies, are there some patients who will do better if chemotherapies are omitted completely prior to resection, and likewise is there a group that requires even more intensive neoadjuvant therapies prior to completion surgery? And finally, is this population a cancer specific population, as might be speculated from previously published data on CD39+ TILs, and can increased knowledge about the abundance and characteristics of this population shed light onto patient outcomes in the metastatic setting, and particularly responses to immune checkpoint blockade?

With these questions in mind, the composition and function of the DP population has been investigated with a mixed approach of flow cytometric immune profiling, bulk transcriptomic assessment, and functional analysis. Flow cytometry has shown that the DP group is potentially heterogeneous, but with a majority population of cells that could correspond to a precursor exhausted phenotype as implied by a majority possessing a T-bet^{High} Eomes^{Low} transcription factor profile. Additionally, while the DP group possessed a higher frequency of TILs positive for the exhaustion markers TIM3 and LAG3, as well as TIGIT, 2B4 and the marker of lymphocyte activation CD38, this was not at frequencies that may be expected were this group predominantly terminally exhausted. The DP population is also seen to be composed of TILs with a range of levels of PD-1 expression, with those at the higher end of this spectrum increasingly positive for additional surface markers of exhaustion.

Multi-parametric flow cytometry data interrogating a subset of samples with a view on assessing T-bet and Eomes expression in the experimental groups, alongside TIM3 and LAG3 expression has

Chapter 6

suggested that the DP and LExh groups do not conform to precursor exhausted and terminally differentiated exhausted phenotypes as may have been expected, but represent more heterogeneous cell groupings. Indeed when the T-bet^{low} Eomes^{high} group is assessed it is by no means wholly comprised of TILs possessing multiple markers of exhaustion which would suggest that while there may be processes underway that are akin to lymphocyte exhaustion, it is not representative of the classical picture developed from the LCMV model.

Interpreting this data together, it has been speculated that the DP population is heterogeneous, and comprised of lymphocytes conforming to an exhausted phenotype given PD-1 and CD39 both being strongly correlated with this type of CD8⁺ lymphocyte dysfunction (126), though it may also contain other PD-1 and CD39 positive CD8⁺ T cell populations such as tissue resident memory cells (129).

To further understand the composition and nature of the DP population, a transcriptomic approach has been adopted to allow comparison with the PD-1⁻ CD39⁻ group and lymphocytes possessing additional positivity for TIM3 and LAG3. This has revealed the DP group, when compared to the DN, to be enriched for signatures related to lymphocyte activation and proliferation, as well as TCR signalling, CD28 co-stimulation and PD-1 signalling. There was also evidence for enrichment of downstream effects of IL-2, IFN- γ , IL-10, and IL-12 signalling. Such results suggest the DP group to be active and proliferating, responding to stimulatory cytokines, and the effects of TCR complex engagement.

The possibility of this DP group being a T_{RM} population is supported by enrichment of gene sets for T_{RM} described in breast cancer by Savas et al (141) and in lung cancer by Kumar et al (136). It is further reinforced by enrichment for IL-10 signalling as well as downstream effects of RUNX3 and Id3 transcription factors which are known to drive development and maintenance of the T_{RM} phenotype (134,138,140).

Comparisons of the DP and LExh groups showed the DP group to be enriched for signatures of cell survival, and migration. There was enrichment for the transcription factor of precursor exhausted lymphocytes TCF1, as well as the T_{RM} transcription factor Notch as well as STAT3 and STAT4 which play roles in memory cell differentiation and maintenance.

Conversely the LExh group demonstrated a tendency towards cell death and restriction of mitosis, and was enriched for the effects of the transcription factors initiating a terminally differentiated exhausted phenotype TOX and Eomes. There was again enrichment for the downstream effects of TCR engagement suggesting persistent antigen exposure, as well as PD-1 signalling. The LExh

group was enriched for gene sets describing T_{RM} phenotypes, as well as for signatures relating to terminally differentiated and precursor exhausted expression profiles.

When the transcriptomic data set was analysed as a whole there was evidence of increasing enrichment for gene sets related to TCR, PD-1, IFN- γ , and IL-12 signalling with progression from DN, through DP and EExh to LExh groups. Similarly there was observed a trend towards increasing enrichment for gene sets describing terminally exhausted, T_{RM} and some precursor exhausted lymphocyte populations, with progression through experimental groups. Most enriched in the DP group included gene sets for T cell activation, proliferation and migration, as well as for some progenitor exhausted lymphocyte populations.

The DP, EExh and LExh groups showed persistent transcription of genes encoding for IFN- γ , TNF- α , Granzyme B and Perforin. There was also increasing transcriptional activity for the canonical T_{RM} marker CD103.

Considering the functional analyses completed in chapter 5 in light of the transcriptomic assessment we can observe the DP population maintains capacity to proliferate when subject to a high degree of cytokine stimulation. Additionally they possess an ability to produce IFN- γ and TNF- α cytokines on mitogenic stimulation, all be it at a lower level than the DN group, but not on stimulation by autologous tumour alone. Maintained Granzyme B production is in keeping with transcriptomic data while reduced Perforin production does not quite fit with the transcriptomic picture. Of note the DP group retains a higher capacity to degranulate than the DN group, on stimulation by autologous cancer cells, stimulatory antibodies or mitogens.

Finally assessment of expression levels among the experimental groups of interest, for the integrin and T_{RM} marker CD103, as well as CD57 an NK and lymphocyte marker upregulated in some epithelial T_{RM} populations, was assessed. This showed that the DP group was almost exclusively CD103 positive, with a mean of 91.2% cells expressing this marker, and this fell slightly through the EExh to LExh groups to a mean of 81.6%. The DN group contained only a modest number of cells expressing CD103. CD57 expression was lowest in the DP and LExh groups, resulting in a majority of TILs in the DP group being labelled as CD103+ CD57-.

6.3 Interpretation of results

The results summarised above point to a PD-1 CD39 double positive lymphocyte population in human OAC tumours, comprising cells of varying TIM3 and LAG3 expression, which can be variously described as precursor exhausted, terminally exhausted or T_{RM} lymphocytes.

Chapter 6

This PD-1 and CD39 double positive population does not conform to a classically exhausted phenotype as described within the context of the LCMV model, and this is demonstrated both by the heterogeneous T-bet and Eomes transcription factor profile of this population, the low abundance of additional cell surface markers of exhaustion, and by the transcriptomic profiles of this population.

Instead, this PD-1 and CD39 double positive population can be more accurately described as a tissue resident memory cell population, subsets of which have been demonstrated to play crucial roles in immune control of human cancers.

T_{RM} cells are reported as deriving from memory precursor cells and are subsequently retained in the periphery (139), and as such sit outside of the classical view of lymphocyte exhaustion where by effector cells are subjected to sustained antigen exposure and are driven into a precursor and then terminally differentiated exhausted state (34). However, as the understanding of T_{RM} biology has developed in recent years, it is becoming apparent that T_{RM} in tumours are comprised of a heterogeneous collection of states (140), including those that while they possess core T_{RM} transcriptional profiles and cell surface integrins suggesting T_{RM} origin, also possess shared characteristics with exhausted lymphocytes (114,142). Milner et al have published data suggesting that tumour specific TILs are enriched for core tissue residency gene expression signatures and that T_{RM} heterogeneity in TILs corresponds to the heterogeneity described in infection (140). They describe an Id3 high population of T_{RM} in murine tumours that are multipotent and respond to immune checkpoint blockade and that are consistent with precursor or progenitor exhausted lymphocytes. Likewise, evidence presented by Clarke et al and others describe the presence of T_{RM} populations that correspond to terminally differentiated exhausted lymphocyte population and possess PD-1 and TIM3 expression as well as CD39 and CD103 positivity (114,129).

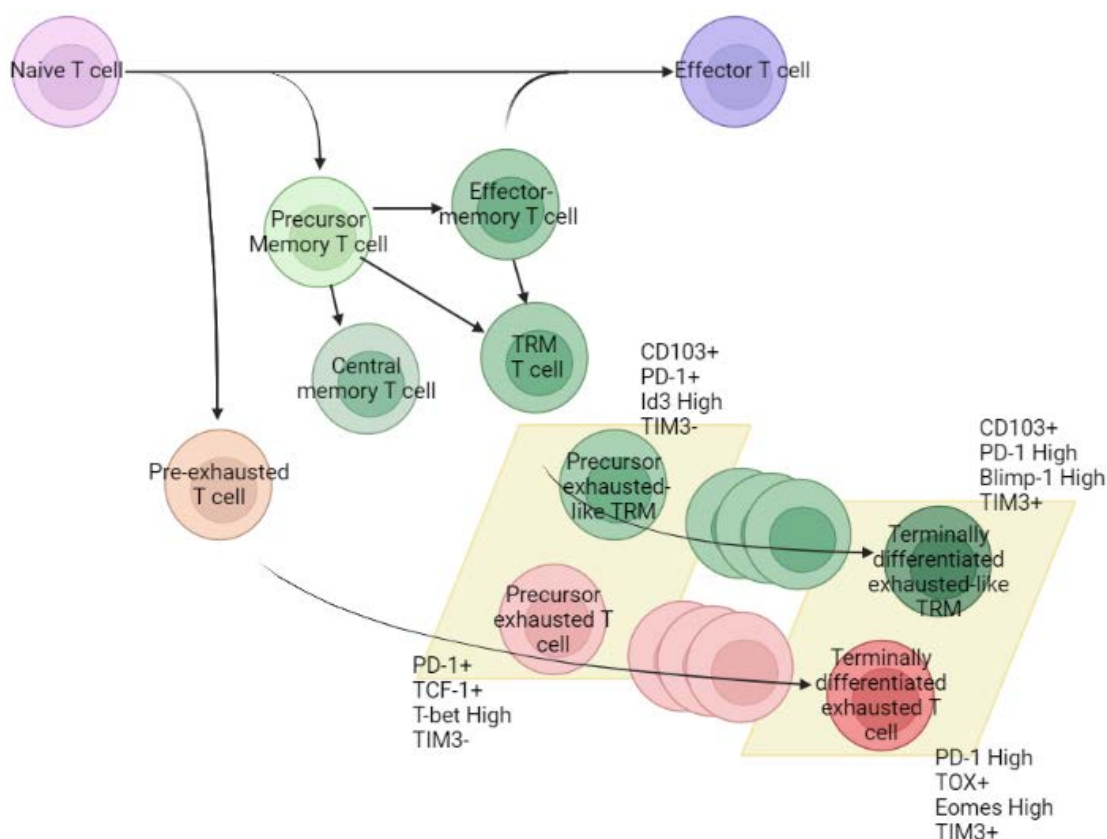


Figure 42 Similarities between tissue resident memory cell and classically exhausted lymphocyte populations of interest.

Schematic displaying development and characteristics of precursor exhausted-like and terminally differentiated exhausted-like tissue resident memory lymphocytes, and their similarities with classical precursor exhausted and terminally differentiated exhausted lymphocytes. It is proposed that the DP and LExh populations investigated in human oesophageal adenocarcinomas correspond with the pre-cursor exhausted-like and terminally differentiated-like T_{RM} populations displayed here. Created with BioRender.com.

The data summarised above supports an assumption that human oesophageal adenocarcinomas are variably, but often highly, infiltrated by an antigen experienced $CD8^+$ lymphocyte population that is $PD-1$ and $CD39^+$, but $TIM3$ and $LAG3$ negative, and comprised predominantly of tissue resident memory cells. This population is consistent with those described by Milner et al. as being $Id3^{high}$ T_{RM} that share many transcriptional and protein level similarities with a precursor exhausted population (140). The DP population would also correspond to a similar $CD103^+$ $CD57^-$ population has been described by Cheng et al among HBV specific TILs extracted from hepatocellular carcinomas, that remain highly functional, and are associated with improved survival (142).

The human OAC samples analysed here also demonstrate a population of CD8+ TILs that possess multiple inhibitory markers including TIM3 and LAG3, described as late exhausted (LExh) that is of very low abundance. There is evidence that this group corresponds with a PD-1^{high} TIM3+ terminally exhausted-like T_{RM} population described in a range of scenarios as being in possession of multiple inhibitory markers suggesting terminal exhaustion, but maintaining core T_{RM} expression profiles, as well as an ability to proliferate, produce effector molecules and kill cancer cells (114,140,142). This phenotype is associated with improved outcomes on treatment with anti-PD-1 therapies.

Aligning the experimental groups characterised in this project with T_{RM} phenotypes described in recently published studies, allows consideration of the mechanism by which an abundance of PD-1 and CD39 double positive TILs may be associated with improved overall survival. This population of tumour reactive and functional lymphocytes has been associated with improved survival elsewhere and it can be considered that the same is true in oesophageal adenocarcinoma (114,140,202). Certainly it can be hypothesised that a relative lack of these TILs that possess the potential for tumour reactivity and an ability to rapidly proliferate and undertake effector functions, within a tumour would be associated with reduced tumour control and poorer prognosis.

As to why better responses to immunotherapy are observed following priming with previous or concurrent chemotherapy it is difficult to find a clear answer from the data presented. It can be speculated that the LEExh population which is of low abundance in the analysed OAC tumours, and appears to correspond with the CD103+PD-1+TIM3+ population described by Clarke et al as associated with improved responses to anti-PD-1 therapy in lung cancer, is responsible for immunotherapy induced tumour regression in oesophageal cancer too. The current data set is comprised of a limited number of patient samples and as such has limited granularity, but it appears that TIM3 expression is highest in CD8+ TILs after pre-treatment with chemoradiotherapy. While chemotherapy treated samples appear to have a similar percentage of TIM3 positive TILs to treatment naïve samples, it can be postulated that the priming with chemotherapy or chemoradiotherapy, increases the relative abundance of these terminally exhausted-like T_{RM} within the tumour microenvironment, creating a scenario more responsive to immune checkpoint blockade.

6.4 Limitations

This project has focused on intrinsic CD8+ T lymphocyte factors that influence dysfunction in human oesophageal adenocarcinoma, however lymphocytes exist within and rely upon a complex

immune microenvironment in order to survive, proliferate and undertake effector functions. Investigation of other components of this environment, including CD4+ T lymphocytes, has not been within the remit of this project but are of course of huge significance when interrogating CD8+ T lymphocyte responses.

When considering the specific limitations of this project, it must be conceded that the patient sample size available for analysis is small. Despite this project being undertaken on the site of a tertiary referral hospital acting as the principle location for resection of upper gastrointestinal tumours for a large region, the numbers of patients operated on and also recruited to the overarching studies, was relatively small each year. Recruitment was also hampered by the coronavirus disease 2019 pandemic halting access to non-essential clinical trials. The nature of the methods used for analysis, principally flow cytometric based analysis of manually disaggregated tumour samples, meant that up-scaling analysis pipelines would always be a challenge.

The limited number of patients recruited, as well as time constraints on this study and experimental issues, have limited the number of samples available for some work-streams. In particular, the transcriptomic analyses detailed in chapter 4. For this body of work, power calculations had set the minimum number of biological replicates to allow DEG assessment and GSEA, at 6, with 10 an ideal number. It had therefore been planned to undertake RNA sequencing of all 4 experimental groups on samples from 8 treatment naïve patients, and then up to 8 chemotherapy pre-treated patients to allow detailed comparison between treatment groups. This was ultimately not possible but in excess of 6 samples were collected for each experimental group, and adequate power achieved to allow gene set based analysis to be completed with confidence.

The nature of the tissue available for analysis also resulted in a relatively narrow focus for this project. There were limited samples of normal adjacent tissue available for comparative analysis, and no tumour draining lymph node specimens available, with the latter being important for patient diagnostic staging and prognostication at the time of surgery. Such access to nodal tissue would require additional consent and ethical approval. At the outset of this study the focus was upon the presence of lymphocyte exhaustion and as such access to adjacent tissue was not considered essential, as focus has shifted towards tissue resident memory cells as a crucial CD8+ subgroup in oesophageal adenocarcinomas there has been an appreciation that looking at analogous populations in normal, organ matched tissue would have been very informative, in the same way as healthy non-cancerous lung tissue was used by Clarke et al in their work much cited throughout this project (114,202).

A final consideration regarding sample availability related to the size of the tumour sample accessed. These varied but were often small, typically fragments of an 8mm punch biopsy on arrival at the research laboratory. Given the priority not to interfere with routine pathological assessments post resection, research samples were limited and sampling undertaken from the centre of each tumour to allow assessment of resection margins. Given this, the amount of disaggregated tumour cells accessed and available for experimentation was limited. For some experimental work streams, such as routine flow cytometric analysis, this was certainly sufficient to provide accurate results. For others such as transcriptomic assessment, high sensitivity approaches were chosen to account for the limited number of cells available for experimentation. However for some experiments, particularly the cell proliferation assays measured after staining with CFSE, the limited cell number did have a bearing on the validity of results. There were real challenges in completing these experiments on such limited cell numbers, making numerical quantification of proliferation between groups very difficult, though the results presented do provide a real suggestion of the proliferative capacity of the cell populations of interest.

Despite these limitations, it is considered that the data presented here is robust, with clear flow cytometric data, sufficient depth of sequencing and biological replicates for gene set based enrichment analysis techniques, and representative functional data particularly cell stimulation and degranulation assays, that correspond with the published literature and transcriptomic analysis. This has allowed the characterisation of the DP and LExh populations of interest described in this work as precursor and terminally exhausted-like T_{RM} populations, with a clear mechanism for the improved patient outcomes associated with their abundance.

6.5 Future research

As described above this project has identified exhausted-like T_{RM} populations as potential effectors of anti-cancer immune responses in human oesophageal adenocarcinoma, leading to multiple potential future strands for this research project. These results raise a number of important questions worthy of future investigation. Firstly, would these findings remain were the number of samples accessible for analysis to be increased? Secondly, what are the developmental origins of the T_{RM} populations of interest, and how could conditions be manipulated to enhance these populations if they do prove to play an important role in anti-tumour responses. Thirdly, are these T_{RM} populations enriched for cancer specific CTLs that can undertake effective killing of cancer cells and are the terminally exhausted-like T_{RM} cells responsible for reactivation after immune checkpoint blockade. Could these TILs be manipulated either in vivo or ex-vivo as a future therapeutic strategy to control this aggressive cancer. Finally, what are the effects of neoadjuvant treatments on these populations of interest, and are their relative abundances and

therefore potential to bring about tumour control, influenced by exposure to cytotoxic chemotherapy and, or, radiation.

Moving forward it would be of interest to look for evidence of these T_{RM} populations in further patient samples, but also to assess the ability of this cell type to control disease, in particular in the context of immune checkpoint blockade. There would be potential to repeat the current experimental analysis, such as flow cytometry assessment and even RNA sequencing on more patient samples. If this was to be undertaken, it would be interesting to again prioritise treatment naïve patients, allowing the greatest window into the emerging biology of these cancers. With increasing use of immune checkpoint blockade in the adjuvant and metastatic setting for treatment of oesophageal cancer since conclusion of experimental work on this project, there is also scope to assess the effects that PD-1 blockade has upon the cell populations of interest within in human cancers.

There is scope to look at data sets and samples collected by collaborators, and explore if observations made here are repeated elsewhere. Single cell RNA sequencing analysis has been undertaken by close collaborators on resected oesophageal adenocarcinoma samples, and there is significant interest in exploring these data libraries for the presence of a dominant T_{RM} population, as well as gathering information on the potential subtypes of these cells. The added detail about individual cells, may also provide further evidence of the developmental origins of the tumour infiltrating T_{RM} populations, an issue that remains up for debate in the wider field of cancer immunology, where the precise pathway for differentiation of tumour specific T_{RM} is not wholly accepted.

Additionally, other members of the wider research group, are using tissue microarrays for microscopic analysis of collections of multiple tumour samples from analogous sources as those studied here. As has been discussed there are challenges to using simple immunohistochemistry techniques to identify and classify the PD-1 CD39 double positive group, given the number of stains required to identify them, but with increasing adoption of multiplex immunohistochemistry protocols, it would be possible, following optimisation, to assess for the T_{RM} populations of interest in multiple samples using the wealth of historic histology samples.

To address questions of tumour reactivity among the populations of interest studied here remains a real challenge. In the absence of knowledge about the target peptide for these TILs, assumptions are reliant upon extrapolations from viral models or cancers with known dominant neoantigens or tumour associated antigens, molecules such as MART in melanoma or the E6 and E7 antigens presented by HPV associated tumours. It would be of great interest to utilise collaborations with university colleagues who are uncovering peptidomic profiles of cancer cells,

including those working on historic oesophageal adenocarcinoma samples, in order to test the reactivity of this population for potential immunogenic peptides. Such analysis would be a significant undertaking, and highly experimental, however were it able to confirm that the T_{RM} populations observed are highly enriched for cancer cells presenting neoantigens, this would confirm these as cell types of significant interest when characterising anti-cancer immune responses.

6.6 Concluding summary

It is demonstrated here that human oesophageal adenocarcinomas are infiltrated to a varying degree with CD8+ tissue resident memory lymphocyte populations that display precursor exhausted-like and terminally exhausted-like phenotypes. These TILs are likely enriched for tumour reactive clones and while the former, precursor-like group, appears associated with improved patient outcomes in this study as well as published data sets, the latter is often described as being responsive to immune checkpoint blockade. It has been shown that an abundance of PD-1+ CD39+ TILs appears to be associated with improved patient progression free and overall survival in the study cohort. It is also demonstrated that this double positive group are dominated by CD103+ antigen experienced lymphocytes, with a maintained proliferative potential and an ability to produce effector molecules under conducive stimulation. Additionally this group is enriched for transcriptional signatures in keeping with lymphocyte activation, proliferation and migration, as TCR and CD28 signalling, as well as gene sets enriched for T_{RM} and precursor exhausted expression profiles. Meanwhile the PD-1+CD39+ population also contains a minority population of TIM3 and LAG3 positive TILs, that are consistent with a terminally exhausted-like T_{RM} population, showing increased IFN- γ and TNF- α production at both the transcriptional and protein level, as well as similarly maintained Granzyme B and Perforin production. These terminally exhausted-like T_{RM} cells are highly enriched for signatures of TCR engagement suggesting interaction with cognate peptide-MHC. They are also enriched for gene sets describing both terminal exhaustion from viral models and human cancers, as well as core tissue resident memory cell transcriptional profiles.

This knowledge adds to a growing appreciation of the role of T_{RM} populations in controlling cancers in a range of settings, including other cancers of the upper gastrointestinal tract, but whose specific phenotype is context specific. These T_{RM} lymphocyte populations are understood to play a vital role in immune activation after immune checkpoint blockade and their characterisation in oesophageal adenocarcinoma, adds to our appreciation of the mechanisms behind the variable responses observed to such treatments.

Appendix A Classification and staging of human oesophagogastric cancer

A.1 Siewert system of classification for adenocarcinomas of the oesophagogastric junction

Siewert group	Siewert description	Practical description
Type I tumour	Adenocarcinoma of the distal oesophagus which usually arises from an area with specialized intestinal metaplasia of the oesophagus (i.e. Barrett's oesophagus) and which may infiltrate the oesophagogastric junction from above.	Tumour centre located between 5 and 1 cm proximal to the anatomical cardia (surgical approach as oesophageal or OG junctional cancer).
Type II tumour	True carcinoma of the cardia arising from the cardiac epithelium or short segments with intestinal metaplasia at the oesophagogastric junction; this entity is also often referred to as 'junctional carcinoma'.	Tumour centre located between 1cm proximal and 2 cm distal to the anatomical cardia (surgical approach as oesophageal or OG junctional cancer).
Type III tumour	Subcardial gastric carcinoma which infiltrates the oesophagogastric junction and distal oesophagus from below.	Tumour centre located between 2cm and 5cm distal to the anatomical cardia (surgical approach typically as gastric cancer).

Table 5 Siewert classification of oesophagogastric adenocarcinomas.

Classification of oesophagogastric adenocarcinomas with respect to the anatomical cardia, as defined by Siewert and Stein (158). Included are the description of each

tumour classification as defined in the original publication, and the commonly accepted practical description.

A.2 TNM cancer staging categories for cancer of the oesophagus and oesophagogastric junction

T category	
TX	Tumour cannot be assessed
T0	No evidence of primary tumour
Tis	High-grade dysplasia, defined as malignant cells confined by the basement membrane
T1	Tumour invades the lamina propria, muscularis mucosae, or submucosa
T1a	Tumour invades the lamina propria or muscularis mucosae
T1b	Tumour invades the submucosa
T2	Tumour invades the muscularis propria
T3	Tumour invades adventitia
T4	Tumour invades adjacent structures
T4a	Tumour invades the pleura, pericardium, azygos vein, diaphragm, or peritoneum
T4b	Tumour invades other adjacent structures, such as aorta, vertebral body, or trachea
N category	
NX	Regional lymph nodes cannot be assessed
N0	No regional lymph node metastasis
N1	Metastasis in 1–2 regional lymph nodes
N2	Metastasis in 3–6 regional lymph nodes
N3	Metastasis in 7 or more regional lymph nodes
M category	
M0	No distant metastasis

M1	Distant metastasis
----	--------------------

Table 6 Cancer staging for cancer of the oesophagus and oesophagogastric junction.

Tumour, Lymph node and Metastasis (TNM) scoring detailed by the 8th edition of the American Joint Committee on Cancer (AJCC) staging of epithelial cancers of the oesophagus and oesophagogastric junction, applicable to both squamous cell and adenocarcinomas (159).

A.3 Mandard tumour regression score

Tumour regression score	Description
TRG1	No residual cancer cells
TRG2	Rare residual cancer cells
TRG3	Fibrosis outgrowing residual cancer cells
TRG4	Residual cancer cells outgrowing fibrosis
TRG5	Absence of regressive changes

Table 7 Classification of tumour regression using the Mandard scoring system.

Description of tumour regression following neoadjuvant therapies as described by tumour regression scoring detailed by Mandard and colleagues (207).

Appendix B List of flow cytometry antibodies

Antibody	Fluorophore	Clone	Isotype	Supplier	Amount (μ L) per 100 μ L
Anti-human 2B4 (CD244)	PerCP/Cy5.5	C1.7	Mouse IgG1, K	BioLegend	1.25
Anti-human CD103 (Integrin α E)	PE	Ber-ACT8	Mouse IgG1, K	BioLegend	5
Anti-human CD107a (LAMP-1)	PE/Cy7	H4A3	Mouse IgG1, K	BioLegend	5
Anti-human CD3	BV421	OKT3	Mouse IgG2a, κ	BioLegend	5
Anti-human CD38	PE/Cy7	HIT2	Mouse IgG1, K	BioLegend	1.25
Anti-human CD39	APC	A1	Mouse IgG1, K	BioLegend	2.5
Anti-human CD39	FITC	A1	Mouse IgG1, K	BioLegend	2.5
Anti-human CD4	BV711	OKT4	Mouse IgG2b, κ	BioLegend	5
Anti-human CD44	Pacific Blue	BJ18	Mouse IgG1, K	BioLegend	2.5
Anti-human/mouse CD44	BV510	IM7	Rat IgG1, κ	BioLegend	2.5
Anti-human CD57	APC	HNK-1	Mouse IgM, κ	BioLegend	5
Anti-human CD8a	FITC	HIT8a	Mouse IgG1, K	BioLegend	2.5
Anti-human CD8a	APC/Cy7	RPA-T8	Mouse IgG1, K	eBioscience	5
Anti-human CD8a	APC	HIT8a	Mouse IgG1, K	BioLegend	5
Anti-human EOMES	PE/Cy7	WD1928	Mouse IgG1, K	eBioscience	2.5
Anti-human/mouse Granzyme B	BV421	QA18A28	Rat IgG1, κ	BioLegend	2.5

Anti-human IFN gamma	APC	4S.B3	Mouse IgG1, K	BioLegend	5
Anti-human LAG3 (CD233)	PerCP/eFluor710	3DS223H	Mouse IgG1, K	eBioscience	5
Anti-human LAG3 (CD233)	BV650	11C3C65	Mouse IgG1, K	BioLegend	5
Anti-human PD-1 (CD279)	PE	EH12.2H7	Mouse IgG1, K	BioLegend	2.5
Anti-human PD-1 (CD279)	BV785	EH12.2H7	Mouse IgG1, K	BioLegend	2.5
Anti-human Perforin	BV711	dG9	Mouse IgG2b, κ	BioLegend	2.5
Anti-human T-bet	PerCP/Cy5.5	eBio4B10	Mouse IgG1, K	eBioscience	0.625
Anti-human TIGIT	PerCP/eFluor710	MBSA43	Mouse IgG1, K	eBioscience	2.5
Anti-human TIM3 (CD366)	PE/Cy7	F38-2E2	Mouse IgG1, K	eBioscience	5
Anti-human TIM3 (CD366)	PE/Cy5.5	F38-2E2	Mouse IgG1, K	eBioscience	5
Anti-human TNF alpha	PE	MAB11	Mouse IgG1, K	BioLegend	5

Table 8 Fluorophore labelled antibodies used for flow cytometry

Details of all fluorophore labelled antibodies used for flow cytometry based experiments. Included are the antibody target, fluorophore, antibody clone and isotype, supplier, and the volume of antibody added to a 100 μ L staining reaction as defined by antibody titration.

Appendix C SmartSeq 2 reaction mixtures and reaction conditions

Description of the reaction mixtures and conditions used for the modified SmartSeq2 protocol used for the preparation of cDNA and subsequently amplified adapter-ligated fragments used for RNA sequencing experiments as described in Chapter 2 with results presented in Chapter 4.

C.1 Reverse transcription and template switching reaction

C.1.1 Reverse transcription/template switching reaction mixture

Component	Volume per sample (μL)	Final Concentration
RNA/Primer/dNTP product	4.30	-
SuperScript II reverse transcriptase (200U/ μL)	0.50	100
SuperScript II first-strand buffer (5x)	2.00	1x
DTT (100mM)	0.50	5mM
RNase Inhibitor (40U/ μL)	0.25	10U
Betaine (5M)	2.00	1M
MgCl ₂ (1M)	0.06	6mM
TSO primer (100 μM)	0.10	1 μM
Nuclease-free water	0.29	-
Total volume	10.00	-

Table 9 Reverse transcription/template switching reaction mixture.

Reaction mixture for reverse transcription and template switching.

C.1.2 Reverse transcription PCR conditions

Cycle	Temperature ($^{\circ}\text{C}$)	Time	Purpose
1	42	90 min	RT and template switching
2-11	50	2 min	Unfolding of secondary RNA structures
	42	2 min	Completion/continuation of RT and template switching

12	70	15 min	Enzyme inactivation
-	4	Hold	

Table 10 Reverse transcription PCR conditions.

PCR conditions for the reverse transcription and template switching reaction as modified from the SmartSeq2 protocol (197).

C.2 PCR pre-amplification reaction

C.2.1 PCR pre-amplification reaction mixture

Component	Volume (μL)	Final Concentration
First-strand reaction	10.00	-
KAPA HiFi HotStart (2x)	12.50	1x
ISPCR primers (10 μM)	0.25	0.1 μM
Nuclease-free water	2.25	-
Total volume	25.00	-

Table 11 PCR pre-amplification reaction mixture.

Reaction mixture for PCR pre-amplification reaction.

C.2.2 Pre-amplification PCR conditions

Cycle	Denature	Anneal	Extend	Hold
1	98°C, 3 min	-	-	-
2-23	98°C, 20 s	67°C, 15 s	72°C, 6 min	-
24	-	-	72°C, 5 min	-
25	-	-	-	4°C

Table 12 Pre-amplification PCR conditions.

PCR conditions for the pre-amplification reaction as modified from the SmartSeq2 protocol (197).

C.3 Tagmentation and adapter-ligated fragment amplification

C.3.1 Tagmentation reaction mixture

Component	Volume (μL)	Final Concentration
Tagment DNA Buffer (2X)	10	1x
Amplicon tagment mix	5	-
DNA from PCR	Variable	-
Nuclease-free water	Variable	-
Total volume	20	-

Table 13 Tagmentation reaction mixture.

Reaction mixture for Tagmentation reaction utilising the Illumina NexteraXT library preparation procedure as detailed in the SmartSeq2 protocol (197).

C.3.2 Amplification of adapter-ligated fragment reaction mixture

Component	Volume (μL)
DNA	25
Nextera PCR master mix	15
Index 1 primers	5
Index 2 primers	5
Total volume	50

Table 14 Amplification of adapter-ligated fragment reaction mixture.

Reaction mixture for amplification of adapter-ligated fragment reaction as modified from the SmartSeq2 protocol (197).

C.3.3 Adapter-ligated fragment amplification PCR conditions

Cycle	Denature	Anneal	Extend	Hold
1	-	-	72°C, 3 min	-

Appendix C

2	95°C, 30 sec	-	-	-
3-14	95°C, 10 sec	55°C, 30 sec	72°C, 30 sec	-
15	-	-	72°C, 5 min	-
16	-	-	-	4°C

Table 15 Adapter-ligated fragment amplification PCR conditions.

PCR conditions for the adapter-ligated fragment amplification reaction as modified from the SmartSeq2 protocol (197).

Appendix D Script for DEG analysis using DESeq2

Exemplar script for differential gene expression analysis using DESeq2 package in the statistical package R detailed below. Descriptions in black following a # symbol, exemplar script in grey following a > symbol and exemplar data output in blue.

```
## Load important packages for analysis.
>library(DESeq2)
>library(DEGreport)
>library(pheatmap)
>library(EnhancedVolcano)
>library(AnnotationDbi)
>library(org.Hs.eg.db)

## Load and view read count data and metadata. Columns names of read count data and row
names of metadata files assessed to ensure accurately aligned and corresponding.
>data <- read.table("~/Current Work/PhD - Chapter 2/OAC TIL RNAseq Final
analysis/Read_counts_naive+chemo.txt", header=T, row.names=1)
>meta <- read.table("~/Current Work/PhD - Chapter 2/OAC TIL RNAseq Final
analysis/Metadata_naive+chemo.txt", header=T, row.names=1)

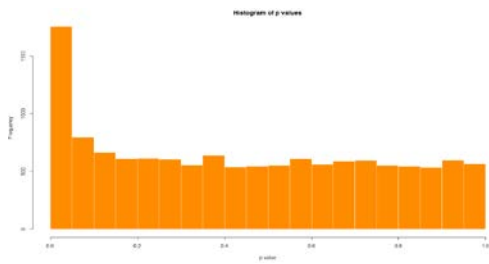
>View(data)
>View(meta)

>all(colnames(data) %in% rownames(meta))
>all(colnames(data) == rownames(meta))

## DESeq2Dataset object produced for initiaion of DESeq2 analysis.
## Manual filtering of genes which do not have more than 5 normalized counts in at least 5
samples.
## DESeq2 assessment undertaken.
>dds <- DESeqDataSetFromMatrix (countData = data, colData = meta, design = ~ Sequencing_Run
+ Population_Type)
>dds <- estimateSizeFactors(dds)
>idx <- rowSums( counts(dds, normalized=TRUE) >= 5 ) >= 5
>dds <- dds[idx,]
>dds <- DESeq(dds)

## Analysis undertaken to assess for differential expression of genes between samples in the DP
and DN groups. Shrinkage estimation undertaken using the ashhr package.
## Histogram of p values produed to give approximation of the impact of false positives on data
set.
>res <- results(dds, contrast = c('Population_Type', 'DP', 'DN'))
>res <- lfcShrink(dds, contrast = c('Population_Type', 'DP', 'DN'), res=res, type = 'ashr')
>hist(res$pvalue, breaks=20, col="darkorange", border="white", xlab = 'p value', main =
'Histogram of p values')
```

Appendix D



```
##Gene symbol added to Ensembl ID labels for ease of analysis.
```

```
##Results inspected for differential gene expression between DP and DN groups
```

```
>ens.str <- substr(rownames(res), 1, 15)
```

```
>res$symbol <- mapIds(org.Hs.eg.db,  
  keys=ens.str,  
  column="SYMBOL",  
  keytype="ENSEMBL",  
  multiVals="first")
```

```
>res
```

```
>View(res)
```

```
>summary(res)
```

log2 fold change (MMSE): Population_Type DP vs DN

Wald test p-value: Population Type DP vs DN

DataFrame with 19322 rows and 6 columns

	baseMean	log2FoldChange	pvalue	padj	symbol
ENSG00000186827	443.67048	1.134524	0.11241690	0.5261350	TNFRSF4
ENSG00000186891	1032.83806	4.482928	0.00165704	0.0461722	TNFRSF18
ENSG00000160072	51.07995	0.100188	NA	NA	ATAD3B
ENSG00000041988	90.94042	0.226525	0.58823126	0.9109791	THAP3
ENSG00000198744	6.54537	0.310347	0.30494047	0.7682752	MTCO3P12
...
ENSG00000210196	384.49110	1.09305	0.106172	0.511925	NA
ENSG00000273748	6.19817	1.04169	0.919367	0.989698	NA
ENSG00000275063	248.37684	1.46100	NA	NA	LOC102723407
ENSG00000277856	313.22470	1.70941	NA	NA	NA
ENSG00000271254	3.31480	1.20129	0.530545	NA	LOC102724250

out of 19322 with nonzero total read count

adjusted p-value < 0.1

LFC > 0 (up) : 113, 0.58%

LFC < 0 (down) : 573, 3%

outliers [1] : 6297, 33%

low counts [2] : 291, 1.5%

(mean count < 4)

```
## Differentially expressed genes identified and viewed
```

```
>SigDEGs_DP_vs_DN <- data.frame(significants(res, fc = 0, padj = 0.05 ,full=TRUE))
```

```
>View (SigDEGs_DP_vs_DN)
```

```
>summary(SigDEGs_DP_vs_DN)
```

log2 fold change (MMSE): Population_Type DP vs DN

Wald test p-value: Population Type DP vs DN

DataFrame with 19322 rows and 6 columns

	baseMean	log2FoldChange	pvalue	padj	symbol
--	----------	----------------	--------	------	--------

ENSG00000186827	443.67048	1.134524	0.11241690	0.5261350	TNFRSF4
ENSG00000186891	1032.83806	4.482928	0.00165704	0.0461722	TNFRSF18
ENSG00000160072	51.07995	0.100188	NA	NA	ATAD3B
ENSG00000041988	90.94042	0.226525	0.58823126	0.9109791	THAP3
ENSG00000198744	6.54537	0.310347	0.30494047	0.7682752	MTCO3P12
...
ENSG00000210196	384.49110	1.09305	0.106172	0.511925	NA
ENSG00000273748	6.19817	1.04169	0.919367	0.989698	NA
ENSG00000275063	248.37684	1.46100	NA	NA	LOC102723407
ENSG00000277856	313.22470	1.70941	NA	NA	NA
ENSG00000271254	3.31480	1.20129	0.530545	NA	LOC102724250

out of 19322 with nonzero total read count

adjusted p-value < 0.1

LFC > 0 (up) : 113, 0.58%

LFC < 0 (down) : 573, 3%

outliers [1] : 6297, 33%

low counts [2] : 291, 1.5%

(mean count < 4)

Variance stabilizing transformation undertaken to stabilize the variance across the mean and presented as a log2 figure.

```
>vsd <- vst(dds, blind=FALSE)
```

```
>head(assay(vsd), 3)
```

	OAC25_B1	OAC25_B2	OAC25_B3	OAC15_B1
ENSG00000186827	6.445049	4.759465	1.325451	7.320498
ENSG00000186891	6.574652	6.144873	6.641733	7.852158
ENSG00000160072	5.447882	1.325451	5.568860	1.325451
	OAC15_B3	OAC06_B1	OAC06_B2	OAC06_B3
ENSG00000186827	3.288006	8.582943	3.893173	8.648183
ENSG00000186891	7.491654	10.701636	10.411038	8.092306
ENSG00000160072	6.897549	1.325451	1.874026	5.948208

##Volcano plot produced to compare gene expression between DP and DN groups.

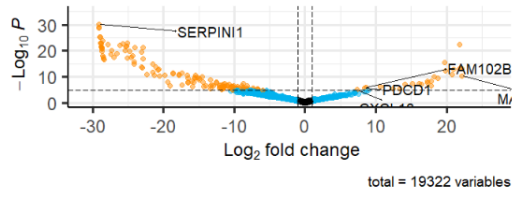
```
>EnhancedVolcano(res,
  lab = as.character(res$symbol),
  x = 'log2FoldChange',
  y = 'pvalue',
  drawConnectors = TRUE,
  title = 'Differentially expressed genes',
  subtitle = 'Double Positive vs Double Negative',
  col = c('black', 'deepskyblue2','black', 'darkorange'),
  legendLabels=c('Not sig.', 'Log fold change > 2', 'p-value < 0.05',
    'p-value < 0.05 and Log2FC > 2'),
  labSize = 5.0)
```

Appendix D

Differentially expressed genes

Double Positive vs Double Negative

- Not sig.
- Log fold change > 2
- p-value < 0.05 and Log2FC >



Appendix E Metadata and read count example

E.1 RNA sequencing metadata

	Patient ID	Population	Patient No	Sequencing Run	Neoadjuvant Therapy
OAC25_B1	OAC25	EExh	1	1	Chemotherapy
OAC25_B2	OAC25	LExh	1	1	Chemotherapy
OAC25_B3	OAC25	DP	1	1	Chemotherapy
OAC15_B1	OAC15	EExh	3	1	Naïve
OAC15_B2	OAC15	LExh	3	1	Naïve
OAC15_B3	OAC15	DP	3	1	Naïve
OAC06_B1	OAC6	EExh	4	2	Naïve
OAC06_B2	OAC6	LExh	4	2	Naïve
OAC06_B3	OAC6	DP	4	2	Naïve
OAC06_B6	OAC6	DN	4	2	Naïve
OAC16_B1	OAC16	EExh	5	2	Naïve
OAC16_B2	OAC16	LExh	5	2	Naïve
OAC16_B3	OAC16	DP	5	2	Naïve
OAC16_B6	OAC16	DN	5	2	Naïve
OAC20_B1	OAC20	EExh	6	2	Naïve
OAC20_B2	OAC20	LExh	6	2	Naïve
OAC20_B3	OAC20	DP	6	2	Naïve
OAC20_B6	OAC20	DN	6	2	Naïve
OAC28_B1	OAC28	EExh	7	3	Chemotherapy
OAC28_B2	OAC28	LExh	7	3	Chemotherapy
OAC28_B3	OAC28	DP	7	3	Chemotherapy
OAC28_B6	OAC28	DN	7	3	Chemotherapy
OAC33_B1	OAC33	EExh	8	3	Naïve
OAC33_B3	OAC33	DP	8	3	Naïve
OAC33_B6	OAC33	DN	8	3	Naïve
OAC37_B3	OAC37	DP	9	3	Naïve
OAC37_B6	OAC37	DN	9	3	Naïve
OAC38_B3	OAC38	DP	10	3	Chemotherapy
OAC38_B6	OAC38	DN	10	3	Chemotherapy

Table 16 Metadata for RNA sequencing analysis

Metadata for RNA sequencing analysis of full data set comprising samples obtained from patients treatment naïve and pre-treated with neoadjuvant chemotherapy. The data displayed here for each sample allows analysis of differential gene expression for each group as well as normalisation for potential confounding variables such as patient ID and sequencing run.

E.2 Example RNA sequencing read counts data for analysis

	OAC25_ B1	OAC25_ B2	OAC25_ B3	OAC15_ B1	OAC15_ B2	OAC15_ B3	OAC06_ B1	OAC06_ B2
ENSG00000138078	200	202	1482	0	21	994	136	20
ENSG00000162924	2293	1865	1626	1003	86	745	0	2580
ENSG00000186487	132	29	4	0	2427	397	0	89
ENSG00000135976	442	382	421	33	327	189	4	230
ENSG00000128656	602	238	1673	1326	4273	887	32	2
ENSG00000152256	313	238	437	96	0	329	0	462
ENSG00000080293	8	42	0	0	0	69	57	0
ENSG00000143870	1762	2586	4724	553	2879	2265	2	2700
ENSG00000115275	100	134	5	0	0	2	0	0
ENSG00000115523	23639	37511	25041	617	3219	1041	1357	32121
ENSG00000244474	0	0	0	0	0	0	0	0
ENSG00000115415	5103	2957	4395	4453	6153	3968	1007	4026
ENSG00000115839	329	673	64	776	0	970	107	950
ENSG00000138449	830	638	966	1149	61	1042	3	19
ENSG00000115687	251	120	0	59	0	398	5	711
ENSG00000144036	122	161	5	53	107	170	10	795
ENSG00000135956	181	228	1074	5	0	139	1	601
ENSG00000115392	371	203	552	54	703	724	36	676
ENSG00000134313	951	545	388	555	2168	113	33	1069
ENSG00000144524	133	186	923	310	5	20	0	1863

Table 17 Example of read counts generated by RNA sequencing.

Example section of read count data generated by Illumina based RNA sequencing, following gene alignment and sample de-multiplexing. Shown here is a randomly selected portion of 20 genes from the first 8 samples. The full dataset is comprised of

information relating to 60,664 labelled gene products for 29 samples. This dataset was used as input for downstream analysis including differential gene expression analysis and gene set enrichment analysis.

Glossary of Terms

- Adenocarcinoma Malignant tumour arising from glandular epithelial structures.
- Apoptosis A highly regulated form of programmed cell death occurring in multicellular organisms.
- Barrett's Oesophagus..... A complication of gastro-oesophageal reflux disease where by the distal oesophagus undergoes metaplasia from its usual stratified squamous epithelium to simple columnar epithelium interspersed with goblet cells.
- Complementary DNA (cDNA) DNA synthesised from single stranded RNA template catalysed by the reverse transcriptase enzyme. Commonly generated to allow transcriptomic analysis from bulk samples or single cells.
- Cluster of differentiation A protocol used for identifying and labelling cell surface molecules for use in immunophenotyping.
- Cytotoxic t lymphocyte A class of thymic derived lymphocytes characterised by positivity for CD8 that possess and ability to kill cells affected by intracellular pathogens or malignant change. In possession of unique T-cell receptors, they recognise target cells by identifying cognate peptides bound to major-histocompatibility complex class I molecules.
- DESeq2 A statistical package for use in the R programming language to allow differential gene expression analysis of RNA sequencing data.
- Differential gene expression analysis Statistical analysis to discover quantitative changes in expression levels between normalised genes counts in different experimental groups.
- Fluorescence-activated cell sorting (FACS) A specialized flow-cytometry technique allowing sorting of cells from a heterogeneous mixture into two or more containers based upon light scattering and fluorescent characteristics.
- Flow cytometry A technique allowing rapid analysis of single particles or cells as they pass single or multiple lasers while suspended in a solution, based upon physical characteristics and fluorescence staining.

Glossary of Terms

Gastro-oesophageal junction The transition between the distal oesophagus and the stomach at the approximate level of the diaphragm where there is an abrupt transition from the oesophageal squamous epithelium to the gastric columnar epithelium.

Gastro-oesophageal reflux disease A common condition where by stomach contents are allowed to pass proximal to the gastro-oesophageal junction, causing irritation to the oesophagus and symptoms of discomfort and potential injury to the oesophagus, pharynx or respiratory tract.

Gene ontology A framework for describing the functions of gene products, supporting the computational representation of biological systems. The outcome of the gene ontology project, a major bioinformatics initiative to develop a comprehensive computational model of biological systems.

Gene set enrichment analysis A statistical method for identification of classes of genes over-represented in large datasets such as those produced by RNA sequencing, allowing identification of an association with specific disease or phenotype.

Immune checkpoint inhibitors A class of immunotherapeutic agents that block the action of inhibitory mechanisms that prevent immune destruction of cancer cells.

Indexed sequencing..... A technique when applied to genomic sequencing experiments of adding unique identifiers, typically short segment of DNA added to sample DNA through specific PCR primers, allowing analysis of material from multiple samples in the same experiment.

Malignant melanoma An often aggressive skin cancer, characterised by malignant change to the pigmented skin cells melanocytes. Historically outcomes were poor once unresectable, but disease trajectories have been greatly altered through use of immune checkpoint blockade.

Neoadjuvant therapy..... relating to administration of therapeutic agents before a treatment. For example use of chemotherapy prior to surgery in order to improve survival and reduce the scale of the operation required.

Neoantigen A novel protein, produced by cancer cells as a result of mutations that occur in cancer DNA. Neoantigens can play a crucial role in detection of malignant cells by the immune system.

- OesophagectomySurgical removal of the oesophagus either in part or in its entirety, typically for treatment of early stage cancer. A commonly used technique is the Ivor Lewis oesophagectomy combining a transabdominal and transthoracic approach.
- Principle component analysis A dimensionality-reduction method allowing reduction of large data sets by reducing the large number of variables into a smaller number and allowing plotting in two dimensional space.
- QIAGEN ingenuity pathway analysis A web based application, developed by the biotechnology company QIAGEN, that readily allows bioinformatics analysis of results from high-throughput experiments such as next-generation sequencing or microarray techniques. Utilises the extensive QIAGEN database of curated content to provide information regarding enrichment of certain cellular phenotypes, effects of upstream regulators and impact on downstream processes.
- ReactomeAn open source, open access, manually curated and peer reviewed database of biological pathways. While information related to many organisms has been created, this predominantly relates to human biology. Gene signatures related to a wide range of cellular processes are described including cell cycling processes, metabolic pathways, cell signalling and immune system functions.
- Read countWhen related to RNA sequencing experiments defines a summary of the expression level of a gene of interest, though does not necessarily distinguish between isoforms. It can relate to the number of reads that align to a specific reference gene sequence.
- Reverse transcriptionA reverse of normal transcription, catalysed by the reverse transcriptase enzyme, and undertaken by some RNA viruses as well as in many laboratory practices including RNA sequencing experiments, to produce complimentary DNA from RNA.
- SmartSeq2A single cell RNA sequencing technique allowing generation of full length cDNA and sequencing libraries using standard reagents. The protocol can be completed in a relatively short time period, and can be adapted to use RNA extracted from bulk samples of cells.

Glossary of Terms

- Squamous cell carcinoma A collective term for a range of cancers arising from the squamous cells that form the surface of the skin as well as the lining of hollow organs including the digestive and respiratory tracts.
- Tagmentation A stage in many DNA analysis protocols where by unfragmented DNA is simultaneously cleaved and tagged with an index, utilising an engineered transposome. A key process in the commercial RNA sequencing library preparation systems developed by the biotechnology company Illumina, particularly in their Nextera XT products.
- Regulatory T cells (T_{reg}) A specialised sub population of T lymphocytes characterised by positivity for CD4 and the transcription factor FOXP3, that play a role in suppressing an immune response, ensuring tolerance to self-antigens and avoiding autoimmune disease.
- Tissue resident memory cells (T_{RM}) A subset of T lymphocytes identified as resident in peripheral mucosal or epithelial tissues, which do not recirculate via secondary lymphoid organs. Transcriptionally and functionally distinct from other memory T lymphocyte populations they are increasingly considered important mediators of anticancer immune responses, particularly in the context of immune checkpoint blockade.
- Wald test..... A statistical test for identifying if explanatory variables in a data set are significant, utilises the weighted distance between the unrestricted estimates and a hypothesised value based upon the null hypothesis. This statistical function forms the basis of the assessment of significance in the DESeq2 differential gene expression analysis pipeline.

List of References

1. Hill SL, Johnson PWM. Immunotherapy: Past, present and future. In: Board RE, Nathan P, Newsom-Davis T, Papa S, Johnson PWM, editors. *Problem Solving in Cancer Immunotherapy*. 1st ed. 2019. p. 1–7.
2. Coley WB. The treatment of malignant tumors by repeated inoculations of erysipelas: With a report of ten original cases. Vol. 105, *American Journal of Medical Sciences*. 1893. p. 487–511.
3. Nathanson L. Spontaneous regression of malignant melanoma: a review of the literature on incidence, clinical features, and possible mechanisms. *Natl Cancer Inst Monogr*. 1976 Nov;No. 44:67–76.
4. Morales A, Eidinger D, Bruce AW. Intracavitary Bacillus Calmette Guerin in the treatment of superficial bladder tumors. *J Urol*. 1976 Aug;116(2):180–2.
5. Kirkwood JM, Butterfield LH, Tarhini AA, Zarour H. Immunotherapy of Cancer in 2012. *CA Cancer J Clin*. 2012;62(5):309–35.
6. Garbe C, Eigentler TK, Keilholz U, Hauschild A, Kirkwood JM. Systematic Review of Medical Treatment in Melanoma: Current Status and Future Prospects. *Oncologist*. 2011 Jan;16(1):5–24.
7. Rosenberg SA, Yang JC, Topalian SL, Schwartzentruber DJ, Weber JS, Parkinson DR, et al. Treatment of 283 Consecutive Patients With Metastatic Melanoma or Renal Cell Cancer Using High-Dose Bolus Interleukin 2. *JAMA J Am Med Assoc*. 1994;271(12):907–13.
8. Köhler G, Milstein C. Continuous cultures of fused cells secreting antibody of predefined specificity. *Nature*. 1975 Aug;256(5517):495–7.
9. Hale G, Dyer MJ, Clark MR, Phillips JM, Marcus R, Riechmann L, et al. Remission induction in non-Hodgkin lymphoma with reshaped human monoclonal antibody CAMPATH-1H. *Lancet*. 1988 Dec;2(8625):1394–9.
10. Lim SH, Beers SA, French RR, Johnson PWM, Glennie MJ, Cragg MS. Anti-CD20 monoclonal antibodies: Historical and future perspectives. Vol. 95, *Haematologica*. 2010. p. 135–43.
11. World Health Organization. *WHO Model List of Essential Medicines*. 20th Ed.

List of References

- 2017;(March):58.
12. Hodi FS, Chiarion-Sileni V, Gonzalez R, Grob JJ, Rutkowski P, Cowey CL, et al. Nivolumab plus ipilimumab or nivolumab alone versus ipilimumab alone in advanced melanoma (CheckMate 067): 4-year outcomes of a multicentre, randomised, phase 3 trial. *Lancet Oncol.* 2018;19(11):1480–92.
 13. Wolchok JD, Chiarion-Sileni V, Gonzalez R, Grob J-J, Rutkowski P, Lao CD, et al. Long-Term Outcomes With Nivolumab Plus Ipilimumab or Nivolumab Alone Versus Ipilimumab in Patients With Advanced Melanoma. *J Clin Oncol.* 2021 Nov 24;
 14. Masopust D, Vezys V, Wherry EJ, Ahmed R. A brief history of CD8 T cells. *Eur J Immunol.* 2007;37(SUPPL. 1):103–10.
 15. Zhang N, Bevan MJ. CD8+ T Cells: Foot Soldiers of the Immune System. Vol. 35, *Immunity.* Elsevier Inc.; 2011. p. 161–8.
 16. Lieberman J. Cytotoxic Lymphocytes. In: *Encyclopedia of Immunobiology.* Elsevier; 2016. p. 363–73.
 17. Shah DK, Zúñiga-Pflücker JC. An Overview of the Intrathymic Intricacies of T Cell Development. *J Immunol.* 2014;192(9):4017–23.
 18. Krangel MS. Mechanics of T cell receptor gene rearrangement. Vol. 21, *Current Opinion in Immunology.* 2009. p. 133–9.
 19. Moran AE, Hogquist KA. T-cell receptor affinity in thymic development. Vol. 135, *Immunology.* 2012. p. 261–7.
 20. Halle S, Halle O, Förster R. Mechanisms and Dynamics of T Cell-Mediated Cytotoxicity In Vivo. Vol. 38, *Trends in Immunology.* Elsevier Ltd; 2017. p. 432–43.
 21. Martínez-Lostao L, Anel A, Pardo J. How Do Cytotoxic Lymphocytes Kill Cancer Cells? *Clin Cancer Res.* 2015;21(22):5047–56.
 22. Chen DS, Mellman I. Oncology meets immunology: The cancer-immunity cycle. Vol. 39, *Immunity.* 2013. p. 1–10.
 23. Motz GT, Coukos G. Deciphering and Reversing Tumor Immune Suppression. Vol. 39, *Immunity.* Elsevier Inc.; 2013. p. 61–73.
 24. Di Virgilio F, Sarti AC, Falzoni S, De Marchi E, Adinolfi E. Extracellular ATP and P2 purinergic

- signalling in the tumour microenvironment [Internet]. Vol. 18, *Nature Reviews Cancer*. 2018 [cited 2022 Jan 5]. p. 601–18. Available from: <https://doi.org/10.1038/>
25. Joyce AJ, Fearon DT. T cell exclusion, immune privilege and tumour microenvironment. *Science* (80-). 2015;348(6230):74–80.
 26. Naito Y, Saito K, Shiiba K, Ohuchi A, Saigenji K, Nagura H, et al. CD8+ T cells infiltrated within cancer cell nests as a prognostic factor in human colorectal cancer. *Cancer Res*. 1998;58(16):3491–4.
 27. Noble F, Mellows T, McCormick Matthews LH, Bateman AC, Harris S, Underwood TJ, et al. Tumour infiltrating lymphocytes correlate with improved survival in patients with oesophageal adenocarcinoma. *Cancer Immunol Immunother*. 2016;65(6):651–62.
 28. Schreiber RD, Old LJ, Smyth MJ. Cancer immunoediting: Integrating immunity's roles in cancer suppression and promotion [Internet]. Vol. 331, *Science*. 2011 [cited 2022 Oct 18]. p. 1565–70. Available from: <https://www.science.org>
 29. Thommen DS, Schumacher TN. T Cell Dysfunction in Cancer [Internet]. Vol. 33, *Cancer Cell*. *Cancer Cell*; 2018 [cited 2022 Jan 6]. p. 547–62. Available from: <https://pubmed.ncbi.nlm.nih.gov/29634943/>
 30. Wherry EJ. T cell exhaustion. Vol. 12, *Nature Immunology*. Nature Publishing Group; 2011. p. 492–9.
 31. Moskophidis D, Lechner F, Pircher H, Zinkernagel RM. Virus persistence in acutely infected immunocompetent mice by exhaustion of antiviral cytotoxic effector T cells. *Nature* [Internet]. 1993 [cited 2022 Jan 5];362(6422):758–61. Available from: <https://pubmed.ncbi.nlm.nih.gov/8469287/>
 32. Zajac AJ, Blattman JN, Murali-Krishna K, Sourdive DJD, Suresh M, Altman JD, et al. Viral immune evasion due to persistence of activated T cells without effector function. *J Exp Med*. 1998;188(12):2205–13.
 33. Klein MR, Van Der Burg SH, Pontesilli O, Miedema F. Cytotoxic T lymphocytes in HIV-1 infection: A killing paradox? Vol. 19, *Immunology Today*. Elsevier Current Trends; 1998. p. 317–24.
 34. Blank CU, Haining WN, Held W, Hogan PG, Kallies A, Lugli E, et al. Defining 'T cell exhaustion.' *Nat Rev Immunol* [Internet]. 2019 Nov 1 [cited 2021 Feb 1];19(11):665–74. Available from: <https://pubmed.ncbi.nlm.nih.gov/31570879/>

List of References

35. Gallimore A, Glithero A, Godkin A, Tissot AC, Plückthun A, Elliott T, et al. Induction and exhaustion of lymphocytic choriomeningitis virus-specific cytotoxic T lymphocytes visualized using soluble tetrameric major histocompatibility complex class I-peptide complexes. *J Exp Med*. 1998;187(9):1383–93.
36. Matloubian BM, Somasundaram T, Kolhekar SR, Selvakumar R, Ahmed R. Genetic Basis of Viral Persistence : Single Amino Acid. *J Exp Med*. 1990;172(October):2944–51.
37. Wherry EJ, Blattman JN, Murali-Krishna K, van der Most R, Ahmed R. Viral Persistence Alters CD8 T-Cell Immunodominance and Tissue Distribution and Results in Distinct Stages of Functional Impairment. *J Virol*. 2003;77(8):4911–27.
38. Barber DL, Wherry EJ, Masopust D, Zhu B, Allison JP, Sharpe AH, et al. Restoring function in exhausted CD8 T cells during chronic viral infection. *Nature*. 2006;439(7077):682–7.
39. Pauken KE, Wherry EJ. Overcoming T cell exhaustion in infection and cancer. Vol. 36, *Trends in Immunology*. Elsevier Ltd; 2015. p. 265–76.
40. Tajan M, de Rocca Serra A, Valet P, Edouard T, Yart A. SHP2 sails from physiology to pathology. Vol. 58, *European Journal of Medical Genetics*. 2015. p. 509–25.
41. Wherry EJ, Ha SJ, Kaech SM, Haining WN, Sarkar S, Kalia V, et al. Molecular Signature of CD8+ T Cell Exhaustion during Chronic Viral Infection. *Immunity*. 2007;27(4):670–84.
42. Blackburn SD, Shin H, Haining WN, Zou T, Workman CJ, Polley A, et al. Coregulation of CD8+ T cell exhaustion by multiple inhibitory receptors during chronic viral infection. *Nat Immunol*. 2009;10(1):29–37.
43. Doering TA, Crawford A, Angelosanto JM, Paley MA, Ziegler CG, Wherry EJ. Network Analysis Reveals Centrally Connected Genes and Pathways Involved in CD8+ T Cell Exhaustion versus Memory. *Immunity*. 2012;37(6):1130–44.
44. Bengsch B, Ohtani T, Khan O, Setty M, Manne S, O'Brien S, et al. Epigenomic-Guided Mass Cytometry Profiling Reveals Disease-Specific Features of Exhausted CD8 T Cells. *Immunity*. 2018;48(5):1029-1045.e5.
45. Betts MR, Nason MC, West SM, De Rosa SC, Migueles SA, Abraham J, et al. HIV nonprogressors preferentially maintain highly functional HIV-specific CD8+ T cells. *Blood*. 2006;107(12):4781–9.
46. Day CL, Kaufmann DE, Kiepiela P, Brown JA, Moodley ES, Reddy S, et al. PD-1 expression on

- HIV-specific T cells is associated with T-cell exhaustion and disease progression. *Nature* [Internet]. 2006 Sep 21 [cited 2022 Jan 6];443(7109):350–4. Available from: <https://pubmed.ncbi.nlm.nih.gov/16921384/>
47. Hoffmann M, Pantazis N, Martin GE, Hickling S, Hurst J, Meyerowitz J, et al. Exhaustion of Activated CD8 T Cells Predicts Disease Progression in Primary HIV-1 Infection. *PLoS Pathog.* 2016;12(7):1–19.
 48. Osuch S, Metzner KJ, Cortés KC. Reversal of t cell exhaustion in chronic HCV infection [Internet]. Vol. 12, *Viruses*. Multidisciplinary Digital Publishing Institute; 2020 [cited 2022 Jan 7]. p. 799. Available from: <https://www.mdpi.com/1999-4915/12/8/799/htm>
 49. Penna A, Pilli M, Zerbini A, Orlandini A, Mezzadri S, Sacchelli L, et al. Dysfunction and functional restoration of HCV-specific CD8 responses in chronic hepatitis C virus infection. *Hepatology* [Internet]. 2007 Mar 1 [cited 2022 Jan 7];45(3):588–601. Available from: <https://onlinelibrary.wiley.com/doi/full/10.1002/hep.21541>
 50. Alfei F, Kanev K, Hofmann M, Wu M, Ghoneim HE, Roelli P, et al. TOX reinforces the phenotype and longevity of exhausted T cells in chronic viral infection. *Nature*. 2019;571(7764):265–9.
 51. Barili V, Vecchi A, Rossi M, Montali I, Tiezzi C, Penna A, et al. Unraveling the multifaceted nature of cd8 t cell exhaustion provides the molecular basis for therapeutic t cell reconstitution in chronic hepatitis b and c [Internet]. Vol. 10, *Cells*. Multidisciplinary Digital Publishing Institute; 2021 [cited 2022 Jan 7]. p. 2563. Available from: <https://www.mdpi.com/2073-4409/10/10/2563/htm>
 52. Jayaraman P, Jacques MK, Zhu C, Steblenko KM, Stowell BL, Madi A, et al. TIM3 Mediates T Cell Exhaustion during Mycobacterium tuberculosis Infection. *PLoS Pathog.* 2016;12(3):1–21.
 53. Rha MS, Shin EC. Activation or exhaustion of CD8+ T cells in patients with COVID-19 [Internet]. Vol. 18, *Cellular and Molecular Immunology*. 2021 [cited 2022 Jan 7]. p. 2325–33. Available from: <https://doi.org/10.1038/s41423-021-00750-4>
 54. Iwai Y, Terawaki S, Honjo T. PD-1 blockade inhibits hematogenous spread of poorly immunogenic tumor cells by enhanced recruitment of effector T cells. *Int Immunol.* 2005;17(2):133–44.
 55. Ahmadzadeh M, Johnson LA, Heemskerk B, Wunderlich JR, Dudley ME, White DE, et al.

List of References

- Tumor antigen-specific CD8 T cells infiltrating the tumor express high levels of PD-1 and are functionally impaired. *Blood* [Internet]. 2009 Aug 20 [cited 2022 Jan 7];114(8):1537–44. Available from: <http://ashpublications.org/blood/article-pdf/114/8/1537/1323807/zh803409001537.pdf>
56. Baitsch L, Baumgaertner P, Devèvre E, Raghav SK, Legat A, Barba L, et al. Exhaustion of tumor-specific CD8+ T cells in metastases from melanoma patients. *J Clin Invest* [Internet]. 2011 Jun 1 [cited 2022 Jan 9];121(6):2350–60. Available from: <http://www.jci.org>
57. Thommen DS, Schreiner J, Müller P, Herzig P, Roller A, Belousov A, et al. Progression of lung cancer is associated with increased dysfunction of T cells defined by coexpression of multiple inhibitory receptors. *Cancer Immunol Res*. 2015;3(12):1344–54.
58. Lu X, Yang L, Yao D, Wu X, Li J, Liu X, et al. Tumor antigen-specific CD8+ T cells are negatively regulated by PD-1 and Tim-3 in human gastric cancer. *Cell Immunol*. 2017 Mar 1;313:43–51.
59. Baitsch L, Legat A, Barba L, Marraco SA, Rivals JP, Baumgaertner P, et al. Extended co-expression of inhibitory receptors by human CD8 T-cells depending on differentiation, antigen-specificity and anatomical localization. *PLoS One*. 2012;7(2):1–10.
60. Topalian SL, Hodi FS, Brahmer JR, Gettinger SN, Smith DC, McDermott DF, et al. Safety, Activity, and Immune Correlates of Anti-PD-1 Antibody in Cancer. *N Engl J Med* [Internet]. 2012 Jun 28 [cited 2022 Jan 10];366(26):2443–54. Available from: <https://www.nejm.org/doi/full/10.1056/nejmoa1200690>
61. Postow MA, Callahan MK, Wolchok JD. Immune checkpoint blockade in cancer therapy. Vol. 33, *Journal of Clinical Oncology*. American Society of Clinical Oncology; 2015. p. 1974–82.
62. Krummel MF, Allison JP. CTLA-4 engagement inhibits IL-2 accumulation and cell cycle progression upon activation of resting T cells. *J Exp Med* [Internet]. 1996 [cited 2022 Jan 10];183(6):2533–40. Available from: <http://rupress.org/jem/article-pdf/183/6/2533/1108172/2533.pdf>
63. Leach DR, Krummel MF, Allison JP. Enhancement of antitumor immunity by CTLA-4 blockade. *Science (80-)* [Internet]. 1996 Mar 22 [cited 2022 Jan 10];271(5256):1734–6. Available from: <https://pubmed.ncbi.nlm.nih.gov/8596936/>
64. Ribas A, Camacho LH, Lopez-Berestein G, Pavlov D, Bulanagui CA, Millham R, et al.

- Antitumor activity in melanoma and anti-self responses in a phase I trial with the anti-cytotoxic T lymphocyte-associated antigen 4 monoclonal antibody CP-675,206. *J Clin Oncol*. 2005 Sep 21;23(35):8968–77.
65. Phan GQ, Yang JC, Sherry RM, Hwu P, Topalian SL, Schwartzentruber DJ, et al. Cancer regression and autoimmunity induced by cytotoxic T lymphocyte-associated antigen 4 blockade in patients with metastatic melanoma. *Proc Natl Acad Sci U S A* [Internet]. 2003 Jul 8 [cited 2022 Jan 10];100(14):8372–7. Available from: <https://pubmed.ncbi.nlm.nih.gov/12826605/>
66. Hodi FS, O’Day SJ, McDermott DF, Weber RW, Sosman JA, Haanen JB, et al. Improved Survival with Ipilimumab in Patients with Metastatic Melanoma. *N Engl J Med*. 2010;363(8):711–23.
67. Weber JS, D’Angelo SP, Minor D, Hodi FS, Gutzmer R, Neyns B, et al. Nivolumab versus chemotherapy in patients with advanced melanoma who progressed after anti-CTLA-4 treatment (CheckMate 037): A randomised, controlled, open-label, phase 3 trial. *Lancet Oncol*. 2015 Apr 1;16(4):375–84.
68. Blackburn SD, Shin H, Freeman GJ, Wherry EJ. Selective expansion of a subset of exhausted CD8 T cells by α PD-L1 blockade. *Proc Natl Acad Sci U S A* [Internet]. 2008 Sep 30 [cited 2022 Jan 10];105(39):15016–21. Available from: <https://www.pnas.org/content/105/39/15016>
69. Sade-Feldman M, Yizhak K, Bjorgaard SL, Ray JP, de Boer CG, Jenkins RW, et al. Defining T Cell States Associated with Response to Checkpoint Immunotherapy in Melanoma. *Cell*. 2018 Nov 1;175(4):998-1013.e20.
70. Miller BC, Sen DR, Al Abosy R, Bi K, Virkud Y V., LaFleur MW, et al. Subsets of exhausted CD8+ T cells differentially mediate tumor control and respond to checkpoint blockade. *Nat Immunol* [Internet]. 2019 Mar 1 [cited 2021 Feb 9];20(3):326–36. Available from: <https://pubmed.ncbi.nlm.nih.gov/30778252/>
71. Chen Z, Ji Z, Ngiow SF, Manne S, Cai Z, Huang AC, et al. TCF-1-Centered Transcriptional Network Drives an Effector versus Exhausted CD8 T Cell-Fate Decision. *Immunity*. 2019;51(5):840-855.e5.
72. Beltra JC, Manne S, Abdel-Hakeem MS, Kurachi M, Giles JR, Chen Z, et al. Developmental Relationships of Four Exhausted CD8+ T Cell Subsets Reveals Underlying Transcriptional and Epigenetic Landscape Control Mechanisms. *Immunity* [Internet]. 2020 May 19 [cited

List of References

- 2022 Jan 10];52(5):825-841.e8. Available from:
<https://pubmed.ncbi.nlm.nih.gov/32396847/>
73. Angelosanto JM, Blackburn SD, Crawford A, Wherry EJ. Progressive Loss of Memory T Cell Potential and Commitment to Exhaustion during Chronic Viral Infection. *J Virol*. 2012 Aug 1;86(15):8161–70.
74. Virgin HW, Wherry EJ, Ahmed R. Redefining Chronic Viral Infection. Vol. 138, *Cell*. 2009. p. 30–50.
75. Wherry EJ, Ahmed R. Memory CD8 T-Cell Differentiation during Viral Infection. *J Virol*. 2004;78(11):5535–45.
76. Blank CU, Haining WN, Held W, Hogan PG, Kallies A, Lugli E, et al. Defining ‘T cell exhaustion.’ *Nat Rev Immunol* [Internet]. 2019 Sep 30 [cited 2022 Jan 6];19(11):665–74. Available from: <https://www.nature.com/articles/s41577-019-0221-9>
77. Kurtulus S, Madi A, Escobar G, Klapholz M, Nyman J, Christian E, et al. Checkpoint Blockade Immunotherapy Induces Dynamic Changes in PD-1 – CD8 + Tumor-Infiltrating T Cells. *Immunity* [Internet]. 2019 Jan 15 [cited 2021 Feb 1];50(1):181-194.e6. Available from: <https://pubmed.ncbi.nlm.nih.gov/30635236/>
78. Im SJ, Hashimoto M, Gerner MY, Lee J, Kissick HT, Burger MC, et al. Defining CD8+ T cells that provide the proliferative burst after PD-1 therapy. *Nature* [Internet]. 2016 [cited 2022 Jan 17];537(7620):417–21. Available from: <https://pubmed.ncbi.nlm.nih.gov/27501248/>
79. Dolina JS, Van Braeckel-Budimir N, Thomas GD, Salek-Ardakani S. CD8+ T Cell Exhaustion in Cancer [Internet]. Vol. 12, *Frontiers in Immunology*. *Front Immunol*; 2021 [cited 2022 Jan 10]. Available from: <https://pubmed.ncbi.nlm.nih.gov/34354714/>
80. Utzschneider DT, Gabriel SS, Chisanga D, Gloury R, Gubser PM, Vasanthakumar A, et al. Early precursor T cells establish and propagate T cell exhaustion in chronic infection. *Nat Immunol* [Internet]. 2020 Oct 1 [cited 2021 Feb 1];21(10):1256–66. Available from: <https://doi.org/10.1038/s41590-020-0760-z>
81. Schietinger A, Philip M, Krisnawan VE, Chiu EY, Delrow JJ, Basom RS, et al. Tumor-Specific T Cell Dysfunction Is a Dynamic Antigen-Driven Differentiation Program Initiated Early during Tumorigenesis. *Immunity*. 2016 Aug 16;45(2):389–401.
82. Buggert M, Tauriainen J, Yamamoto T, Frederiksen J, Ivarsson MA, Michaëlsson J, et al. T-bet and Eomes Are Differentially Linked to the Exhausted Phenotype of CD8+ T Cells in HIV

- Infection. *PLoS Pathog.* 2014;10(7).
83. Li J, He Y, Hao J, Ni L, Dong C. High Levels of Eomes Promote Exhaustion of Anti-tumor CD8+ T Cells. *Front Immunol* [Internet]. 2018 [cited 2021 Feb 2];9:2981. Available from: <https://pubmed.ncbi.nlm.nih.gov/30619337/>
 84. Viganò S, Utzschneider DT, Perreau M, Pantaleo G, Zehn D, Harari A. Functional avidity: A measure to predict the efficacy of effector T cells? Vol. 2012, *Clinical and Developmental Immunology*. 2012.
 85. Zhang J, Lyu T, Cao Y, Feng H. Role of TCF-1 in differentiation, exhaustion, and memory of CD8+ T cells: A review [Internet]. Vol. 35, *FASEB Journal*. *FASEB J*; 2021 [cited 2022 May 7]. Available from: <https://pubmed.ncbi.nlm.nih.gov/33913198/>
 86. Utzschneider DT, Charmoy M, Chennupati V, Pousse L, Ferreira DP, Calderon-Copete S, et al. T Cell Factor 1-Expressing Memory-like CD8+ T Cells Sustain the Immune Response to Chronic Viral Infections. *Immunity* [Internet]. 2016 [cited 2022 May 7];45(2):415–27. Available from: <http://dx.doi.org/10.1016/j.immuni.2016.07.021>
 87. Kao C, Oestreich KJ, Paley MA, Crawford A, Angelosanto JM, Ali MAA, et al. Transcription factor T-bet represses expression of the inhibitory receptor PD-1 and sustains virus-specific CD8+ T cell responses during chronic infection. *Nat Immunol.* 2011;12(7):663–71.
 88. Paley MA, Kroy DC, Odorizzi PM, Johnnidis JB, Dolfi D V., Barnett BE, et al. Progenitor and terminal subsets of CD8+ T cells cooperate to contain chronic viral infection. *Science* (80-) [Internet]. 2012 Nov 30 [cited 2022 Jan 10];338(6111):1220–5. Available from: <https://www.science.org/doi/abs/10.1126/science.1229620>
 89. Scott AC, Dünder F, Zumbo P, Chandran SS, Klebanoff CA, Shakiba M, et al. TOX is a critical regulator of tumour-specific T cell differentiation. *Nature* [Internet]. 2019 Jul 11 [cited 2021 Feb 1];571(7764):270–4. Available from: <https://pubmed.ncbi.nlm.nih.gov/31207604/>
 90. Yao C, Sun HW, Lacey NE, Ji Y, Moseman EA, Shih HY, et al. Single-cell RNA-seq reveals TOX as a key regulator of CD8+ T cell persistence in chronic infection. *Nat Immunol* [Internet]. 2019 Jul 1 [cited 2021 Feb 1];20(7):890–901. Available from: <https://pubmed.ncbi.nlm.nih.gov/31209400/>
 91. Ishida Y, Agata Y, Shibahara K, Honjo T. Induced expression of PD-1, a novel member of the immunoglobulin gene superfamily, upon programmed cell death. *EMBO J* [Internet]. 1992

List of References

- Nov 1 [cited 2022 Jan 11];11(11):3887–95. Available from:
<https://onlinelibrary.wiley.com/doi/full/10.1002/j.1460-2075.1992.tb05481.x>
92. Nishimura H, Nose M, Hiai H, Minato N, Honjo T. Development of lupus-like autoimmune diseases by disruption of the PD-1 gene encoding an ITIM motif-carrying immunoreceptor. *Immunity*. 1999 Aug 1;11(2):141–51.
93. Keir ME, Butte MJ, Freeman GJ, Sharpe AH. PD-1 and its ligands in tolerance and immunity [Internet]. Vol. 26, *Annual Review of Immunology*. Annual Reviews; 2008 [cited 2022 Jan 11]. p. 677–704. Available from:
<https://www.annualreviews.org/doi/abs/10.1146/annurev.immunol.26.021607.090331>
94. Thommen DS, Koelzer VH, Herzig P, Roller A, Trefny M, Dimeloe S, et al. A transcriptionally and functionally distinct pd-1 + cd8 + t cell pool with predictive potential in non-small-cell lung cancer treated with pd-1 blockade. *Nat Med* [Internet]. 2018 Jun 11 [cited 2021 Jan 28];24(7). Available from: <https://pubmed.ncbi.nlm.nih.gov/29892065/>
95. Pisibon C, Ouertani A, Bertolotto C, Ballotti R, Cheli Y. Immune checkpoints in cancers: From signaling to the clinic [Internet]. Vol. 13, *Cancers*. Multidisciplinary Digital Publishing Institute; 2021 [cited 2022 Jan 11]. p. 4573. Available from: <https://www.mdpi.com/2072-6694/13/18/4573/htm>
96. Yamazaki T, Akiba H, Iwai H, Matsuda H, Aoki M, Tanno Y, et al. Expression of Programmed Death 1 Ligands by Murine T Cells and APC. *J Immunol* [Internet]. 2002 Nov 15 [cited 2022 Jan 11];169(10):5538–45. Available from:
<https://www.jimmunol.org/content/169/10/5538>
97. Sun JM, Shen L, Shah MA, Enzinger P, Adenis A, Doi T, et al. Pembrolizumab plus chemotherapy versus chemotherapy alone for first-line treatment of advanced oesophageal cancer (KEYNOTE-590): a randomised, placebo-controlled, phase 3 study. *Lancet* [Internet]. 2021 Aug 28 [cited 2022 Jan 11];398(10302):759–71. Available from:
<http://www.thelancet.com/article/S0140673621012344/fulltext>
98. Young S, Griego-Fullbright C, Wagner A, Chargin A, Patterson BK, Chabot-Richards D. Concordance of PD-L1 Expression Detection in Non-Small Cell Lung Cancer (NSCLC) Tissue Biopsy Specimens between OncoTect iO Lung Assay and Immunohistochemistry (IHC). *Am J Clin Pathol* [Internet]. 2018 Aug 30 [cited 2022 May 7];150(4):346–52. Available from:
<https://academic.oup.com/ajcp/article/150/4/346/5058159>
99. Waterhouse P, Penninger JM, Timms E, Wakeham A, Shahinian A, Lee KP, et al.

- Lymphoproliferative disorders with early lethality in mice deficient in Ctlα-4. *Science* (80-) [Internet]. 1995 [cited 2022 Jan 11];270(5238):985–8. Available from: <https://pubmed.ncbi.nlm.nih.gov/7481803/>
100. Tivol EA, Borriello F, Schweitzer AN, Lynch WP, Bluestone JA, Sharpe AH. Loss of CTLA-4 leads to massive lymphoproliferation and fatal multiorgan tissue destruction, revealing a critical negative regulatory role of CTLA-4. *Immunity* [Internet]. 1995 [cited 2022 Jan 11];3(5):541–7. Available from: <https://pubmed.ncbi.nlm.nih.gov/7584144/>
 101. Rowshanravan B, Halliday N, Sansom DM. CTLA-4: A moving target in immunotherapy [Internet]. Vol. 131, *Blood*. American Society of Hematology; 2018 [cited 2022 Jan 17]. p. 58–67. Available from: <http://ashpublications.org/blood/article-pdf/131/1/58/1367947/blood741033.pdf>
 102. Quezada SA, Peggs KS. Lost in translation: Deciphering the mechanism of action of anti-human CTLA-4 [Internet]. Vol. 25, *Clinical Cancer Research*. American Association for Cancer Research; 2019 [cited 2022 Jan 17]. p. 1130–2. Available from: <https://clincancerres.aacrjournals.org/content/25/4/1130>
 103. Monney L, Sabatos CA, Gaglia JL, Ryu A, Waldner H, Chernova T, et al. Th1-specific cell surface protein Tim-3 regulates macrophage activation and severity of an autoimmune disease. *Nature* [Internet]. 2002 Jan 31 [cited 2022 Jan 17];415(6871):536–41. Available from: <https://www.nature.com/articles/415536a>
 104. Wolf Y, Anderson AC, Kuchroo VK. TIM3 comes of age as an inhibitory receptor [Internet]. Vol. 20, *Nature Reviews Immunology*. *Nat Rev Immunol*; 2020 [cited 2022 Jan 17]. p. 173–85. Available from: <https://pubmed.ncbi.nlm.nih.gov/31676858/>
 105. Chihara N, Madi A, Kondo T, Zhang H, Acharya N, Singer M, et al. Induction and transcriptional regulation of the co-inhibitory gene module in T cells. *Nature* [Internet]. 2018 Jun 13 [cited 2022 Jan 17];558(7710):454–9. Available from: <https://www.nature.com/articles/s41586-018-0206-z>
 106. Anderson AC, Lord GM, Dardalhon V, Lee DH, Sabatos-Peyton CA, Glimcher LH, et al. T-bet, a Th1 transcription factor regulates the expression of Tim-3. *Eur J Immunol* [Internet]. 2010 Mar 1 [cited 2022 Jan 17];40(3):859–66. Available from: <https://onlinelibrary.wiley.com/doi/full/10.1002/eji.200939842>
 107. Triebel F, Jitsukawa S, Baixeras E, Roman-Roman S, Genevee C, Viegas-Pequignot E, et al. LAG-3, a novel lymphocyte activation gene closely related to CD4. *J Exp Med* [Internet].

List of References

- 1990 May 1 [cited 2022 Jan 17];171(5):1393–405. Available from:
<http://rupress.org/jem/article-pdf/171/5/1393/1100342/1393.pdf>
108. Maruhashi T, Sugiura D, Okazaki IM, Okazaki T. LAG-3: from molecular functions to clinical applications [Internet]. Vol. 8, Journal for immunotherapy of cancer. BMJ Specialist Journals; 2020 [cited 2022 Jan 17]. p. e001014. Available from:
<https://jitc.bmj.com/content/8/2/e001014>
109. Baixeras E, Huard B, Miossec C, Jitsukawa S, Martin M, Hercend T, et al. Characterization of the Lymphocyte Activation Gene 3-Encoded Protein. A New Ligand for Human Leukocyte Antigen Class II Antigen Presenting Cell Antigen Presenting Cell. J Exp Med [Internet]. 1992 Aug 1 [cited 2022 Jan 17];176(2):327–37. Available from: <http://rupress.org/jem/article-pdf/176/2/327/1102754/327.pdf>
110. Wang J, Sanmamed MF, Datar I, Su TT, Ji L, Sun J, et al. Fibrinogen-like Protein 1 Is a Major Immune Inhibitory Ligand of LAG-3. Cell. 2019 Jan 10;176(1–2):334–347.e12.
111. Khan O, Giles JR, McDonald S, Manne S, Ngiow SF, Patel KP, et al. TOX transcriptionally and epigenetically programs CD8+ T cell exhaustion. Nature. 2019;571(7764):211–8.
112. Okazaki T, Okazaki IM, Wang J, Sugiura D, Nakaki F, Yoshida T, et al. PD-1 and LAG-3 inhibitory co-receptors act synergistically to prevent autoimmunity in mice. J Exp Med [Internet]. 2011 Feb 14 [cited 2022 Jan 17];208(2):395–407. Available from:
www.jem.org/cgi/doi/10.1084/jem.20100466
113. Sen DR, Kaminski J, Barnitz RA, Kurachi M, Gerdemann U, Yates KB, et al. The epigenetic landscape of T cell exhaustion. Science (80-) [Internet]. 2016 Dec 2 [cited 2022 Jan 19];354(6316):1165–9. Available from:
<https://www.science.org/doi/abs/10.1126/science.aae0491>
114. Clarke J, Panwar B, Madrigal A, Singh D, Gujar R, Wood O, et al. Single-cell transcriptomic analysis of tissue-resident memory T cells in human lung cancer. J Exp Med [Internet]. 2019 Sep 1 [cited 2021 Jan 28];216(9):2128–49. Available from:
<https://pubmed.ncbi.nlm.nih.gov/31227543/>
115. Yu X, Harden K, Gonzalez LC, Francesco M, Chiang E, Irving B, et al. The surface protein TIGIT suppresses T cell activation by promoting the generation of mature immunoregulatory dendritic cells. Nat Immunol [Internet]. 2009 [cited 2022 Jan 19];10(1):48–57. Available from: <https://pubmed.ncbi.nlm.nih.gov/19011627/>
116. Pauken KE, Wherry EJ. TIGIT and CD226: Tipping the Balance between Costimulatory and

- Coinhibitory Molecules to Augment the Cancer Immunotherapy Toolkit. Vol. 26, Cancer Cell. Cell Press; 2014. p. 785–7.
117. Johnston RJ, Comps-Agrar L, Hackney J, Yu X, Huseni M, Yang Y, et al. The Immunoreceptor TIGIT Regulates Antitumor and Antiviral CD8+ T Cell Effector Function. *Cancer Cell*. 2014 Dec 8;26(6):923–37.
118. Boles KS, Nakajima H, Colonna M, Chuang SS, Stepp SE, Bennett M, et al. Molecular characterization of a novel human natural killer cell receptor homologous to mouse 2B4. *Tissue Antigens* [Internet]. 1999 [cited 2022 Jan 19];54(1):27–34. Available from: <https://pubmed.ncbi.nlm.nih.gov/10458320/>
119. Agresta L, Hoebe KHN, Janssen EM. The emerging role of CD244 signaling in immune cells of the tumor microenvironment [Internet]. Vol. 9, *Frontiers in Immunology*. *Front Immunol*; 2018 [cited 2022 Jan 19]. Available from: <https://pubmed.ncbi.nlm.nih.gov/30546369/>
120. Ezinne CC, Yoshimitsu M, White Y, Arima N. HTLV-1 specific CD8+ T cell function augmented by blockade of 2B4/CD48 interaction in HTLV-1 infection. *PLoS One* [Internet]. 2014 [cited 2022 Jan 19];9(2). Available from: www.plosone.org
121. Kar A, Mehrotra S, Chatterjee S. CD38: T Cell Immuno-Metabolic Modulator [Internet]. Vol. 9, *Cells*. *Cells*; 2020 [cited 2022 Jan 19]. Available from: <https://pubmed.ncbi.nlm.nih.gov/32709019/>
122. Moesta AK, Li XY, Smyth MJ. Targeting CD39 in cancer. *Nature Reviews Immunology*. 2020.
123. Ohta A, Gorelik E, Prasad SJ, Ronchese F, Lukashev D, Wong MKK, et al. A2A adenosine receptor protects tumors from antitumor T cells. *Proc Natl Acad Sci U S A* [Internet]. 2006 Aug 29 [cited 2022 Jan 19];103(35):13132–7. Available from: [/pmc/articles/PMC1559765/](https://pubmed.ncbi.nlm.nih.gov/16250000/)
124. Mascanfroni ID, Takenaka MC, Yeste A, Patel B, Wu Y, Kenison JE, et al. Metabolic control of type 1 regulatory T cell differentiation by AHR and HIF1- α . *Nat Med* [Internet]. 2015 Jun 9 [cited 2022 Jan 19];21(6):638–46. Available from: <https://pubmed.ncbi.nlm.nih.gov/26005855/>
125. Deaglio S, Dwyer KM, Gao W, Friedman D, Usheva A, Erat A, et al. Adenosine generation catalyzed by CD39 and CD73 expressed on regulatory T cells mediates immune suppression. *J Exp Med* [Internet]. 2007 Jun 11 [cited 2022 Jan 19];204(6):1257–65. Available from: www.jem.org/cgi/doi/10.1084/jem.20062512

List of References

126. Gupta PK, Godec J, Wolski D, Adland E, Yates K, Pauken KE, et al. CD39 Expression Identifies Terminally Exhausted CD8+ T Cells. *PLoS Pathog* [Internet]. 2015 [cited 2022 Jan 19];11(10). Available from: <https://pubmed.ncbi.nlm.nih.gov/26485519/>
127. Allard D, Allard B, Stagg J. On the mechanism of anti-CD39 immune checkpoint therapy. *Journal for ImmunoTherapy of Cancer*. 2020.
128. Simoni Y, Becht E, Fehlings M, Loh CY, Koo SL, Teng KWW, et al. Bystander CD8+ T cells are abundant and phenotypically distinct in human tumour infiltrates. *Nature* [Internet]. 2018 May 24 [cited 2021 Feb 10];557(7706):575–9. Available from: <https://doi.org/10.1038/s41586-018-0130-2>
129. Duhén T, Duhén R, Montler R, Moses J, Moudgil T, De Miranda NF, et al. Co-expression of CD39 and CD103 identifies tumor-reactive CD8 T cells in human solid tumors. *Nat Commun* [Internet]. 2018 Dec 1 [cited 2021 Feb 11];9(1):1–13. Available from: www.nature.com/naturecommunications
130. Tallón de Lara P, Castañón H, Vermeer M, Núñez N, Silina K, Sobottka B, et al. CD39+PD-1+CD8+ T cells mediate metastatic dormancy in breast cancer. *Nat Commun* [Internet]. 2021 Feb 3 [cited 2022 Jan 19];12(1):1–14. Available from: <https://www.nature.com/articles/s41467-021-21045-2>
131. Canale FP, Ramello MC, Núñez N, Furlan CLA, Bossio SN, Serrán MG, et al. CD39 expression defines cell exhaustion in tumor-infiltrating CD8+ T cells. *Cancer Res* [Internet]. 2018 Jan 1 [cited 2022 Jan 19];78(1):115–28. Available from: <https://pubmed.ncbi.nlm.nih.gov/29066514/>
132. Jiang X, Clark RA, Liu L, Wagers AJ, Fuhlbrigge RC, Kupper TS. Skin infection generates non-migratory memory CD8 + T RM cells providing global skin immunity. *Nature* [Internet]. 2012 Feb 29 [cited 2022 May 7];483(7388):227–31. Available from: <https://www.nature.com/articles/nature10851>
133. Edwards J, Wilmott JS, Madore J, Gide TN, Quek C, Tasker A, et al. CD103+ tumor-resident CD8+ T cells are associated with improved survival in immunotherapy-naïve melanoma patients and expand significantly during anti-PD-1 treatment. *Clin Cancer Res* [Internet]. 2018 Jul 1 [cited 2022 Apr 17];24(13):3036–45. Available from: <https://aacrjournals.org/clincancerres/article/24/13/3036/80949/CD103-Tumor-Resident-CD8-T-Cells-Are-Associated>
134. Okla K, Farber DL, Zou W. Tissue-resident memory T cells in tumor immunity and

- immunotherapy [Internet]. Vol. 218, *Journal of Experimental Medicine*. J Exp Med; 2021 [cited 2022 Apr 27]. Available from: <https://pubmed.ncbi.nlm.nih.gov/33755718/>
135. Gebhardt T, Wakim LM, Eidsmo L, Reading PC, Heath WR, Carbone FR. Memory T cells in nonlymphoid tissue that provide enhanced local immunity during infection with herpes simplex virus. *Nat Immunol* [Internet]. 2009 Mar 22 [cited 2022 May 7];10(5):524–30. Available from: <https://www.nature.com/articles/ni.1718>
136. Kumar B V., Ma W, Miron M, Granot T, Guyer RS, Carpenter DJ, et al. Human Tissue-Resident Memory T Cells Are Defined by Core Transcriptional and Functional Signatures in Lymphoid and Mucosal Sites. *Cell Rep*. 2017 Sep 19;20(12):2921–34.
137. Milner JJ, Goldrath AW. Transcriptional programming of tissue-resident memory CD8 + T cells [Internet]. Vol. 51, *Current Opinion in Immunology*. Elsevier Ltd; 2018 [cited 2022 May 7]. p. 162–9. Available from: <https://doi.org/10.1016/j.coi.2018.03.017>
138. Milner JJ, Toma C, Yu B, Zhang K, Omilusik K, Phan AT, et al. Runx3 programs CD8+ T cell residency in non-lymphoid tissues and tumours. *Nature* [Internet]. 2017 Dec 6 [cited 2022 May 2];552(7684):253–7. Available from: <https://www.nature.com/articles/nature24993>
139. MacKay LK, Rahimpour A, Ma JZ, Collins N, Stock AT, Hafon ML, et al. The developmental pathway for CD103+ CD8+ tissue-resident memory T cells of skin. *Nat Immunol* [Internet]. 2013 Oct 27 [cited 2022 Apr 17];14(12):1294–301. Available from: <https://www.nature.com/articles/ni.2744>
140. Milner JJ, Toma C, He Z, Kurd NS, Nguyen QP, McDonald B, et al. Heterogenous Populations of Tissue-Resident CD8+ T Cells Are Generated in Response to Infection and Malignancy. *Immunity*. 2020 May 19;52(5):808-824.e7.
141. Savas P, Virassamy B, Ye C, Salim A, Mintoff CP, Caramia F, et al. Single-cell profiling of breast cancer T cells reveals a tissue-resident memory subset associated with improved prognosis. *Nat Med* [Internet]. 2018 Jul 1 [cited 2022 Jan 29];24(7):986–93. Available from: <https://pubmed.ncbi.nlm.nih.gov/29942092/>
142. Cheng Y, Gunasegaran B, Singh HD, Dutertre CA, Loh CY, Lim JQ, et al. Non-terminally exhausted tumor-resident memory HBV-specific T cell responses correlate with relapse-free survival in hepatocellular carcinoma. *Immunity*. 2021 Aug 10;54(8):1825-1840.e7.
143. Mei X, Li H, Zhou X, Cheng M, Cui K. The Emerging Role of Tissue-Resident Memory CD8+ T Lymphocytes in Human Digestive Tract Cancers. Vol. 11, *Frontiers in Oncology*. Frontiers

List of References

- Media S.A.; 2022. p. 5828.
144. Jinhua X, Ji W, Shouliang C, Liangfeng Z, Feiyue J, Lin Y, et al. Expression of immune checkpoints in T cells of esophageal cancer patients. *Oncotarget* [Internet]. 2016 [cited 2021 Feb 10];7(39):63669–78. Available from: <https://pubmed.ncbi.nlm.nih.gov/27577071/>
145. Han L, Gao QL, Zhou XM, Shi C, Chen GY, Song YP, et al. Characterization of CD103+ CD8+ tissue-resident T cells in esophageal squamous cell carcinoma: may be tumor reactive and resurrected by anti-PD-1 blockade. *Cancer Immunol Immunother* [Internet]. 2020 Aug 1 [cited 2022 May 9];69(8):1493–504. Available from: <https://pubmed.ncbi.nlm.nih.gov/32285170/>
146. Asia S, Asia S, Hdi H. Oesophagus Source: Globocan 2018. *Int Agency Res Cancer* [Internet]. 2018;876:2018–9. Available from: <http://gco.iarc.fr/today>
147. Bray F, Ferlay J, Soerjomataram I. *Global Cancer Statistics 2018 : GLOBOCAN Estimates of Incidence and Mortality Worldwide for 36 Cancers in 185 Countries*. 2018;394–424.
148. Oesophageal cancer statistics | Cancer Research UK [Internet]. [cited 2022 Jan 12]. Available from: <https://www.cancerresearchuk.org/health-professional/cancer-statistics/statistics-by-cancer-type/oesophageal-cancer>
149. Edgren G, Adami HO, Vainio EW, Nyrén O. A global assessment of the oesophageal adenocarcinoma epidemic. *Gut* [Internet]. 2013 Oct 1 [cited 2022 Jan 12];62(10):1406–14. Available from: <https://gut.bmj.com/content/62/10/1406>
150. Rustgi AK, El-Serag HB. Esophageal carcinoma. *N Engl J Med*. 2014;371(26):2499–509.
151. Al-Batran SE, Homann N, Pauligk C, Goetze TO, Meiler J, Kasper S, et al. Perioperative chemotherapy with fluorouracil plus leucovorin, oxaliplatin, and docetaxel versus fluorouracil or capecitabine plus cisplatin and epirubicin for locally advanced, resectable gastric or gastro-oesophageal junction adenocarcinoma (FLOT4): a ra. *Lancet* [Internet]. 2019 May 11 [cited 2021 Jan 14];393(10184):1948–57. Available from: <https://pubmed.ncbi.nlm.nih.gov/30982686/>
152. Shapiro J, van Lanschot JJB, Hulshof MCCM, van Hagen P, van Berge Henegouwen MI, Wijnhoven BPL, et al. Neoadjuvant chemoradiotherapy plus surgery versus surgery alone for oesophageal or junctional cancer (CROSS): Long-term results of a randomised controlled trial. *Lancet Oncol* [Internet]. 2015 Sep 1 [cited 2021 Jan 14];16(9):1090–8.

- Available from: <https://pubmed.ncbi.nlm.nih.gov/26254683/>
153. The National Institute for Health and Care Excellence (NICE). Oesophago-gastric cancer: Assessment and management in adults (NG83). NICE Guidel [Internet]. 2018 [cited 2022 Jan 12];4(January 2018):970–6. Available from: <http://www.nice.org.uk/guidance/ng83>
 154. Bhat S, Coleman HG, Yousef F, Johnston BT, McManus DT, Gavin AT, et al. Risk of malignant progression in Barrett’s Esophagus patients: Results from a large population-based study. *J Natl Cancer Inst* [Internet]. 2011 Jul 6 [cited 2022 Jan 12];103(13):1049–57. Available from: </pmc/articles/PMC3632011/>
 155. Sawas T, Killcoyne S, Iyer PG, Wang KK, Smyrk TC, Kisiel JB, et al. Identification of Prognostic Phenotypes of Esophageal Adenocarcinoma in 2 Independent Cohorts. *Gastroenterology* [Internet]. 2018 Dec 1 [cited 2022 Jan 12];155(6):1720-1728.e4. Available from: <https://pubmed.ncbi.nlm.nih.gov/30165050/>
 156. Killcoyne S, Fitzgerald RC. Evolution and progression of Barrett’s oesophagus to oesophageal cancer [Internet]. Vol. 21, *Nature Reviews Cancer*. *Nat Rev Cancer*; 2021 [cited 2022 Jan 12]. p. 731–41. Available from: <https://pubmed.ncbi.nlm.nih.gov/34545238/>
 157. Frankell AM, Jammula SG, Li X, Contino G, Killcoyne S, Abbas S, et al. The landscape of selection in 551 esophageal adenocarcinomas defines genomic biomarkers for the clinic. *Nat Genet* [Internet]. 2019 Feb 4 [cited 2022 Jan 12];51(3):506–16. Available from: <https://www.nature.com/articles/s41588-018-0331-5>
 158. Siewert JR, Stein HJ. Classification of adenocarcinoma of the oesophagogastric junction. *Br J Surg* [Internet]. 1998 [cited 2022 Jan 12];85(11):1457–9. Available from: <https://pubmed.ncbi.nlm.nih.gov/9823902/>
 159. Rice TW, Patil DT, Blackstone EH. 8th edition AJCC/UICC staging of cancers of the esophagus and esophagogastric junction: Application to clinical practice. *Ann Cardiothorac Surg* [Internet]. 2017 Mar 1 [cited 2022 May 8];6(2):119–30. Available from: </pmc/articles/PMC5387145/>
 160. Hulscher JBF, van Sandick JW, de Boer AGEM, Wijnhoven BPL, Tijssen JGP, Fockens P, et al. Extended Transthoracic Resection Compared with Limited Transhiatal Resection for Adenocarcinoma of the Esophagus. *N Engl J Med* [Internet]. 2002 Oct 7 [cited 2022 Jan 13];347(21):1662–9. Available from: <https://www.nejm.org/doi/10.1056/NEJMoa022343>

List of References

161. Chang AC, Morse CR, Pramesh CS, Pera M, Naftoux P, Kuppusamy MK, et al. Benchmarking Complications Associated with Esophagectomy. *Ann Surg*. 2017;269(2):291–8.
162. Lordick F, Mariette C, Haustermans K, Obermannová R, Arnold D, on behalf of the ESMO Guidelines Committee clinicalguidelines@esmo.org. Oesophageal cancer: ESMO clinical practice guidelines for diagnosis, treatment and follow-up. *Ann Oncol*. 2016;27:v50–7.
163. Girling DJ, Bancewicz J, Clark PI, Smith DB, Donnelly RJ, Fayers PM, et al. Surgical resection with or without preoperative chemotherapy in oesophageal cancer: A randomised controlled trial. *Lancet*. 2002 May 18;359(9319):1727–33.
164. Cunningham D, Allum WH, Stenning SP, Thompson JN, Van de Velde CJH, Nicolson M, et al. Perioperative Chemotherapy versus Surgery Alone for Resectable Gastroesophageal Cancer. *N Engl J Med* [Internet]. 2006 Jul 6 [cited 2022 Jan 13];355(1):11–20. Available from: <https://pubmed.ncbi.nlm.nih.gov/16822992/>
165. Pühr HC, Preusser M, Ilhan-Mutlu A. Immunotherapy for esophageal cancers: What is practice changing in 2021? [Internet]. Vol. 13, *Cancers*. Multidisciplinary Digital Publishing Institute; 2021 [cited 2022 Jan 13]. p. 4632. Available from: <https://www.mdpi.com/2072-6694/13/18/4632/htm>
166. Kelly RJ, Ajani JA, Kuzdzal J, Zander T, Van Cutsem E, Piessen G, et al. Adjuvant Nivolumab in Resected Esophageal or Gastroesophageal Junction Cancer. *N Engl J Med* [Internet]. 2021 Apr 1 [cited 2022 Jan 13];384(13):1191–203. Available from: <https://www.nejm.org/doi/full/10.1056/NEJMoa2032125>
167. Food and Drug Administration. FDA Approves Pembrolizumab for Esophageal or GEJ Carcinoma [Internet]. 2021 [cited 2022 Jan 13]. Available from: <https://www.fda.gov/drugs/resources-information-approved-drugs/fda-approves-nivolumab-resected-esophageal-or-gej-cancer>
168. National Institute for Health and Care Excellence. Overview | Nivolumab for adjuvant treatment of resected oesophageal or gastro-oesophageal junction cancer | Guidance | NICE. NICE; 2021.
169. Linder G, Klevebro F, Edholm D, Johansson J, Lindblad M, Hedberg J. Burden of in-hospital care in oesophageal cancer: national population-based study. *BJS open* [Internet]. 2021 May 7 [cited 2022 Jan 13];5(3). Available from: <https://academic.oup.com/bjsopen/article/5/3/zrab037/6271348>

170. Cunningham D, Starling N, Rao S, Iveson T, Nicolson M, Coxon F, et al. Capecitabine and Oxaliplatin for Advanced Esophagogastric Cancer. *N Engl J Med* [Internet]. 2008 Jan 3 [cited 2022 Jan 13];358(1):36–46. Available from: <https://www.nejm.org/doi/full/10.1056/nejmoa073149>
171. Van Cutsem E, Moiseyenko VM, Tjulandin S, Majlis A, Constenla M, Boni C, et al. Phase III study of docetaxel and cisplatin plus fluorouracil compared with cisplatin and fluorouracil as first-line therapy for advanced gastric cancer: A report of the V25 study group. *J Clin Oncol*. 2006 Nov 1;24(31):4991–7.
172. Bang YJ, Van Cutsem E, Feyereislova A, Chung HC, Shen L, Sawaki A, et al. Trastuzumab in combination with chemotherapy versus chemotherapy alone for treatment of HER2-positive advanced gastric or gastro-oesophageal junction cancer (ToGA): A phase 3, open-label, randomised controlled trial. *Lancet*. 2010;376(9742):687–97.
173. Ford HER, Marshall A, Bridgewater JA, Janowitz T, Coxon FY, Wadsley J, et al. Docetaxel versus active symptom control for refractory oesophagogastric adenocarcinoma (COUGAR-02): An open-label, phase 3 randomised controlled trial. *Lancet Oncol*. 2014 Jan 1;15(1):78–86.
174. Kim J, Bowlby R, Mungall AJ, Robertson AG, Odze RD, Cherniack AD, et al. Integrated genomic characterization of oesophageal carcinoma. *Nature* [Internet]. 2017 Jan 12 [cited 2022 Jan 14];541(7636):169–74. Available from: <https://pubmed.ncbi.nlm.nih.gov/28052061/>
175. Hao D, He S, Harada K, Pizzi MP, Lu Y, Guan P, et al. Integrated genomic profiling and modelling for risk stratification in patients with advanced oesophagogastric adenocarcinoma. *Gut* [Internet]. 2021 Nov 1 [cited 2022 Jan 14];70(11):2055–65. Available from: <https://gut.bmj.com/content/70/11/2055>
176. Lonie JM, Barbour AP, Dolcetti R. Understanding the immuno-biology of oesophageal adenocarcinoma: Towards improved therapeutic approaches. Vol. 98, *Cancer Treatment Reviews*. W.B. Saunders; 2021. p. 102219.
177. Marabelle A, Fakih M, Lopez J, Shah M, Shapira-Frommer R, Nakagawa K, et al. Association of tumour mutational burden with outcomes in patients with advanced solid tumours treated with pembrolizumab: prospective biomarker analysis of the multicohort, open-label, phase 2 KEYNOTE-158 study. *Lancet Oncol* [Internet]. 2020 Oct 1 [cited 2022 Jan 14];21(10):1353–65. Available from: <https://pubmed.ncbi.nlm.nih.gov/32919526/>

List of References

178. Le DT, Uram JN, Wang H, Bartlett BR, Kemberling H, Eyring AD, et al. PD-1 Blockade in Tumors with Mismatch-Repair Deficiency. *N Engl J Med* [Internet]. 2015 Jun 25 [cited 2022 Jan 14];372(26):2509–20. Available from: <https://www.nejm.org/doi/full/10.1056/nejmoa1500596>
179. Yarchoan M, Hopkins A, Jaffee EM. Tumor Mutational Burden and Response Rate to PD-1 Inhibition. *N Engl J Med* [Internet]. 2017 Dec 21 [cited 2022 Jan 14];377(25):2500–1. Available from: <https://www.nejm.org/doi/10.1056/NEJMc1713444>
180. Janjigian YY, Bendell J, Calvo E, Kim JW, Ascierto PA, Sharma P, et al. CheckMate-032 Study: Efficacy and Safety of Nivolumab and Nivolumab Plus Ipilimumab in Patients With Metastatic Esophagogastric Cancer. *J Clin Oncol*. 2018 Oct;36(28):2836–44.
181. Thorsson V, Gibbs DL, Brown SD, Wolf D, Bortone DS, Ou Yang TH, et al. The Immune Landscape of Cancer. *Immunity*. 2018;48(4):812-830.e14.
182. Schumacher K, Haensch W, Röefzaad C, Schlag PM. Prognostic Significance of Activated CD8+ T Cell Infiltrations within Esophageal Carcinomas. *Cancer Res*. 2001;61(10).
183. Zheng X, Song X, Shao Y, Xu B, Hu W, Zhou Q, et al. Prognostic role of tumor-infiltrating lymphocytes in esophagus cancer: A meta-analysis. *Cell Physiol Biochem* [Internet]. 2018 Feb 1 [cited 2022 Jan 14];45(2):720–32. Available from: <https://pubmed.ncbi.nlm.nih.gov/29414812/>
184. Jung H, Choi JK, Lee EA. Immune signatures correlate with L1 retrotransposition in gastrointestinal cancers. *Genome Res* [Internet]. 2018 Aug 1 [cited 2022 Jan 14];28(8):1136–46. Available from: </pmc/articles/PMC6071633/>
185. Sohn BH, Hwang JE, Jang HJ, Lee HS, Oh SC, Shim JJ, et al. Clinical significance of four molecular subtypes of gastric cancer identified by The Cancer Genome Atlas project. *Clin Cancer Res* [Internet]. 2017 Aug 1 [cited 2022 Jan 14];23(15):4441–9. Available from: <https://clincancerres.aacrjournals.org/content/23/15/4441>
186. Thompson ED, Zahurak M, Murphy A, Cornish T, Cuka N, Abdelfatah E, et al. Patterns of PD-L1 expression and CD8 T cell infiltration in gastric adenocarcinomas and associated immune stroma. *Gut* [Internet]. 2016 Jan 22 [cited 2022 Jan 14];66(5):794–801. Available from: </pmc/articles/PMC4958028/>
187. Kang YK, Boku N, Satoh T, Ryu MH, Chao Y, Kato K, et al. Nivolumab in patients with advanced gastric or gastro-oesophageal junction cancer refractory to, or intolerant of, at

- least two previous chemotherapy regimens (ONO-4538-12, ATTRACTION-2): a randomised, double-blind, placebo-controlled, phase 3 trial. *Lancet* [Internet]. 2017 Dec 2 [cited 2021 Feb 2];390(10111):2461–71. Available from: <https://pubmed.ncbi.nlm.nih.gov/28993052/>
188. Smyth EC, Gambardella V, Cervantes A, Fleitas T. Checkpoint inhibitors for gastroesophageal cancers: dissecting heterogeneity to better understand their role in first-line and adjuvant therapy. Vol. 32, *Annals of Oncology*. Elsevier; 2021. p. 590–9.
189. Fuchs CS, Doi T, Jang RW, Muro K, Satoh T, Machado M, et al. Safety and efficacy of pembrolizumab monotherapy in patients with previously treated advanced gastric and gastroesophageal junction cancer: Phase 2 clinical KEYNOTE-059 trial. *JAMA Oncol* [Internet]. 2018 May 1 [cited 2022 Jan 14];4(5). Available from: <https://pubmed.ncbi.nlm.nih.gov/29543932/>
190. Shitara K, Özgüroğlu M, Bang YJ, Di Bartolomeo M, Mandalà M, Ryu MH, et al. Pembrolizumab versus paclitaxel for previously treated, advanced gastric or gastro-oesophageal junction cancer (KEYNOTE-061): a randomised, open-label, controlled, phase 3 trial. *Lancet*. 2018 Jul 14;392(10142):123–33.
191. Shitara K, Van Cutsem E, Bang YJ, Fuchs C, Wyrwicz L, Lee KW, et al. Efficacy and Safety of Pembrolizumab or Pembrolizumab plus Chemotherapy vs Chemotherapy Alone for Patients with First-line, Advanced Gastric Cancer: The KEYNOTE-062 Phase 3 Randomized Clinical Trial. *JAMA Oncol* [Internet]. 2020 Oct 1 [cited 2022 Jan 14];6(10):1571–80. Available from: <https://jamanetwork.com/journals/jamaoncology/fullarticle/2769922>
192. Janjigian YY, Shitara K, Moehler M, Garrido M, Salman P, Shen L, et al. First-line nivolumab plus chemotherapy versus chemotherapy alone for advanced gastric, gastro-oesophageal junction, and oesophageal adenocarcinoma (CheckMate 649): a randomised, open-label, phase 3 trial. *Lancet* [Internet]. 2021 Jul 3 [cited 2022 Jan 14];398(10294):27–40. Available from: <http://www.thelancet.com/article/S0140673621007972/fulltext>
193. QIAGEN. RNeasy® Plus Micro Handbook. 2020 [cited 2022 May 8];(January):1–68. Available from: <https://www.qiagen.com/us/resources/resourcedetail?id=1961e574-091d-42cc-8b51-1bc3747da874&lang=en>
194. Zymo-Research. Quick-RNA Miniprep Kit [Internet]. 2021 [cited 2022 May 8]. Available from: <https://www.zymoresearch.com/products/quick-rna-miniprep-kit>
195. Zymo-Research. Direct-zol RNA Microprep Kits [Internet]. 2021 [cited 2022 May 8]. Available from: <https://www.zymoresearch.com/collections/direct-zol-rna->

List of References

kits/products/direct-zol-rna-microprep-kits

196. Toni LS, Garcia AM, Jeffrey DA, Jiang X, Stauffer BL, Miyamoto SD, et al. Optimization of phenol-chloroform RNA extraction. *MethodsX* [Internet]. 2018 Jan 1 [cited 2021 Jan 28];5:599–608. Available from: [/pmc/articles/PMC6031757/?report=abstract](https://pubmed.ncbi.nlm.nih.gov/30111111/)
197. Picelli S, Faridani OR, Björklund ÅK, Winberg G, Sagasser S, Sandberg R. Full-length RNA-seq from single cells using Smart-seq2. *Nat Protoc*. 2014;9(1):171–81.
198. Thermo Fisher Scientific. Qubit™ RNA High Sensitivity (HS), Broad Range (BR), and Extended Range (XR) Assay Kits. [Internet]. 2020 [cited 2022 May 8]. Available from: <https://www.thermofisher.com/order/catalog/product/Q32852>
199. Agilent. High Sensitivity RNA Electrophoresis, RIN, Bioanalyzer Pico | Agilent [Internet]. 2022 [cited 2022 May 8]. Available from: <https://www.agilent.com/en/product/automated-electrophoresis/bioanalyzer-systems/bioanalyzer-rna-kits-reagents/bioanalyzer-high-sensitivity-rna-analysis-228255>
200. Mueller O, Schroeder A. RNA Integrity Number (RIN) – Standardization of RNA Quality Control Application [Internet]. Agilent Technologies. 2016 [cited 2021 Jan 28]. Available from: <https://www.agilent.com/cs/library/applications/5989-1165EN.pdf>
201. Illumina. TruSeq DNA Sample Preparation Guide, Part 15026486 Rev. C [Internet]. Sample Prep Guide. San Diego, CA; 2012 [cited 2022 Jan 24]. Available from: <https://support.illumina.com/>
202. Ganesan AP, Clarke J, Wood O, Garrido-Martin EM, Chee SJ, Mellows T, et al. Tissue-resident memory features are linked to the magnitude of cytotoxic T cell responses in human lung cancer. *Nat Immunol* [Internet]. 2017 Jul 19 [cited 2021 Jan 28];18(8):940–50. Available from: <https://pubmed.ncbi.nlm.nih.gov/28628092/>
203. Agilent. Quality control NGS libraries, Bioanalyzer High Sensitivity DNA [Internet]. 2022 [cited 2022 May 8]. Available from: <https://www.agilent.com/en/product/automated-electrophoresis/bioanalyzer-systems/bioanalyzer-dna-kits-reagents/bioanalyzer-high-sensitivity-dna-analysis-228249>
204. Quah BJC, Warren HS, Parish CR. Monitoring lymphocyte proliferation in vitro and in vivo with the intracellular fluorescent dye carboxyfluorescein diacetate succinimidyl ester. *Nat Protoc* [Internet]. 2007 Aug 23 [cited 2022 May 3];2(9):2049–56. Available from: <https://www.nature.com/articles/nprot.2007.296>

205. Gao Y, Guo W, Geng X, Zhang Y, Zhang G, Qiu B, et al. Prognostic value of tumor-infiltrating lymphocytes in esophageal cancer: an updated meta-analysis of 30 studies with 5,122 patients. *Ann Transl Med.* 2020;
206. Kelly RJ. The emerging role of immunotherapy for esophageal cancer. *Curr Opin Gastroenterol* [Internet]. 2019 Jul 1 [cited 2021 Feb 10];35(4):337–43. Available from: <https://journals.lww.com/00001574-201907000-00013>
207. Mandard A -M, Dalibard F, Mandard J -C, Marnay J, Henry-Amar M, Petiot J -F, et al. Pathologic assessment of tumor regression after preoperative chemoradiotherapy of esophageal carcinoma. Clinicopathologic correlations. *Cancer* [Internet]. 1994 [cited 2021 Jan 14];73(11):2680–6. Available from: <https://pubmed.ncbi.nlm.nih.gov/8194005/>
208. Cancer Research UK. Oesophageal cancer incidence statistics | Cancer Research UK [Internet]. Cancer Research UK. 2018. Available from: <https://www.cancerresearchuk.org/health-professional/cancer-statistics/statistics-by-cancer-type/oesophageal-cancer/incidence#heading-One>
209. Waise S, Parker R, Rose-Zerilli MJ, Layfield DM, Wood O, West J, et al. An optimised tissue disaggregation and data processing pipeline for characterising fibroblast phenotypes using single-cell RNA sequencing. *Sci Rep.* 2019;
210. Leelatian N, Doxie DB, Greenplate AR, Sinnaeve J, Ihrie, Rebecca A, Irish JM. Preparing Viable Single Cells from Human Tissue and Tumors for Cytomic Analysis *Current Protocols in Molecular Biology.* Current Protocol Molecular Biology. 2018.
211. Gooden M, de Bock G, Leffers N, Daemen T, Nijman H. The prognostic influence of tumour-infiltrating lymphocytes in cancer: a systematic review with meta-analysis. *Br J Cancer* [Internet]. 2011 [cited 2021 Sep 23];105:93–103. Available from: www.bjccancer.com
212. Zingg U, Montani M, Frey DM, Dirnhofer S, Esterman AJ, Went P, et al. Tumour-infiltrating lymphocytes and survival in patients with adenocarcinoma of the oesophagus. *Eur J Surg Oncol.* 2010 Jul 1;36(7):670–7.
213. Direct-zol RNA Microprep Kits [Internet]. [cited 2022 Apr 26]. Available from: <https://www.zymoresearch.com/products/direct-zol-rna-microprep-kits>
214. Love MI, Huber W, Anders S. Moderated estimation of fold change and dispersion for RNA-seq data with DESeq2. *Genome Biol* [Internet]. 2014 Dec 5 [cited 2021 Feb 12];15(12):550. Available from: <http://genomebiology.biomedcentral.com/articles/10.1186/s13059-014->

List of References

0550-8

215. Stephens M. False discovery rates: A new deal. *Biostatistics* [Internet]. 2017 Apr 1 [cited 2022 Jan 26];18(2):275–94. Available from: </pmc/articles/PMC5379932/>
216. Subramanian A, Tamayo P, Mootha VK, Mukherjee S, Ebert BL, Gillette MA, et al. Gene set enrichment analysis: A knowledge-based approach for interpreting genome-wide expression profiles. *Proc Natl Acad Sci U S A* [Internet]. 2005 Oct 25 [cited 2022 Jan 26];102(43):15545–50. Available from: <https://www.pnas.org/content/102/43/15545>
217. Mootha VK, Lindgren CM, Eriksson KF, Subramanian A, Sihag S, Lehar J, et al. PGC-1 α -responsive genes involved in oxidative phosphorylation are coordinately downregulated in human diabetes. *Nat Genet* [Internet]. 2003 Jun 15 [cited 2022 Jan 26];34(3):267–73. Available from: <https://www.nature.com/articles/ng1180>
218. Anders S, Huber W. Differential expression analysis for sequence count data. *Genome Biol* [Internet]. 2010 Oct 27 [cited 2022 Jan 26];11(10):1–12. Available from: <https://genomebiology.biomedcentral.com/articles/10.1186/gb-2010-11-10-r106>
219. Busby MA, Stewart C, Miller CA, Grzeda KR, Marth GT. Scotty: A web tool for designing RNA-Seq experiments to measure differential gene expression. *Bioinformatics* [Internet]. 2013 Mar 1 [cited 2022 Apr 27];29(5):656–7. Available from: <https://academic.oup.com/bioinformatics/article/29/5/656/252753>
220. Sowell RT, Goldufsky JW, Rogozinska M, Quiles Z, Cao Y, Castillo EF, et al. IL-15 Complexes Induce Migration of Resting Memory CD8 T Cells into Mucosal Tissues. *J Immunol* [Internet]. 2017 Oct 1 [cited 2022 Apr 27];199(7):2536–46. Available from: <https://www.jimmunol.org/content/199/7/2536>
221. Andreatta M, Corria-Osorio J, Müller S, Cubas R, Coukos G, Carmona SJ. Interpretation of T cell states from single-cell transcriptomics data using reference atlases. *Nat Commun* [Internet]. 2021 May 20 [cited 2022 Feb 27];12(1):1–19. Available from: <https://www.nature.com/articles/s41467-021-23324-4>
222. Goldrath AW, Luckey CJ, Park R, Benoist C, Mathis D. The molecular program induced in T cells undergoing homeostatic proliferation. *Proc Natl Acad Sci U S A* [Internet]. 2004 Nov 30 [cited 2022 Jan 29];101(48):16885–90. Available from: <https://www.pnas.org/content/101/48/16885>
223. Hänzelmann S, Castelo R, Guinney J. GSEA: Gene set variation analysis for microarray and

- RNA-Seq data. *BMC Bioinformatics* [Internet]. 2013 [cited 2022 Mar 7];14:7. Available from: <http://www.biomedcentral.com/1471-2105/14/7><http://www.bioconductor.org>.Background
224. Thompson EA, Darrah PA, Foulds KE, Hoffer E, Caffrey-Carr A, Norenstedt S, et al. Monocytes Acquire the Ability to Prime Tissue-Resident T Cells via IL-10-Mediated TGF- β Release. *Cell Rep* [Internet]. 2019 [cited 2022 May 2];28(5):1127-1135.e4. Available from: <https://doi.org/10.1016/j.celrep.2019.06.087>
225. Hadrup SR, Brændstrup O, Jacobsen GK, Mortensen S, Pedersen LØ, Seremet T, et al. Tumor infiltrating lymphocytes in seminoma lesions comprise clonally expanded cytotoxic T cells. *Int J Cancer* [Internet]. 2006 Aug 15 [cited 2022 May 3];119(4):831–8. Available from: <https://pubmed.ncbi.nlm.nih.gov/16557580/>
226. Lorenzo-Herrero S, Sordo-Bahamonde C, Gonzalez S, López-Soto A. CD107a degranulation assay to evaluate immune cell antitumor activity. In: *Methods in Molecular Biology* [Internet]. *Methods Mol Biol*; 2019 [cited 2022 May 3]. p. 119–30. Available from: <https://pubmed.ncbi.nlm.nih.gov/30465198/>
227. Overgaard NH, Jung J-W, Steptoe RJ, Wells JW. CD4 + /CD8 + double-positive T cells: more than just a developmental stage? *J Leukoc Biol* [Internet]. 2015 Jan 1 [cited 2022 Apr 17];97(1):31–8. Available from: <https://onlinelibrary.wiley.com/doi/full/10.1189/jlb.1RU0814-382>
228. Behr FM, Chuwonpad A, Stark R, van Gisbergen KPJM. Armed and Ready: Transcriptional Regulation of Tissue-Resident Memory CD8 T Cells. Vol. 9, *Frontiers in Immunology*. Frontiers Media S.A.; 2018. p. 1770.
229. Mami-Chouaib F, Tartour E. Editorial: Tissue resident memory T cells. Vol. 10, *Frontiers in Immunology*. Frontiers Media S.A.; 2019. p. 1018.
230. Flynn M, Young K, Cunningham D, Starling N. The evolving immunotherapeutic landscape in advanced oesophagogastric cancer [Internet]. Vol. 10, *Therapeutic Advances in Medical Oncology*. SAGE Publications; 2018 [cited 2022 May 9]. Available from: </pmc/articles/PMC6048671/>

